



22nd

NRB

Yellowknife
Canada

**22nd Northern Research Basins (NRB)
Symposia & Workshop: *Partners in
Learning***

August 18-23, 2019

On behalf of the Organizing Committee, I would like to welcome you to the 22nd Northern Research Basins Symposium & Workshop – *Partners in Learning*, and to Yellowknife, Canada!

The theme "*Partners in Learning*" emphasises the need for two-way information flow and collaboration between Indigenous communities and scientists/scientific programmes. It also reflects the need for us to come together, regardless of our backgrounds, and different ways of knowing, so that we can collectively meet the challenges of climate warming. The meeting will include unique opportunities to exchange experiences and ideas with members of other circum-polar nations, and to discuss the science, community engagement activities and partnerships.

This week is an excellent opportunity for you to meet colleagues from around the circumpolar region and share experiences and insights. Registered NRB participants also have a full schedule of events to experience the life and history of NWT peoples:

- Viewing artifacts & emerging archaeology projects in the region.
- Experiencing a feast in a Dene village.
- Touring Great Slave Lake by boat & a shore side fish fry lunch.
- Walking tour of Yellowknife and Old Town.
- Dancing to traditional Métis music.
- Meeting community members from across the NWT.

With your participation we can all learn from each other as partners, and gain new insights to inform our research and engagement activities in the North.

Kind Regards,



William (Bill) Quinton, Chief Delegate, Canada
Director, Cold Regions Research Centre, Wilfrid Laurier University.
scottycreek.com, coldregions.ca, scottycreek.com/DCoP

NORTHERN RESEARCH BASINS (NRB) WORKING GROUP

HISTORY

In 1975, the International Hydrological Program (IHP) National Committees of Canada, Denmark/Greenland, Finland, Norway, Sweden, the United States of America, and the Union of Soviet Socialist Republics (USSR) established the **IHP Working Group on Northern Research Basins**, now called the “**NRB Working Group**”. In 1992, Iceland joined the group and Russia took over the responsibilities of the former USSR.

OBJECTIVES

The overall objective of the NRB Working Group is to **encourage research in hydrological basins in cold regions where snow, ice and frozen ground have a dominant role in the hydrological cycle.**

Over the years, the objectives of the NRB Working Group have evolved to include the following:

1. Gain a better understanding of hydrological processes, particularly those in which snow, ice, and frozen ground have a major influence on the hydrological regime, and to determine the relative importance of each component of the water balance.
2. Provide data for the development and testing of transposable models which may be applied to regional, national, and international water and land resource programmes.
3. Relate hydrological processes to the chemical and biological evolution of northern basins.
4. Assess and predict the effect of human activities on the hydrological regime in northern environments.
5. Encourage the exchange of personnel (technicians, scientists, research officers, students, and others) among participating countries.
6. Provide information for the improvement and standardisation of measurement techniques and network design in northern regions.
7. Encourage exchange of information on a regular basis, and
8. Set up task forces to promote research initiatives on topics of special interest to northern research basins.

FOCUS ON CLIMATE WARMING

Since the NRB’s inception, climate warming has developed as a major scientific issue of direct importance to cold regions hydrology and water science throughout the circumpolar region. From the perspective of the Indigenous communities of cold regions, climate warming has introduced new and troubling uncertainties in regards to the future quantity and quality of water resources. In recent years there is a growing realization that climate warming adaptation strategies are most successful if the communities directly affected play a leading role in their development and application.

22nd Northern Research Basins (NRB) Symposium Proceedings

Long-term Evidence for Hydrological System Regime Change from the Fish Creek Watershed Observatory in northern Alaska, U.S.A.

Christopher D. Arp¹, Matthew S. Whitman², and Richard Kemnitz²

¹*Water and Environmental Research Center, University of Alaska Fairbanks, Fairbanks, Alaska, 99775, U.S.A.*

²*Bureau of Land Management, Arctic District Office, Fairbanks, Alaska, 99709, U.S.A.*

**Corresponding author's email address: cdarp@alaska.edu*

ABSTRACT

Rapid changes in climate coupled with expanding development on the Arctic Coastal Plain of northern Alaska (ACP) make sustaining hydrological observations increasingly important. Fish Creek drains a 4600 km² area of the ACP in the National Petroleum Reserve in Alaska (NPR-A). While oil production in this watershed unit only began in 2016, environmental monitoring began much earlier in 2001. Hydroclimatic datasets for this watershed now span 18 years and record notable changes in precipitation, total runoff, and runoff regimes. Discharge records from three adjacent rivers representing varying geologic conditions and lake extents provide the framework for the Fish Creek Watershed Observatory (FCWO). Three periods with distinct hydrologic regimes were identified from this record. The 2001-2008 period had average mean annual runoff (MAR) of 90 mm with a severe drought in 2007. 2009-2015 was characterized by higher MAR of 120 mm and several years with early and high snowmelt runoff. The most recent three years, 2016-2018, had even higher MAR of 146 mm, but relatively low and late snowmelt. Hydrograph separation suggests a regime shift to rainfall dominated runoff in the most recent period compared to approximately 75% of runoff contributed from snowmelt in the previous 15 years. Our analysis suggest that this shift in runoff contributions and increase in total runoff is partially due to greater open water extent with declining sea ice. Future development on the ACP will require careful planning to avoid flood and channel change hazards, permafrost degradation, and ecosystem damage.

KEYWORDS

Arctic Coastal Plain; Hydrologic intensification; Runoff regimes; Hydrograph separation; Petroleum development

1. INTRODUCTION

Runoff from arctic coastal watersheds has long been characterized by a short season initiated by large snowmelt peakflows that decline rapidly to much lower runoff supplied by rainfall and storage from the active-layer and lake basins (Marsh & Woo 1981; Bowling et al. 2003; Kane & Yang 2004). Evapotranspiration can often exceed traditionally low rainfall amounts during the summer leading to periods of extremely low flow and disconnectivity in smaller streams. While snowmelt-dominated runoff regimes and associated sharp peakflow events present hazards to infrastructure (Instanes et al. 2016), channel and floodplain soils are typically frozen and more resistant to erosion during this period (McNamara and Kane 2009; Beel et al. 2018). Accordingly, most hydrologic monitoring programs have focused on capturing snowmelt runoff events relative to watershed snowpacks (Kane & Yang 2004) with more recent interest in summer lowflows and affects on connectivity relative to weather and climate conditions (Arp et al. 2019).

Large summer rainfall-runoff events are traditionally rare on the Arctic Coastal Plain of northern Alaska (ACP) (Kane et al. 2003), but potentially most effective at moving sediment and reshaping channels (McNamara & Kane 2009). Extreme rainfall-generated floods have been captured in arctic foothills watersheds, yet the same weather system failed to produce similar responses in coastal watersheds (Kane et al. 2003). Hydrological process studies have focused on calculating watershed water balance from networks of intensive hydrometrological stations compared to discharge records (Kane et al. 1991; Kane and Yang 2004). Such studies typically suggest that 60-80% of runoff comes from snowpack and antecedent surface storage plays an important role in runoff efficiency from year to year. Research into source-water contribution to runoff events show that old storage water can accompany snowmelt using both graphical hydrograph separation and chemical tracer end-member (McNamara et al. 1997). Using natural tracers in arctic systems, such as hydrogen and oxygen isotopes or specific conductance, are often challenging because similarities between snow, activelayer, and permafrost water signatures and high variability in storm-track rainfall signatures. Graphical hydrograph separation in temperate watersheds with continuous baseflow are often considered subjective in isolating stormwater from groundwater contributions (Sujono et al. 2004). However, in small to medium sized continuous permafrost watersheds where flow initiates almost entirely from snowmelt, the removal of groundwater baseflow simplifies graphical separation approaches, allowing for useful hydrological analyses of hydrographs from year to year and among basins (Woo et al. 2008).

Arctic watersheds are increasingly sensitive to hydrologic intensification in response to both cold and warm season climate change that is predicted to drive higher snowfall and rainfall (Déry et al. 2009; Rawlings et al. 2010). Evidence of such higher overall runoff are already emerging from several watershed with long-term runoff records in the Canadian (Déry et al. 2009; Beel et al. 2018) and Siberian (Peterson et al. 2002; Makarieva et al. 2019) Arctic. Coincident with hydrologic intensification may be a shift from snowmelt-dominated to rainfall-dominated runoff regimes (Instanes et al. 2016). In ACP watersheds, enhanced open-ocean extents as sea ice declines can provide an additional source of rainfall adding to such a regime shift (Bintanja & Selten 2014). Understanding if and to what extent such hydrologic changes are occurring on the ACP, and particularly the NPR-A where development is pushing into new terrain (Arp et al. 2019), will help inform better design of infrastructure and management of natural resources in the future.

2. METHODS

The Fish Creek Watershed (FCW) drains an 4600 km² area of the northeastern National Petroleum Reserve in Alaska (NPR-A) on the central ACP approximately equal distance between Prudhoe Bay to the East and Utqiagvik to the West (Figure 1). Three alluvial rivers compose the FCW and representing varying geologic, hypsographic, and lake basin compositions (Arp et al. 2012). Upper Fish Creek (2016 km²) drains mostly tundra set atop inactive eolian sand dunes with many large deep lakes and distinctively slow snowmelt recession. Judy Creek (1647 km²) has its headwaters in lower bedrock-controlled foothills, is very elongate, and has intermediate densities of lakes and drained lake basins. The Ublutuoch River (483 km²) has a beaded channel through most of its course running through alluvial-marine silt terrain with high densities of thermokarst lake basins.

Beginning in 2000, river gauging stations were established near the confluence of each of these three rivers within the FCW by the Bureau of Land Management (BLM) (Whitman et al. 2011). Stations consist of vented pressure transducers set at high and low channel elevations to avoid ice

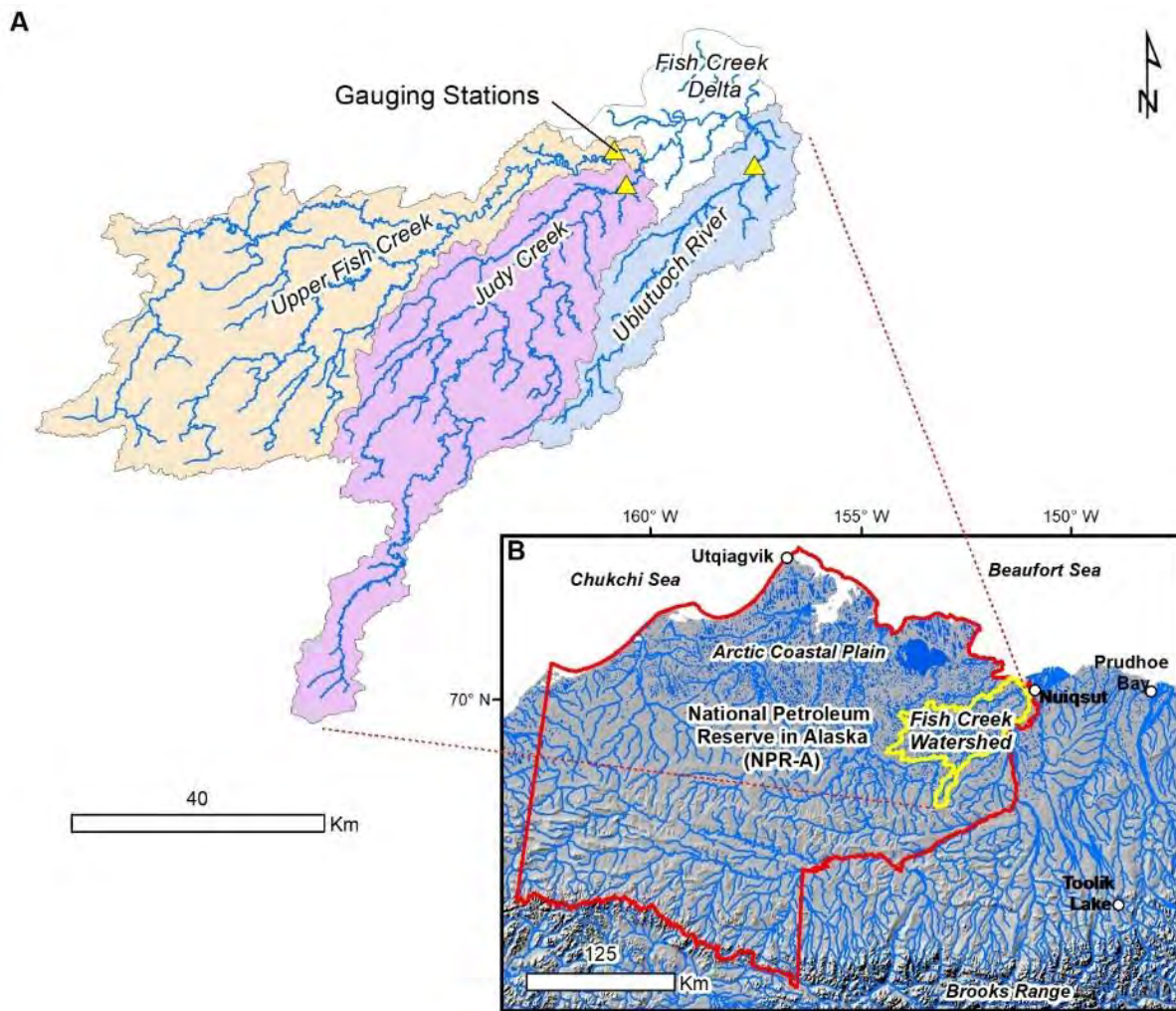


Figure 1. Map of the Fish Creek Watershed showing the three gauged catchments and location within the National Petroleum Reserve in Alaska (NPR-A) relative to major villages, industrial centers, and field stations.

interference and low flow conditions, respectively, and log and transmit in near real-time via GOES telemetry system. Velocity-area discharge measurements have been consistently collected through a full range of flows over this period (average of 50 per station) to develop rating curves to compute hydrographs from 2001-2018 (Vas et al. 2018). During ice-affected flows, records were interpolated to rated flow peaks aided with point discharge measurements and time-lapse camera images for each station. Ice-affected late season records were also interpolated to flow minima aided by time-lapse cameras, water temperature sensors, and air temperature data at each station. Records from 2005-2009 were officially published by the U.S. Geological Survey (USGS) and records before and after this period were officially published in 2018 following rating curve refinements by BLM and University of Alaska Fairbanks (UAF) (Kemnitz et al. 2018).

Hydrograph analysis was performed on mean daily flow data for the three individual catchments from 2001 to 2018 by identifying snowmelt and rainfall peaks and corresponding peakflow recessions then fitting an exponential decay function from the peak to the next event (McNamara et al. 1998). Snowmelt recession were evaluated from peakflow to the number of days corresponding flow initiation on the rising limb, typically 5 to 20 days depending on the catchment and rapidity of melt conditions. In cases where detectable rainfall peaks occurred during the early portion of snowmelt peakflow recession, the period of snowmelt recession fit was shortened or rainfall-affected flows were removed to calculate snowmelt recession rates. Flows below the snowmelt recession curve were considered snowmelt-generated runoff (Fig 2). Rainfall recession curves were calculated for the first major rainfall peak in each hydrograph to the rising limb of the next rainfall event. All flows above this curve were considered rainfall-generated runoff (Fig 2). Flows between the snowmelt- and rainfall-runoff curves were categorized as storage-generated runoff, though it is recognized that presumably most originated from either meteoric sources in that or previous years. Our analysis did not attempt to consider or quantify any contributions from permafrost melt-water or sub-permafrost groundwater. Additionally, snowmelt runoff may be over-estimated in some years due to undetectable rainfall events during the snowmelt runoff rise and recession and also storage contributions from lake basins, though we suggest these are minor in most cases.

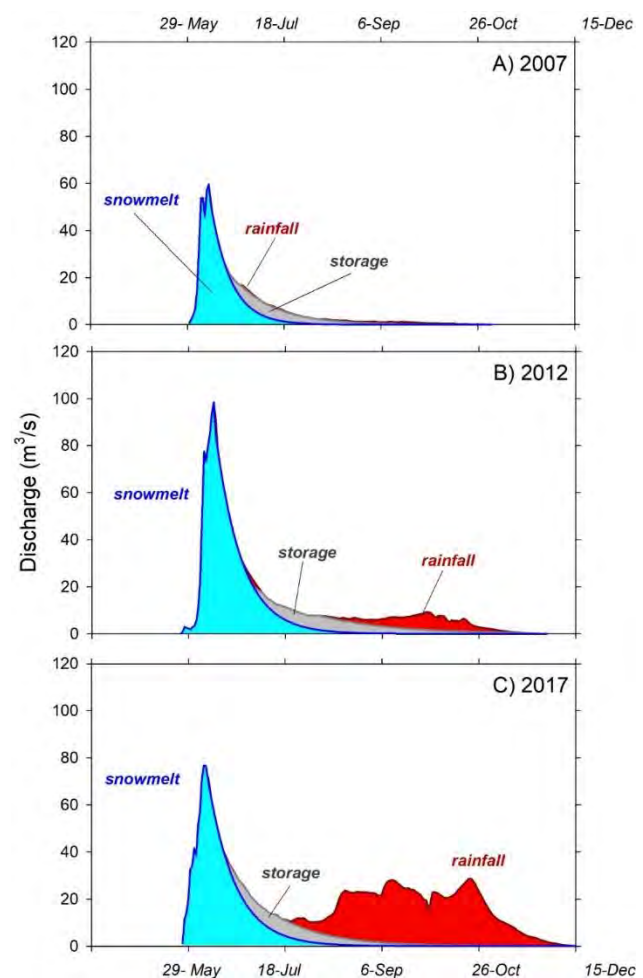


Figure 2. Examples of hydrograph separation for the Upper Fish Creek Watershed in years of contrasting runoff behavior.

3. RESULTS AND DISCUSSION

Mean annual runoff (MAR) increased significantly in all three catchment from 2001 to 2018 despite very low runoff in 2007 and 2008 and relatively high runoff in 2004 (Figure 3). The lowest MAR was observed in the Ublutuoch River in 2007, 46 mm, and the highest in the Upper Fish Creek in 2018, 195 mm (Figure 3). Interannual variation in MAR among the three catchments behaved coherently; average correlation among catchment runoff records is +0.91. Analysis of the longer record ending in 2015 for the Putulguyik River, a catchment similar in size to the Ublutuoch River in FCW, identified the same set of years showing contrasting runoff extremes (Stuefer et al. 2017).

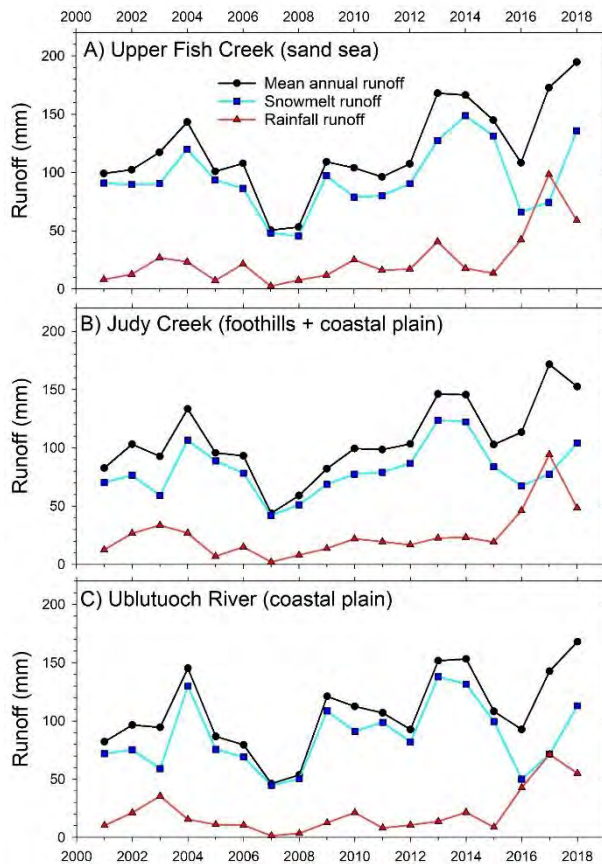


Figure 3. Mean annual runoff (MAR) for three study watersheds (A-C) and runoff portioned into snowmelt and rainfall over an 18 year record.

rainstorm-driven peak flows occasionally observed in arctic foothill watersheds (Kane et al. 2003).

Hydrograph separation results suggest that snowmelt contributed 71% of total annual runoff averaged over the three catchments and the 18 year period. Highest snowmelt contributions among all three basins averaged 83% in 2008 and averaged as low as 44% in 2017. Rainfall runoff was estimated to contribute 17% of total annual runoff over the entire period accounting for only 3% in 2007 and up to 51% in 2017 (Figure 2). Rainfall records from a station set lower in the Fish Creek Watershed (Figure 1) also show very low total rainfall in 2007, 22 mm, and much higher rainfall in 2017, 140 mm. Estimated storage runoff averaged 12% of total runoff over the entire record

Annual peak discharge in all three catchments over the period of record were always snowmelt driven and occurred on May-27 on average with no trend in peakflow magnitude or timing over this 18 year period. Highest peakflows averaged among catchments occurred in 2010 when Judy Creek’s mean daily peak was 246 m³/s and the Ublutuoch River’s mean daily peak was 89 m³/s. The lowest average peakflow occurred in 2016 when Judy Creek’s mean daily flow peak was 97 m³/s and the Ublutuoch River’s mean daily peak was 25 m³/s. Similar to inter-catchment patterns described for a three year period in the FCW in Arp et al. (2012), peakflows in Upper Fish Creek were consistently lower and smaller, per unit drainage area as runoff, than Judy Creek or Ublutuoch River. Upper Fish Creek consistently had higher overall MAR, 119 mm, compared to the other catchments averaging 107 mm; corresponding snowmelt recession were consistently slower and summer low flows higher at Upper Fish Creek, a pattern noted by Arp et al. (2012) for a shorter record. In 2016, 2017, and 2018, several late summer rainfall peakflows approached 50% of snowmelt peakflows of the same year in each river system—still far from observations of

tended to be lower during year with higher runoff contributions from either snowmelt or rainfall suggesting more storage recharge in these year and more storage discharge in years with more balanced contributions. This pattern of shifting storage excess and deficit follows more detailed storage process observations from other lake-rich watershed on the ACP (Bowling et al. 2003).

Table 1. Hydrologic, climatic, and sea ice data summarized relevant to the Fish Creek Watershed according to distinct period with differing patterns of discharge and runoff contributions. All values are averaged across three study catchments with reported standard deviations.

Variable	2001-2008	2009-2015	2016-2018
Mean Annual Runoff (mm)	90 ± 29	120 ± 26	146 ± 35
Annual Peak Discharge (m³/s)	87 ± 42	107 ± 54	76 ± 35
Time of Peak Discharge	6-Jun ± 6	4-Jun ± 7	7-Jun ± 12
Annual Flow Duration (days)	150 ± 32	187 ± 15	184 ± 31
Annual # of Rainfall Peaks	3.6 ± 1.7	4.0 ± 1.5	5.8 ± 1.3
Snowmelt Runoff (%)	74.2 ± 9.7	75.5 ± 6.8	49.5 ± 6.6
Storage Runoff (%)	12.6 ± 7.4	11.3 ± 4.4	13.1 ± 7.3
Rainfall Runoff (%)	13.3 ± 8.2	13.3 ± 4.3	37.3 ± 11.2
Annual Rainfall* (mm)	69 ± 24	72 ± 29	127 ± 24
Seasonal Rainfall* (Aug-Sep, mm)	28 ± 16	41 ± 22	80 ± 20
Mean Air Temperature (Aug-Sep, ° C)	6.8 ± 2.2	6.3 ± 1.1	5.7 ± 1.0
Open-ocean Extent** (km)	350 ± 244	559 ± 218	735 ± 182

*Record only spans from 2003 to 2018; **Data NSIDC sea ice concentrations averaged for August and September.

Comparing composite (all three catchments) runoff records together over 18 years suggest three periods with distinctive regimes based on quantitative breakpoint analysis, qualitative comparison of hydrograph analysis statistics, and hydrograph separation results (Table 1). The period from 2001 to 2008 had lower overall runoff driven in part by drought conditions in 2007 (Arp et al. 2012). Snowmelt peakflow discharge were moderate in magnitude and timing compared to the next two periods (Table 1). Hydrograph separation suggested snowmelt contributed 74% of runoff, rainfall 13%, and storage another 13% in this earliest eight year period. The middle seven years appeared distinct with 30% higher MAR (120 mm) than the previous period, primarily driven by higher snowmelt peakflows 107 m³/s than the earlier and later record averaging 82 m³/s across catchments (Table 1). Runoff contributions during the 2009-2015 period were similar to the previous 2001-2008 period, as were summer rainfall totals, though average late summer rainfall was 46% higher in the middle period. The last period identified as distinct, 2016-2018, is much shorter in comparison to the previous two, but had distinctly higher rainfall contributions, 37% on average, and corresponding higher rainfall totals, 127 mm, and over 2-X greater during the late summer compared to previous periods (Table 1). Snowmelt peakflows were lower in this period,

76 m³/s, and slightly later on average. Late summer temperature was also cooler during these last three years in comparison the previous record (Table 1). Stuefer et al. (2017) also identified a very recent pattern of higher runoff for a longer ACP watershed record terminating in 2015 that was suggestive of hydrologic intensification. Our analyses that extends to 2018 show even wetter, more rainfall dominated conditions leading to what we see as more evidence of hydrologic intensification and even a hydrologic regime shift.

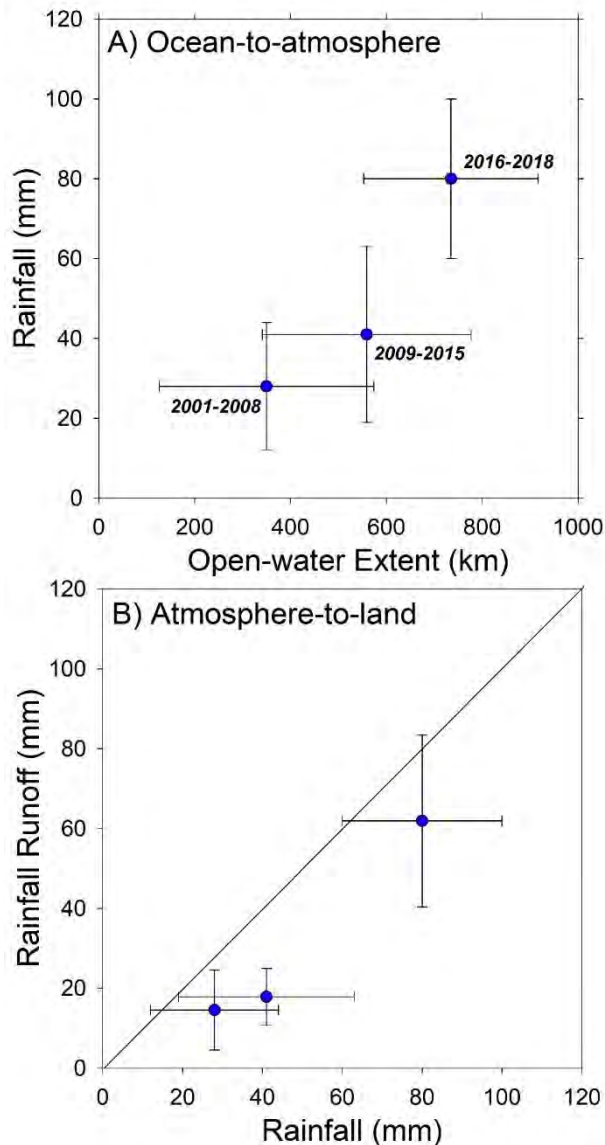


Figure 4. Relationships between August and September open-water extent of the Beaufort Sea to rainfall during the same period (A) and the same rainfall period to total rainfall runoff averaged across the three study catchments and grouped by distinctive flow periods in Table 1.

The most obvious arctic response to warming climate in decreasing sea ice extent and much larger extents of open-water persisting into late fall (Serreze and Barry 2011). We summarized the extent of open ocean North of FCW in August and September from sea ice concentration datasets available from the National Snow Ice Data Center (NSIDC), which showed progressive increases from 350 km in the first period, to 559 km in the second period, to 735 km in the third period (Table 1). Plotting late summer rainfall versus open-water extent averaged over FCW runoff periods it Table 1 shows a positive relationship (Figure 4), suggesting that enhance moisture supply may be driving more rainfall. In turn comparing mean values across runoff periods, more late season rainfall directly corresponded to more rainfall runoff and perhaps more importantly high rainfall runoff efficiency over the last three years of record.

Hydrologic intensification in arctic coastal watershed is expected to result in both enhanced precipitation and evapotranspiration, making runoff outcomes less certain (Rawlings et al. 2010). The additional moisture supply from more open ocean along the coast is highly dependent on the direction and intensity of storm tracks contributing significant precipitation inland (Homan 2015). Results from this study suggest at least some of the enhanced rainfall in recent years is coming from marine sources, which is may then be driving much higher proportions of rainfall contributions to runoff and the emergence of a new flow regime for ACP rivers.

4. CONCLUSIONS

Snowmelt-driven flow regimes have been a defining characteristic of many arctic watersheds. This dominant hydrologic pattern has formed the basis for planning, design, and maintenance of infrastructure, land management and municipal and industrial operations, and how ecosystems function in arctic coastal plains. The emergence of a rainfall-dominated hydrologic regimes, as is suggestive from our data in the FCW and other long-term monitored watershed in the Arctic, as implications for a wide range of social-ecological systems. In many respects, rainfall-dominated hydrologic regimes are more common and thus human and ecosystem adaptation to this pattern should have many examples. What is uncertain is how the rate of change will drive responses and if adaptation can keep pace, particularly with respect to how rapidly arctic coastal climates shift to a maritime regime and how enhanced late season river flows, high lake levels, and soil moisture interact with already degrading permafrost landforms. Far-sighted programs of consistent environmental monitoring, such as BLM's hydrologic monitoring program in the NPR-A, are providing reliable long-term data to understand such complex changes. Policy makers, land managers, and other stakeholders in the FCW and ACP should be aware of these valuable programs and ensure their continuance in the future.

ACKNOWLEDGMENTS

This research has been supported by the Bureau of Land Management's Arctic Office with additional funding provided by the U.S. Fish and Wildlife Service's Arctic Landscape Conservation Cooperative, National Fish and Wildlife Foundation, U.S. Geological Survey, and the National Science Foundation (#1806213). Important field work and data analysis were conducted by Dragos Vas, Allen Bondurant, and other research professionals at UAF's Water and Environmental Research Center.

REFERENCES

- Arp, C.D., Whitman, M.S., Jones, B.M., Kemnitz, R., Grosse, G. & Urban, F.E. 2012 Drainage network structure and hydrologic behavior of three lake-rich watersheds on the Arctic Coastal Plain, Alaska. *Arctic, Antarctic, and Alpine Research* 44(3), 385-398.
- Arp, C.D., Whitman, M.S., Jones, B.M., Nigro, D.A., Alexeev, V.A., Gädeke, A., Fritz, S., Daanen, R., Liljedahl, A.K., Adams, F.J., Gaglioti, B.V., Grosse, G., Heim, K.C., Beaver, J.R., Cai, L., Engram, M. and Uher-Koch, H.R. 2019 Ice roads through lake-rich Arctic watersheds: Integrating climate uncertainty and freshwater habitat responses into adaptive management. *Arctic, Antarctic, and Alpine Research* 51(1), 9-23.
- Beel, C.R., Lamoureux, S.F. & Orwin, J.F. 2018 Fluvial Response to a Period of Hydrometeorological Change and Landscape Disturbance in the Canadian High Arctic. *Geophysical Research Letters* 45(19), 10,446-410,455.
- Bintanja, R. & Selten, F.M. 2014 Future increases in Arctic precipitation linked to local evaporation and sea-ice retreat. *Nature* 509(7501), 479-+.
- Bowling, L.C., Kane, D.L., Gieck, R.E., Hinzman, L.D. & Lettenmaier, D.P. 2003 The role of surface storage in a low-gradient Arctic watershed. *Water Resources Research* 39(4), 1087, doi:10.1029/2002WR0010466.
- Déry, S.J., Hernández-Henríquez, M.A., Burford, J.E. & Wood, E.F. 2009 Observational evidence of an intensifying hydrological cycle in northern Canada. *Geophysical Research Letters* 36(13).

- Instones, A., Kokorev, V., Janowicz, R., Bruland, O., Sand, K. & Prowse, T. 2016 Changes to freshwater systems affecting Arctic infrastructure and natural resources. *Journal of Geophysical Research: Biogeosciences* 121(3), 567-585.
- Kane, D.L., Hinzman, L.D., Benson, C.S. & Liston, G.E. 1991 Snow hydrology of a headwater Arctic basin 1. Physical measurements and process studies. *Water Resources Research* 27(6), 1099-1109.
- Kane, D.L., McNamara, J.P., Yang, D., Olsson, P.Q. & Gieck, R.E. 2003 An extreme rainfall/runoff event in Arctic Alaska. *Journal of Hydrometeorology* 4(6), 1220-1228.
- Kane, D.L. & Yang, D. 2004 Northern Research Basins Water Balance. Kane, D. & Yang, D. (eds), p. 12, IAHS, Fairbanks, AK.
- Kemnitz, R., Arp, C., Whitman, M., & Vas, D. 2018 River discharge data, National Petroleum Reserve, Alaska, 2001-2017. *Arctic Data Center*, doi:10.18739/A2P55DG5N.
- Makarieva, O., Nesterova, N., Andrew Post, D., Sherstiukov, A. & Lebedeva, L. 2019 Warming temperatures are impacting the hydrometeorological regime of Russian rivers in the zone of continuous permafrost. *The Cryosphere* 13, 1635-1659.
- Marsh, P. & Woo, M. K. 1981 Snowmelt, glacier melt, and high arctic streamflow regimes. *Canadian Journal of Earth Sciences*. 18(8), 1380-1384.
- McNamara, J.P., Kane, D.L. & Hinzman, L.D. 1998 An analysis of streamflow hydrology in the Kuparuk River Basin, Arctic Alaska: a nested watershed approach. *Journal of Hydrology* 206, 39-57.
- McNamara, J.P. and Kane, D.L. 2009 The impact of a shrinking cryosphere on the form of arctic alluvial channels. *Hydrological Processes* 23, 159-168.
- Peterson, B.J., Holmes, R.M., McClelland, J.W., Vorosmarty, C.J., Lammers, R.B., Shiklmanov, A.I., Shiklomanov, I.A. & Rahmstorf, S. 2002 Increasing river discharge to the Arctic Ocean. *Science* 298(13 December 2002), 2171-2173.
- Rawlins, M.A., Steele, M., Holland, M.M., Adam, J.C., Cherry, J.E., Francis, J.A., Groisman, P.Y., Hinzman, L.D., Huntington, T.G. & Kane, D.L. 2010 Analysis of the Arctic system for freshwater cycle intensification: Observations and expectations. *Journal of Climate* 23(21), 5715-5737.
- Serreze, M.C. & Barry, R.G. 2011 Processes and impacts of Arctic amplification: A research synthesis. *Global and Planetary Change* 77(1-2), 85-96.
- Stuefer, S.L., Arp, C.D., Kane, D.L., & Liljedahl, A.K. 2017) Recent extreme runoff observations from coastal arctic watersheds in Alaska. *Water Resources Research*, 53, 9145–9163. <https://doi.org/10.1002/2017WR020567>
- Sujono, J., Shikasho, S. & Hiramatsu, K. 2004 A comparison of techniques for hydrograph recession analysis. *Hydrological Processes*, 18, 403-413. doi:10.1002/hyp.1247
- Vas, D., Toniolo, H., LaMesjerant, E., & Bailey, J. 2018 *Hydrological and meteorological observations on seven streams in the National Petroleum Reserve – Alaska (NPR-A)*. Final Project Report, Water and Environmental Research Center, University of Alaska Fairbanks, Fairbanks, AK.
- Whitman, M.S., Arp, C.D., Jones, B., Morris, W., Grosse, G., Urban, F. & Kemnitz, R. 2011 Developing a long-term aquatic monitoring network in a complex watershed of the Alaskan Arctic Coastal Plain. *Proceedings of the Fourth Interagency Conference on Research in Watersheds: Observing, Studying, and Managing for Change*. Medley, C.N., Patterson, G. and Parker, M.J. (eds), pp. 15-20, USGS, Reston.
- Woo, M. Kane, D. L., Carey, S. K. & Yang, D. 2008 Progress in permafrost hydrology in the new millennium. *Permafrost Periglac. Process.*, 19: 237-254. doi:10.1002/ppp.6
-

Water Quality Trends in Three Rivers near Yellowknife, NT, Canada

Pieter J. K. Aukes^{1,2*}, S. L. Schiff¹, M. C. English², R. Staples³, M. Palmer⁴

¹Earth & Environmental Sciences, University of Waterloo, Waterloo, ON, N2L 3G1, CANADA

²Geography & Environmental Studies, Wilfrid Laurier University, Waterloo, ON, N2L 3C5, CANADA

³Water Resources Division, Environment & Natural Resources, Government of Northwest Territories, Yellowknife, NT, X1A 2L9, CANADA

⁴Department of Geography and Environmental Studies, Carleton University, Ottawa, ON, K1S 5B6

*Corresponding author's email address: paukes@uwaterloo.ca

ABSTRACT

Northern environments are some of the most sensitive to a warming climate, yet monitoring the responses of watersheds in these regions to climate warming can be difficult due to its remoteness. Long-term monitoring of river water quality provides a method to evaluate the response of a watershed to climate or anthropogenic drivers. Here we focus on three major rivers around Yellowknife, Northwest Territories, to understand how water chemistry has changed over the past 30 years. Historical water quality data, collected by the Water Resources Division, Environment Natural Resources, was compiled for the Yellowknife (YK), Cameron (CAM), and Marian (MR) rivers. We focussed on cations (K^+ , Na^+ , Ca^{2+} , Mg^{2+}), anions (Cl^- , SO_4^{2-} , alkalinity), nutrients (NH_3 , $NO_3^-+NO_2^-$, TP, DOC), and total dissolved solids. River discharge (YK and CAM only) and climate data were also analysed where available. Differences in underlying geology dictated differences in water chemistry among the three rivers. Mean annual air temperature increased over the sampling period. No significant change was observed in total annual precipitation or annual discharge in the YK and CAM rivers but winter discharge increased over the study period in the YK river. Increased solute and inorganic-nitrogen concentrations within YK and CAM indicate changing water quality and suggest enhanced subsurface flow through mineral rather than organic soils. Hence, seasonal changes in geochemistry are indicative of enhanced subsurface contributions during winter months, similar to recent observations at smaller scales, while future water quality may be influenced by inter-annual variability in discharge rather than uni-directional change with time.

KEYWORDS

Water quality; northern rivers; geochemistry; hydrology; time trend

1. INTRODUCTION

The Northwest Territories (NT), Canada, is an area that is rapidly responding to a warming climate in terms of hydrology and biogeochemical cycling. Changes to northern environments include shifts to the amount and timing of precipitation, increases to mean annual air and subsurface temperature, and increases in river discharge among Eurasian and Canadian rivers (McClelland *et al.* 2006; Spence *et al.* 2011; Déry *et al.* 2016; Bintanja *et al.* 2017). In particular, increased active-layer thickness and permafrost degradation can alter subsurface hydrologic pathways and the export of solutes, nutrients, and carbon that were previously immobilized within permafrost (Kokelj *et al.* 2013; Reyes *et al.* 2015; Tank *et al.* 2016; Toohey *et al.* 2016; Salmon *et al.* 2016). Long-term

monitoring of river water quality offers a method to observe how hydrology and geochemistry of northern watersheds are changing on longer timescales, allowing for future predictions of water quality as environmental conditions continue to change. Many studies have generally focused on large river systems among ice-rich subsurface areas that drain into the Arctic Ocean. The objective of this study is to use a 35-year record of water quality from three rivers near Yellowknife, NT, to determine whether significant changes to hydrologic discharge, solute and nutrient concentration, and loads into Great Slave Lake have occurred over the time period.

2. METHODS

Water samples have been collected from the Yellowknife (YK), Cameron (CAM), and Marian (MR) rivers since the late 1980s by the Water Resources Division, Environment & Natural Resources, Government of Northwest Territories. The MR (basin area: 23,608 km²) drains the boundary between the taiga shield and taiga plains, while the YK (19,353 km²) and CAM (3,630 km²) drain the taiga shield. The taiga shield is underlain by Precambrian bedrock, till deposits, eskers, and a number of peat plateaux (Ecosystem Classification Group, 2008), while the taiga plains is comprised of extensive peatlands and till plains (Ecosystem Classification Group, 2009). Permafrost extent in the NT ranges from sporadic and discontinuous in the south to continuous in the north (Burn & Kokelj, 2009; Morse *et al.* 2015). The hydrology around Yellowknife is characterized by a series of lakes connected by wetlands and streams, with flow among these systems described as ‘fill and spill’ (Woo *et al.* 2008). Within these systems, snowmelt is the primary source water and flow and connectivity are dictated by precipitation, storage, and landscape topography (Spence & Woo, 2008). Increased autumn rainfall among and a shift from a nival to combined nival/pluvial streamflow regime has been observed within small catchments within the western Canadian sub-arctic (Spence *et al.* 2011).

Climate data was retrieved from online Environment Canada records of the Yellowknife Airport Station #1706 (from 1942 to 2013) and Station #51058 (from 2013 to 2016). Daily surface air temperature and total precipitation data were aggregated into monthly and yearly averages. Hydrologic discharge was retrieved from the WaterOffice, Government of Canada, for the YK and CAM rivers (there is no gauging of the MR). Water samples were collected by Water Resources Division, Government of Northwest Territories, once a month between 1985 to 2013 for YK and CAM, and 1997 to 2013 for the MR. Samples were analysed by the Taiga Environmental Laboratory, Yellowknife, for cations (potassium, sodium, calcium, magnesium), anions (chloride, sulphate, alkalinity), nutrients (ammonia, nitrate plus nitrite, total phosphorus, dissolved organic carbon), and total dissolved solids (TDS). Values under analytical detection limits were kept in the dataset at the concentration of the detection limit.

Significant trends over time were calculated using a non-parametric Mann-Kendall test. Data was pre-whitened to remove autocorrelation. Annual trends were determined for temperature, precipitation, and geochemical fluxes, while monthly trends were calculated for discharge. Differences in the magnitude of discharge over the year were used to determine the season, later used to determine seasonal trends in geochemical data. Mean annual fluxes for cations, anions, nutrients, and TDS were calculated for the YK and CAM river using LOADEST (Runkel *et al.* 2004) via LoadRunner (Booth & Raymond, 2007).

3. RESULTS

Mean annual air temperature around Yellowknife significantly increased over the past 80 years ($3.2 \times 10^{-2} \text{ }^\circ\text{C/yr}$), with little change to total annual precipitation (Figure 1). In particular, increases to the monthly average air temperature were observed for the months of January to April.

The YK had higher discharge than the CAM (up to 5x; MR is ungauged; Figure 2) but contained similar yields when corrected for watershed area. Both rivers exhibited a typical flow pattern of northern rivers where flow is highest during the spring freshet, recedes over the summer, and is low during the fall and winter. The YK and CAM exhibited large annual variability in average monthly discharge, especially during the spring and summer seasons. Although there is no significant change to the mean annual discharge in both rivers over the past 35 years, the CAM had significant increases in winter discharge over the past 35 years.

The MR had higher dissolved constituents and more pronounced seasonality than either the YK or CAM. Significant increases were determined for all seasons in most dissolved solutes over the past 35 years for the YK and CAM. Alternatively, the MR only showed significant decreases to K^+ and Cl^- during the spring (Table 1). Nutrients (NH_3 , $\text{NO}_2^- + \text{NO}_3^-$, TP, and DOC) show little change within each season over the time period, except for a recent increase to $\text{NO}_2^- + \text{NO}_3^-$ within the YK and CAM during the fall and winter. Calculated loads for the YK and CAM find no significant change to annual fluxes into Great Slave Lake except for decreased NH_3 in YK and decreased DOC in CAM (Figure 3). Although not significant, YK and CAM TP loads decrease since ~2005.

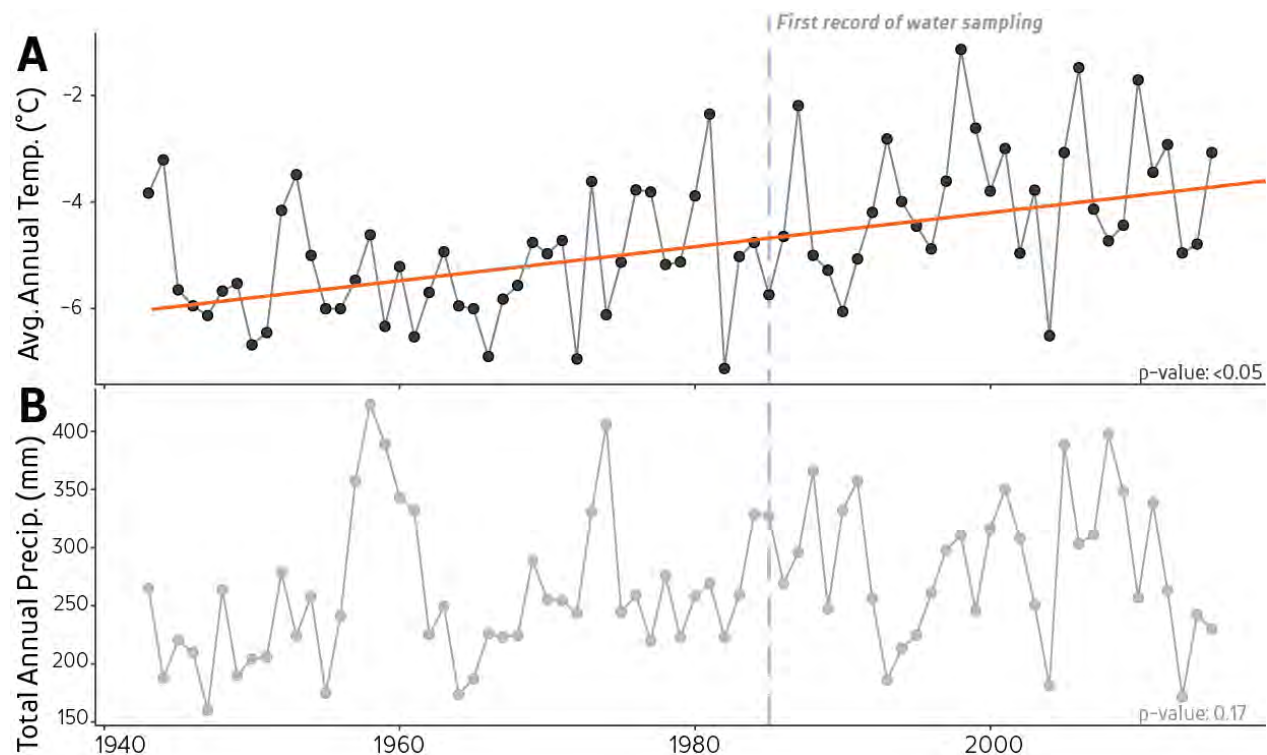


Figure 1. Average annual air temperature (panel A) and total annual precipitation (panel B) for Yellowknife, Northwest Territories, over the past 80 years. Significant trends were determined using a Mann-Kendall test. Dotted blue line represents the time of the first water quality sampling.

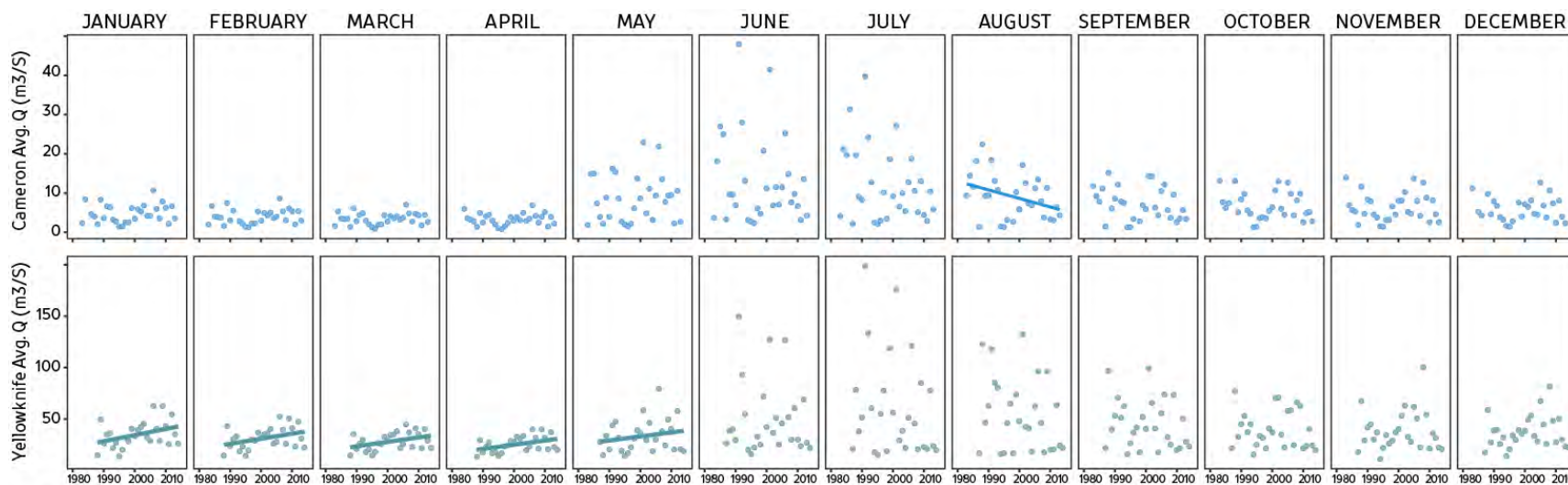
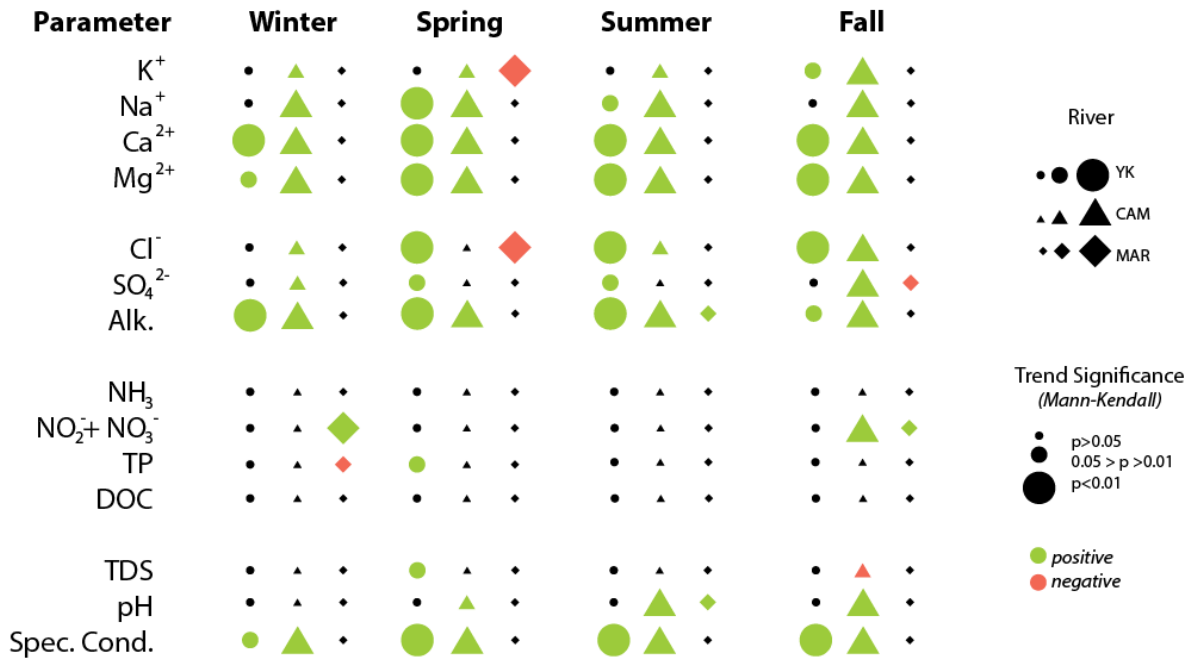


Figure 2. Average annual discharge per month for the Cameron River (top panel) and the Yellowknife River (bottom panel) for the past ~35 years. Lines indicate significant Mann-Kendall trends ($p < 0.05$)

Table 1. Summary of all Mann-Kendall statistical analyses and direction of geochemical trends for the Yellowknife (YK; circle), Cameron (CAM; triangle), and Marian (MR; diamond) rivers for each season. Geochemical parameters includes potassium (K⁺), sodium (Na⁺), calcium (Ca²⁺), magnesium (Mg²⁺), chloride (Cl⁻), sulphate (SO₄²⁻), alkalinity (as total concentration of CaCO₃), ammonia (NH₃), nitrate plus nitrite (NO₃⁻+NO₂⁻), total phosphorus (TP), dissolved organic carbon (DOC), total dissolved solute (TDS), pH, and specific conductivity (Spec. Cond.).



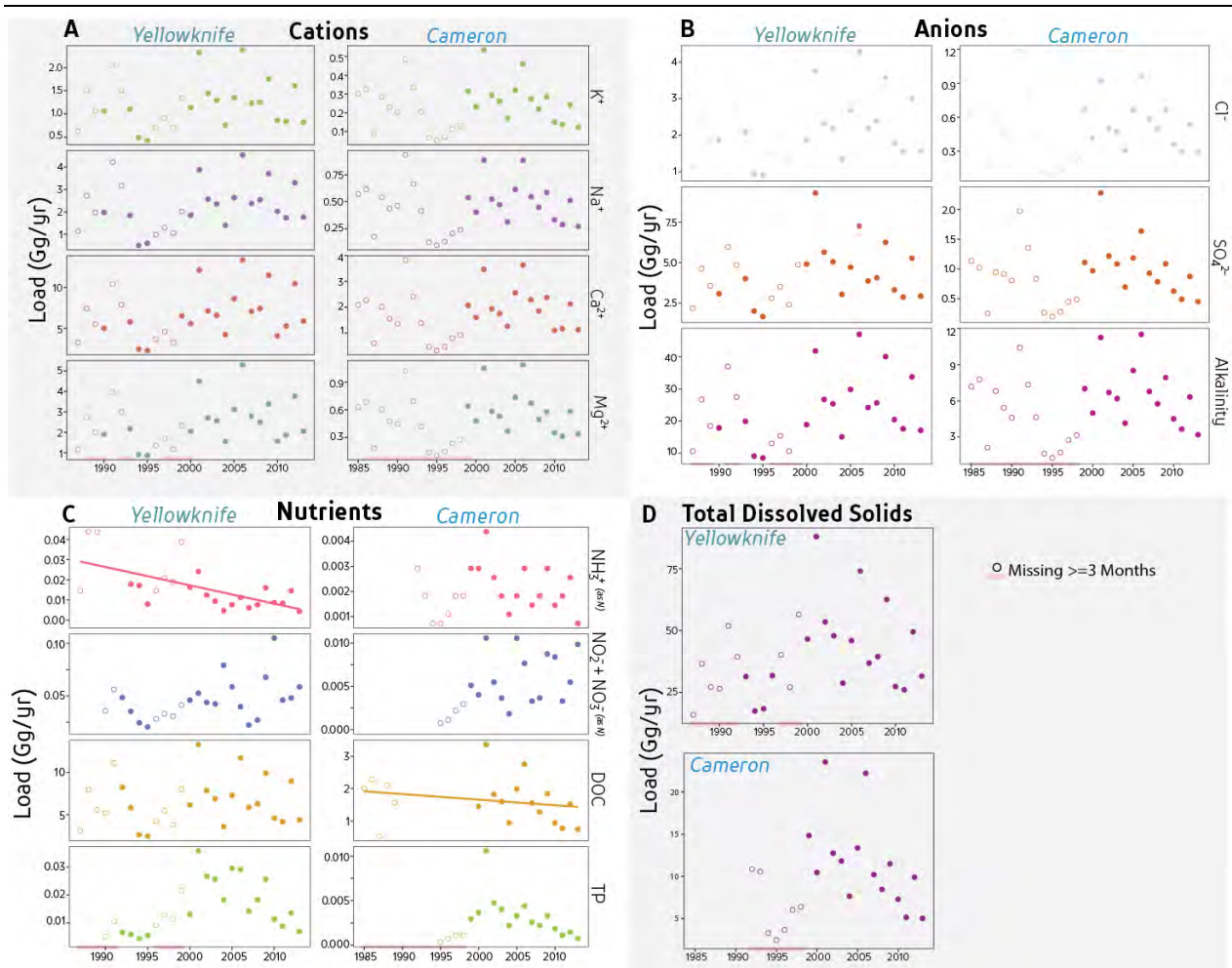


Figure 3. Calculated annual loads for the Yellowknife (left column) and Cameron (right column) rivers for cations (panel A), anions (panel B), nutrients (panel C) and total dissolved solids (panel D). Statistical trends (Mann-Kendall, $p < 0.05$) are signified with lines, whereas open symbols represent annual loads containing data with three or more missing months.

4. DISCUSSION

The underlying geology dictates the difference in concentrations of various geochemical constituents in rivers draining the taiga shield and taiga plains. The MR flows between the taiga plains and taiga shield, whereas the YK and CAM both drain the taiga shield. The taiga plains are comprised of deeper glacial tills and calcareous soils and are relatively easier to erode than the Precambrian bedrock found in the taiga shield; hence, the MR contains higher concentrations of solutes than either the YK or CAM. Similarity in trends between the YK and CAM illustrate the role watershed characteristics can have upon overall water quality.

Changes to climate can be an important driver of hydrologic change within northern rivers, influencing watershed processes and flow pathways (Connon *et al.* 2014; Dery *et al.* 2016; Rood *et al.* 2016). In particular, warming temperatures around Yellowknife impact permafrost extent

and degradation in the area (Morse *et al.* 2015) and result in altered subsurface flow pathways and residence times. Although permafrost degradation can impact river discharge (St. Jacques & Sauchyn, 2009), our results indicate there is no clear response of warming temperatures influencing annual hydrologic discharge within the YK or CAM. This may be due to the lack of change in total annual precipitation, coupled with projected increases to evapotranspiration in the area (Kicklighter *et al.* 2013; Vihma *et al.* 2016).

Permafrost degradation and increased active-layer thickness can result in two water quality scenarios: 1) flow pathways move into deeper, mineral rich soils, and/or 2) organic-rich layers become unfrozen and contribute organic carbon and nutrients. Increased active-layer thickness resulted in enhanced weathering and increased solute fluxes within the Yukon River Basin (Toohey *et al.* 2016) and Mackenzie River Basin (Tank *et al.* 2016). Although a study at this scale cannot identify the predominant drivers of water quality change in the watersheds, the results showing increased solute export over the study period are consistent with changes expected of enhanced subsurface flow pathways. Further, DOC concentrations and loads show little change over the time period, yet mean annual air temperatures near Yellowknife have rarely met or surpassed the threshold of -2°C determined to enhance DOC export from high-organic permafrost watersheds (Frey & Smith, 2005). Hence, the YK and CAM exhibit changes in water quality that represents subsurface flow within mineral soils.

Seasonal changes observed to water quality and quantity in the YK and CAM are similar to processes observed at smaller catchment scales and highlight the importance of year-long monitoring. Increased winter baseflow and increased solute and nutrient concentrations can result from enhanced soil and lake storage due to late fall precipitation arriving as rain rather than snow before freeze-up (Spence *et al.* 2014). Similar observations are found in all three rivers and indicate that processes observed at smaller scales may be occurring to larger systems. Further, increased concentrations of inorganic nitrogen in the fall and winter are indicative of build up within subarctic lakes (Spence *et al.* 2014, 2015) and could have implication for downstream river productivity. Thus, quantifying seasonal changes to river water quality identifies changes to certain processes that dictate the export of nutrients across these systems.

5. CONCLUSION

Long-term climate and water quality records of three rivers around Yellowknife indicate a geochemical response to a warming climate. Significant increases to mean annual air temperature are observed around Yellowknife; however, no change to annual discharge for the YK or CAM was found. The MR, flowing between the taiga shield and taiga plains, showed no response in water quality over time for most parameters, whereas the YK and CAM contained various significant changes to cation and anion concentrations that suggest an increasing contribution of subsurface flow pathways. These pathways are likely flowing through mineral-rich soils as DOC concentrations have not changed. Increased winter discharge in the YK and increased inorganic nitrogen within all three rivers is similar to the biogeochemical response observed within smaller systems, and illustrates the importance of year-long monitoring to identify seasonal changes. Although most geochemical concentrations changed with time, no significant changes to the loads of cations, anions, or nutrients into Great Slave Lake were observed. This suggests that the magnitude of solute and nutrient export is dictated by changes to the inter-annual variability of

river discharge, rather than uni-directional change with time. Hence, long-term records of climate, hydrology, and geochemistry indicate differences in the response from three rivers near Yellowknife, and provide evidence on how these systems may continue to respond to a changing climate.

REFERENCES

- Bintanja, R., Andry, O. 2017. Towards a Rain-Dominated Arctic. *Nat. Clim. Chang.* 17(7), 263–268. Doi: 10.1038/nclimate3240.
- Burn, C. R., & Kokelj, S. V. 2009. The Environment and Permafrost of the Mackenzie Delta Area. *Permafr. Periglac. Process.* 20: 83-105. Doi: 10.1002/ppp.655.
- Booth, G.; Raymond, P. & Oh, N.-H. 2007. LoadRunner: <http://Environment.Yale.Edu/Raymond/Loadrunner>. Yale University: New Haven, CT, USA.
- Connon, R. F., Quinton, W. L., Craig, J. R. & Hayashi, M. 2014. Changing Hydrologic Connectivity Due to Permafrost Thaw in the Lower Liard River Valley, NWT, Canada. *Hydrol. Process.* 28(14), 4163–4178. Doi: 10.1002/hyp.10206.
- Déry, S. J., Stadnyk, T. A., MacDonald, M. K., & Gaudi-Sharma, B. 2016. Recent Trends and Variability in River Discharge across Northern Canada. *Hydrol. Earth Syst. Sci.* 20(12), 4801–4818. Doi: 10.5194/hess-20-4801-2016.
- Ecosystem Classification Group. 2008. Ecological Regions of the Northwest Territories - Taiga Shield; Yellowknife, NT, Canada.
- Ecosystem Classification Group. 2009. Ecological Regions of the Northwest Territories - Taiga Plains; Yellowknife, NT, Canada.
- Frey, K. E. & Smith, L. C. 2005. Amplified Carbon Release from Vast West Siberian Peatlands by 2100. *Geophys. Res. Lett.* 32(9), L09401. Doi: 10.1029/2004GL022025.
- Kicklighter, D. W., Hayes, D. J., McClelland, J. W., Peterson, B. J., McGuire, A. D. & Melillo, J. M. 2013. Insights and Issues with Simulating Terrestrial DOC Loading of Arctic River Networks. *Ecol. Appl.* 23(8), 1817–1836. Doi: 10.1890/11-1050.1.
- Kokelj, S. V., Lacelle, D., Lantz, T. C., Tunnicliffe, J., Malone, L., Clark, I. D. & Chin, K. S. 2013. Thawing of Massive Ground Ice in Mega Slumps Drives Increases in Stream Sediment and Solute Flux across a Range of Watershed Scales. *J. Geophys. Res. Earth Surf.* 118(2), 681–692. Doi: 10.1002/jgrf.20063.
- McClelland, J. W., Déry, S. J., Peterson, B. J., Holmes, R. M. & Wood, E. F. 2006. A Pan-Arctic Evaluation of Changes in River Discharge during the Latter Half of the 20th Century. *Geophys. Res. Lett.* 33(6), 2–5. Doi:10.1029/2006GL025753.
- Morse, P. D., Wolfe, S. A., Kokelj, S. V. & Gaanderse, A. J. R. 2015. The Occurrence and Thermal Disequilibrium State of Permafrost in Forest Ecotopes of the Great Slave Region, Northwest Territories, Canada. *Permafr. Periglac. Process.* 27(2), 145–162. Doi: 10.1002/ppp.1858.
- Reyes, F. R. & Loughheed, V. L. 2015. Rapid Nutrient Release from Permafrost Thaw in Arctic Aquatic Ecosystems. *Arctic, Antarct. Alp. Res.* 47(1), 35–48. Doi: 10.1657/AAAR0013-099.
- Rood, S. B., Kaluthota, S., Philipsen, L. J., Rood, N. J. & Zanewich, K. P. 2016. Increasing Discharge from the Mackenzie River System to the Arctic Ocean. *Hydrol. Process.* 160, 150–160. Doi: 10.1002/hyp.10986.

- Runkel, R. L., Crawford, C. G. & Cohn, T. A. 2004. Load Estimator (LOADEST): A FORTRAN Program for Estimating Constituent Loads in Streams and Rivers: U.S. Geological Survey Techniques and Methods Book 4; U.S. Geological Survey.
- Salmon, V. G., Soucy, P., Mauritz, M., Celis, G., Natali, S. M., Mack, M. C. & Schuur, E. A. G. Nitrogen Availability Increases in a Tundra Ecosystem during Five Years of Experimental Permafrost Thaw. *Glob. Chang. Biol.* 22(5), 1927–1941. Doi: 10.1111/gcb.13204
- Spence, C. & M-K Woo. 2008. Hydrology of the Northwestern Subarctic Canadian Shield. In: Woo, M-K. (ed.), *Cold Region Atmospheric and Hydrologic Studies*, Springer-Verlag, Berlin, pp235-256.
- Spence, C., Kokelj, S. V. & Ehsanzadeh, E. 2011. Precipitation Trends Contribute to Streamflow Regime Shifts in Northern Canada. In: *Cold Region Hydrology in a Changing Climate*, pp 3–8.
- Spence, C., Kokelj, S. A., Kokelj, S. V. & Hedstrom, N. 2014. The Process of Winter Streamflow Generation in a Subarctic Precambrian Shield Catchment. *Hydrol. Process.* 28(14), 4179–4190. Doi: 10.1002/hyp.10119.
- Spence, C., Kokelj, S. V., Kokelj, S. A., McCluskie, M. & Hedstrom, N. 2015. Evidence of a Change in Water Chemistry in Canada’s Subarctic Associated with Enhanced Winter Streamflow. *J. Geophys. Res. Biogeosciences*, 120(1), 113–127. Doi: 10.1002/2014JG002809.
- St. Jacques, J. M. & Sauchyn, D. J. 2009. Increasing Winter Baseflow and Mean Annual Streamflow from Possible Permafrost Thawing in the Northwest Territories, Canada. *Geophys. Res. Lett.* 36(1), 1–6. Doi: 10.1029/2008GL035822.
- Tank, S. E., Striegl, R. G., McClelland, J. W. & Kokelj, S. V. 2016. Multi-Decadal Increases in Dissolved Organic Carbon and Alkalinity Flux from the Mackenzie Drainage Basin to the Arctic Ocean. *Environ. Res. Lett.* 11(5), 54015. Doi: 10.1088/1748-9326/11/5/054015.
- Toohey, R. C., Herman-Mercer, N. M., Schuster, P. F., Mutter, E. & Koch, J. C. 2016. Multi-Decadal Increases in the Yukon River Basin of Chemical Fluxes as Indicators of Changing Flowpaths, Groundwater, and Permafrost. *Geophys. Res. Lett.* 43(23), 120-130. Doi: 10.1002/2016GL070817.
- Vihma, T., Screen, J., Tjernström, M., Newton, B., Zhang, X., Popova, V., Deser, C., Holland, M. & Prowse, T. 2016. The Atmospheric Role in the Arctic Water Cycle: A Review on Processes, Past and Future Changes, and Their Impacts. *J. Geophys. Res. Biogeosciences*. 121(3), 586–620. Doi: 10.1002/2015JG003132.
- Woo, M. K. & Mielko, C. Flow Connectivity of a Lake-Stream System in a Semi-Arid Precambrian Shield Environment. In: Woo, M. K (ed.), *Cold Region Atmospheric and Hydrologic Studies*. Springer-Verlag: Berlin, Heidelberg, 2008; Vol. 2, pp 221–233. Doi: 10.1007/978-3-540-75136-6_12

A Regional Hydrologic Model of the Liard River Basin

Genevieve Brown^{1*} and James R. Craig¹

¹*Department of Civil and Environmental Engineering, University of Waterloo, Waterloo, Ontario, N2L 3G1, CANADA*

**Corresponding author's email address: g7brown@uwaterloo.ca*

ABSTRACT

A hydrologic model of the Liard river basin in northern Canada was developed with the objective of appropriately representing the varying hydrologic processes and responses within this large basin. Like many northern river basins in Canada, the hydrologic data network is relatively sparse. The calibration process was optimized to exploit available information within the basin while minimizing model uncertainty. The resulting model shows strong performance across the basin and can respect multiple data sources for varying hydrologic processes and responses within the basin.

KEYWORDS

Hydrologic Model; Canada; Calibration; Model Structure

1. INTRODUCTION

The Liard basin, located in northern Canada, is a large, spatially heterogeneous watershed with relatively sparse data. The basin has a total contributing area of 275,000 km² and spans multiple provinces and territories. There is a wide range of hydrological processes and responses across the basin due to the varying climate and physiography. The landscape and hydrology of the Nahanni, Upper and Central Liard regions, as shown in Figure 1, are largely influenced by several mountain ranges which result in a freshet dominated hydrograph. The Fort Nelson, Petitot and Lower Liard regions are primarily wetland dominated with little topographic relief. These regions are much more complicated and difficult to model than the mountainous regions due to influences like the connectivity between wetland forms and thawing permafrost.

A hydrological model of the Liard basin was developed with the objective of constructing a model which provides valid and realistic results across the large, spatially heterogeneous basin. The model will be used operationally for flood forecasting within the Northwest Territories and as a platform for testing improvements to models of wetlands, permafrost, and long-term land cover change.

The development of the model and calibration process emphasized exploiting available data to help constrain parameters and reduce uncertainty within the model. The calibration process drew on a variety of methods including internal process calibration, multi-objective calibration, and model structure calibration (Gupta et al. 1998; Cao et al. 2006; Fenicia et al. 2008).

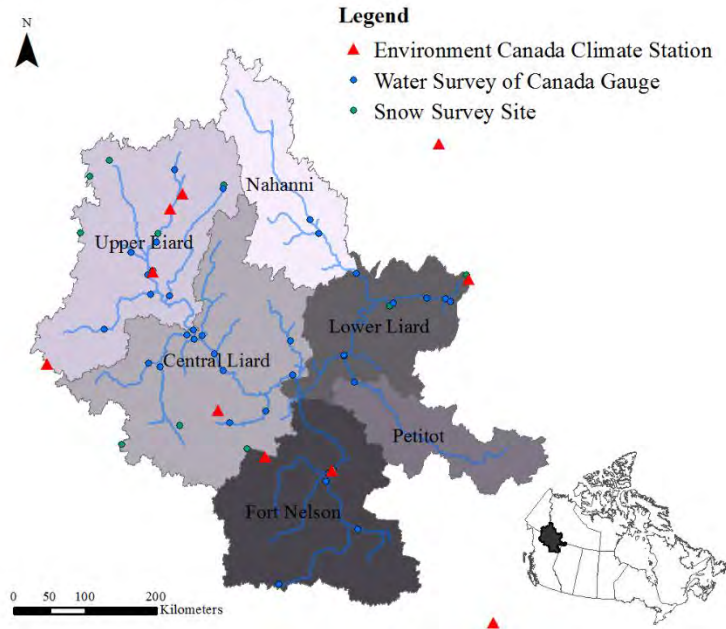


Figure 1. Primary regions within the Liard Basin and hydrometric data used in the model development

2. MODEL DESCRIPTION

The hydrological model was developed using Raven, a flexible modelling framework (Craig & Raven Development Team 2018). The model is based on a semi-distributed discretization scheme in which the basin is subdivided into 64 smaller subbasins. These subbasins are then characterized by 1100 hydrological response units which are defined based on land cover, elevation, slope, and aspect.

Due to the dominant influence of the mountainous regions in the basin, the initial model structure was based on the HBV-EC model. The HBV-EC model is a model which was originally built for Nordic countries and has been successfully applied to many mountainous basins (Bergstrom & Forsman 1973; Hamilton et al. 2001). The HBV-EC model structure allows for consideration of cold region hydrological processes including glaciers and snow accumulation and melt. A strict HBV-EC model structure was not kept throughout, as the calibration process explicitly included the modification of the model structure to better represent the regional hydrology.

3. CALIBRATION PROCESS

The calibration and validation of the model relied on hydrometric data from 29 Water Survey of Canada gauges over a 20 year period. Of the 29 gauges, only nine have data which cover the full calibration and validation period. The gauges with partial data were still included within the analysis as they provide data to inform the model and can be particularly useful in regions within the basin with very sparse data.

The calibration process followed an iterative and stepwise approach working from upstream to downstream in the basin. Multiple diagnostic metrics were used to analyze gauge performance

including Nash Sutcliffe Efficiency (NSE), Kling Gupta Efficiency (KGE), percent bias, and root mean square error (RMSE). In addition to the traditional modification of model parameters during calibration, the model structure was also modified in regions where the original model structure did not adequately represent the hydrological processes.

Internal processes within the model were also calibrated using alternate data sources. Snow accumulation and melt within the model was verified with data from 12 snow survey sites around the basin. Annual evapotranspiration rates were also verified at regional and basin wide scales.

4. RESULTS AND DISCUSSION

The manual calibration process described above was able to provide a model which performs well and respects the basin hydrology. Results for the nine gauges with complete data across the 20 year calibration and validation period are summarized in Table 1.

Table 1. Model calibration and validation results at select gauges within the Liard basin

Station	Station Name	Area, km ²	Calibration			Validation		
			NSE	% Bias	KGE	NSE	% Bias	KGE
10AA001	Liard River at Upper Crossing	32,600	0.86	4	0.91	0.83	0	0.88
10AB001	Frances River near Watson Lake	12,800	0.63	-16	0.69	0.67	-14	0.72
10BE001	Liard River at Lower Crossing	104,000	0.86	3	0.90	0.88	4	0.89
10BE004	Toad River above Nonda Creek	2,540	0.70	-11	0.78	0.82	-5	0.90
10CB001	Sikanni Chief River near Fort Nelson	2,180	0.42	7	0.68	0.48	16	0.70
10CD001	Muskwa River near Fort Nelson	20,300	0.64	10	0.71	0.59	27	0.69
10EB001	South Nahanni River above Virginia Falls	14,500	0.66	-9	0.69	0.76	-4	0.76
10ED001	Liard River at Fort Liard	222,000	0.80	7	0.83	0.83	7	0.89
10ED002	Liard River near the Mouth	275,000	0.68	7	0.81	0.72	11	0.84

The model is also able to respect snow accumulation and melt and evapotranspiration rates at different locations and scales within the basin. The calibration process was able to highlight regions within the basin which required modification of the original model structure to better respect the hydrological processes and responses. The model structure was modified within the more wetland dominated region through modifications to the soil structure and the addition of a simple wetland structure. As well, the model structure within the Nahanni range was modified to better represent the underlying Karst geology.

5. CONCLUSIONS

Through the use of partial gauge data, model structure modification, and multi-objective and internal process calibration, a high-quality model of the Liard basin was developed. The model performs well across the large, spatially heterogeneous basin and can respect multiple data sources. The calibration process was able to provide insight to the regions which required modification to the model structure to better represent the regional hydrological processes and responses. Automatic calibration of the model is expected to further improve model performance.

ACKNOWLEDGEMENTS

This work is supported by the Natural Sciences and Engineering Research Council of Canada and the Northern Water Futures project.

REFERENCES

- Bergstrom, S., & Forsman, A. 1973 Development of a conceptual deterministic rainfall-runoff model. *Nordic Hydrology*. 4(3), 147–170.
- Cao, W., Bowden, W.B., Davie, T., & Fenemor, A. 2006 Multi-variable and multi-site calibration and validation of SWAT in a large mountainous catchment with high spatial variability. *Hydrological Processes*. 20(5), 1057–1073.
- Craig, J. R., & Raven Development Team. 2018 Raven user's and developer's manual (Version 2.9.1). Available online: <http://www.civil.uwaterloo.ca/jrcraig/Raven/Main.html>. 17 June 2019
- Fenicia, F., Savenije, H. H. G., Matgen, P., & Pfister, L. 2008 Understanding catchment behavior through stepwise model concept improvement. *Water Resources Research*. 44(1), 1–13.
- Gupta, H. V., Sorooshian, S., & Yapo, P. O. 1998 Toward improved calibration of hydrologic models: Multiple and noncommensurable measures of information. *Water Resources Research*. 34(4), 751–763.
- Hamilton, A. S., Hutchinson, D. G., & Moore, R. D. 2001 Estimation of winter streamflow using a conceptual hydrological model: a case study, Wolf Creek, Yukon Territory. Proc. *11th Workshop on the Hydraulics of Ice Covered Rivers, Ottawa, Ontario*, pp 111-124.

How extreme can unit discharge become in steep Norwegian catchments?

Oddbjörn Bruland¹

¹*Department of Civil and Environmental Engineering, Faculty of Engineering, Norwegian University of Science and Technology, Trondheim, NORWAY.*

**Corresponding author's email address: sschiff@uwaterloo.ca*

ABSTRACT

This study presents results of observations and analysis of the flood in Utvik 24 July 2017. The author was present during the event and documented the flood during and after the event. Observations and calculations suggest a discharge between 200 m³/s and 250 m³/s from the 25 km² large catchment. With the majority of water coming from a contributing area found from observations in the watershed of about 50% of the catchment this gives unit discharges of 10 m³/s,km² to 20 m³/s,km². This is two to four times higher than previously documented unit discharges in Norway and in the range of the highest observed peak unit discharges in Southern Europe. The precipitation causing this event is estimated to be two to three times higher than IDF curves give for 200 year precipitation in this region.

KEYWORDS

Arctic environments; flooding; hydrology.

The trajectory of permafrost environments in northwestern Canada's discontinuous permafrost zone

Olivia Carpino^{1*}, Kristine Haynes¹, Ryan Connon², Élise Devoie³, and William Quinton¹

¹*Cold Regions Research Centre, Wilfrid Laurier University, Waterloo, Ontario, N2L 3C5, CANADA*

²*Environment and Natural Resources, Government of the Northwest Territories, Yellowknife, Northwest Territories, X1A 2L9, CANADA*

³*Department of Civil and Environmental Engineering, University of Waterloo, Waterloo, Ontario, N2L 3G1, CANADA*

**Corresponding author's email address: ocarpino@wlu.ca*

ABSTRACT

The discontinuous permafrost zone is among the most environmentally vulnerable regions on Earth as it is undergoing a significant transformation associated with rapid climate change and the resultant impacts of permafrost thaw. While this region is characterized as a patchwork of both mineral and organic terrain, permafrost is effectively isolated to areas of high peatland coverage but is still typically at or very near to melting point temperatures. Rapid climate warming over recent decades has significantly decreased the area underlain by permafrost and has catalyzed dramatic landscape transition from forest to wetland in these peatland areas. These permafrost thaw-induced landscape transformations indicate the region is particularly sensitive to warming temperatures and will continue to respond to climatic changes and landscape disturbances. This study explores the future trajectory of these transitioning landscapes by proposing a space-for-time substitution spanning the approximately 600 km long and 300,000 km² latitudinal gradient of northwestern Canada's discontinuous permafrost zone. Forested peatlands overlying permafrost dominate more northerly landscapes while forest-wetland patchworks dominate more southerly landscapes. Similarly, a warming climate over time acts as a catalyst to begin the same transition. Here we present the distribution of peatland-rich environments that govern permafrost coverage in the discontinuous permafrost zone and propose a conceptual model to represent the landcover changes within these environments across both time and space.

KEYWORDS

Discontinuous permafrost zone; taiga; peatland; climate change; boreal forest; hydrology

1. INTRODUCTION

Arctic and subarctic regions are undergoing rapid and accelerating climate warming and experiencing widespread permafrost thaw as a result. Permafrost thaw is one of the most dramatic manifestations of climate warming yet the degree that it will transform these landscapes moving forward is more uncertain. Land and water resources across the circumpolar region therefore have an ambiguous future, emphasizing the need for further research to quantify current and future permafrost thaw-induced changes. This is particularly important in the discontinuous permafrost zone as substantial changes have already been observed to both the landscape (Quinton et al. 2011; Carpino et al. 2018) and the regional hydrology (Connon et al. 2014; Korosi et al. 2017).

While permafrost (i.e. perennially cryotic soil) only occupies 16% of the global land area (Tarnocai 2009), up to 80% of the world's boreal forests occur on these permafrost soils (Helbig et al. 2016). The relationship between forest and permafrost is becoming increasingly important as over 20% of these permafrost regions are now covered by terrain comprised of thermokarst features or vulnerable to future thermokarst formation (Olefeldt et al. 2016). In the discontinuous permafrost zone, much of the permafrost is isothermal at, or very near to, its melting point temperature (Kwong & Gan 1994), indicating it may be in disequilibrium with current climate conditions (Helbig et al. 2016). This signifies that permafrost is limited to areas of high peatland coverage because it is being preserved by the insulating properties of peat rather than the climatic conditions (Camill 1999; Wright et al. 2009; Helbig et al. 2016). Moreover, in the discontinuous permafrost zone permafrost preferentially exists beneath unsaturated, forested peat plateaus while surrounding saturated peatlands (e.g. collapse scar bogs and channel fens) are permafrost-free (Zoltai & Tarnocai 1975; Hayashi et al. 2004; Quinton et al. 2009).

The relationship between permafrost, peat, and the overlying boreal forest indicates that landcover change is one of the most apparent consequences of climate change in the discontinuous permafrost zone. Specifically, permafrost thaw in this region triggers a transformation from forest-dominated peatlands to those that are wetland-dominated and permafrost-free (Quinton et al. 2011; Baltzer et al. 2014; Carpino et al. 2018). However, previous work has also established that forests may return to these newly wetland-dominated landscapes after a gradual dewatering process (Ketteridge et al. 2013; Chasmer & Hopkinson 2017) via drainage (Camill 1999) and evapotranspiration (Warren et al. 2018) has occurred. While this indicates a cyclical process, it is unlikely for permafrost to return to these environments in response to afforestation trends due to the warmer climatic conditions that originally initiated permafrost thaw (Robinson & Moore 2000; Turetzky et al. 2007; Jorgenson et al. 2010).

The climate change-driven succession experienced by boreal peatlands exemplifies the widespread vulnerability of the discontinuous permafrost zone in response to climate perturbations. In addition to the drastically different surficial appearances between forest-dominated and wetland-dominated peatlands, the landcovers that represent permafrost (e.g. forested peat plateaus) and permafrost-free (e.g. tree-free collapse scar bogs) ground also have contrasting energy balances (Ketteridge et al. 2013; Chasmer & Hopkinson 2017) and hydrological regimes (Connon et al. 2014). Specifically, peat plateaus function principally as runoff generators, collapse scar bogs act as storage features, and channel fens transport water across the landscape (Wright et al. 2009; Hayashi et al. 2014). Additionally, the transition from relatively dry, forest-dominated peatlands to peatlands that are saturated and exposed due to a lack of canopy cover, increases both thermal conductivity (Wright et al. 2009) and received shortwave radiation (Quinton et al. 2009).

There is a growing acceptance that permafrost thaw is impacting the region and that landcover changes have the potential to significantly affect the energy balances and hydrological regimes that govern the landscape. However, predicting these responses across the discontinuous permafrost zone is challenging due to the remoteness and size of the region, spatial and temporal heterogeneity, limited data availability, and incomplete monitoring networks. Despite these challenges, northern communities and decision-makers still require more effective tools and proper knowledge to respond to the impacts of climate change. Livelihoods, particularly in indigenous communities, are directly intertwined with the environment indicating that new approaches are critical to better understanding present conditions and predicting the future of the region's permafrost, forests and water. Researching these environments is critical but to do so, researchers must develop more innovative approaches to improve the understanding of how permafrost thaw affects these environments.

There is a need for more resolved and comprehensive approaches, including establishing broader predictive techniques, in order to expose and describe the factors driving variability in forest and permafrost distribution across northwestern Canada's discontinuous permafrost zone. Using landcover as a proxy for permafrost condition across the peatlands in this region has emerged as an appropriate and innovative method of monitoring these vulnerable and remote environments (Baltzer et al. 2014; Quinton et al. 2011). This study examines over 300,000km² of the discontinuous permafrost zone and aims to determine the future trajectory of permafrost environments under the impacts of climate change. Firstly, we establish the current patterning of permafrost and forest distribution across the boreal peatlands of Canada's taiga plains. Secondly, we present a conceptual model of peatland transition following permafrost thaw and propose that this conceptual model can be applied locally to represent changes over time or regionally to represent changes across space.

2. METHODS

2.1 Study Region

Much of northwestern Canada's boreal ecoregion is located within the discontinuous zone, which ranges latitudinally from extensive-discontinuous (50-90% areal coverage) in the north to sporadic-discontinuous (10-50%) in the south. The study area is located within the taiga plains ecozone and is characterized as a patchwork of both mineral and organic terrain where permafrost is preserved but effectively isolated to areas of high peatland coverage (Wright et al. 2009; Helbig et al. 2016). The parallel distributions of permafrost and peatlands in this environment are due to the associated thermal offset created by insulating peat soil layers (Vitt et al. 1994; Camill and Clark 1998) as permafrost in this region is typically at or very near to, melting point temperatures throughout its thickness (Kwong & Gan 1994). The insulating properties of dry peat throughout the study area define a pattern where permafrost occurs preferentially below unsaturated, forested peatlands such as peat plateaus, while adjacent peatlands occupying lower, and often saturated, topographic positions are permafrost free (Zoltai & Tarnocai 1975; Hayashi et al. 2004; Quinton et al. 2009). However, even despite peat's typically resilient insulating properties, rapid climatic warming over recent decades has significantly decreased the area underlain by permafrost (Wright et al. 2009; Olefeldt et al. 2016).

The discontinuous permafrost zone of the taiga plains ecozone used in this study was further divided into the areas corresponding with extensive-discontinuous and sporadic-discontinuous

classifications (Figure 1). The entire study region covers approximately 312,000 km² where, 151,000 km² falls in the more northerly extensive discontinuous zone and 161,000 km² falls in the more southerly sporadic discontinuous zone. The study area is characterized by a continental climate with short, warm summers and long, cold winters (Quinton et al., 2019). Climate normal data indicate mean annual air temperature (MAAT) values of approximately -4.4°C to -2.5°C across the latitudinal gradient (Natural Resources Canada 2018). The latitudinal extent of the study region has also experienced average MAAT increases of approximately 2.1°C since 1970 (Natural Resources Canada 2018), which is consistent with a widely-documented pan-Arctic warming trend.

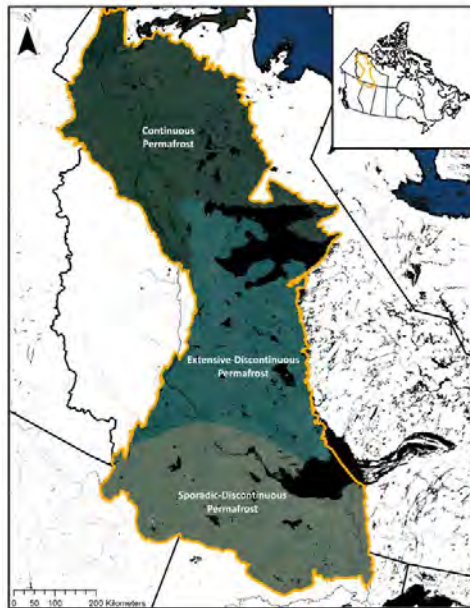


Figure 4. Distribution of permafrost zones within the Taiga Plains study region.

2.1.1 Scotty Creek Research Station

Scotty Creek Research Station (61.3°N, 121.3°W) is located near the confluence of the Mackenzie and Liard Rivers approximately 50 km south of Fort Simpson in the Northwest Territories. Scotty Creek is a peatland-dominated basin within the discontinuous permafrost zone that typifies the southern taiga plains and much of the circumpolar subarctic. Scotty Creek Research Station is located in the headwaters of the 152 km² Scotty Creek basin where a 2-8 m thick cover of continuous peat overlays a clay and silt dominated glacial till (Quinton et al., 2019). While permafrost is isolated to areas of high peatland coverage in this region of the discontinuous permafrost zone, landcover also represents a controlling factor on permafrost distribution (Quinton et al. 2011; Baltzer et al. 2014; Carpino et al. 2018). Specifically, permafrost in the discontinuous zone has been observed, both at Scotty Creek and across the broader region, to predominantly occur below forested peat plateaus, while surrounding tree-free peatlands such as collapse scar bogs and channel fens, typify permafrost-free landcovers (Zoltai & Tarnocai 1975; Hayashi et al. 2004; Quinton et al. 2009).

Scotty Creek presents a unique opportunity to study the taiga plains ecozone as intensive field and modelling studies have been ongoing since the 1990s, spanning a period of rapid climate warming and many associated environmental changes. The data and research Scotty Creek Research Station has provided over recent decades offers an unprecedented look at the impacts of climate change on

a landscape that is representative of much of the taiga plains. Furthermore, there is growing support that peatland-dominated environments are highly susceptible to shifts in the distribution of water and energy fluxes in response to climatic change (St. Jacques & Sauchyn 2009; Quinton et al. 2019).

2.2 Geomatics Methods

The discontinuous portion of the taiga plains ecozone was selected as the boundary for the geomatics work completed in this study. Multispectral Landsat 8 imagery (30 m resolution) was acquired across over 300,000 km², totalling 70 Landsat scenes. Of these, 59 scenes were used to construct the base of the mosaic and 11 were used as secondary data to patch and minimize cloud cover. The 59 primary scenes were acquired in 2017 or 2018 while the 11 secondary scenes were acquired between 2013 and 2016 as data of suitable quality was unavailable during the preferred time period. All 70 Landsat tiles were acquired in June, July, or August rendering the images seasonally comparable and allowing for a simpler mosaicking process. In addition to prioritizing snow-free scenes, seasonal variations in soil moisture can also alter surface albedo particularly near wetland boundaries, which dominate patchwork environments such as the taiga plains (Chasmer et al. 2010).

A colour infrared mosaic (Landsat 8 bands 5, 4, 3 displayed as R, G, B) was created across the study region in ArcGIS (ESRI, Redlands, California) using a Lambert Conformal Conic projection. The mosaic dataset was then colour balanced and the boundary was amended to the taiga plains ecozone including the delineations dividing the sporadic and extensive discontinuous zones. Classifications were then completed separately between the two zones using a hybrid classification approach. Firstly, clouds, cloud shadows and waterbodies were masked out across both regions using spectral thresholds. Secondly, unsupervised classifications were applied to both regions targeting 50-75 classes (72 created). The results of this preliminary classification were then combined with two pre-existing datasets: a digital elevation model (DEM) (Natural Resources Canada 2017) and The Northern Circumpolar Soil Carbon Database (NCSCD) (Bolin Centre for Climate Research 2013). The DEM data was collected and applied to the study region given the role topography plays on governing the distribution of permafrost due to associated climatic and hydrologic factors. Furthermore, the NCSCD, was used to further inform the locations of the targeted peatland-dominated landscapes (Olefeldt et al. 2016; Gibson et al. 2018). The preliminary unsupervised classification, the DEM, and the NCSCD were combined to predict the areas of high peatland coverage that this study focuses on. The classifications within those identified areas were then tested at 10 peatland-dominated training sites that had previously undergone intensive remote sensing analysis and manual classification (10km² at 0.3m resolution) (see Carpino et al. 2018). Those 10km² sites were then used as training sites to advise final classification results. The 72 classes from the preliminary unsupervised classification were then aggregated into 12 final classes that could be observed within the peatlands outlined across the study region. Further work will be completed to assess the accuracy of this classification. Additional work will also be completed to statistically analyse the distribution of landcovers across the distribution of peatlands.

3. RESULTS AND DISCUSSION

The results presented are based on preliminary findings. Additional analysis is being completed to further support these findings as well as expand on the significance of these observations.

The work presented in this study indicates that the distribution of peatlands, and thus the environments that are likely to contain permafrost, is largely dispersed across the study region. Expectedly, large peatland clusters are located in lowland areas with high histel soil percentages. In the sporadic-discontinuous zone the distribution of these high density peatland clusters is more longitudinally dispersed, while in the extensive-discontinuous permafrost zone, high density peatlands are effectively isolated to the western portion, nearest to the Mackenzie River, and notably absent from the area directly south of Great Bear Lake where the taiga plains borders the taiga shield. We estimate that landscapes with high peatland coverage account for approximately 30% of the discontinuous permafrost zone contained within the taiga plains ecozone (Figure 2).

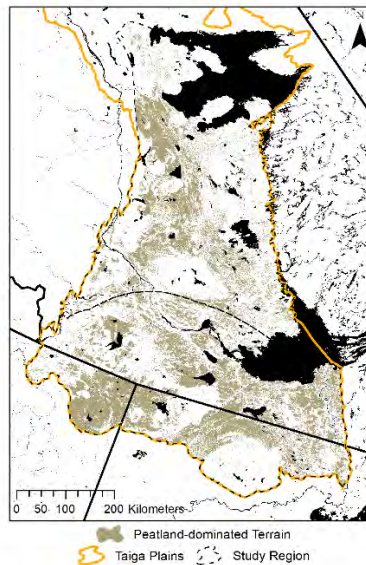


Figure 5. Predicted distribution of peatland-dominated terrain in the discontinuous permafrost zone of the taiga plains.

Within the identified areas of high peatland coverage, a latitudinal trend appears to be present. In the extensive-discontinuous permafrost zone, forested peatlands are dominant. This indicates that the permafrost in these environments is largely intact due to the insulating properties of the dry peat that covers these forest-dominated landscapes (Zoltai & Tarnocai 1975; Hayashi et al. 2004). Along the boundary between the extensive-discontinuous and sporadic-discontinuous permafrost zones that makes up the centre of the study region, wetlands become more prevalent within the identified peatland landscapes. Here, the predominant transition from forest-dominated to more wetland-dominated peatlands appears to be widespread indicating ongoing permafrost thaw and increased inundation and waterlogging of previously dry peat plateaus (Islam & Macdonald 2004; Iwata et al. 2012). A near-even patchwork of both forested and tree-free peatlands make up the majority of the sporadic-discontinuous permafrost zone. However, afforestation trends appear to be responsible for some of the forested area along the southern boundary of the study region, particularly in the areas of northern British Columbia and Alberta, a pattern also observed in Carpino et al. (2018) as well as proposed by Camill (1999) and supported by Ketteridge et al. (2013). This indicates that a large portion of permafrost has already been lost from these environments as peatland dewatering (Ketteridge et al. 2013) has clearing water from the landscape, allowing for forest cover to return to newly unsaturated areas (Camill 1999).

The landcover patterns observed across the taiga plains indicate that variability in both forest cover and permafrost across boreal peatlands is climate-driven. This suggests that a space for time substitution may be appropriate in these environments. The transitional nature of these peatland environments is presented in Figure 3 and can be represented by seven distinct phases: (1) Forested permafrost plateaus dominate; (2) Forested permafrost plateaus with small, isolated wetlands; (3) Forested permafrost plateaus with larger, interconnected wetlands; (4) Wetland complexes with small plateau islands; (5) Wetland complexes with small-scale hummock development and tree establishment; (6) Hummock growth with forest establishment; (7) Forest dominated peatlands. This transition not only represents the dominant trajectory of change over recent decades but also corresponds with the parallel climatic transition from the extensive permafrost found beneath treed peatlands in the north, to patchwork landscapes at more moderate latitudes, and finally to more widespread permafrost-free environments at the southern extent of the study region. Interestingly, each of these stages, and the transitional steps between them, can also be found on smaller scales at local sites including Scotty Creek, which is located on the boundary between the sporadic-discontinuous and extensive-discontinuous zones.

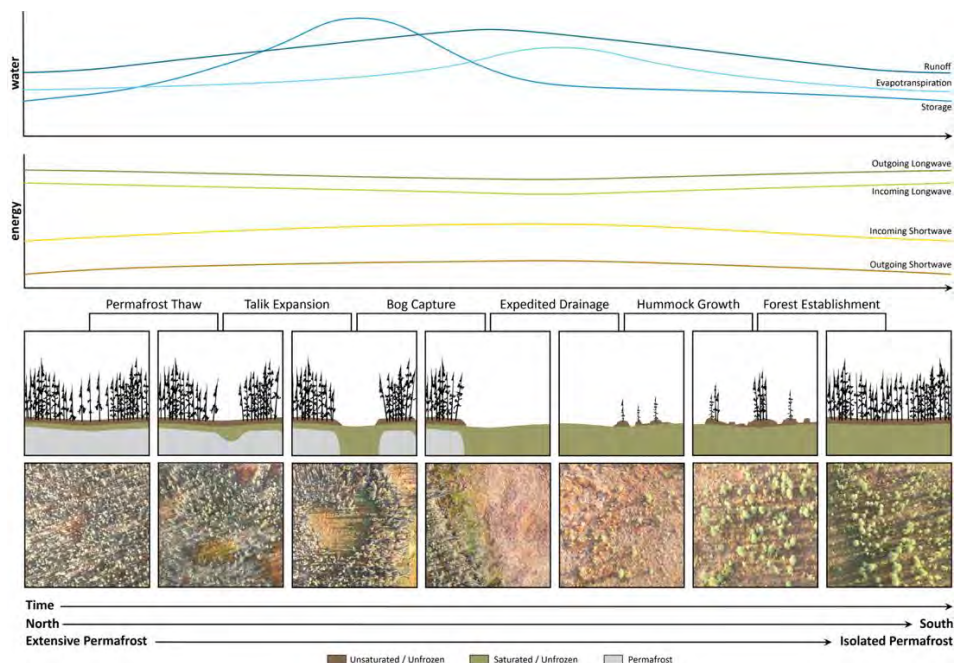


Figure 6. (Bottom) Proposed conceptual model of landscape trajectory including a space-for-time substitution for changes to both permafrost and landcover. Drone imagery is presented alongside conceptual diagrams to further support this proposal. (Top) Relative changes to local water and energy balances are presented.

Scotty Creek serves as an effective microcosm of the transition observed across the taiga plains. As the trajectory progresses through the proposed stages the processes governing hydrological pathways also transition. The early stages of the proposed successional trajectory are dominated by hydrologically isolated wetlands where outflow from the basin is limited to primary runoff from plateau features into nearby fens (Connon et al. 2014; Quinton et al. 2019). The contributions of evapotranspiration during the forest-dominated stages are similarly minor due to the limited transpiration produced by black spruce on organic soils (Warren et al. 2018). Even when forest is

the predominant landcover, the sunlight penetration associated with sparse canopy cover allows for understory vegetation to be the principal contributor to evapotranspiration (Chasmer et al., 2011).

The middle stages of the trajectory are defined by peaks in runoff, storage and evapotranspiration. Storage peaks during wetland expansion but before secondary pathways have been activated, therefore preceding the runoff peak slightly. Water arriving directly into one of the isolated, but rapidly expanding wetlands, will be stored in the collapse scar wetland as it is unlikely to reach a fen at this stage (Quinton et al. 2019). The elevated observed runoff that follows the storage peak is due to primary runoff being amplified by the introduction of secondary runoff in the form of connected and cascading wetlands (Connon et al. 2015; Haynes et al. 2018). A decrease in runoff then follows as plateau loss continues to accelerate, eliminating contributing interior collapse scar wetlands and discontinuing any secondary runoff paths (Quinton et al. 2019). While the water storage runoff terms experience gradual decreases as the trajectory progresses, evapotranspiration then peaks in the stages where wetland is the predominant landcover due to standing water and moss evaporation (Warren et al. 2018).

Finally, the advanced stages of the successional trajectory correspond with continued decreases across the three hydrological terms as peatland dewatering acts as the initiatory mechanism for hummock and tree reestablishment (Ketteridge et al. 2013; Chasmer & Hopkinson 2017). This results in similar evapotranspiration relationships to the forested permafrost plateaus that dominate the early stages despite being permafrost-free. Storage and runoff are slightly increased from the original forest-dominated landscape due to the lack of underlying permafrost.

4. CONCLUSIONS

The results of this study provide a comprehensive picture of peatland and permafrost distribution across the discontinuous permafrost zone in the taiga plains ecozone. Furthermore the results of this study are of relevance to other peatland-rich permafrost environments across the circumpolar north. This research also generates an understanding of how changes to permafrost distribution and ongoing permafrost thaw may impact these environments. Proposing a broadly applicable conceptual model may assist in developing decision-making tools that will more effectively contribute to maintaining the regions resources as well as the health of its communities.

ACKNOWLEDGEMENTS

We gratefully acknowledge the support of the Dehcho First Nations and in particular, the Liidlii Kue First Nation. This work was supported by the Natural Sciences and Engineering Research Council of Canada and Polar Knowledge Canada.

REFERENCES

- Baltzer, J., Veness, T., Chasmer, L., Sniderhan, A., & Quinton, W. (2014). Forests on thawing permafrost: Fragmentation, edge effects, and net forest loss. *Global Change Biology*, 20(3), 824-834.
- Camill, P. (1999). Peat accumulation and succession following permafrost thaw in the boreal peatlands of Manitoba, Canada. *Ecoscience*, 6(4), 592-602.
- Camill, P. & J. S. Clark, 1998. Climate change disequilibrium of boreal permafrost peatlands caused by local processes. *American Naturalist*, 151, 207-222.

- Carpino, O.A., Berg, A.A., Quinton, W.L., & Adams, J.R. (2018). Climate change and permafrost thaw-induced boreal forest loss in northwestern Canada. *Environmental Research Letters*, 13(8).
- Chasmer, L. & Hopkinson, C. (2017). Threshold loss of discontinuous permafrost and landscape evolution. *Global Change Biology*, 23, 2672-2686.
- Chasmer, L., Hopkinson, C. & Quinton, W. (2010). Quantifying errors in discontinuous permafrost plateau change from optical data, Northwest Territories, Canada: 1947-2008. *Canadian Journal of Remote Sensing*, 36(2), 211-223.
- Chasmer, L., Hopkinson, C., Veness, T., Quinton, W., & Baltzer, J. (2014). A decision-tree classification for low-lying complex land cover types within the zone of discontinuous permafrost, *Remote Sensing of Environment*, 143, 73–84.
- Chasmer, L., Quinton, W., Hopkinson, C., Petrone, R., & Whittington, P. (2011). Vegetation Canopy and Radiation Controls on Permafrost Plateau Evolution within the Discontinuous Permafrost Zone, Northwest Territories, Canada. *Permafrost and Periglacial Processes*, 22(3).
- Connon, R.F., Quinton, W.L., Craig, J.R., & Hayashi, M. (2014) Changing hydrologic connectivity due to permafrost thaw in the lower Liard River valley, NWT, Canada *Hydrol. Process.*, 28, 4163–78.
- Connon, R. F., Quinton, W.L., Craig, J.R., Hanisch, J., & Sonnentag, O. (2015). The hydrology of interconnected bog complexes in discontinuous permafrost terrains *Hydrol. Process.* 29, 3831-47.
- Gibson, C.M., Chasmer, L.E., Thompson, D.K., Quinton, W.L., Flannigan, M.D., & Olefeldt, D. (2018). Wildfire as a major driver of recent permafrost thaw in boreal peatlands, *Nature Communications*, 9, 3041.
- Hayashi, M., Quinton, W. L., Pietroniro, A., & Gibson, J. J. (2004). Hydrologic functions of wetlands in a discontinuous permafrost basin indicated by isotopic and chemical signatures. *Journal of Hydrology*, 296, 81-97.
- Helbig, M., Pappas, C. & Sonnetag, O. (2016). Permafrost thaw and wildfire: Equally important drivers of boreal tree cover changes in the Taiga Plains, Canada. *Geophysical Research Letters*, 43, 1598-1606.
- Ketteridge, N., Thompson, D. K., Bombonato, L., Turetsky, M. R., Benscoter, B. W., Waddington, J. M. (2013). The ecohydrology of forested peatlands: simulating the effects of tree shading on moss evaporation and species composition. *Journal of Geophysical Research – Biogeosciences*, 118, 422-435.
- Korosi, J.B., Thienpont, J.R., Pisaric, M.F.J., deMontigny, P., Perreault, J.T., McDonald, J., Simpson, M.J., Armstrong, T., Kokelj, S.V., Smol, J.P., & Blais, J.M. (2017). Broad-scale lake expansion and flooding inundates essential wood bison habitat, *Nature Communications*, 8, 14510.
- Kwong, J. T. & Gan, T. Y. (1994). Northward migration of permafrost along the Mackenzie Highway and climatic warming. *Climate Change*, 26, 399-419.
- Olefeldt, D., Goswami, S., Grosse, G., Hayes, D., Hugelius, G., Kuhry, P., McGuire, A.D., Romanovsky, V.E., Sannel, A.B.K., Schuur, E.A.G. & Turetsky, M.R. (2016). Circumpolar distribution and carbon storage of thermokarst landscapes, *Nature Communications*, 7, 13043.
- Quinton, W., Berg, A., Braverman, M., Carpino, O., Chasmer, L., Connon, R., Craig, J., Devoie, É., Hayashi, M., Haynes, K., Olefeldt, D., Pietroniro, A., Rezanezhad, F., Schincariol, R.,
-

- and Sonnentag, O. (2019). A synthesis of three decades of hydrological research at Scotty Creek, NWT, Canada, *Hydrol. Earth Syst. Sci.*, 23, 2015-2039.
- Quinton, W. L., Hayashi, M., & Chasmer, L. E. (2009). Peatland hydrology of discontinuous permafrost in the Northwest Territories: overview and synthesis. *Canadian Water Resources Journal*, 34(4), 311–328.
- Quinton, W., Hayashi, M., & Chasmer, L. (2011). Permafrost-thaw-induced land- cover change in the Canadian subarctic: Implications for water resources. *Hydrological Processes*, 25, 152-158.
- Robinson, S. D., & Moore, T. R. (2000). The influence of permafrost and fire upon carbon accumulation in high boreal peatlands, Northwest Territories, Canada. *Arctic, Antarctic, and Alpine Research*, 32(2), 155–166.
- St. Jacques, J.M. & Sauchyn, D.J. (2009). Increasing winter baseflow and mean annual streamflow from possible permafrost thawing in the Northwest Territories, Canada. *Geophysics Research Letters* 36.
- Tarnocai, C. (2009) The impact of climate change on Canadian peatlands *Can. WaterRes. J.*, 34, 453-66.
- Turetsky, M. R., Wieder, R. K., Vitt, D. H., Evans, R. J., & Scott, K. D. (2007). The disappearance of relict permafrost in boreal north America: effects on peatland carbon storage and fluxes. *Global Change Biology*, 13, 1922-1934.
- Vitt, D. H., Halsey, L. A., & Zoltai, S. C. (1994). The bog landforms of continental Western Canada in relation to climate and permafrost patterns. *Arctic and Alpine Research*, 26(1), 1– 13.
- Warren, R.K., Pappas, C., Helbig, M., Chasmer, L.E., Berg, A.A., Baltzer, J.L., Quinton, W.L., & Sonnetag, O. (2018). Minor contribution of overstory transpiration to landscape evapotranspiration in boreal permafrost peatlands, *Ecohydrology* 11, 1975.
- Wright, N., Hayashi, M., & Quinton, W. (2009). Spatial and temporal variations in active layer thawing and their implication on runoff generation in peat-covered permafrost terrain. *Water Resources Research*, 45(5).
- Zoltai, S. C., & Tarnocai, C. (1975). Perennially frozen peatlands in the Western Arctic and Subarctic of Canada. *Canadian Journal of Earth Science*, 12, 28–43.

Spatial Drivers of Permafrost Thaw using Lidar Remote Sensing, Machine Learning and *in situ* Methods

L. Chasmer¹, C. Mahoney², Alissia Paluck³, Ryan Connon⁴,
W. Quinton⁵, and C. Hopkins¹

¹Department of Geography, University of Lethbridge, Lethbridge Alberta, T1J 3M4, CANADA

²Alberta Environment and Parks, Government of Alberta, Lethbridge Alberta, T1J 3M4, CANADA

³Farmers Edge Inc., Lethbridge Alberta, T1H 6N3, CANADA

⁴Government of Northwest Territories, Yellowknife, Northwest Territories, X1A 2L9, CANADA

⁵Department of Geography, Wilfrid Laurier University, Waterloo Ontario, N2L 3C5, CANADA

*Corresponding author's email address: laura.chasmer@uleth.ca

ABSTRACT

Spatial quantification of the drivers of permafrost thaw over time is difficult to determine due to complex, non-linear and proximal interactions of the overlying land surface and hydrological influences on energy balance. Here we use time series lidar data acquired for the Scotty Creek watershed NWT in August 2008 and August 2015 to develop a predictive surface of permafrost thaw based on the subtraction of lidar-derived elevation of 2015 from that of 2008, assuming that elevation changes represent loss of permafrost between years. In addition, textural, structural, and spectral observations from airborne lidar and high resolution satellite imagery acquired for the watershed in 2010 were used within a regression-tree machine learning framework. These were used in correspondence to identify spatial land surface attributes and ranking (in importance) associated with variable rates of thaw. We find that that ground surface curvature and aspect, and understory canopy height were the most important correlates of permafrost thaw. Based on application of the most important correlates within the random forest framework, we were able to predict permafrost thaw along the edges of permafrost to within 4 cm compared with lidar-derived thaw (RMSE = 0.11 m). Accuracies improve when applying correlate variables to entire plateaus (mean difference = -0.01 m, RMSE = 0.11 m). Such models show promise for estimating permafrost loss and the volume of runoff from northern basins and may be an improvement over empirical and physical models.

KEYWORDS

Permafrost Thaw, Remote Sensing, Machine Learning, Volumetric Water Loss

1. INTRODUCTION

Sporadic and discontinuous permafrost thaw especially within the southern Taiga Plains ecozone and parts of Alaska has been accelerating in recent decades (Jorgenson et al., 2001; Quinton et al. 2011; Lara et al. 2016; Chasmer & Hopkins, 2016). Permafrost underlays a significant portion (~40%) of Canada's boreal region (Price et al. 2013) and is viewed as an important feedback mechanism for the global climate system (Lenton et al. 2011; Helbig et al. 2016). More locally, the loss of long-term water storage within permafrost through melt may greatly increase the volume of runoff through northern basins and into rivers and streams adjacent to communities (Connon et al. 2015; St Jacques & Sauchyn, 2009). This is of concern to northern communities, where peaks in runoff are starting to rival and surpass peaks occurring during the freshet (summer and fall).

To understand the implications of increasing permafrost meltwater on northern communities, there is a need to determine volumetric loss of permafrost in relation to cumulative discharge across broad regions. However, understanding and quantifying permafrost thaw is notoriously complex due to spatial variations in energy balance. Direct measurements of permafrost thaw are also expensive and difficult to collect often due to inaccessibility of remote sites. Further, while stream gauges provide cumulative measurement of water balance, lags between permafrost thaw, storage, runoff, and environmental changes within watersheds (e.g. Quinton et al. 1999; Connon et al. 2015; Chasmer & Hopkinson, 2016) may be missed. Other tools such as optical remote sensing provide an indicator of vegetation mortality over broad areas, which may be related to permafrost thaw over periods of years to decades (Quinton et al. 2009; Chasmer et al. 2011; Baltzer et al. 2014), but do not measure thaw *in situ*. Active remote sensing, such as lidar, penetrates through tree canopies to provide accurate and high-resolution three-dimensional data of the ground surface (Hopkinson et al. 2005). Despite the utility of these datasets, multi-temporal lidar data may also be expensive and logistically difficult to acquire in some remote northern regions.

Understanding of permafrost thaw and volumetric water input requires quantification of environmental influences on permafrost thaw (Wright et al. 2009), within a spatial framework. One way to approach this is to examine indicators or correlates of permafrost thaw within the environment and land surface attributes that are related to greater and lesser amounts of loss over a period of years (Jorgenson et al. 2001). If these can be determined for all situations and characteristics of permafrost thaw, then a model fed by geospatial and remotely sensed data may be developed to estimate this.

In this study, we use digital elevation models (DEMs) derived from time-series lidar data collected in 2008 and 2015 to train a machine learning model of permafrost thaw. The model is based on spatial correlates of permafrost thaw (land surface attributes that are indicative of permafrost thaw) and spatial predictors of permafrost thaw (land surface attributes that correlate with variable rates of thaw) observed from lidar and optical remote sensing data acquired in 2010. The objective of this study, therefore, is to demonstrate a new method for modelling permafrost rate of thaw based on land surface attributes that do not require time series remotely sensed data.

2. METHODS

Lidar data were planned and collected by the authors within the same week in early August of 2008 and 2015 using a Teledyne Optech Inc. ALTM 3100 discrete return lidar within a small sub-area of the Scotty Creek watershed, NWT (Figure 1). Lidar data were then classified into ground returns in TerraScan (Terrasolid Inc.) and used to create two 1 m x 1 m DEMs. The 2008 DEM area of interest was then subtracted from the 2015 DEM area of interest, such that loss of permafrost (indicated by a reduction in ground surface elevation) is negative. The difference dataset was then defined as the response variable and re-sampled to 2 m. In addition to this, lidar data acquired in 2010 for the entire watershed was used to create a number of predictor variables including vegetation structure metrics (e.g. canopy height, cover, understory height) and ground surface topographical data layers (e.g. ground surface slope, curvature, topographic position). These were then divided into correlate variables (those that are indicative of permafrost thaw) and predictor variables (those that are drivers of permafrost thaw) and resampled to 2 m. WorldView-2 data were also acquired in September 2010 and were used to derive numerous optical vegetation, ground cover, and water indices. Approximately 7100 sample points were distributed within 2 m of permafrost edges determined from a landcover classification (Figure 1). In addition, ~38,000

sample points were distributed within plateau areas for the entire sub-areas. These sampled layer characteristics within identical locations from the response variable (permafrost thaw map) and all correlate and predictor layers. Predictors were then examined for covariance. If they covaried, then they were removed from the analysis, leaving only independent predictors. The response and independent predictors and correlate variable layers were then submitted to a random forest machine learning model (Breiman 2003; Mahoney et al. 2016; 2018) and iterated 20 times using 75% of the variables as training data to determine those that were most highly correlated with permafrost thaw. The best predictors and correlates from 2010 were then used to train the random forest model and output an independent map of permafrost thaw within the sub-area.

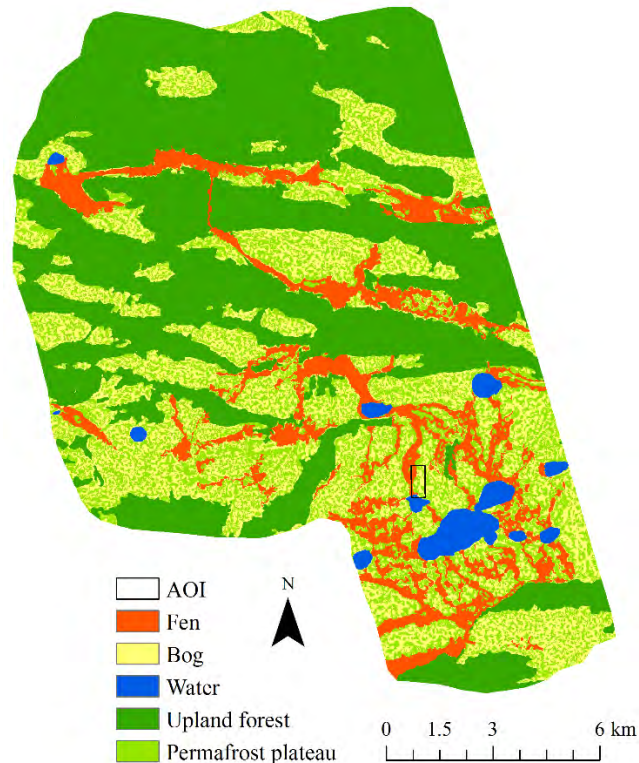


Figure 1. Scotty Creek watershed land cover classification (Chasmer et al. 2014) with the area of interest (AOI) (approximately 1500 m x 500 m) used to parameterize the random forest model.

3. RESULTS AND DISCUSSION

3.1 Ranking of Correlates and Predictors of Permafrost Thaw

Correlates of permafrost thaw are indicators that permafrost thaw is occurring, such that the environment is different from that in areas where there is minimal thaw. These are more numerous than predictors of permafrost thaw ($n = 19$ vs. 5 for non-covarying correlates and predictors, respectively). These consist of land surface and vegetation attributes that may contribute to permafrost thaw. Mean squared error (MSE) between permafrost thaw and positive correlates at randomly distributed point locations ranges from 0.0010 m and 0.0020 m. For example, decreased ground surface curvature corresponds with greater rates of thaw within randomly distributed points

along edges. This is the most important indicator of permafrost thaw. We assume that ground ice is more likely to thaw if the surface topography has greater convexity, thus increasing the surface area available for incident radiation. Aspect also negatively correlates with increased permafrost thaw, though is not as important an indicator of permafrost thaw as ground surface convexity. In addition, once thaw commences, higher moisture content within soils becomes a positive feedback for further thaw. Other correlates such as the height of understory vegetation is a positive indicator of permafrost thaw. Colonization of shrubs, especially along permafrost margins and into peatlands may indicate areas of comparatively reduced soil moisture (Chasmer & Hopkinson, 2016) during the years following lateral contraction of permafrost plateaus (Fafard 2014). In addition, variable foliage cover of taller shrubs may also result in increased snow accumulation in winter, which would insulate permafrost from colder temperatures (e.g. Hinkel & Hurd 2006). Variable importance for predictors of permafrost thaw along edges include slope (negatively related to thaw) and the normalised difference soil index (positively related to thaw). Mean square error ranges from 0.0005 to 0.0025 m, indicating slightly reduced predictive capacity than correlates of permafrost thaw.

3.2 Predicted Permafrost Thaw

Permafrost thaw predicted from correlates identified and ranked using the random forest model and input into a thaw-based classification. Mean differences between correlates applied to edges only within the random forest model and permafrost thaw (DEM differences) from 2008 to 2015 is -0.04 m (mean, RMSE = 0.11 m). When correlates from whole plateaus are compared with permafrost thaw, mean difference is -0.01 m (RMSE = 0.11). Differences in the lidar DEMs (thaw), compared with deviation between edge correlates vs. whole plateau correlates (and thaw) are illustrated in Figure 2 for a small sub-area of the broader region.

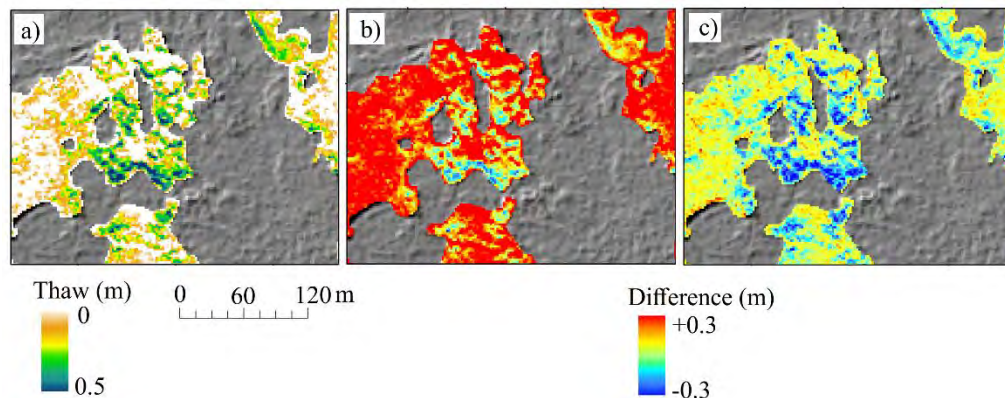


Figure 2. Permafrost thaw inferred from a) the difference between lidar DEMs in 2008 and 2015; b) difference between lidar-derived thaw and random forest modelled permafrost thaw from edge correlates only; and c) whole plateau correlates. Positive differences indicate that random forest methods overestimate losses, whereas negative differences indicate under-estimation of losses.

Figure 2b illustrates smaller differences including slight overestimation of thaw by up to 0.1 m towards plateau centres (along edges) and underestimation of thaw by as much as 0.3 m along edges adjacent to wetlands. Further, modelled thaw is overestimated when using edge correlates only (Figure 2b), which are governed by different processes than what is found along edges. When

applying whole plateau correlates within the random forest framework to plateaus, the differences are smaller, especially within the central plateau areas, with slight overestimation of thaw up to 0.12 m. However, by using this method, modelled thaw is underestimated by up to 0.3 m or more when compared with thaw from lidar time series DEMs. Despite this, the patterns of modelled thaw and sensitivity are spatially similar within both model results, illustrating the potential utility of this method. When compared with *in situ* measurements of cumulative permafrost thaw collected along a transect traversing from edge to edge across a plateau between 2011 and 2015, lidar-derived differences in elevation correlation coefficient (R^2) is 0.37. This is reduced slightly to $R^2 = 0.26$ when compared using the random forest model for whole plateau correlates. More comparisons with field data are required to better understand the relationship between changes in surface elevation over time and depth to frost table.

4. CONCLUSIONS

The methods introduced in this study illustrate the utility for using machine learning as a predictive tool for permafrost thaw when time series remote sensing data do not exist. While this shows promise, it is likely that environmental conditions influencing rates of permafrost thaw will vary between sites, and therefore requires more universal comparisons and parameterisation. Further, the influence of proximal drivers of permafrost thaw also require consideration and inclusion in future permafrost thaw modelling activities. Differences between rates of thaw and basin runoff, both from lidar time series derivations and modelling exercises will provide communities with more informed estimates of the impacts of permafrost thaw on downstream flooding.

ACKNOWLEDGEMENTS

We would like to acknowledge a start-up grant provided by the University of Lethbridge to Chasmer. NSERC Discovery Grants provided to Chasmer and Hopkinson and an NSERC Accelerator provided to Hopkinson. CFI is also acknowledged for field equipment. Finally, we would like to thank Canadian Forest Service Northern Forestry Centre (Drs. G. Castilla and R. Hall) for partial support for this project and Aurora Research Institute for research permits to Chasmer, Hopkinson, and Quinton.

REFERENCES

- Baltzer J.L., Veness T., Chasmer L.E., Sniderhan A.E., Quinton W.L. 2014 Forests on thawing permafrost: fragmentation, edge effects, and net forest loss. *Global Change Biology*. 20(3), 824-34.
- Breiman, L. 2003 Random Forests. *Machine Learning*, 45: 5-32
- Chasmer L., Hopkinson C., and Quinton W. 2011. Quantifying errors in permafrost plateau change from optical data, Northwest Territories, Canada: 1947 to 2008. *Canadian Journal of Remote Sensing – CRSS Special Issue*. 36(2), S211-S223.
- Chasmer L., Hopkinson C., Quinton W., Veness T., and Baltzer J. 2014. A decision-tree classification for low-lying complex land cover types within the zone of discontinuous permafrost. *Remote Sensing of Environment*. 143, 73-84.
- Chasmer, L. and C. Hopkinson, 2017. Threshold loss of discontinuous permafrost and landscape evolution. *Global Change Biology*. 23(7), 2672-2686. Doi:10.1111/gcb.13537.

- Connon R.F., Quinton W.L., Craig J.R., and Hayashi M. 2014. Changing hydrologic connectivity due to permafrost thaw in the lower Liard River valley, NWT, Canada. *Hydrological Processes*. 28, 4163-4178.
- Fafard M. 2014 Musical chairs in a boreal peatland: how permafrost thaw reverses successional processes. Master's thesis. Wilfrid Laurier University. Paper 1637.
- Helbig M., Wischniewski K., Kljun N., Chasmer L., Quinton Q., Detto M., and Sonnentag O. 2016. Permafrost disappearance impacts on near-surface climates of boreal forests. *Global Change Biology*. 22(12), 4048-4066. 10.1111/gcb.13348.
- Hinkel K.M. and Hurd, J.K. 2006. Permafrost destabilization and thermokarst following snow fence installation, Barrow, Alaska, U.S.A. *Arctic, Antarctic and Alpine Research*. 38(4), 530-539.
- Hopkinson C, Chasmer L, Sass G, Creed I, Sitar M, Kalbfleisch W, Treitz P 2005 Vegetation class dependent errors in lidar ground elevation and canopy height estimates in a boreal wetland environment. *Canadian Journal of Remote Sensing*. 31(2), 191-206.
- Jorgenson MT, Racine CH, Walters JC, Osterkamp TE 2001 Permafrost degradation and ecological changes associated with a warming climate in central Alaska. *Climatic Change*. 48(4), 551-579.
- Lara MJ, Genet H, McGuire AD, et al. 2016 Thermokarst rates intensify due to climate change and forest fragmentation in an Alaskan boreal forest lowland. *Global Change Biology*. 22(2), 816-829.
- Lenton, T. M. 2011 Early warning of climate tipping points. *Nature Climate Change*, 1(4), 201-209.
- Mahoney, C., Hopkinson, C., Held, A., Simard, M. 2016 Continental-scale canopy height modelling by integrating nations, spaceborne and airborne LiDAR data. *Canadian Journal of Remote Sensing*. DOI: 10.1080/07038992.2016.1196580
- Mahoney, C., Hall, R., Hopkinson, C., Filiatrault, M., Beaudoin, A., Chen, Q. 2018. A forest attribute mapping framework: a pilot study in a northern boreal forest, Northwest Territories, Canada. *Remote Sensing* 10(9), 1338
- Price DT, Alfaro RI, Brown KJ, et al. 2013 Anticipating the consequences of climate change for Canada's boreal forest ecosystems 1. *Environmental Reviews*. 21(4), 322-365.
- Quinton, W. L., & Marsh, P. 1999. Image analysis and water tracing methods for examining runoff pathways, soil properties and residence times in the continuous permafrost zone. *IAHS Publication 258*, 257-264.
- Quinton WL, Hayashi M, Chasmer LE 2011 Permafrost-thaw-induced land-cover change in the Canadian subarctic: implications for water resources. *Hydrological Processes*. 25(1), 152-158.
- St Jacques JM, Sauchyn DJ 2009 Increasing winter baseflow and mean annual streamflow from possible permafrost thawing in the Northwest Territories, Canada. *Geophysical Research Letters*. 36, L01401, doi:10.1029/2008GL035822.
- Wright, N., Hayashi, M., & Quinton, W. L. 2009. Spatial and temporal variations in active layer thawing and their implication on runoff generation in peat-covered permafrost terrain. *Water Resources Research*, 45(5).

Subarctic Lake Responses to Thawing Permafrost

K.A. Coleman^{1*}, J.R. Thienpont¹, and J.B. Korosi¹

¹*Department of Geography, York University, Toronto, Ontario, M3J 13P, CANADA*

**Corresponding author's email address: kcoleman@yorku.ca*

ABSTRACT

At the southern limit of permafrost degradation in the southern Northwest Territories (NT), Canada, permafrost is typically restricted to forested peat plateaus, that are elevated above the surrounding wetland complex. With climate warming, permafrost thaw can result in the waterlogging of the trees and collapse of the forested plateaus. These landscape changes can impact lake ecosystems by altering watershed hydrological connections and the amount and the nature of terrestrial organic material that is entering the lakes, contributing to lake “browning”. This in turn can affect important aquatic ecological processes. To understand how lakes have responded to accelerated permafrost degradation over the past few decades in the southern NT, where long-term monitoring records are scarce, the field of paleolimnology offers an indirect way to reconstruct long-term environmental change by using proxy data preserved in lake sediment cores. A study that paired paleolimnology and remote sensing to investigate the response of two small lakes in the Tathlina Lake watershed to permafrost thaw showed that although both lakes experienced substantial permafrost thaw in their catchments, their sediments recorded divergent environmental trajectories, with only one tracking increased dissolved organic carbon concentrations (i.e. lake browning). Drawing on this study, research in the Scotty Creek basin, where landscape changes over the last several decades have been well-established, is investigating how hydrologic setting might be driving the variability in response of small lakes to permafrost thaw. Future studies will focus on a chain of cascading lakes that differ in their lake water chemistry and hydrological connections.

KEYWORDS

Permafrost thaw; dissolved organic carbon; lake browning; paleolimnology; subarctic

1. INTRODUCTION

At the southern limit of permafrost, rapid permafrost degradation is resulting in dramatic and widespread alterations of the landscape as mean annual air temperatures approach 0°C. In the southern Northwest Territories (NT), Canada, permafrost is typically restricted to forested patches, or peat plateaus, that are elevated above the surrounding wetland complex. As the permafrost thaws, soils become waterlogged, resulting in the transition of forests into wetlands and altering the connectivity of waterbodies. Another consequence of permafrost thaw is the increased availability of terrestrial organic matter (t-OM) that was previously stored in the permafrost and, coupled with alterations in hydrologic connectivity in the catchment (which increases the potential for transport of this liberated t-OM), can result in increased export of dissolved organic material (DOM) into aquatic ecosystems. Dissolved organic carbon (DOC), which constitutes a large fraction of DOM, has been described as the “great modulator” of aquatic ecosystems as it influences other variables such as temperature, light, and dissolved oxygen concentrations (Prairie 2008; Vonk et al. 2015). For example, the browning of lakes caused by increases in chromophoric dissolved

organic matter (CDOM), reduces the amount of light that can penetrate into the water column, limiting primary productivity and increasing carbon subsidies for heterotrophic respiration. These changes can result in a shift from an autotrophic to a heterotrophic system, with implications for lake oxygen dynamics (Vonk et al. 2015). Increased lake water DOC concentrations in permafrost thaw-affected catchments has been observed across the circumpolar north (e.g. Coleman et al. 2015; Wauthy et al. 2018).

Understanding the long-term impacts of permafrost degradation on aquatic ecosystems is challenging due to a scarcity of long-term monitoring records in these remote regions. Fortunately, the field of paleolimnology offers an indirect way to reconstruct long-term environmental change by using chemical, biological, and physical proxy data preserved in lake sediment cores. Diatoms, a group of unicellular algae with siliceous cell walls that preserve well in sediments, are an important paleolimnological proxy that have been useful for tracking changes in lake habitat, lake depth, and water quality variables such as pH and DOC (dissolved organic carbon)(e.g. Pienitz & Smol 1999; Michelutti et al. 2003; Coleman et al. 2015; Hargan et al. 2015). Therefore, diatoms can be a useful proxy for tracking lake response to permafrost thaw, including changes in DOC and water depth that may occur as a result of thermokarst processes.

In this study, we reconstructed long-term environmental change in two small lakes in the sporadic discontinuous permafrost zone near Kakisa, Northwest Territories (NT), which is experiencing widespread permafrost degradation. (Coleman et al. 2015). Our objective was to assess the potential limnological implications of the northward migration of the permafrost boundary as a result of climate warming.

2. METHODS

2.1 Study Site Description

Two study lakes (KAK-1 and TAH-7; unofficial names) were selected from the Taiga Plains Mid-Boreal ecozone near Tathlina Lake and Kakisa Lake (Figure 1), within the sporadic permafrost zone (10-50% areal extent of permafrost). This region has been warming since at least the end of the 19th century (Coleman et al. 2015). Both lakes are shallow (maximum depth <2m) and have a surface area of <4ha. DOC in KAK-1 is 36.1 mg/L, and colour is 32 TCU. TAH-7 has DOC of 46.7 mg/L, and colour of 91 TCU.

2.2 Aerial Imagery Analysis

Collapsed peat scars, where permafrost degradation has resulted in the waterlogging and collapse of forested plateaus, are evident in aerial images and can be used to track permafrost thaw in the catchment (Quinton et al. 2011). Manual digitization of collapsed scars and calculation of areal extent of scars of a 1 km² area centred around the two study lakes were done in ArcMap (v. 10).

2.2.1 Sedimentary analysis

Sediment cores were collected from KAK-1 and TAH-7 in March of 2013, and sectioned at 0.5 cm intervals. Core chronologies were established using ²¹⁰Pb activity and the constant rate of supply (CRS) model (Appleby & Oldfield 1978). Diatom valves were identified and counted to reconstruct environmental change in the study lakes (e.g. Smol et al. 2005), and visible reflectance spectroscopy was used to reconstruct sedimentary chlorophyll *a* to infer changes in lake primary production (Michelutti et al. 2005). Diatom species diversity for each interval was calculated using

the Hills N2 index (Hill 1973). Biostratigraphic zones of similar species assemblages were delineated using a constrained incremental sum of squares cluster analysis (CONISS) (Grimm 1987).

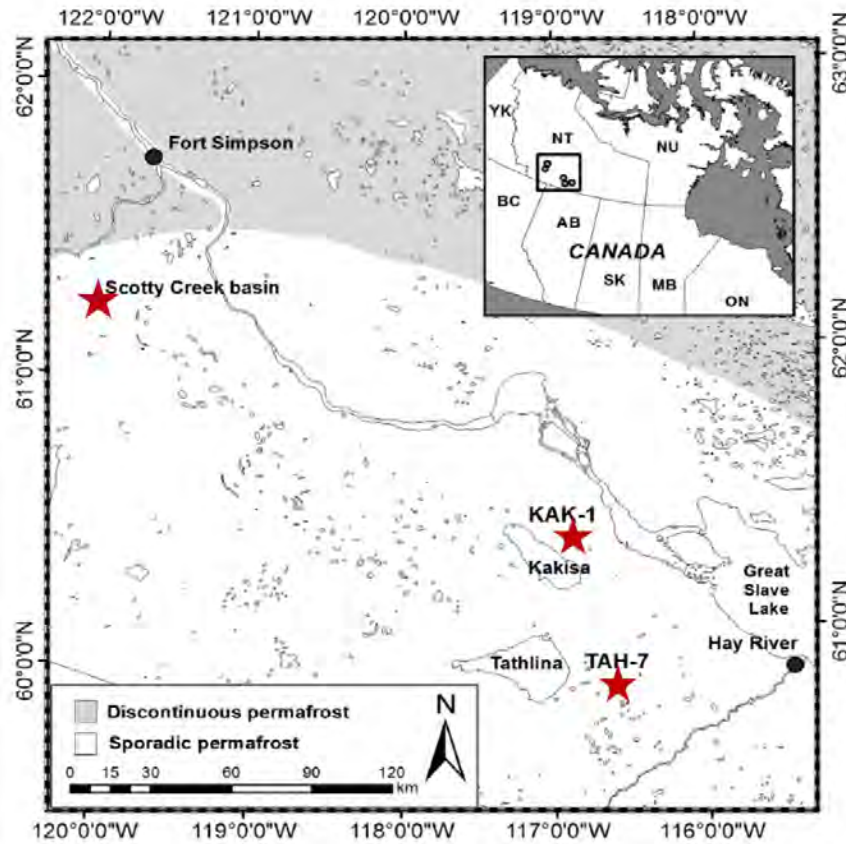


Figure 1. Map of locations of study lakes in the Tathlina Lake watershed (KAK-1 and TAH-7) and site of ongoing research in the Scotty Creek basin. Inset shows location of study regions within Canada. Figure modified from Coleman et al. (2015).

3. RESULTS AND DISCUSSION

Substantial permafrost collapse was identified in the analysis of the remotely-sensed images for both lake catchments, with a collapsed area of 0.24 km² in 1970 compared to 0.34 km² in 2012 for KAK-1, and 0.14 km² in 1971 compared to 0.25 km² in 2012 for TAH-7 (Figure 2).

The sediment core retrieved from KAK-1 recorded fairly stable lake conditions until ~1991 when the assemblage shifted from large benthic species (e.g. large *Navicula* species) to an increased proportion of species that attach to substrates (e.g. *Encyonopsis descripta*, *Encyonema hebridicum* and *E. silesiacum*, and *Kobayasiella jaagii* and *K. subtilissima*) (Figure 3). This is indicative of the development of a more complex periphytic habitat. Coincident with this shift was an increase in diatom species diversity and an increase in primary production. These trends have been observed in other northern lakes, and are consistent with a warming climate that results in a longer growing season and a more developed littoral habitat (E.g. Smol & Douglas 2007).

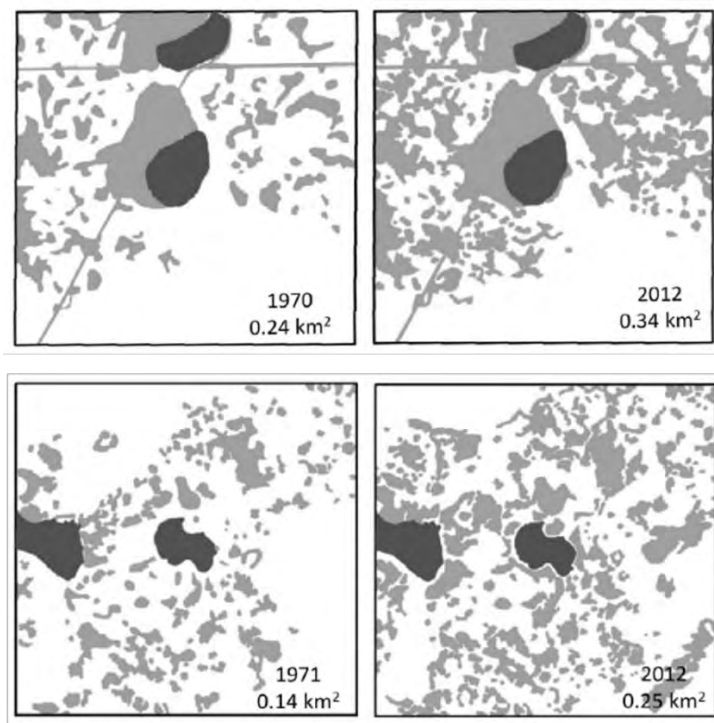


Figure 2. The area occupied by collapsed permafrost scars in a 1 km² area centred around A) KAK-1 in 1970 and 2012; and B) TAH-7 in 1971 and 2012. Modified from Coleman et al. (2015).

Analysis of the sediment core retrieved from TAH-7 captures a longer time period, and a more dynamic environmental history, compared to KAK-1 (Figure 4). In the earliest part of the sediment record, the species assemblage was dominated by epiphytic species that commonly attach to submerged vegetation (e.g. *Encyonema* species and *Kobayasiella jaagii*) and is indicative of a dry or shallow lake environment at this time. At 32 cm, the epiphytic species decline and are replaced by large *Navicula* species, similar to what was identified in the earlier zone in the KAK-1 core and is indicative of a wetter lake environment. At 17.5 cm (~1845) a decrease in large *Navicula* species and a corresponding increase in epiphytic species was recorded (e.g. *Encyonema minuta*), similar to the recent changes that are recorded in KAK-1. The most recent species assemblage shift that occurred in TAH-7 (~1960) was a decrease in epiphytic species and an increase in small benthic species (*Navicula* spp. and *Fragilaria* spp.), which are typically found in harsher, low light conditions (Smol et al. 2005), for example as a result of increasing DOC concentrations, (e.g. Pienitz et al. 1999).

We inferred that this change in diatom species assemblage is tracking an increase in DOC in TAH-7 occurring as a result of the thawing of permafrost peat plateaus; however, no increase in DOC was inferred for KAK-1, despite also being impacted by thawing permafrost. We suggest that the differing trajectories of limnological change in TAH-7 and KAK-1 may be related to present-day hydrological connectivity that modulates the response of these lakes to permafrost degradation.

Wetland-dominated basins are common at the southern extent of permafrost in the NT, and consist of forested peat plateaus, which generate runoff to neighbouring wetlands, flat bogs, which function as water storage, and channel fens, which convey water towards the basin outlet (Hayashi et al.

2004; Quinton et al. 2009; 2011). As plateaus collapse, the proportion of previously isolated bogs that become hydrologically connected to channel fens increases, thereby increasing the contributing runoff area within basins (Connon et al 2014). The number and the type of wetlands that are hydrologically connected to inflows may influence how lakes respond to permafrost degradation as wetlands are sites of DOM transformation and, additionally, bogs and fens process DOM differently (Gordon et al. 2016; Olefeldt et al. 2012). Hydrologic connections to other lakes may also serve to mute the response of lakes to changes in the catchment (Bertolet et al. 2018).

The hydrology of TAH-7 and KAK-1 is unknown. Therefore, in order to further investigate the influence of hydrological connectivity on trajectories of limnological change (particularly for DOC), we have initiated new research on lakes at the Scotty Creek field station near Fort Simpson, NT (Figure 1), where extensive hydrological studies and permafrost mapping have been conducted (Quinton et al. 2009; 2011).

KAK-1

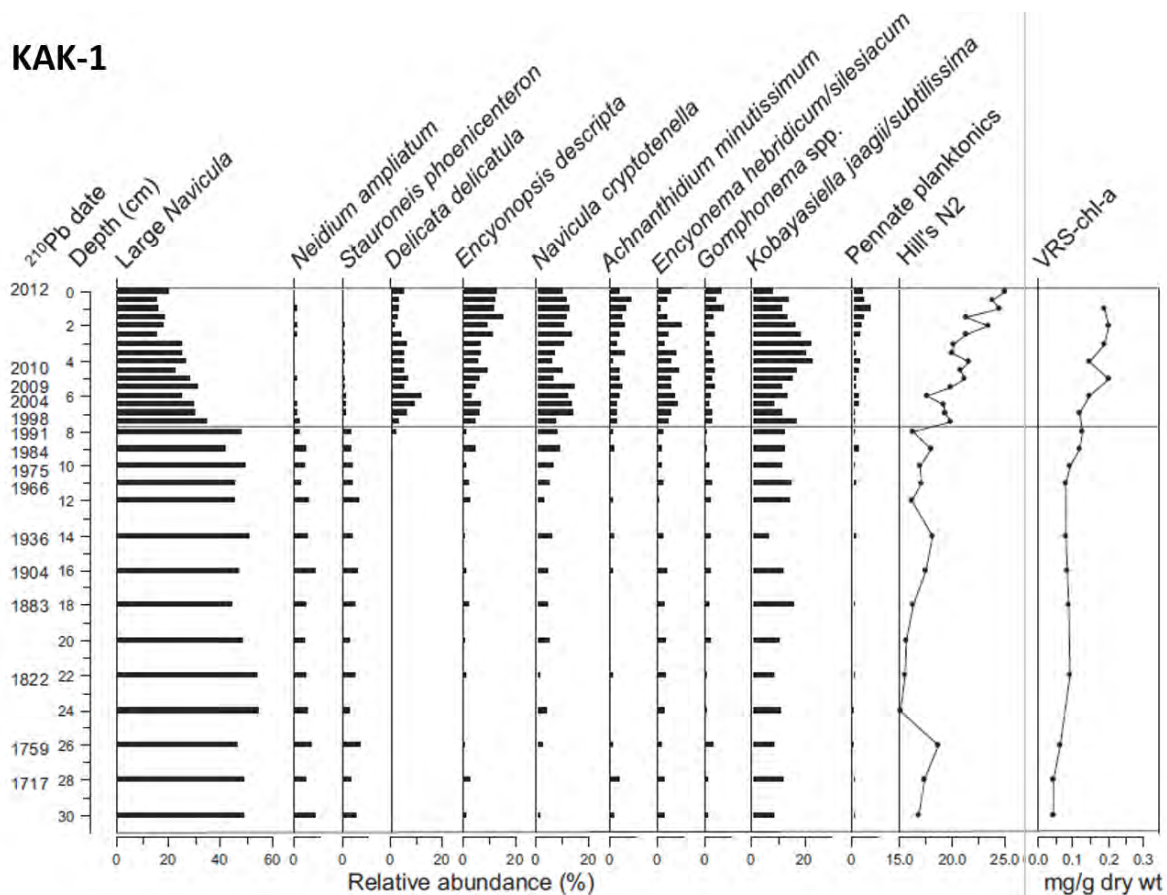


Figure 3. Relative abundance diagram for KAK-1 displaying changes in relative diatom species abundance, Hill's N2 diversity index, and visible reflectance spectroscopy inferred sedimentary chlorophyll-a (VRS-chl-a). Vertical lines delineate biostratigraphic zones based on CONISS cluster analysis. Figure modified from Coleman et al. (2015).

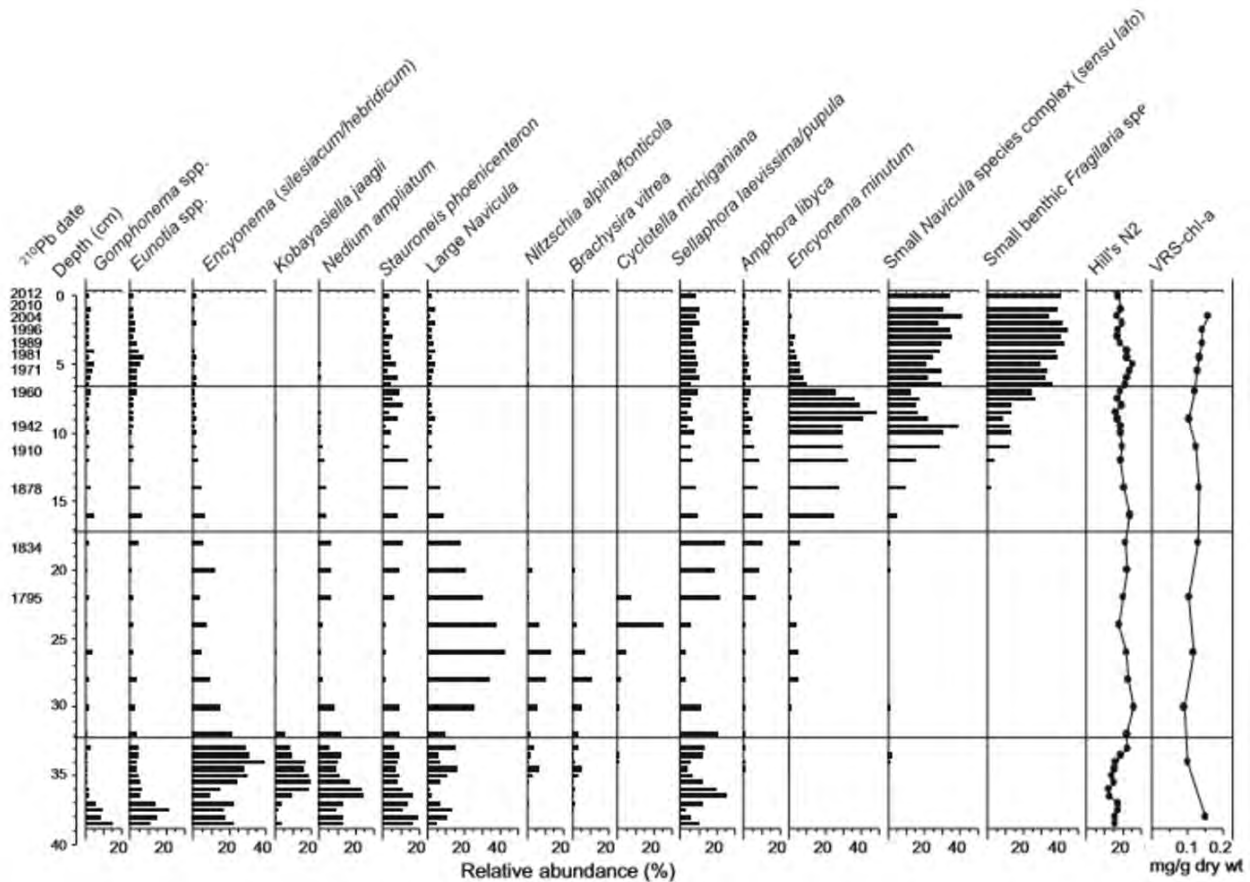


Figure 4. Relative abundance diagram for TAH-7 displaying changes in relative diatom species abundance, Hill's N2 diversity index, and visible reflectance spectroscopy inferred sedimentary chlorophyll-a (VRS-chl-a). Vertical lines delineate biostratigraphic zones based on CONISS cluster analysis. Figure modified from Coleman et al. (2015).

4. FUTURE RESEARCH: THE SCOTTY CREEK BASIN

The Scotty Creek basin (Figure 1) is situated in the lower Liard River valley within the sporadic permafrost zone and is the site of intensive research investigating the impacts of permafrost thaw on basin hydrology that has been ongoing for the past ~ two decades (e.g. Hayashi et al. 2004; Quinton et al. 2003; 2009; 2011; Connon et al. 2014). Drawing on research from the Tathlina Lake watershed as described above, current and future research objectives at Scotty Creek basin are aimed at understanding the variability in lake responses to permafrost degradation.

In order to investigate the range of variability in trajectories of lake ecosystem change, water samples and sediment cores were retrieved in July 2018 from 16 lakes within the lower Liard River valley, including the Scotty Creek basin (Figure 5). Sediment cores will be analysed in a “before/after” study design, where diatoms will be identified in the top surface sample (representing present-day conditions), and compared against a sediment sample that was deposited prior to the onset of warming and rapid permafrost thaw in this region (~1850). This will provide a snapshot of regional variation in post-industrial lake ecosystem change. Preliminary examination of analyses of water chemistry variables indicates that lakes in close proximity to each other can have markedly

different water chemistry. For example Goose Lake and First Lake (unofficial name), which are located less than 700 metres apart and are connected by a channel fen, both have similar DOC (23 mg/L and 22 mg/L, respectively); however First Lake has remarkably higher colour (249 TCU) than Goose Lake (53 TCU). This suggests that the DOC is compositionally different between the two lakes.

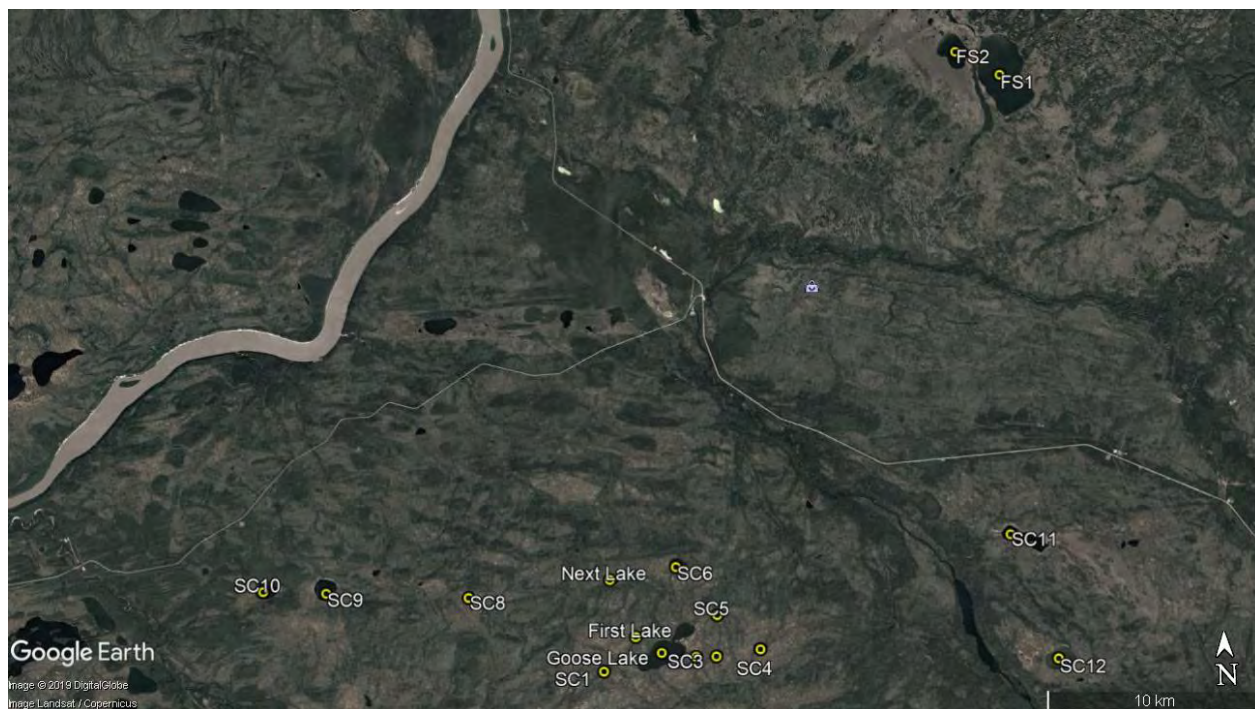


Figure 5: Map showing of the locations of 16 study lakes in the lower Liard River valley sampled in July 2018.

To understand the role of hydrologic connectivity as a driver of present-day limnology and lake response to permafrost degradation, a subset of lakes [Goose L., First L. and Next L. (unofficial name)] were selected for detailed study. These lakes are a part of a chain of cascading lakes connected by channel fens, situated within the well-studied Scotty Creek basin (Figure 6). In June, 2019, light, temperature, oxygen, and water depth data loggers were deployed in Goose Lake and First Lake to track changes in these variables over the open-water season (June to September). Similar to research in the Tathlina Lake watershed, detailed analyses (diatoms, organic content, chl-*a*) of sediment cores collected from these lakes will be used to reconstruct environmental conditions over the past ~300 years, to examine the variability in response of these lakes to permafrost degradation in the context of their hydrological setting. Surface sediment samples and water samples from sites within the lake and along connecting channel fens, and one bog site (Figure 6), were also collected. Water samples will be analysed for water chemistry, including DOM quantity and quality (composition), to assess how connecting channel fens and surrounding bogs may affect lake water chemistry, particularly through processing of DOM. Sediment samples will be used to examine how hydrological setting influences diatom assemblages, and will assist in the interpretation of sediment core analyses. This research will increase our understanding of the mechanisms underlying lake ecological and biogeochemical responses to permafrost degradation

and assist in making predictions on how aquatic ecosystems will respond in the future, particularly as the permafrost boundary moves northward.

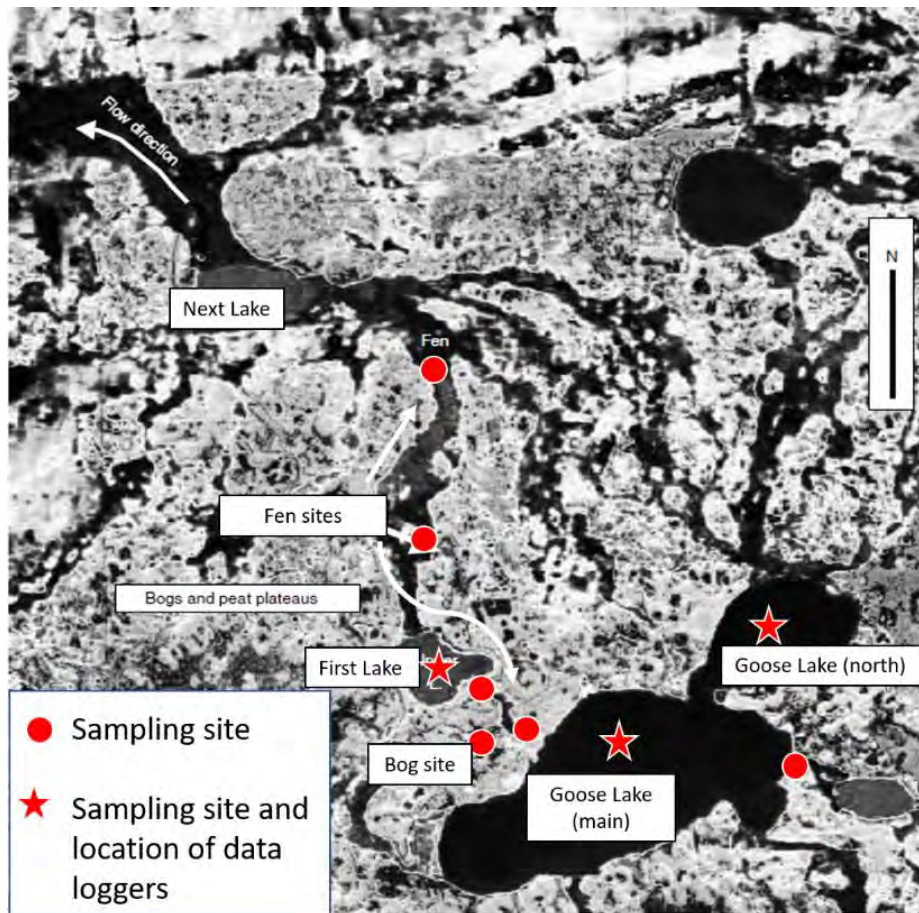


Figure 6. Location of water and surface sediment sampling sites and data loggers deployed in June 2019, within the cascading chain of lakes, including lake, fen, and bog sites.

ACKNOWLEDGMENTS

This research is funded by the Natural Sciences and Engineering Research Council of Canada (NSERC) and the Government of the Northwest Territories Cumulative Impacts Monitoring program (CIMP). Logistics and fieldwork support was provided by the Ka'a'gee Tu First Nation in Kakisa, NT. These projects are the result of collaborations with Dr. John Smol (Queen's University), Dr. Jules Blais (University of Ottawa), Dr. Mike Pisaric (Brock University), Michael Palmer (Carleton University) and Dr. William Quinton (Wilfrid Laurier University). Arnab Shuvo (York University) assisted with fieldwork.

REFERENCES

- Appleby, P.G. & Oldfield, F., 1978. The calculation of lead-210 dates assuming a constant rate of supply of unsupported ^{210}Pb to the sediment. *Catena*. 5(1): 1-8.
- Coleman, K.A., Palmer, M.J., Korosi, J.B., Kokelj, S.V., Jackson, K., Hargan, K.E., Mustaphi,

- C.J.C., Thienpont, J.R., Kimpe, L.E., Blais, J.M. & Pisaric, M.F. 2015. Tracking the impacts of recent warming and thaw of permafrost peatlands on aquatic ecosystems: a multi-proxy approach using remote sensing and lake sediments. *Boreal Environ. Res.* 20: 363-377.
- Connon, R.F., Quinton, W.L., Craig, J.R., & Hayashi, M. 2014. Changing hydrologic connectivity due to permafrost thaw in the lower Liard River valley, NWT, Canada: Changing hydrologic connectivity due to permafrost thaw. *Hydrol. Process.* 28: 4163–4178.
- Gordon, J., Quinton, W., Branfireun, B.A., & Olefeldt, D. 2016. Mercury and methylmercury biogeochemistry in a thawing permafrost wetland complex, Northwest Territories, Canada. *Hydrol. Process.* 30: 3627-3638.
- Grimm, E. 1987. CONISS: A Fortran 77 Program for stratigraphically constrained cluster analysis by the method of incremental sum of squares. *Comput. Geosci.* 13: 13–35.
- Hargan, K.E., Rühland, K.M., Paterson, A.M., Finkelstein, S.A., Holmquist, J.R., MacDonald, G.M., Keller, W. and Smol, J.P. 2014. The influence of water-table depth and pH on the spatial distribution of diatom species in peatlands of the Boreal Shield and Hudson Plains, Canada. *Botany.* 93(2): 57-74.
- Hayashi, M., Quinton, W.L., Pietroniro, A., & Gibson, J.J. 2004. Hydrologic functions of wetlands in a discontinuous permafrost basin indicated by isotopic and chemical signatures. *J. Hydrol.* 296: 81–97.
- Hill, M.O. 1973. Diversity and evenness - unifying notation and its consequences. *Ecology.* 54: 427–432.
- Michelutti, N., Holtham, A.J., Douglas, M.S. & Smol, J.P. 2003. Periphytic diatom assemblages from ultra-oligotrophic and UV transparent lakes and ponds on Victoria Island and comparisons with other diatom surveys in the Canadian arctic. *J. Phycol.* 39(3): 465-480.
- Michelutti, N., Wolfe, A.P., Vindebrooke, R.D., Rivard, B. & Briner, J. 2005. Recent primary production increases in arctic lakes. *Geophys. Res. Lett.* 32, L19715.
- Olefeldt, D., & Roulet, N.T., 2012. Effects of permafrost and hydrology on the composition and transport of dissolved organic carbon in a subarctic peatland complex: DOC in a subarctic peatland complex. *J. Geophys. Res. Biogeosci.* 117: G1
- Pienitz, R., Smol, J.P. & MacDonald, G.M. 1999. Paleolimnological reconstruction of Holocene climatic trends from two boreal treeline lakes, Northwest Territories, Canada. *Arc. Antarc. Alp. Res.* 31(1): 82-93.
- Prairie, Y.T. 2008. Carbocentric limnology: looking back, looking forward. *Can. J. Fish. Aquat. Sci.* 65: 543–548.
- Quinton, W.L., Hayashi, M., & Pietroniro, A. 2003. Connectivity and storage functions of channel fens and flat bogs in northern basins. *Hydrol. Process.* 17: 3665–3684
- Quinton, W.L., Hayashi, M., & Chasmer, L.E. 2009. Peatland Hydrology of Discontinuous Permafrost in the Northwest Territories: Overview and Synthesis. *Can. Water Resour. J.* 34: 311–328.

- Quinton, W.L., Hayashi, M., & Chasmer, L.E. 2011. Permafrost-thaw-induced land-cover change in the Canadian subarctic: implications for water resources. *Hydrol. Process.* 25: 152–158.
- Smol, J.P. & Douglas, M.S.V. 2007. From controversy to consensus: making the case for recent climate change in the Arctic using lake sediments. *Front Ecol. Environ.* 59: 466–474.
- Smol, J.P., Wolfe, A.P., Birks, H.J.B., Douglas, M.S.V., Jones, V.J., Korhola, A., Pienitz, R., Rühland, K.M., Sorvari, S., Antoniades, D., Brooks, S.J., Fallu, M.-A., Hughes, M., Keatley, B. E., Laing, T.E., Michelutti, N., Nazarova, L., Nyman, M., Paterson, A.M., Perren, B., Quinlan, R., Rautio, M., Saulnier-Talbot, E., Siitonen, S., Solovieva, N. & Weckstrom, J. 2005. Climate-driven regime shifts in the biological communities of arctic lakes. *PNAS USA*, 102: 4397–4402
- Vonk, J.E., Tank, S.E., Bowden, W.B., Laurion, I., Vincent, W.F., Alekseychik, P., Amyot, M., Billet, M.F., Canario, J., Cory, R.M. & Deshpande, B.N. 2015. Reviews and syntheses: Effects of permafrost thaw on Arctic aquatic ecosystems. *Biogeosciences*. 12(23): 7129-7167.
- Wauthy, M., Rautio, M., Christoffersen, K.S., Forsström, L., Laurion, I., Mariash, H.L., Peura, S., and Vincent, W.F. 2018. Increasing dominance of terrigenous organic matter in circumpolar freshwaters due to permafrost thaw: Increasing allochthony in arctic freshwaters. *Limnol. Oceanogr. Lett.* 3: 186–198.

Changing streamflow patterns in Canada's Northwest Territories

R.F. Connon^{1*}, A. E. Coles¹, and S.A. Kokelj¹

¹*Environment and Natural Resources, Government of the Northwest Territories, Yellowknife, Northwest Territories, X1A 2L9, Canada*

**Corresponding author's email address: Ryan_Connon@gov.nt.ca*

ABSTRACT

Air temperatures in northern Canada are increasing at a rapid rate. In a region that is underlain by permafrost of varying temperature and distribution, and where snow and ice blanket the landscape for six to eight months of the year, changes in air temperature and precipitation regimes can have a direct impact on surface and subsurface hydrological processes, especially in the late fall and early winter. For example, the length of the season with snow cover is decreasing, allowing a greater proportion of incoming energy to be consumed by evapotranspiration and ground thaw. In the Northwest Territories (NWT), Canada, many streams are undergoing regime change, which is not always concomitant with changes in precipitation patterns. Here, we use Water Survey of Canada gauged streamflow data from nival regime-dominated streams to investigate the ubiquity of these changes. Although streamflow patterns are not changing everywhere across the NWT, commonalities are evident in most regions. For example, there is a general trend towards earlier freshet (*i.e.* spring snowmelt). While total freshet volumes remain relatively unchanged, the proportion of annual streamflow that occurs during the freshet is decreasing, while there is an increase in fall and winter flows. This additional volume of water flowing in winter is leading to increased icing formation, which has implications for infrastructure where flowpaths intersect highways.

KEYWORDS

Northern hydrology; subsurface flow; winter flow; permafrost

1. INTRODUCTION

Northern basins are being affected by changes to the timing and magnitude of precipitation events, (Spence *et al.*, 2011; Vincent *et al.*, 2015), changes to the physical properties of the subsurface in response to thawing permafrost and shifting seasonal freeze-thaw patterns (Connon *et al.*, 2018; St. Jacques and Sauchyn, 2009), and by changes in river icing dynamics (Morse and Wolfe, 2017). An improved understanding of hydrological processes is necessary to predict how northern basins will respond to the threats of climate change on decadal timescales.

There are three major long-term research basins in the Northwest Territories (NWT), each in a distinct ecological region. Collectively, the process-based research in these basins greatly improves our understanding of the cycling and storage of water, and provides an indication of how these processes may be changing in response to a warming climate. These research basins are located in Baker Creek (Taiga Shield, discontinuous permafrost), Scotty Creek (Taiga Plains, sporadic-discontinuous permafrost), and Trail Valley Creek (Southern Arctic tundra, continuous permafrost). This paper focuses on runoff processes and regimes in these three main ecological regions.

1.1 Taiga Shield

Runoff generation in the Taiga Shield is controlled primarily by fill-and-spill processes that drive rapidly expanding and contracting contributing areas in response to basin wetness (Spence and Woo, 2003, 2006). Runoff in these basins is generally controlled by large headwater lakes, which act as ‘gatekeepers’, and do not release runoff until their internal storage capacity has been met and the water level of the lake exceeds the level of the outlet sill (Mielko and Woo, 2006; Phillips *et al.*, 2011). Pre-existing dry or wet conditions therefore exert a primary control on hydrological connectivity and contributing area of the basin (Spence *et al.*, 2010). Changing precipitation patterns in this region have led to an increase in fall rainfall events (Spence *et al.*, 2011) that can increase soil moisture content prior to freeze-up. This changing precipitation regime has caused a regime shift in small catchments in the Taiga Shield towards a combined nival-pluvial streamflow regime, where autumn runoff peaks can rival those of the spring freshet (Spence *et al.*, 2011). Furthermore, icing development in river networks in the Canadian Shield is related to antecedent fall moisture conditions and winter runoff (Morse and Wolfe, 2017), suggesting that climatic shifts that result in a higher frequency of fall and winter flow events may lead to increased icing events in the Shield region (Morse and Wolfe, 2017).

1.2 Taiga Plains

Streamflow generation in the Taiga Plains is initiated in wetland-dominated headwaters, before being routed through upland sites once a stream network is formed. Near the southern end of the NWT, wetlands are comprised mainly of peatland complexes and are underlain by discontinuous permafrost, whereas the upland terrain is typically permafrost-free. In the headwaters, permafrost bodies often take the form of forested peat plateaus, which shed water to adjacent permafrost-free wetlands (Wright *et al.*, 2008). Once water enters wetlands, it is either routed to a channel fen which drains into the stream network, or retained internally as storage if lateral drainage is prevented by the presence of permafrost bodies (Quinton *et al.*, 2003). As permafrost thaws, these impermeable barriers to subsurface flow are disappearing and hydrological connectivity is increasing (Connon *et al.*, 2014). Recent studies have shown dewatering of wetlands as hydrological connectivity increases, leading to a transient increase in basin streamflow (Connon *et al.*, 2015; Haynes *et al.*, 2018). Although it is evident that thawing permafrost is changing the routing of water to the stream network, the long term trajectory of hydrological change in these regions is still uncertain.

1.3 Arctic Tundra

The Arctic tundra is underlain by thick continuous permafrost which serves as an effective aquitard between near-surface suprapermafrost groundwater and deep subpermafrost groundwater stores (Woo, 2012). Runoff generation in tundra environments is dependent largely on soil properties in the thawed portion of the active layer. Runoff in these environments is driven largely by snowmelt (Woo, 1983); however recent studies have demonstrated the increasing importance of summer rainfall events on the basin hydrograph (Lamoureux and Lafrenière, 2017). In southern tundra sites in the NWT, organic materials frequently blanket the surface. The high porosity and hydraulic conductivity of an organic and/or peat cover typically prevent overland flow (Woo, 2012). As a result, subsurface flow is the predominant hillslope runoff mechanism. As the hydraulic conductivity of peat can drop by orders of magnitude within the top 30 cm (Quinton *et al.*, 2008), runoff is most rapid when the water table is in the highly conductive upper peat layer (Quinn and Marsh, 1999). This indicates that basin storage capacity increases as the active layer thaws, but late

summer/early fall precipitation events that saturate the soil can provide a mechanism for sustained streamflow events during this period given sufficient antecedent moisture conditions. Shi *et al.* (2015) showed a changing streamflow regime at Trail Valley Creek in the southern Arctic tundra. They found a non-intuitive coupling of an earlier onset of snowmelt and a delayed onset of streamflow. Slightly further south, at Havikpak Creek, Krogh and Pomeroy (2019) used the Cold Regions Hydrological Model to demonstrate both an earlier and increased volume of the spring freshet under a climate warming scenario. The uncertainty in the literature about how these regions are responding and will continue to respond to warming temperatures implies that more work must be completed to understand the complex interplay between these climatic and hydrological processes.

This study will attempt to build on previous process-based field and modelling studies completed in the NWT to investigate observed changes to streamflow regimes. The main objective of this study is to explore annual and seasonal changes in streamflow and to suggest causal effects.

2. METHODOLOGY AND STUDY SITE

Ten hydrometric stations operated by the Water Survey of Canada in the Northwest Territories were chosen for analysis (Table 1). These stations were selected as they cover a range of basin sizes ($5.4 \times 10^2 - 1.3 \times 10^6 \text{ km}^2$) and terrain types across the territory (see Figure 1). Trends were evaluated using the non-parametric Mann-Kendall test at significance levels of $p \leq 0.1$, $p \leq 0.05$, and $p \leq 0.01$. Hydrometric data were acquired from the HYDAT database.

Table 1. Selected hydrometric stations operated by the Water Survey of Canada in the Northwest Territories

Station ID	Station Name	Lat	Long	Period of Record		Basin Area (km ²)
				Start	End	
10GC001	Mackenzie River at Fort Simpson	61.868	-121.359	1938	2017	1 301 435
10ED002	Liard River near the mouth	61.743	-121.228	1972	2017	275 000
10MC002	Peel River above Fort McPherson	67.259	-134.889	1969	2017	70 600
10PB001	Coppermine River at outlet of Point Lake	65.416	-114.008	1965	2017	19 200
07SB010	Cameron River below Reid Lake	62.491	-113.523	1975	2017	3630
07OB001	Hay River near Hay River	60.743	-115.860	1972	2017	51 700
10EB001	South Nahanni River above Virginia Falls	61.636	-125.979	1962	2017	14 500
10MA003	La Martre River below outlet of Lac La Martre	63.108	-116.975	1975	2017	13 900
10ED003	Birch River at Highway No. 7	61.334	-122.895	1974	2017	542
10LC007	Caribou Creek above Highway No. 8	68.087	-133.492	1975	2017	590

3. RESULTS AND DISCUSSION

In general, there are no significant changes in annual streamflow rates across the NWT (Figure 2). However, the seasonality of flows is showing some significant changes. Most notably, flows in the winter are increasing across the territory. Changes in winter baseflow in northern Canada have been discussed previously (Connon *et al.*, 2014, St. Jacques and Sauchyn 2009, Walvoord and Streigl, 2007), however the mechanisms that cause these changes likely differ in response to geology and soil composition. Spence *et al.* (2011) showed changing precipitation trends – and ultimately, an

increase in fall runoff events, close to Yellowknife, yet our analysis shows that increases to fall runoff events are not common across the territory: while some basins exhibit increasing flows, others show no trend (Figure 3). Again, these changes are likely associated with basin characteristics and are discussed in more detail below.

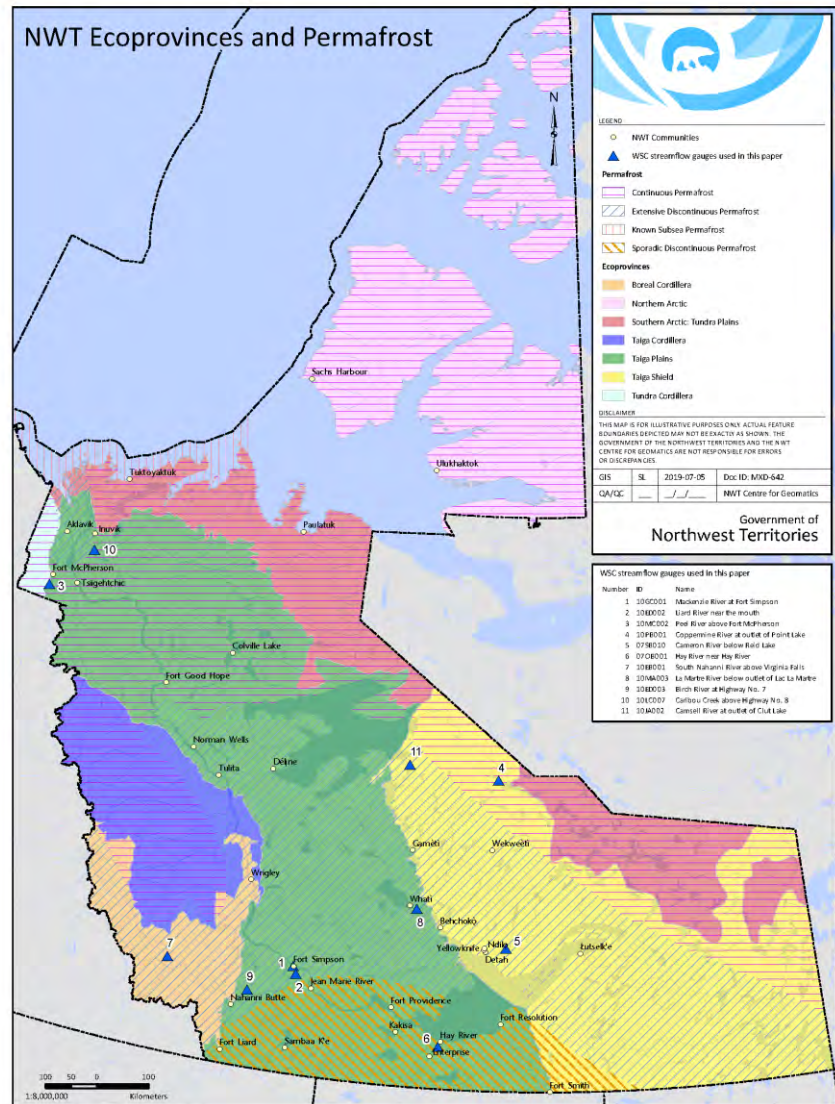


Figure 1. Map of ecological and permafrost regions in the NWT and locations of the ten hydrometric stations used in this analysis (also includes Camsell River, see section 3.4).

3.1 Taiga Shield

Basins within the Taiga Shield (e.g. Cameron River) show neither significant change in flows over time, or in seasonality of flows. As suggested by Spence *et al.* (2010), runoff generation in this region is strongly dependent on antecedent moisture conditions and pre-existing hydrological connectivity. The distribution of annual and seasonal flows for the Cameron River (Figures 2 - 4) provides an indication of this control. For example, annual runoff remained high for two periods in the early 1990s and 2000s, while it remained low during periods in the late 1980s, mid-1990s, and mid-2010s. Due to the strong control that bedrock exerts on runoff generation, hydrological regime

change in these basins would be controlled more strongly by changing precipitation patterns rather than changes to the way in which water is cycled and stored. Warmer temperatures may also induce more frequent instances of river icing formation in the winter, as spatial coverage of icings is a product of sustained winter baseflow and rapid winter warming intervals (Morse and Wolfe, 2017). The building of icings may result in a delayed recession limb after the spring freshet, as the melting of icings can provide sustained runoff to the stream network.

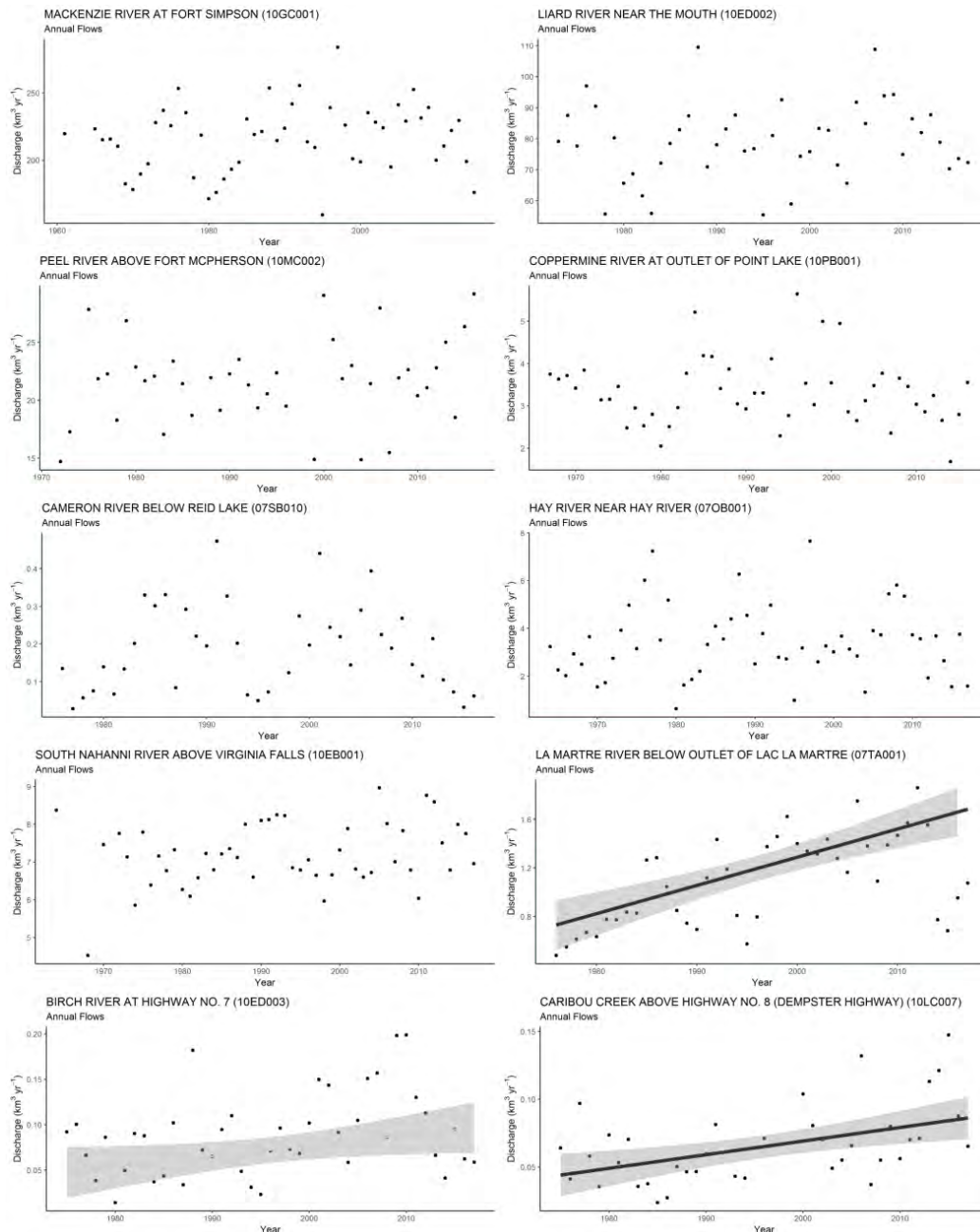


Figure 2. Changes in annual flows over time in the Northwest Territories. Annual flow calculations required a minimum of 350 days of data per year. Dark gray line: $p < 0.01$; medium gray line: $p < 0.05$; light gray line: $p < 0.1$. No trend line indicates no significant trend ($p \geq 0.1$).

3.2 Taiga Plains

Basins in the discontinuous permafrost region of the Taiga Plains are undergoing rapid permafrost thaw (Carpino *et al.*, 2018), which is having a direct impact on runoff generation processes (Wright *et al.*, 2008). Connon *et al.* (2014) documented a significant increase in annual streamflow in the lower Liard River basin between 1996 and 2012, but a series of dry years has slowed that trend (*e.g.* Figure 2, Birch River). It is hypothesized that changes to basin hydrological connectivity resulting from permafrost thaw can significantly increase basin contributing area during years with high precipitation input, but have a negligible effect if a certain precipitation threshold is not reached (Connon *et al.*, 2015). The observed increases in winter baseflow in these regions may be a combined result of talik development between the active layer and permafrost (Connon *et al.*, 2018; Haynes *et al.*, 2018) and increased recharge of subpermafrost groundwater resulting from permafrost thaw (St. Jacques and Sauchyn, 2009). Together, these two processes indicate that over-winter subsurface hydrology is becoming a non-negligible component of the basin water balance. This suggests that changes to hydrology in this region can be driven by a combination of changes to the seasonality of precipitation and climate warming-induced permafrost thaw that alters the structure of subsurface flowpaths.

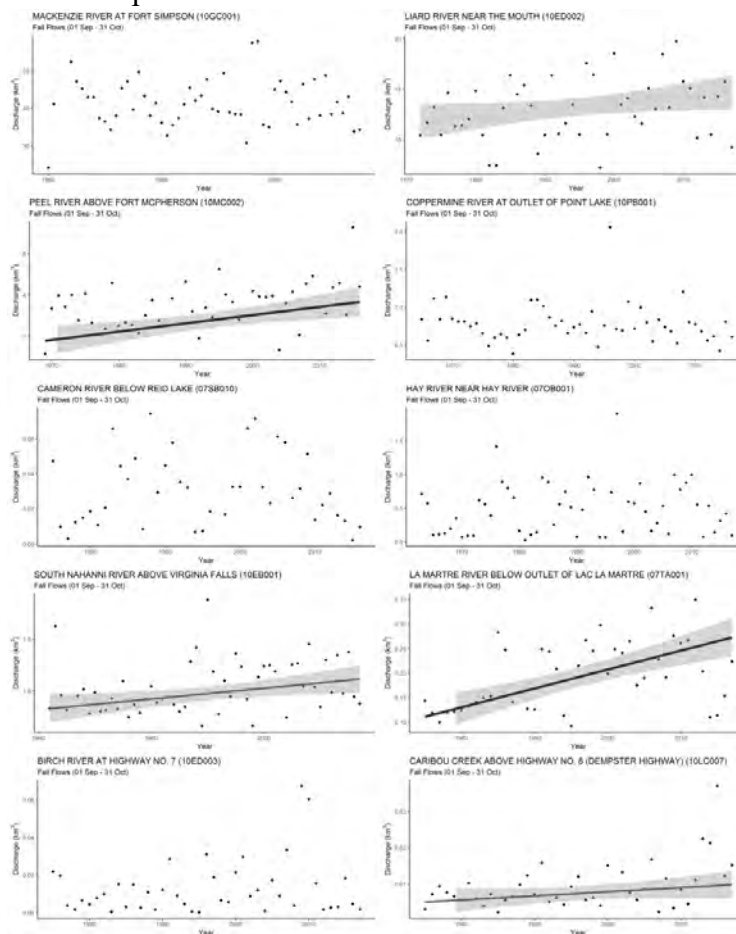


Figure 3. Changes in fall flows over time in the Northwest Territories. Fall flows were calculated between 01 Sep and 30 Nov and required a minimum of 45 days of data per year. Dark gray line: $p < 0.01$; medium gray line: $p < 0.05$; light gray line: $p < 0.01$. No trend line indicates no significant trend ($p \geq 0.1$).

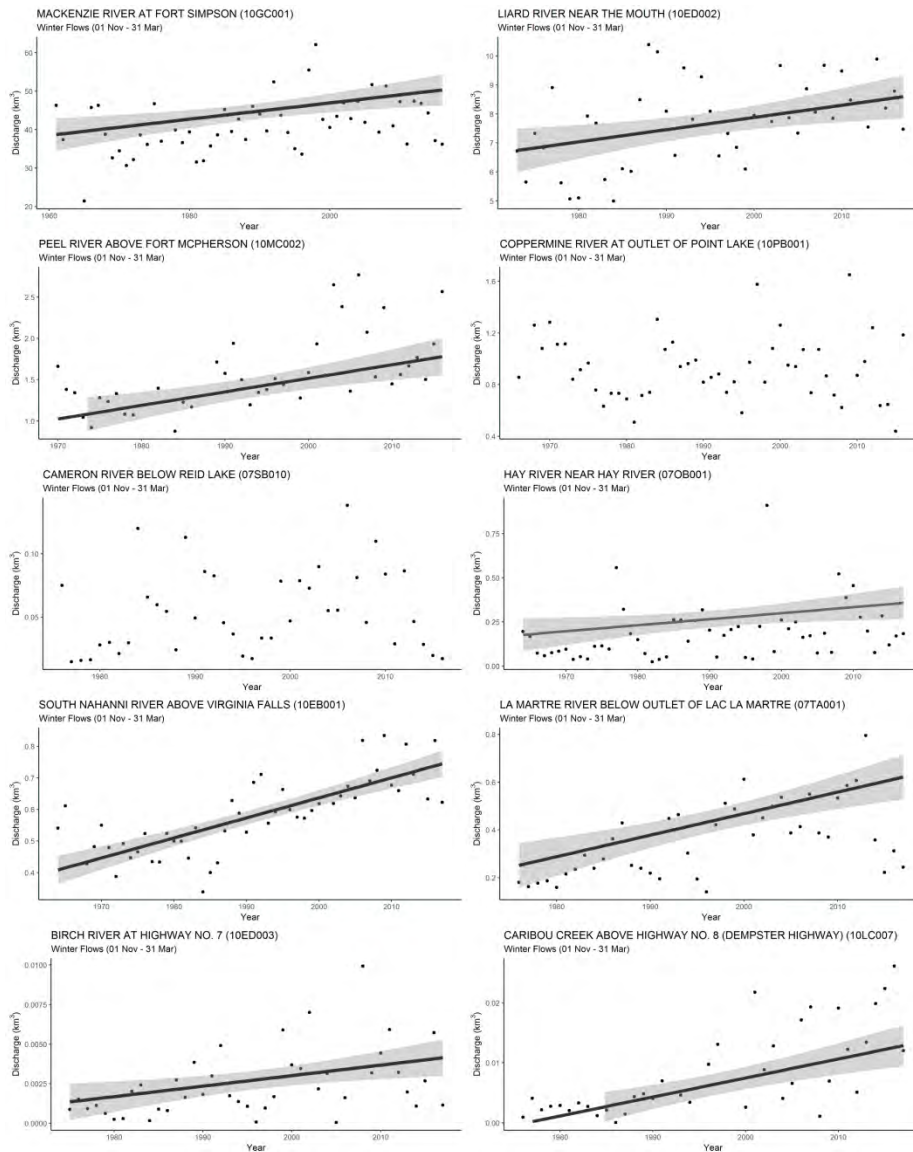


Figure 4: Changes in winter flows over time in the Northwest Territories. Winter flows were calculated between 01 Nov and 31 Mar and required a minimum of 120 days of data per year. Dark gray line: $p < 0.01$; medium gray line: $p < 0.05$; light gray line: $p < 0.01$. No trend line indicates no significant trend ($p \geq 0.1$).

3.3 Arctic Tundra

In regions of continuous permafrost, vertical subsurface drainage is greatly restricted which thereby promotes a reasonably high water table for the duration of summer. It is possible that increasing fall wetness will increase soil moisture prior to winter, thereby altering the thermal regimes of riparian areas and streambed channels by changing latent heat requirements for soil freeze-back. This theory is supported by a significant increase in fall runoff events in basins underlain by continuous permafrost (Figure 3, Caribou Creek and Peel River). In a modelling experiment at Havikpak Creek (near Inuvik, NWT), Krogh and Pomeroy (2019) predict an increase in fall runoff events in the future, but, due to the small basin size (15 km^2), the creek will freeze to the bed and

will not produce runoff in the winter. Due to the thickness of permafrost in tundra environments, it is unlikely that thawing permafrost will change subsurface flowpaths in the same manner as southern sites underlain by discontinuous permafrost. An increase in fall precipitation that saturates the soil can significantly change freeze-back dates, especially in organic-rich soils with high porosity. As a result, subsurface flow can extend further into the winter. When these open subsurface flowpaths intersect frozen ground (e.g. a roadway without significant snow accumulation), subsurface water is extruded to the surface and can form icings. These icings present challenges to northern infrastructure, which can result in costly maintenance.

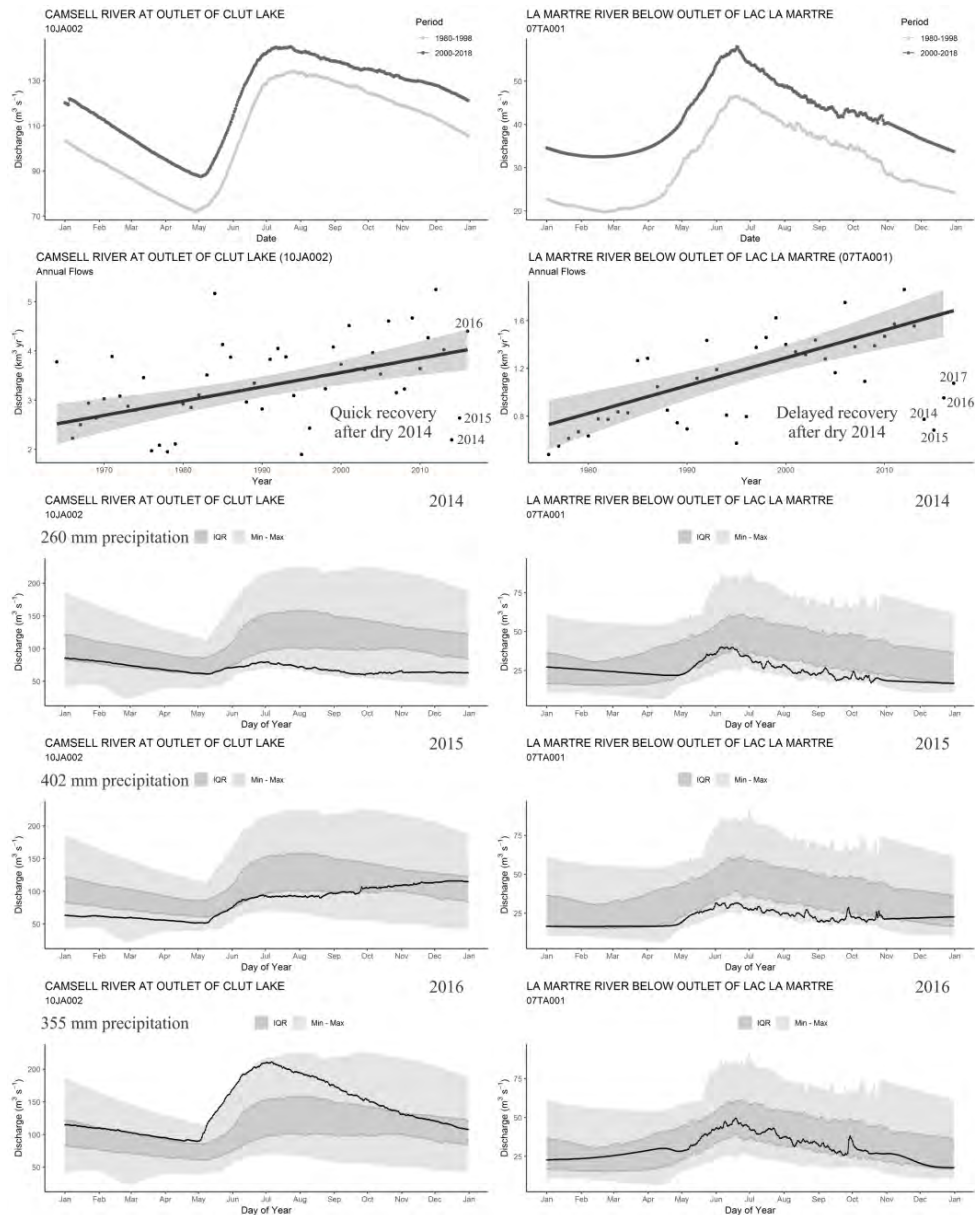


Figure 5: Comparison of Camsell River and La Martre River. Both rivers exhibit a significant increasing annual trend. Runoff events are depicted for 2014 (260 mm precipitation), 2015 (402 mm precipitation), and 2016 (355 mm precipitation) and demonstrates how the basins respond to a dry year.

3.4 Case Study of La Martre and Camsell Rivers

The La Martre and Camsell rivers drain south into Great Slave Lake and north into Great Bear Lake, respectively. The two basins are located near each other geographically (see Figure 1) and both straddle the border of the central Taiga Plains and Taiga Shield. Both basins are in data scarce regions. Both basins are exhibiting high magnitude, significant increases in total annual streamflow (Figure 5). Composite hydrographs for the periods 1980- 1998 and 2000- 2018 show a distinct increase in flow volume for the entire course of the year. Both gauging stations are located at the outlet of a large lake, suggesting that storage is the primary factor governing streamflow. The summer of 2014 was very dry across the whole of the NWT, and provides an interesting case study to investigate how the basins respond to dry years (Figure 5). Both basins eventually return to normal flow levels after the dry summer, however the Camsell River returns more rapidly than the La Martre River. The dry period did not permanently change the increase in flow trajectory of either river, suggesting that the increased streamflow levels are a new normal. This is in contrast to the response of other basins in both the Taiga Shield and the Taiga Plains, where dry years can effectively ‘reset’ basin memory and streamflow returns to low volumes. It is hypothesized that high water levels may be caused by reactivation of large subpermafrost aquifers resulting from permafrost thaw. These aquifers may discharge enough water into basin lakes to create a higher regional hydraulic head, which sustains increased streamflow.

4. SUMMARY AND CONCLUSIONS

The NWT is comprised of many different ecological regions, each with unique geological and surficial predispositions that govern the flux and storage of runoff. The mechanisms by which these basins respond to climate change and permafrost thaw are also unique. With the exception of basins in the central Taiga Plains and Shield (between Great Bear and Great Slave Lakes), total annual flows remain relatively constant. In the central Taiga, significant increases to flows throughout the course of the year suggest a fundamental shift in flow regimes. There have been few process-based field studies in this region to identify how runoff generation is changing, and the mechanisms responsible for this shift. Most rivers in the NWT display increasing winter flows, while approximately half of the gauged basins show an increase in fall flows. The volume of winter streamflow remains relatively low, and therefore has little impact on changing total annual volumes. Increased winter flows may be of concern, however, due to its potential impacts on northern infrastructure, as active flowpaths may result in increases in river and ground icings.

ACKNOWLEDGEMENTS

We would like to thank the Water Survey of Canada for providing streamflow data used for the analysis of this project. We would also like to thank Shawn Larocque and Douglas Sauer of the NWT Centre for Geomatics for preparing the map. We would also like to thank Drs. Steve Kokelj (Northwest Territories Geological Survey), Phil Marsh (Wilfrid Laurier University), William Quinton (Wilfrid Laurier University), and Chris Spence (Environment Canada) for insightful conversations over the past several years to better understand runoff generation processes across the Northwest Territories.

REFERENCES

- Carpino, O.A., A.A. Berg, W.L. Quinton, and J.R. Adams (2018), Climate change and permafrost thaw-induced boreal forest loss in northwestern Canada, *Environ. Res. Lett.* (13) 1-13.
- Connon, R.F., É. Devoie, M. Hayashi, T. Veness, and W.L. Quinton (2018), The influence of shallow taliks on permafrost thaw and active layer dynamics in subarctic Canada, *J. Geophys. Res.*, 123
- Connon, R.F., W.L. Quinton, J.R. Craig, J. Hanisch, and O. Sonnentag (2015). The hydrology of interconnected bog complexes in discontinuous permafrost terrains, *Hydrol. Process.*, 29, 3831-3847.
- Connon, R.F., W.L. Quinton, J.R. Craig, and M. Hayashi (2014), Changing hydrologic connectivity due to permafrost thaw in the lower Liard River valley, NWT, Canada, *Hydrol. Process.*, 28, 4163-4178.
- Haynes, K.M., R.F. Connon, and W.L. Quinton (2018), Permafrost thaw induced drying of wetlands at Scotty Creek, NWT, Canada, *Environ. Res. Lett.*, (13) 1-13.
- Krogh, S.A., and J.W. Pomeroy (2019), Impact of future climate and vegetation on the hydrology of an Arctic headwater basin at the tundra-taiga transition, *J. Hydrometeorol.*, 197-215.
- Lamoureux, S.F., and N.J. Lafrenière (2017), More than just snowmelt: integrated watershed science for changing climate and permafrost at the Cape Bounty Arctic Watershed Observatory, *WIREs Water*. e1255.
- Mielko, C., and M.K. Woo (2006), Snowmelt runoff processes in a headwater lake and its catchment, subarctic Canadian Shield, *Hydrol. Process.*, 20, 987-1000.
- Morse, P.D., and S.A. Wolfe (2017), Lon-term river icing dynamics in discontinuous permafrost, subarctic Canadian Shield, *Permafrost and Periglac. Process.* (28) 580-586.
- Phillips, R.W., C. Spence, and J.W. Pomeroy (2011), Connectivity and runoff dynamics in heterogenous basins, *Hydrol. Process.*, 25, 3061-3075.
- Quinton, W.L., M. Hayashi, and S.K. Carey (2008), Peat hydraulic conductivity in cold regions and its relation to pore size and geometry, *Hydrol. Process.*, 22(15), 2829-2837.
- Quinton, W.L., M. Hayashi, A. Pietroniro (2003), Connectivity and storage functions of channel fans and flat bogs in northern basins, *Hydrol. Process.*, 17, 3665-3684.
- Quinton, W.L., and P. Marsh (1999), A conceptual framework for runoff generation in a permafrost environment, *Permafrost and Periglac. Process.*, 9, 213-228.
- Shi, X., P. Marsh, and D. Yang (2015), Warming spring air temperatures, but delayed spring streamflow in an Arctic headwater basin, *Environ. Res. Lett.* (10) 1-10.
- Spence, C., S.V. Kokelj, and E. Ehsanzadeh (2011), Precipitation trends contribute to stream flow regime shifts in northern Canada, *IAHS*, 346, 3-8.
- Spence, C. X.J. Guan, R. Phillips, N. Hedstrom, R. Granger, and B. Reid (2010), Storage dynamics and streamflow in a catchment with a variable contributing area, *Hydrol. Process.*, 24(16), 2209-2221.
- Spence, C., and M.K. Woo (2006), Hydrology of subarctic Canadian Shield: heterogeneous headwater basins, *J. Hydrol.*, 317(1-2), 138-154.
- Spence, C., and M.K. Woo (2003), Hydrology of subarctic Canadian shield: soil-filled valleys, *J. Hydrol.*, 279(1-4), 151-166.
- St. Jacques, J.M., and D.J. Sauchyn (2009), Increasing winter baseflow and mean annual streamflow from possible permafrost thawing in the Northwest Territories, Canada, *Geophys. Res. Lett.*, 36, L01401.

- Vincent, L., X. Zhang, R. Brown, Y. Feng, E. Mekis, E. Milewska, H. Wan, and X. Wang (2015), Observed trends in Canada's climate and influence of low-frequency variability modes, *J. Climate*, 28, 4545-4560.
- Walvoord, M.A., and R.F. Striegl (2007), Increased groundwater to stream discharge from permafrost thawing in the Yukon River Basin: potential impacts on lateral export of carbon and nitrogen, *Geophys. Res. Lett.*, 34(12), L12402.
- Wright, N., W.L. Quinton, and M. Hayashi (2008), Hillslope runoff from an ice-cored peat plateau in a discontinuous permafrost basin, Northwest Territories, Canada, *Hydrol. Process.*, 22, 2816-2828.
- Woo, M.K. (2012), *Permafrost Hydrology*, Springer-Verlag, Berlin.
- Woo, M.K. (1983), Hydrology of a drainage basin in the Canadian high Arctic, *Ann. Assoc. Am. Geograph.*, (73) 577-596.

Mackenzie DataStream: Mobilizing open water data for decision-making and collaborative water stewardship in the Mackenzie River Basin

Carolyn DuBois¹ and Lindsay Day^{1*}

¹*The Gordon Foundation, Toronto, Ontario M5E 1W1, CANADA*

**Corresponding author's email address: Lindsay@gordonfn.org*

ABSTRACT

Diverse water monitoring programs led by Indigenous and non-Indigenous governments, academic research groups, communities and watershed organizations are generating valuable information to track the health of Northern freshwater ecosystems. Yet these datasets can be difficult to access and, in some cases, are not available at all. DataStream is designed to address this challenge by providing an open access, online platform for sharing and accessing water quality data. DataStream was first launched in the Mackenzie River Basin where it was developed through a unique collaboration between The Gordon Foundation and the Government of the Northwest Territories. In building Mackenzie DataStream (www.MackenzieDataStream.ca), we sought to provide an independent home for data that would facilitate the sharing of information collected through diverse monitoring initiatives of varying scale, focus, and approach; and across multiple, sometimes overlapping, jurisdictional boundaries. DataStream is designed to align with, and support, open data standards and best practices including FAIR (findable, accessible, interoperable and reusable) data principles. With enormous potential to support evidence-based decision-making, DataStream is now being scaled up in collaboration with other regional monitoring networks, most recently in the Lake Winnipeg Basin and Atlantic Canada. In the face of increasingly complex environmental changes, solid, transparent and open data infrastructure will be foundational to sustaining the health of shared water resources so that information can be stored and shared in accessible, effective and sustainable ways.

KEYWORDS

Water quality; open data; data repository; community-based monitoring; Mackenzie River Basin

Predicting Changes in Discontinuous Permafrost using an Interface Model of Soil Freezing and Thawing

É. G. Devoie^{1*}, J. R. Craig¹, and W. L. Quinton²

¹*Civil and Environmental Engineering, University of Waterloo, Waterloo, Ontario, N2L 3G1, CANADA*

²*Cold Regions Research Centre, Wilfrid Laurier University, Waterloo, Ontario, N2L 3C5, CANADA*

**Corresponding author's email address: egdevoie@uwaterloo.ca*

ABSTRACT

A fast physically-based interface model of active layer evolution and permafrost thaw is presented. This computationally efficient, semi-analytical, non-equilibrium solution to soil the freeze-thaw problem is proposed as a component of hydrological models to describe seasonal ground ice, active layer and permafrost evolution. The model is developed and validated against the Stefan problem and a benchmarked numerical model. Unlike similar semi-analytic models, the interface model does not assume a linear temperature profile. It incorporates both saturated and unsaturated soil conditions. Water balance results are compared to a coupled continuum model including the unsaturated Richards equation and thermal energy balance to assess the validity of simplifying assumptions made in model development. The model is implemented for use in discontinuous permafrost peatlands where soil properties are highly dependent on soil ice content. This model is used to simulate the formation and evolution of taliks (perennially thawed soil in permafrost environments) in the discontinuous permafrost region. Simulation results are compared with field data collected at the Scotty Creek Research Station. Long-term simulations are made possible using this efficient model. The efficiency of the model also allows for practical sensitivity and uncertainty analyses which are unwieldy with more computationally expensive representations of active layer and permafrost. Future extensions of the model may include the addition of frost heave. It is proposed that this model be included in hydrological modelling software for better and faster predictions in cold-regions basins and areas underlain by seasonal ground ice.

KEYWORDS

Discontinuous permafrost; freeze-thaw; hydrology; permafrost modelling; semi-analytical

1. INTRODUCTION

Modelling is a useful tool to test hypotheses about system function and project possible future system states. In the discontinuous permafrost environment, the appropriate representation of permafrost and seasonal ground ice thaw is essential. The presence of frozen soil strongly affects not only the hydrology, but also the thermodynamics, soil chemistry and ecology of regions experiencing freezing soils (Hayashi 2013). Practically, it is essential to accurately model soil freeze-thaw because it controls many important processes including infiltration, the migration of soil moisture to the surface during freezing, winter quiescence of hydrological systems, and the destabilization of soils, especially in the permafrost region (Gray et al. 2001; Harlan 1973; Stähli et al. 1999; Woo 2012; Nelson et al. 2001). To date, the most accurate models representing discontinuous permafrost been local continuum models such as SUTRA-ICE (McClymont et al. 2013, McKenzie et al. 2007).

Though these models accurately represent non-equilibrium processes of soil freeze thaw, and have the ability to simulate multiple thawing fronts in complex domains, they are notoriously numerically expensive (Slater et al. 1998). This can make them inappropriate for large-scale modelling, sensitivity analysis, or hypothesis testing, and leads to the desire to use more efficient 1-D vertical freeze-thaw models, such as NEST and many others (Atchley et al. 2015, Goodrich 1978, Yu Zhang et al. 2003). Though these models solve the heat equation only in one spatial dimension, they can be coupled through source/sink terms to approximate important lateral fluxes (Hinzman et al. 1998). A study site can be broken into HRUs representing the thermal properties of the soil allowing for semi-distributed freeze-thaw modelling. However these 1-D models are still computationally demanding (Kurylyk et al. 2014), which can deter multiple simulations.

In an effort to solve the freeze-thaw problem more efficiently, analytical or semi-analytical solutions have been proposed. These solutions make simplifying assumptions so that it is possible to solve the heat equation directly. These simplifications include neglecting sensible heat transfer (Hayashi et al. 2007), assuming an equilibrium temperature profile (Woo et al. 2004), time-invariant soil properties (Semenova and Lebedeva 2013), tracking only one freeze/thaw interface (Krogh et al. 2017) and simplifying surface boundary conditions (Woo et al. 2004), among others. A comprehensive review of current thermal models was completed by Kurylyk & Watanabe (2013).

Freeze-thaw models based on analytic or semi-analytic solutions of the Stefan problem (e.g. Hayashi et al. 2007; Hinzman et al. 1998; Krogh et al. 2017; Semenova & Lebedeva 2013; Woo et al. 2004; Zhang et al. 2003) cannot represent the dynamic three-tiered system (permafrost-talik-active layer). These models may be inappropriate for modelling degrading permafrost at the local scale because they assume a single (often linear) temperature profile between the soil surface and the (single) freeze/thaw front. It is thought that the formation of taliks is the first step in permafrost degradation (Connon et al. 2018). Existing continuum models that do not assume a linear temperature profile (e.g. McKenzie & McKenzie 2007; Zhang et al. 2008; Frampton et al. 2011; Daanen et al. 2008; Karra et al. 2014; Schaefer et al. 2009) have thus far focused on longer-term lateral permafrost extent, water seepage, or other processes not associated with the formation and expansion of isolated taliks.

The initiation of an isolated talik has been simulated by Frampton et al. 2011; Atchley et al. 2015; Yi et al. 2014; Endrizzi et al. 2014 and Rawlins et al. 2013, where controls on the active layer such as saturation, snow cover, and ponded water were quantified. These studies shed light on processes governing active layer thickness as defined by maximum thaw depth, but talik formation was not their focus.

The aim here is to address the need for a computationally efficient, physically-based semi-analytical model of active layer evolution and permafrost thaw. This semi-analytical, non-equilibrium solution to soil the freeze-thaw problem does not place constraints on temperature boundary conditions, allows multiple and dynamic freeze/thaw fronts to be tracked simultaneously, tracks only a small number of state variables and does not neglect sensible heat. This model is proposed as a component of hydrological models to describe seasonal frost, active layer and permafrost evolution.

2. METHODS

The initial proposed interface model represents the ground using one to four (with the potential for more) representative dynamic domain elements, depending on the season and history. This progression is conceptually represented in Figure 1. In order to track the evolution of the system, it is necessary to know the energy stored in each element (in this case the energy is stored as a mean temperature), as well as the temperature gradients at the interface between elements to drive evolution of these interfaces, where the change in interface position is given by:

$$\Delta z = -\frac{1}{\eta\rho L_f} \left[\lambda_{z+} \left(\frac{\partial T}{\partial z} \right)_{z+} - \lambda_{z-} \left(\frac{\partial T}{\partial z} \right)_{z-} \right] \quad [1]$$

Where z is depth, η is porosity, ρ is density, L_f is latent heat of fusion, λ is thermal conductivity and T is temperature.

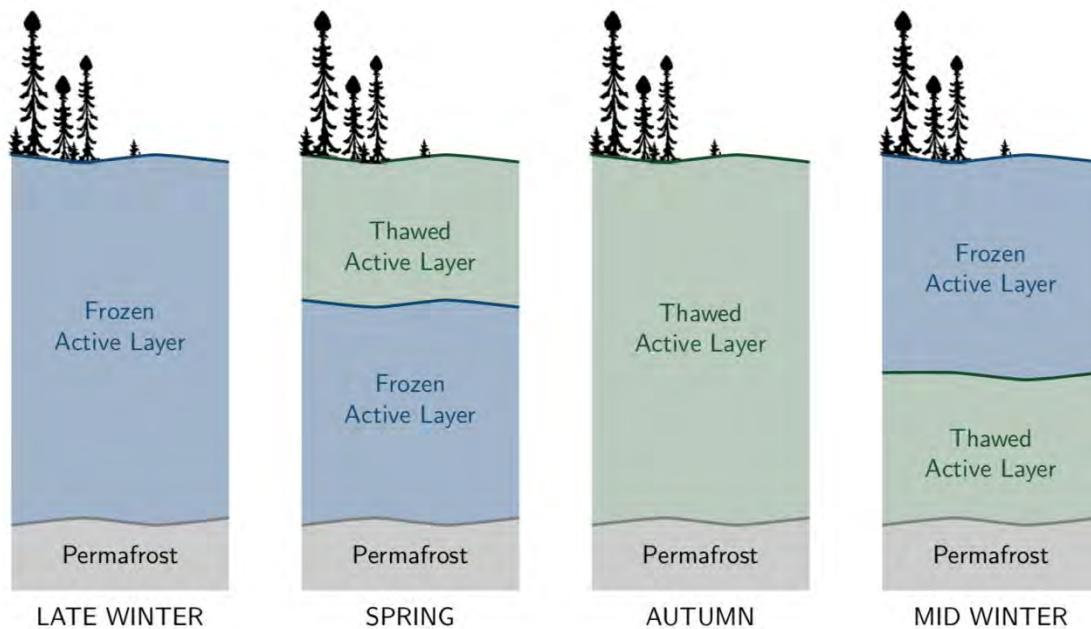


Figure 1. Seasonal transition in soil profile

2.1 Free-boundary Problem

The temperature of the surface element, whether thawed or frozen, is governed by the heat equation with an arbitrary, time-dependent boundary condition. The solution to the heat equation in a fixed domain with constant boundary conditions presented by Carslaw & Jaeger 1959 can be extended to solve this problem by applying the principle of superposition. This principle can be repeated for consecutive arbitrary perturbations in surface temperature, allowing the underlying layer to respond directly to the history of applied surface forcing temperature. Note that this relieves the need to track the entire temperature profile at points in this surface layer, as we need only a representative temperature (energy), and the gradient at the base of the layer to compute the heat flux and consequently the change in thickness and the reduction in mean temperature.

This solution is exact in a domain of fixed length when an infinite number of terms are retained. Given the high thermal conductivity of water and high porosity of peat soils found at the study site, truncating the sum results in little error. In order to account for a change in length, a linear stretching

of the profile is assumed, which results in an over-estimate of the energy contained in the profile. Note that this applies both in the frozen and thawed case, where the difference lies only in the values of thermal conductivity and heat capacity.

2.2 Confined Layer

A confined layer of thawed (or frozen) soil between the frozen (thawed) surface and the underlying permafrost (perennially thawed ground) is possible (e.g. SPRING and MID-WINTER in Figure 1). In these cases, the heat equation is subject to isothermal boundary conditions at the freezing point, and it is assumed that the initial temperature profile can be approximated by a sinusoidal relationship. A linear correction is applied to this solution to account for changes in length of the profile. A zero or a linear gradient is assumed in the underlying permafrost, with some constant temperature defined at the bottom boundary, and the surface of this layer at the freezing point.

2.3 Mass Balance

Mass transport and unsaturated soil is implemented in the profile through an additional surface layer. When the soil column is unsaturated, the water table position is calculated. Above the water table, the soil is assigned a uniform moisture, and instead of explicitly tracking interfaces in this unsaturated layer, it is also assigned a fractional ice content, allowing it to exist in a partially-frozen, partially saturated state. Thermal and hydraulic properties of the soil are dependent on the soil moisture and ice content.

3. RESULTS AND DISCUSSION

Two benchmarking exercises are presented to validate the model, first the free boundary problem is compared to the Neumann solution (Kurylyk et al. 2014), and secondly the confined layer solution is benchmarked against a continuum finite volume model. The utility of the model is demonstrated by comparing the efficiency of the interface model and the continuum model for the confined case. Finally, a representative one-year simulation of a permafrost is presented as an example application of the model.

3.1 Neumann Solution Benchmark

The interface model solution is compared to the analytical Neumann solution for thermal properties of pure water with an initial temperature of 0°C and an imposed surface temperature of 5°C in Figure 2. The error in thaw depth approximation was approximately 0.5 cm over the course of the 100-day simulation, and over a 1000-day simulation the error grew to approximately 1 cm.

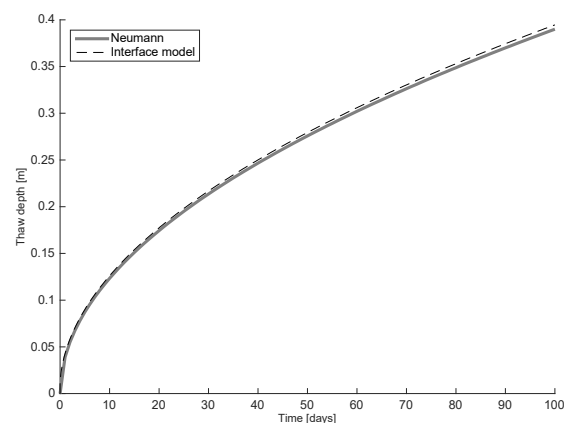


Figure 2. Neumann solution benchmark, interface model subject to constant temperature boundary condition as in Neumann problem.

3.2 Confined Layer Benchmark

The confined problem can be benchmarked against an analytical energy balance, where the sensible heat contained in an initial temperature profile is used as latent heat to determine the expected thaw. This expected thaw is shown as filled circles in Figure 2 while the modelled temperature profile over the course of a 1000-day simulation is shown as curves which get progressively darker with time. After 100 days, the modelled solution reproduces 100.23 % of the predicted thaw with an initial length of $L = 0.1$ m and $T_0 = 1^\circ\text{C}$.

3.3 Model Comparison

The confined case was further compared to a continuum model solving the same problem with the same initial conditions on the same domain. Over the 1000-day simulation, the continuum model resulted in 79 % of the analytically computed thaw, with temperature profiles nearly identical to Figure 3. This comparison was made using the total loss of ice content as a proxy for change in profile length since partially frozen soil is allowed to exist in the continuum model where a soil freezing curve was defined between -0.05 and 0°C . The equilibrium condition for this simulation would be an isothermal, uniformly partially

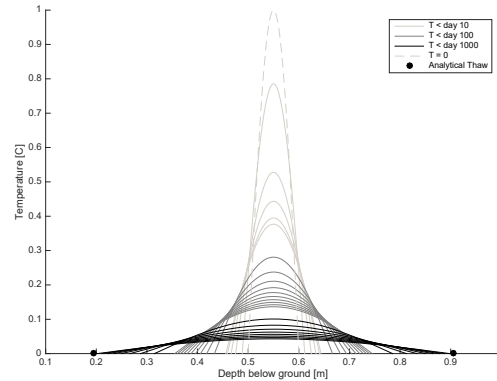


Figure 3. Benchmarking confined problem for a 1000 day simulation, temperature profiles are plotted at uneven timesteps and get darker as time progresses. Note that the profiles are calculated for visualization and are not necessary for tracking the interface.

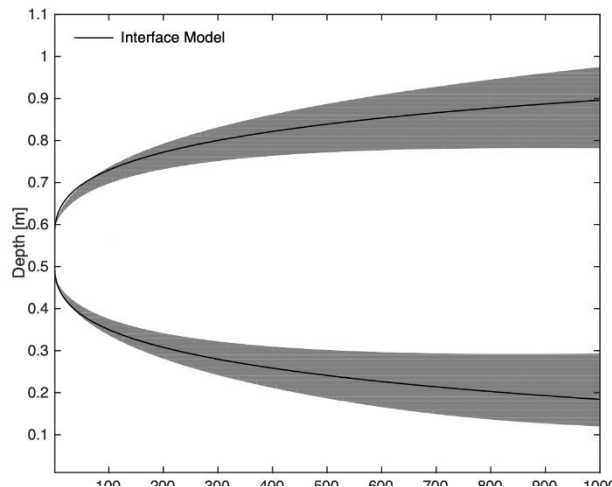


Figure 4. Interface location of interface model (solid line) compared with contour plot of temperature generated from continuum model data. Note that the interface is located between 0 and -0.05 , the region over which the freezing function is defined.

frozen soil column where the change in total ice content is expected to be slightly less than the predicted sharp-interface problem because of the sensible heat included in the non-isothermal phase change. For this reason, the results are also compared in Figure 4, where the freezing front modelled using the interface model falls beyond the -0.025°C isotherm, where the ice content is 50 %.

This simulation had a computational time of 0.681 s using the interface model, while the continuum model ran for 28.1 min s to solve the same problem. This represents a ~ 2500 -fold increase in model efficiency, making previously computationally prohibitive tasks such as sensitivity or uncertainty analyses, model calibration, and Monte-Carlo simulations feasible.

3.4 Example Application

The interface model was developed for the representation of active layer evolution and changes in permafrost table in hydrological modelling. Figure 5 presents a representative one-year simulation of ground ice and soil moisture conditions, forced with a temperature profile measured in the field and a simple sinusoidal surface water flux. The results of this simulation is consistent with field observations made on peat plateaux at the Scotty Creek Research Station, where high porosity soils are near saturation year-round (Connon et al., 2018).

This simulation demonstrates that arbitrary temperature or flux profiles are sufficient as a surface boundary condition. This tool is not only applicable in permafrost environments, it can be easily extended to represent seasonal ground ice in more temperate regions by changing the boundary and initial conditions as well as soil properties.

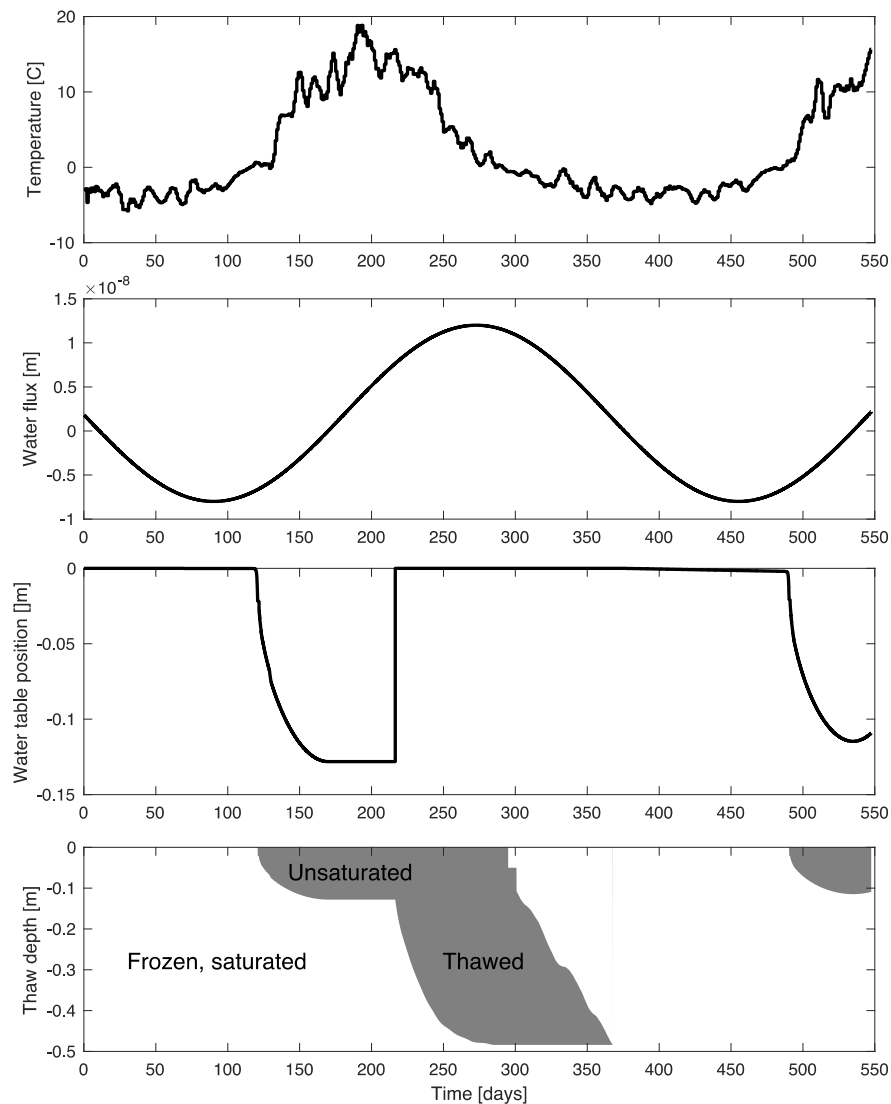


Figure 5. Simulation of hypothetical freeze-thaw system. Top figure denotes surface temperature, followed by surface water flux, water table position and frost table position. Note the unsaturated portion is permitted to have ice content ranging from 0 to 1 but is shaded in the same way as the thawed portion of the soil column.

4. CONCLUSION

The proposed interface model is adequate for the simulation of permafrost degradation and annual freeze-thaw, as well as the representation of seasonal ground ice. Results agree well with analytical solutions and a benchmarked continuum model, though the interface model demonstrates an approximate 2500-fold increase in computational speed. This tool can be applied to better understand the condition of permafrost in peatlands in the SCRS, allowing for sensitivity analysis and calibration to be feasible. The model can easily be extended to represent seasonal ground ice and different soil types. Next steps in model development include incorporation of segregated ice development and its impacts on hydraulic conductivity and pore volume.

REFERENCES

- Atchley, A. L., Painter, S. L., Harp, D. R., Coon, E. T., Wilson, C. J., Liljedahl, A. K., and Romanovsky, V. E. (2015). *Using field observations to inform thermal hydrology models of permafrost dynamics with ATS (v0.83)*, (September).
- Carslaw, H. S., and Jaeger, J. C. (1959). *Conduction of Heat in Solids*.
- Connon, R., Devoie, É., Hayashi, M., Veness, T., and Quinton, W. (2018). *The influence of shallow taliks on permafrost thaw and active layer dynamics in subarctic Canada*. *Journal of Geophysical Research: Earth Surface*, 1–17.
- Daanen, R. P., Misra, D., Epstein, H., Walker, D., and Romanovsky, V. (2008). *Simulating nonsorted circle development in arctic tundra ecosystems*, 113(July), 1–10.
- Endrizzi, S., Gruber, S., Amico, M. D., and Rigon, R. (2014). *GEOtop 2.0: simulating the combined energy and water balance at and below the land surface accounting for soil freezing, snow cover and terrain effects*, 2831–2857.
- Frampton, A., Painter, S., Lyon, S. W., and Destouni, G. (2011). *Non-isothermal, three-phase simulations of near-surface flows in a model permafrost system under seasonal variability and climate change*. *Journal of Hydrology*, 403, 352–359.
- Goodrich, L. E. (1978). *Efficient numerical technique for one-dimensional thermal problems with phase change*. *International Journal of Heat and Mass Transfer*, 21, 615–621.
- Gray, D. M., Toth, B., Zhao, L., Pomeroy, J. W., and Granger, R. J. (2001). *Estimating areal snowmelt infiltration into frozen soils*. *Hydrological Processes*, 15(16), 3095–3111.
- Harlan, R. L. (1973). *Analysis of coupled heat and fluid transport in partially frozen soil*. *Water Resources Research*, 9(5), 1314–1323.
- Hayashi, M. (2013). *The Cold Vadose Zone: Hydrological and Ecological Significance of Frozen-Soil Processes*. *Vadose Zone Journal*, 12, 2136.
- Hayashi, M., Goeller, N., Quinton, W. L., and Wright, N. (2007). *A simple heat-conduction method for simulating the frost-table depth in hydrological models*. *Hydrological Processes*, 2622, 2610–2622.
- Hinkel, K. M., Paetzold, F., Nelson, F. E., and Bockheim, J. G. (2001). *Patterns of soil temperature and moisture in the active layer and upper permafrost at Barrow, Alaska: 1993–1999*, 1993–1999.
- Hinzman, L. D., Goering, D. J., and Kane, D. L. (1998). *A distributed thermal model for calculating soil temperature profiles and depth of thaw in permafrost regions*, 103(98).
- Karra, S., Painter, S. L., and Lichtner, P. C. (2014). *Three-phase numerical model for subsurface hydrology*, 1935–1950.
- Krogh, S. A., Pomeroy, J. W., and Marsh, P. (2017). *Diagnosis of the hydrology of a small Arctic*

- basin at the tundra-taiga transition using a physically based hydrological model.* Journal of Hydrology, 550, 685–703.
- Kurylyk, B. L., McKenzie, J. M., MacQuarrie, K. T. B., and Voss, C. I. (2014). *Analytical solutions for benchmarking cold regions subsurface water flow and energy transport models: One-dimensional soil thaw with conduction and advection.* Advances in Water Resources, 70, 172–184. <https://doi.org/10.1016/j.advwatres.2014.05.005>
- Kurylyk, B. L., and Watanabe, K. (2013). *The mathematical representation of freezing and thawing processes in variably-saturated, non-deformable soils.* Advances in Water Resources, 60(August), 160–177.
- McClymont, A. F., Hayashi, M., Bentley, L. R., and Christensen, B. S. (2013). *Geophysical imaging and thermal modeling of subsurface morphology and thaw evolution of discontinuous permafrost.* Journal of Geophysical Research: Earth Surface, 118, 1826–1837.
- McKenzie, J. M., Voss, C. I., and Siegel, D. I. (2007). *Groundwater flow with energy transport and water-ice phase change: Numerical simulations, benchmarks, and application to freezing in peat bogs.* Advances in Water Resources, 30(4), 966–983.
- Mckenzie, J., and Mckenzie, J. M. (2007). *Groundwater Flow with Energy Transport and Water-Ice Phase Change : Numerical Simulations , Benchmarks , and Application to Freezing in Peat Bogs freezing in peat bogs,* (April 2016).
- Rawlins, M. A., Nicolsky, D. J., McDonald, K. C., and Romanovsky, V. E. (2013). *Simulating soil freeze / thaw dynamics with an improved pan-Arctic water balance model,* 5(October 2012), 659–675.
- Schaefer, K., Zhang, T., Slater, A. G., Lu, L., Etringer, A., and Baker, I. (2009). *Improving simulated soil temperatures and soil freeze / thaw at high-latitude regions in the Simple Biosphere / Carnegie- Ames-Stanford Approach model,* 114, 1–18.
- Semenova, O., and Lebedeva, L. (2013). *Simulation of subsurface heat and water dynamics , and runoff generation in mountainous permafrost conditions , in the Upper Kolyma River basin , Russia,* 107–119.
- Slater, A. G., Pitman, A. J., and Desborough, C. E. (1998). *Simulation of freeze-thaw cycles in a general circulation model land surface scheme.* Journal of Geophysical Research, 103(D10), 11303–11312.
- Stahli, M., Jansson, P., and Lundin, L. (1999). *Soil moisture redistribution and infiltration in frozen sandy soils,* 35(1), 95–103.
- Woo, M., Arain, M. A., Mollinga, M., and Yi, S. (2004). *A two-directional freeze and thaw algorithm for hydrologic and land surface modelling,* 31, 1–4.
- Woo, M. K. (2012). *Permafrost hydrology.* Permafrost Hydrology (Vol. 9783642234).
- Yi, S., Wischniewski, K., Langer, M., Muster, S., and Boike, J. (2014). *Freeze / thaw processes in complex permafrost landscapes of northern Siberia simulated using the TEM ecosystem model : impact of thermokarst ponds and lakes,* 1671–1689.
- Zhang, Y., Carey, S. K., and Quinton, W. L. (2008). *Evaluation of the algorithms and parameterizations for ground thawing and freezing simulation in permafrost regions.* Journal of Geophysical Research Atmospheres, 113(17).
- Zhang, Y., Chen, W., and Cihlar, J. (2003). *A process-based model for quantifying the impact of climate change on permafrost thermal regimes,* 108.
-

Decreasing Precipitation Phase Uncertainty in Cold Region Conceptual Snow Models Weather to Apply Sub-daily Timescales or Supplemental Observation Data

James M Feiccabrino^{1*}

¹*Department of Water Resources Engineering, Lund University, Lund, Sweden*
**Corresponding author's email address: James.Feiccabrino@googlemail.com*

ABSTRACT

Precipitation phase uncertainty in cold regions is a significant source of hydrological, climatological, and environmental model error. These fields often use conceptual models applying a single rain/snow temperature threshold (Trs) to assign precipitation phase irrespective of local to regional influences on climate and weather. Model uncertainty caused by Trs is greatest in areas such as the Scandinavian Peninsula where physiography varies, and over 35% of annual precipitation falls in air temperatures (AT) -3 to 5°C. Another primary source of uncertainty is that many conceptual models use an AT threshold at a 24hr timestep; however, most precipitation events occur on a sub-daily timescale. 22 years of observations from 103 Norwegian and Swedish meteorological stations consisting of over 1.5 million precipitation observations with over 502,000 occurring between -3 and 5°C were used. First AT, dew-point temperature (DP), and Wet-bulb temperature (WB) Trs were determined for 1 and 24hr timesteps. A formula using relative humidity (RH), an essential secondary factor in precipitation formation and phase change, to adjust AT thresholds was also applied. However, parameters needed to calculate DP and WB are often not included in observations. Therefore some stations could only be used for AT analysis. Results indicate that on a 24hr timestep the use of DP, WB, and RH adjusted AT thresholds did little to reduce precipitation phase error (5-10% reduction). However, upgrading to a 1hr timestep, or a sub-model to find and apply temperatures at the time of precipitation reduced over 40% of precipitation phase uncertainty.

KEYWORDS

precipitation phase; snow; snow model; temperature threshold; cold region modelling

1. INTRODUCTION

Precipitation phase uncertainty in cold regions is a major source of error in hydrological, climatological, and environmental models. Conceptual snow models used in these fields often apply a single rain/snow temperature threshold (Trs) irrespective of local to regional influences on climate and weather (Jennings *et al.* 2018). Model uncertainty caused by Trs is greatest in areas such as the Scandinavian Peninsula where over 30% of annual precipitation falls in air temperatures (AT) between -3 and 5°C.

Some studies using hourly observations have found dew-point (DP), wet-bulb (WB), or AT adjusted for RH to yield better model results than using a AT (e.g., Ye *et al.* 2013; Harpold *et al.* 2017b; Jennings *et al.* 2018). However, hydrological or meteorological stations reporting DP, WB, and RH measurements are much less common than AT (ex. Kane & Stuefer 2015) therefore it is beneficial to find techniques using AT to reduce misclassified precipitation.

Prior studies have decreasing hourly AT threshold uncertainty. One study reduced model uncertainty by grouping stations with similar physiographic characteristics (Grigg *et al.* 2019). Another reduced 16% of misclassified precipitation in Norway by adjusting hourly AT thresholds for observed cloud base height and RH (Feiccabrino 2019). However, not many studies of this nature have been attempted on a 24-hour time-step.

The goal of this work is two-fold; 1.) modify some of the recent hourly methods to a 24-hour time-step to decrease misclassified precipitation in daily models, and 2.) answer a good question posed to me, If given the chance to improve a 24-hour snow model would it be better to create a more complex precipitation phase determination scheme to reduce precipitation phase uncertainty, or reduce the time-resolution to 1-hour?

2. METHODS

2.1 Study Area

Weather observations reporting current conditions from 67 Swedish and 44 Norwegian weather stations between 01 September 1997 to 21 January 2019 were collected. Daily minimums, maximums, and mean values for air temperature, and relative humidity were also downloaded for the Norwegian sites. Each weather station was north of 62°N Latitude spanning the Northern Scandinavian peninsula from the Bay of Bothnia over the Scandinavian Alps and the North Sea ocean platforms to Svalbard and Jan Mayen. The observation dataset of just under 1 million Swedish observations and over 500,000 Norwegian observations were obtained freely from the Swedish Meteorological and Hydrological Institute (SMHI 2019) and the Norwegian Meteorological Institute (NMI 2019).

2.2 Data Processing

The initial step was calculating the daily maximum, minimum, and mean values for air temperature and relative humidity for the Swedish stations. After calculating this data, all observations containing a WMO weather code not corresponding to present precipitation were discarded. Next, precipitation codes (e.g., 180) indicating either rain or snow were excluded as these observations are not precise on precipitation phase. Mixed precipitation observations were then removed from the datasets. This is due to A.) an unknown proportion of rain to snow in the mixed observation, B.) a previous study in Sweden (Feiccabrino *et al.* 2013) found an equal distribution of mixed precipitation around a Trs and C.) mixed precipitation is often discarded in precipitation phase threshold studies (Bartlett *et al.* 2006).

An air temperature Trs adjusted by relative humidity (T_{RH}), equation 1 from Feiccabrino *et al.* (2015) and Harpold *et al.* (2017a) was calculated for each observation. This T_{RH} equation is based on; Matsuo *et al.* (1981), Gjertsen & Ødegaard (2005) and Harder & Pomeroy (2013).

$$T_{RH} = 0.75 + 0.085 * (100-RH) \quad \text{Equation 1}$$

Wet-bulb was not reported in the observations, and the true wet-bulb requires some information not commonly reported in meteorological observations. Therefore, an approximate wet-bulb calculation (Stull 2011) (equation 2) requiring AT and RH was used.

$$WB=AT*\text{atan}[0.151977(RH+8.313659)^5]+\text{atan}(AT+RH)-\text{atan}(RH-1.676331)+0.00391838(RH)^{1.5}*\text{atan}(0.023101RH)-4.686035 \quad \text{Equation 2}$$

Dew-point temperature was also not always included even when RH was available. Therefore, equation 3, a common formula for DP was used.

$$TD = \left(\frac{RH}{100}\right)^{0.125} * (112 + 0.9 * AT) + 0.1 * AT - 112 \quad \text{Equation 3}$$

In datasets used to compare WB, DP, and T_{RH} any observation without an RH was removed. This allowed results from identical observation sets to be compared.

For this analysis an energy balance approach was taken to classify freezing precipitation as liquid. It can be classified as either liquid or solid since by definition it freezes on contact. However, the freezing process takes energy from an existing snowpack.

2.3 Calculations

All AT, WB, and DP temperature between -3 and 5°C at a 0.1°C interval were tested to find the T_{rs} resulting in the lowest misclassified precipitation event percentage in each country. Here, a misclassified precipitation event is defined as an observation that has either; A.) Snow predicted due to temperatures cooler or equal to the T_{rs} when rain was observed, or B.) Rain predicted in temperatures warmer than the T_{rs} when snow was observed.

To address possible use of a dual threshold model, the observed 10% rain was used for a snow temperature threshold T_s and observed 10% snow was used for the rain temperature threshold T_r . Between these suggested thresholds precipitation can be considered mixed liquid and solid with a calculated phase that can follow either a linear or non-linear function.

The percent of misclassified precipitation occurring outside of a -3 to 5°C range is also quantified for each method. This analysis determines if simple methods considering all precipitation occurring with temperatures warmer than 5°C to be rain and all precipitation in temperatures colder than 3°C to be snow. If so, more sophisticated methods could be applied in the temperature range and skipped if the temperature is outside of the range.

The amount of rain misclassified as snow and snow misclassified as rain for each T_{rs} was also calculated. This determines if the number of misclassified events was nearly equal or favored the liquid or solid phase. The sum of snow events predicted divided by total precipitation events was compared to the observed solid phase percent of events to determine if a given T_{rs} would result in over or underestimating long term solid precipitation projections.

3. RESULTS AND DISCUSSION

The air temperature thresholds were 1.3°C for Norway and 1.0°C for Sweden. The warmer threshold in Norway is expected to be a result of a more unstable atmosphere over and near the ocean due to warm water modifying the cool near surface winter air.

The T_{rs} with the lowest average station value for 1-hour WB, DP, AT and 24-hour average AT were compared for the Swedish stations. Results indicate that there is 40.7% less misclassified precipitation for the 1-hour AT compared to the 24-hour AT (Figure 1). This more substantial difference in misclassified precipitation using optimal T_{rs} is most likely due to the 1hr AT observations being taken during the precipitation event, while the 24hr AT is averaged over the full day which may not be representative of the conditions during precipitation (see Feiccabrino 2019). Precipitation events more often than not occur on a sub-daily time-scale.

Standard deviation error bars are large when compared to the average error ranging from 31% to 57% for 24hr AT and 1hr WB, respectively (Figure 1). These standard deviations could be further reduced if grouping stations by physiography (e.g., Grigg *et al.* 2019) rather than by region regardless of ocean or terrain influences which has become all too common (Jennings *et al.* 2018). It is also noted that 1-hour WB, DP and AT all have similar misclassified precipitation results, with WB having just over 15% less averaged error than AT.

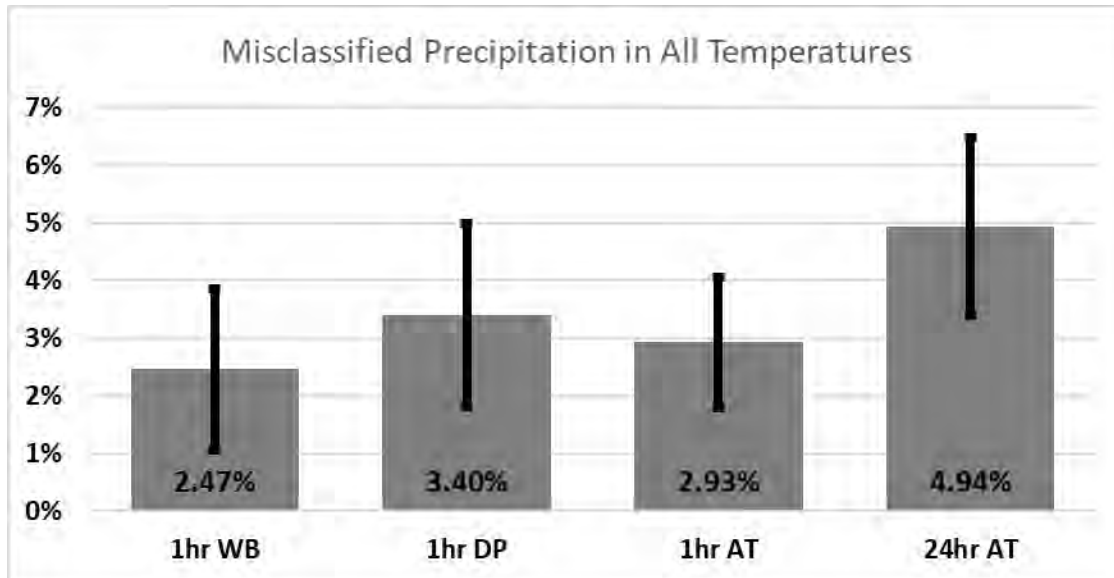


Figure 1. 1hr wet-bulb (WB), 1hr dew-point (DP), 1hr air temperature (AT) and 24hr air temperature (AT) average Swedish station threshold misclassified precipitation with standard deviation error bars.

The increased misclassified precipitation for 24-hour AT (Figure 1) corresponds to a more extensive mixed phase precipitation zone than the 1-hour Tr_s options (Figure 2). Also noted, WB has both the lowest average misclassified precipitation (Figure 1) and the smallest temperature range between the suggest T_s and T_r thresholds in figure 2.

Clearly stated, the lower the precipitation phase uncertainty indicated by misclassified precipitation, the smaller the mixed phase zone should be for a given precipitation phase determination method. In this case, the suggested mixed phase range is bounded by the temperatures at which 10% of precipitation is misclassified as rain or snow using a climatological dataset. The use of a mixed phase range in models also acknowledges that snow in near and above freezing temperatures often has liquid water in its crystal lattice, and rain in near-freezing temperatures can still have some ice in the droplets.

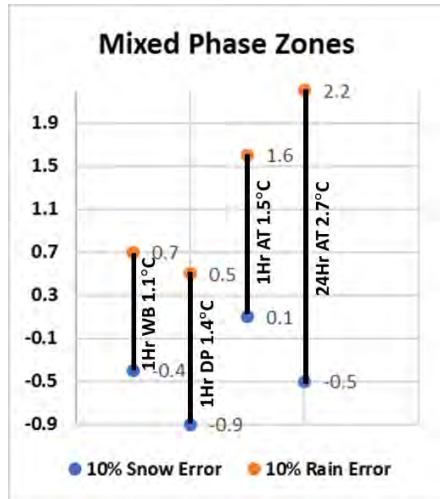


Figure 2. Mixed-phase temperature range for 1-hour WB, DP, AT and 24-hour AT thresholds.

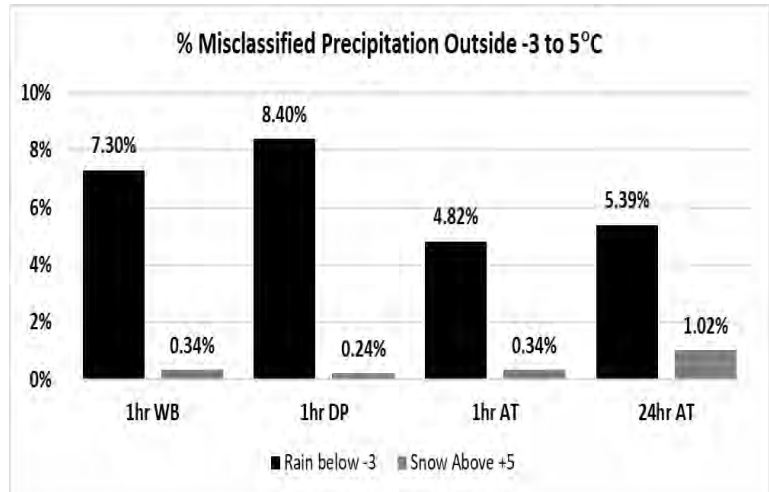


Figure 3. Percent of total misclassified precipitation occurring below -3°C (Black) or above 5°C (Gray) for 1-hour WB, DP, AT and 24-hour AT thresholds.

Most misclassified precipitation occurs in the temperature range -3 to 5°C (Figure 3) supporting the use of more complex precipitation phase determination schemes in this temperature range while assuming all snow in colder temperatures and all rain in warmer temperatures. In all cases no more than 10% misclassified precipitation occurs outside of the range. WB and DP temperatures, and thresholds are always the same or cooler than AT, so the -3 to 5°C temperature range can always be decreased a bit if applying WB or DP Trs. It is also interesting that while misclassified precipitation was over 40% lower for 1-hour AT compared to 24-hour AT, there was not a vast difference in misclassified precipitation outside of the -3 to 5°C range between the two Trs options.

The larger share of misclassified precipitation below -3°C is in part due to classifying freezing precipitation as a liquid. Freezing rain is an atmospheric phenomenon that can occur in well below freezing temperatures if cloud conditions are not correct for snow crystal formation. This makes creating a surface-based precipitation phase determination scheme for a model to identify freezing precipitation nearly impossible.

When comparing 24-hour AT, WB, DP, and T_{RH} mean, minimum, and maximum values for AT and RH were used (Tables 1 and 2). As expected, DP Trs is always \leq WB Trs, which is also always \leq AT Trs.

Table 1. 24-hour rain/snow thresholds using 24-hour minimum, mean, and maximum air temperatures.

Air Temperature Thresholds		
Min AT	Mean AT	Max AT
0.0	1.1	3.3

Table 2. Dew-point temperature, and wet-bulb temperature thresholds determined using 24-hour minimum, mean, and maximum relative humidity and air temperature values.

Dew Point Thresholds				Wet Bulb Thresholds			
	Min AT	Mean AT	Max AT		Min AT	Mean AT	Max AT
Min RH	-3.5	-1.3	0.6	Min RH	-2.0	-0.2	1.6
Mean RH	-1.8	0.1	1.8	Mean RH	-1.3	0.5	2.3
Max RH	-0.7	0.8	2.9	Max RH	-0.4	0.8	3.0

In this analysis using all Swedish observations with a reported RH, the AT Trs of 1.1°C results in 4.81% misclassified precipitation with 14.41% more rain classified as snow resulting in a long term 0.69% overestimation of snow events compared to observed solid phase (Table 3). Interestingly, applying the 24-hour maximum AT Trs in a model while having 6.55% misclassification predicts only 0.51% more rain classified as snow than snow classified as rain resulting in only 0.03% more snow than observed. Therefore if the purpose of a model was long term averages, and not affected by individual event misclassification this 24-hour maximum AT Trs would be a better choice than the 24-hour average AT Trs value.

Table 3. The resulting misclassified precipitation, solid to liquid error imbalance, predicted solid precipitation percentage with a difference from observed 60.98% when applying table 1 air temperature thresholds to the Swedish station dataset.

Misclassified Precipitation			Greater Snow Than Rain Error		
Min AT	Mean AT	Max AT	Min AT	Mean AT	Max AT
7.14%	4.81%	6.55%	68.23%	14.41%	0.51%
Percent Solid Precipitation			Solid Precip Increase From Observed		
Min AT	Mean AT	Max AT	Min AT	Mean AT	Max AT
65.85%	61.68%	61.01%	4.87%	0.69%	0.03%

Table 4. The resulting misclassified precipitation, solid to liquid error imbalance, predicted solid precipitation percentage with a difference from observed 60.98% when applying table 2 dew-point temperature thresholds to the Swedish station dataset.

Misclassified Precipitation				Greater Snow Error Than Rain Error			
	Min AT	Mean AT	Max AT		Min AT	Mean AT	Max AT
Min RH	13.80%	9.95%	7.21%	Min RH	35.24%	41.54%	35.67%
Mean RH	9.35%	5.42%	5.56%	Mean RH	37.89%	43.33%	2.24%
Max RH	7.52%	4.75%	6.38%	Max RH	44.25%	24.23%	4.86%
Percent Solid Precipitation (Full Period)				Increase in Solid Precip From Observed			
	Min AT	Mean AT	Max AT		Min AT	Mean AT	Max AT
Min RH	65.85%	65.12%	63.55%	Min RH	4.86%	4.13%	2.57%
Mean RH	64.53%	63.33%	61.11%	Mean RH	3.54%	2.35%	0.12%
Max RH	64.31%	62.13%	61.29%	Max RH	3.33%	1.15%	0.31%

Dew-point results in table 4 had one notable result of slightly less misclassified precipitation than 24-hour mean AT when calculated using the 24-hour maximum RH with mean AT, but this was only an improvement of 0.06%. WB calculated using Mean 24-hour RH and AT values resulted in the least misclassified precipitation of all 24-hour combinations tested. However, it also had 41.90% more snow than rain errors causing a long-term overestimation of 1.88% solid precipitation (Table 5). This would be an improved solution for rapid models, but worse for models predicting or tracking monthly or seasonal average precipitation. A similar issue arises with the use of 24-hour average RH and AT using T_{RH} (Table 6).

Table 5. The resulting misclassified precipitation, solid to liquid error imbalance, predicted solid precipitation percentage with a difference from observed 60.98% when applying table 2 wet-bulb temperature thresholds to the Swedish station dataset.

Misclassified Precipitation				Greater Snow Error Than Rain Error			
	Min AT	Mean AT	Max AT		Min AT	Mean AT	Max AT
Min RH	8.86%	5.09%	5.24%	Min RH	36.18%	37.51%	5.16%
Mean RH	7.90%	4.48%	5.73%	Mean RH	36.64%	41.90%	-2.97%
Max RH	7.31%	4.67%	6.40%	Max RH	60.39%	19.95%	1.10%
Percent Solid Precipitation (Full Period)				Increase in Solid Precip From Observed			
	Min AT	Mean AT	Max AT		Min AT	Mean AT	Max AT
Min RH	64.19%	62.89%	61.25%	Min RH	3.21%	1.91%	0.27%
Mean RH	63.88%	62.86%	60.81%	Mean RH	2.98%	1.88%	-0.17%
Max RH	65.40%	61.91%	61.05%	Max RH	4.41%	0.93%	0.07%

Table 6. The resulting misclassified precipitation, solid to liquid error imbalance, predicted solid precipitation percentage with a difference from observed 60.98% when applying T_{RH} to the Swedish station dataset.

Misclassified Precipitation				Greater Snow Error Than Rain Error			
	Min AT	Mean AT	Max AT		Min AT	Mean AT	Max AT
Min RH	14.06%	6.52%	6.42%	Min RH	99.69%	86.94%	-61.14%
Mean RH	10.98%	4.55%	8.86%	Mean RH	99.25%	50.14%	-84.32%
Max RH	9.01%	4.76%	10.97%	Max RH	97.57%	1.12%	-90.31%
Percent Solid Precipitation (Full Period)				Increase in Solid Precip From Observed			
	Min AT	Mean AT	Max AT		Min AT	Mean AT	Max AT
Min RH	75.00%	66.42%	57.06%	Min RH	14.02%	5.44%	-3.92%
Mean RH	71.88%	63.27%	53.51%	Mean RH	10.90%	2.29%	-7.47%
Max RH	69.77%	61.04%	51.07%	Max RH	8.79%	0.06%	-9.91%

Using 24-hour maximum and minimum AT to calculate T_{RH} would result in very large overestimations of snow and rain respectively. However, T_{RH} using 24-hour mean AT and max RH has 0.05% less error than 24-hour mean AT and only overestimates long term snow by 0.06%, compared to 0.69% using 24-hour mean AT.

To this point none of these 24-hour methods have come close to decreasing the same amount of misclassified precipitation as reducing the time-step to 1-hour. However, there is still future work to be done such as; using wind speed and wind direction to perhaps decrease misclassified precipitation in coastal areas. Adjusting 24-hour AT for average or lowest cloud height may be able to reduce misclassified precipitation, however the nearly 15% decrease using RH adjusted AT thresholds at the 1-hour time-step (Feiccabrino 2019) did not result in similar reductions at the daily time-scale.

4. CONCLUSIONS

It is clear to this point that time resolution is very important for surface-based precipitation phase determination in conceptual models. None of the tested 24-hour rain/snow temperature threshold options resulted in comparable reductions to the 40.7% improvement from changing from a 24-hour averaged air temperature threshold to a 1-hour air temperature threshold. However, for some uses such as annual snow amounts, or low time-resolution climate forecasts some of the 24-hour solutions such as 24-hour Maximum air temperature thresholds, or 24-hour maximum relative humidity with mean air temperatures have more misclassified precipitation, but balance the errors to result in close to observed long-term solid precipitation percentages.

Results from this study can be applied in new models to reduce precipitation phase misclassification which should result in better in season predictions of snow pack layers and properties, and runoff predictions to name a couple. Results for the Scandinavian Mountains and Sweden should also be applicable in similar coastal mountain areas such as the Rockies and Cascades in the Pacific Northwest and British Columbia, New Zealand, and Japan.

REFERENCES

- Bartlett, P. A., MacKay, M. D., & Verseghy, D. L. 2006 Modified snow algorithms in the Canadian land surface scheme: Model runs and sensitivity analysis at three Boreal forest stands. *Atmosphere-Ocean*, **43**, 207-222. <https://doi.org/10.3137/ao.440301>
- Feiccabrino, J. 2019 Reducing misclassified precipitation phase in conceptual models using air temperature thresholds calibrated for cloud base heights, or adjusted by relative humidity. *Hydrology Research*, Submitted.
- Feiccabrino, J., Graff, W., Lundberg, A. & Sandström, N. 2015 Meteorological knowledge useful for the improvement of snow rain separation in surface based models. *Hydrology*, **2**(4), 266-288. <https://doi.org/10.3390/hydrology2040266>
- Feiccabrino, J., Gustafsson, D. & Lundberg, A. 2013 Surface-based precipitation phase determination methods in hydrological models. *Hydrology Research*, **44**(1), 44-57. <https://doi.org/10.2166/nh.2012.158>
- Gjertsen, U. & Ødegaard, V. 2005 The water phase of precipitation – A comparison between observed, estimated and predicted values. *Atmospheric Research*, **77**, 218-231. <https://doi.org/10.1016/j.atmosres.2004.10.030>
- Grigg, L. D., Feiccabrino, J. M. & Sherenco, F. 2019 Testing the applicability of physiographic classification methods towards improving precipitation phase determination in conceptual models. *Hydrology Research*, Submitted.
- Harder, P. & Pomeroy, J. 2013 Estimating precipitation phase using a psychrometric energy balance method. *Hydrological Processes*, **27**, 1901-1914. <https://doi.org/10.1002/hyp.9799>

- Harpold, A. A., Kaplan, M. L., Klos, P. Z., Link, T., McNamara, J. P., Rajagopal, S., Schumer, R. & Steele, C. M. 2017a Rain or snow: hydrologic processes, observations, prediction, and research needs. *Hydrology and Earth System Sciences*, **21**(1), 1-22. <https://doi.org/10.5194/hess-21-1-2017>
- Harpold, A. A., Rajagopal, S., Crews, J. B., Winchell, T. & Schumer, R. 2017b Relative humidity has uneven effects on shifts from snow to rain over the Western U.S.. *Geophysical Research Letters*, **44**(19), 9742-9750. <https://doi.org/10.1002/2017GL075046>
- Jennings, K. S., Winchell, T. S., Livneh, B. & Molotch, N. P. 2018 Spatial variation of the rain-snow temperature threshold across the Northern Hemisphere. *Nature Communications*, **9**(1148). DOI: 10.1038/s41467-018-03629-7
- Kane, D. L. & Stuefer, S. L. 2015 Reflecting on the status of precipitation data collection in Alaska: a case study. *Hydrology Research*, **46**(4), 478-493. <https://doi.org/10.2166/nh.2014.023>
- Matsuo, T., Sato, Y. & Sasyo, Y. 1981 Relationship between types of precipitation on the ground and surface meteorological elements. *Journal of the Meteorological Society of Japan*, **59**, 462-476. https://doi.org/10.2151/jmsj1965.59.4_462
- Norwegian Meteorological Institute (NMI) 2019 Meteorological Data. Available from: <http://eklima.met.no> (accessed 22 May 2019)
- Swedish Meteorological and Hydrological Institute (SMHI) 2018 Meteorological Data. Available from: <http://opendatadownload-metobs.smhi.se/explore/?parameter=8> (accessed 22 May 2019).
- Stull, R. 2011 Wet-bulb temperature from relative humidity and air temperature. *Journal of Applied Meteorology and Climatology*, **50**, 2267-2269.
- Ye, H., Cohen, J. & Rawlins, M. 2013 Discrimination of solid from liquid precipitation over northern Eurasia using surface atmospheric conditions. *Journal of Hydrometeorology*, **14**(4), 1345-1355. <http://dx.doi.org/10.1175/JHM-D-12-0164.1>

Quantifying spatially distributed shrub biomass in the boreal forest of Northwestern Canada using destructive field sampling, allometry and multi-spectral lidar derivatives

L. Flade¹, L. Chasmer¹, and C. Hopkinson¹

¹Department of Geography, University of Lethbridge, Lethbridge Alberta, T1J 3M4, CANADA

*Corresponding author's email address: linda.flade@uleth.ca

ABSTRACT

In the discontinuous permafrost zone of boreal northwestern Canada vegetation structure, composition and condition have and will change drastically into the foreseeable future. These broad area ecosystem changes, that are associated with climate change, not only have implications for carbon cycling dynamics but also for permafrost condition, ecosystem wildfire susceptibility, and freshwater resources, potentially posing major threats to northern communities in these regions. Understanding of broad area ecosystem changes will improve understanding of the fate of the northern boreal carbon balance in the sensitive transitional zones of sporadic to discontinuous permafrost. In this study, we develop preliminary shrub biomass allometric equations determined from 29 shrub samples of five shrub species for three height classes. We further discuss the use of lidar point cloud return metrics to model shrub aboveground biomass. Early analysis of *in situ* shrub biomass using linear functions indicate that the best fitting allometric equation for all species of all height categories is based on measured volume calculated as line-intercept cover [m²] of shrub individual * average height [m] of shrub individual (Pearson's correlation coefficient $R^2 = 0.89$). Measured average shrub height correlated with all species of all height categories with an R^2 of 0.49. Average stem diameter at ground level had the least predictive capacity in comparison with shrub biomass ($R^2 = 0.21$). The study further discusses the integration of *in situ* biomass data with lidar data. Although more shrub biomass samples need to be collected to improve the applicability of allometric equations, results show promise for the use of airborne lidar data and scaling of shrub biomass to broader regions.

KEYWORDS

Shrub biomass, succession, allometry, remote sensing, lidar, scaling

1. INTRODUCTION

The discontinuous to sporadic permafrost regions of northwestern Canada have undergone rapid environmental change (e.g. Quinton et al. 2009; Connon et al. 2015) due to climate change in the last half century (IPCC 2013). Climate-mediated disturbances such as wildfire (Flannigan et al. 2005; Johnston et al. 2015) and permafrost thaw (e.g. Quinton et al. 2009; Baltzer et al. 2014; Chasmer & Hopkinson 2017) have caused ecosystem changes that are *inter alia* observed as changes of vegetation structure, condition and composition, which will continue in coming decades (IPCC 2013).

Regional observations using time-series of passive optical remote sensing vegetation indices (VIs), associate an increase in VI, such as the NDVI, with enhanced plant net primary productivity (NPP; e.g. Berner et al. 2013), plant biomass (e.g. Epstein et al. 2012; Berner et al. 2018) and shrub

abundance (Myers-Smith et al. 2011; Berner et al. 2018). Positive trends in Vis over periods of years to decades are often referred to as ‘greening’, while negative trends are associated with forest biomass loss and declining NPP trends as well as unchanging spectral pixels are revealed, with a majority of studies reporting browning as decade-long mid-summer forest decline of green foliage (e.g. Goetz et al. 2005; Beck and Goetz 2011). Nevertheless, how these trends in remote sensed data are related to actual trends and processes on the ground is highly uncertain. For example, browning might also be observed coincident with an increase in shrub biomass *in situ*; or changing pixels might be detected where no changes in vegetation have occurred. Furthermore, decreasing growth/browning trends are contrary to expectations of stimulated growth and photosynthesis with anticipated increases in air temperature, which may enhance soil temperature, oxygen supply to roots, and nutrient availability (Shaver et al. 1992; Larcher 1995, Myneni et al. 1997; Tucker et al. 2001; Slayback et al. 2003). In addition to changing air surface temperatures, implications to succession due to permafrost thaw (Baltzer et al. 2014; Chasmer and Hopkinson, 2017) as well as wildfire disturbance might represent different greening and browning trends (Goetz et al. 2007; Beck and Goetz 2011). Therefore, high uncertainties exist when correlating changes in pixels over time with anticipated (but not measured) successional forms on the ground. To quantify changes in aboveground biomass, and thus carbon content due to permafrost thaw and wildfire disturbance across broad areas, there is a need for detailed vegetation structural data of varying scale, ranging from plot-level to ecosystem and regional scales.

While a majority of ecosystem change studies focus on tree succession integrated in regional forest monitoring strategies, less is known about changes in boreal shrub abundance. However, a potential increase of shrub abundance as observed in Arctic environments (Meyer-Smith et al. 2011), in wildfire disturbed ecosystems (Goetz et al. 2007), and in drying wetlands (Chasmer and Hopkinson 2017) could increase ecosystem carbon storage quantities due to a high carbon nitrogen ratio of woody plants (Shaver et al. 1992). In Addition, wildfire frequency, magnitude and severity (e.g. Goetz et al. 2007) might be mitigating due to the less flammable properties of deciduous broadleaf plant species. Hence, knowledge about an increase boreal shrub abundance is important for understanding the fate of the boreal ecosystems and urgently needed for wildfire susceptibility projections.

In this study, we develop shrub biomass allometric equations determined from 29 shrub samples of five different shrub species (*Betula glandulosa*, *Shepherdia canadensis*, *Salix arbusculoides*, *Salix bebbiana*, *Salix glauca*) for three different height classes (< 0.5 m; 0.51 m – 1.00 m, 1.01 m – 1.50 m). We further discuss the use of lidar point cloud return metrics (e.g. average height and percentile return ratios) to model shrub aboveground biomass. The objectives of this study are to a) evaluate height and other measured variables as predictors of shrub aboveground biomass; b) develop shrub biomass allometric equations using destructive sampling for each of the five shrub species of all three height categories; and c) develop one universal allometric equation for all shrub species of all height categories. Finally, d) measured shrub biomass will be compared with the coincident lidar point cloud metrics (lidar acquisition July/August 2018) in order to determine the best performing regression model, which will then be used to model shrub biomass across the study area.

2. METHODS

Shrub individuals were destructively sampled at ground level along nine lidar-coincident field sampling transects (Figure 1) distributed across the Taiga Shield (shrub samples n=4) and Taiga Plains (shrub samples n=25) ecozones. A shrub sample was selected for destructive sampling when it was alive and either the only representing species in one of the three height categories, or when all height categories of the corresponding shrub species were present along the transect. Sampling transects were randomly distributed within areas of lidar data that were collected by the authors in 2010 and/or 2016 and/or 2018 and proximity to roads due to accessibility and safety purposes. Sampling transects were geographically located using global navigation satellite system (GNSS) and tape/level in a chronosequence of previously burned sites (burned in the last 50 years, shrub samples n=14) and in late-succession unburned sites (shrub samples n=15). Additional variables measured along the transect for each individual shrub sample include shrub average height, shrub average diameter of all stems at ground level, and shrub cover using the width at the widest horizontal distribution of foliage cover. These were used to determine the best fitting predictor variable for shrub biomass. Clipped shrub samples were weighed and oven dried at 60°C for 48 hrs. The biomass for each shrub individual is determined as dry weight (g).



Figure 1. Layout of transect to destructively sample shrub species, coincident with lidar survey in 2018 along Highway 3 between Providence and Yellowknife. Species shown is *Betula glandulosa*, coincident lidar data available for the years 2010 and 2016.

3. INITIAL RESULTS AND DISCUSSION

3.1 Shrub Allometric Equations

Initial analysis of in-situ shrub biomass using linear functions indicate that the best fitting allometric equation for all species of all height categories is based on measured volume calculated as ground cover [m²] of shrub individual * average height [m] of shrub individual (Pearson's correlation coefficient $R^2 = 0.89$, n=29). Measured average shrub height correlated with all species of all height categories with an R^2 of 0.49 (n=29). Average stem diameter at ground level had the least predictive capacity in comparison with shrub biomass ($R^2 = 0.21$, n=29). Average shrub height [m] correlated best with *Shepherdia canadensis* ($R^2 = 0.61$), however sampling size was relatively small (n=5). Considering different height categories, height explained 54 % of the biomass

distribution in the middle height category (0.51 m – 1.00 m) of all five shrub species (n=10) based on a linear trend. Shrub biomass for species in the smallest height category (< 0.5 m) was poorly correlated with measured height (14 % (n=12)) and had virtually no correlation with the middle height category (0.51 m – 1.00 m; 0.8 % (n=7)). This might be due to a high biomass content of two shrub individuals of *Betula glandulosa* (height < 0.5 m) and *Salix glauca* (height > 1.01 m). While this study provides early allometry additional shrub biomass samples will be collected to improve analysis results and to develop one shrub allometric equation for all shrub species and heights. Further analysis will evaluate multivariate and non-linear functions for allometry development once candidate metrics are identified.

3.2 Shrub biomass modelling

To enhance the scientific understanding of the dominant *in situ* to ecosystem-scale successional trends (tree mortality and growth, encroachment of shrubs) that represent spectral browning, greening and unchanging trends across the Taiga Shield and Plains ecozones, field observations need to be scaled to an ecosystem level. A promising scaling approach utilizes high-spatial resolution airborne lidar data (≥ 1 return per m²). Lidar can measure structural attributes of single plants, and those within plots, which can be related to spectral VIs (e.g. Wulder et al. 2009, Matasci et al. 2018).

Using multi-temporal lidar data, the spatial variability of 3D vegetation properties will be utilized to quantify cumulative change in topography and vegetation structural attributes measured through time (e.g. Hopkinson et al. 2008 and 2016; Chasmer and Hopkinson 2017). Lidar data were collected over study sites and along transects throughout the NWT in 2007/2008, 2010/2011, 2015, 2016 and 2018 (e.g. Wulder et al. 2012; Hopkinson et al. 2013; Mahoney et al. 20018). In some areas, lidar data were overlapping, providing the ability to examine change in 3D structure over time. These data will be used to spatially extend biomass models trained from historical and contemporary spatially coincident field plot data across burned and non-burned ecosystems of the discontinuous permafrost zone, Northwest Territories, Canada.

4. CONCLUSION

Spatially distributed structural attributes of vegetation are needed to determine how vegetation succession contributes to the spectral characteristics of optical remote sensing pixels of change or no change in the form of greening and browning. While the results of this study are preliminary, the outcome of this study will further understanding if greening trends resemble increases in biomass, and browning trends represent biomass loss respectively, or if no such relationship exists what the pixels might represent. This study describes the initial development of shrub allometric equations for five common boreal shrub species of various heights below 1.50 m. Furthermore, the study discusses the integration of *in situ* transect plot data and lidar coincident point cloud return metrics across the broad and heterogeneous landscape of boreal northwestern Canada. The knowledge gained and developed in ongoing research of this study could be implemented in other biomass studies and support national forest monitoring programs, such as TERN/AusCover and NEON.

ACKNOWLEDGEMENTS

We would like to acknowledge the help of various field and laboratory assistants at the University of Lethbridge, namely Emily A. Jones, Craig Mahoney and Lavinia Haase. Lidar data processing was completed by Maxim Okhrimenko. We also thank Drs. W. Quinton, L. Flanagan, and D.

Peddle for discussions on data analysis and processing. Funding was provided by NSERC Discovery Grant to L. Chasmer and an NSERC Discovery Grant with Accelerator funding to C. Hopkinson. Equipment was provided by a CFI grant to C. Hopkinson and U of Lethbridge start-up funding to L. Chasmer. We also acknowledge Aurora Research Institute research permits to Chasmer, Hopkinson and Quinton.

REFERENCES

- Beck, P. S. and Goetz, S. J. 2011. "Satellite observations of high northern latitude vegetation productivity changes between 1982 and 2008: ecological variability and regional differences." *Environ. Res. Lett.* 6.
- Baltzer, J., Veness, T., Chasmer, L., Sniderhan, A., and Quinton, W. 2014. "Forests on Thawing Permafrost: Fragmentation, Edge Effects, and Net Forest Loss." *Global Change Biology* 20 (3). Wiley/Blackwell (10.1111):824–34.
- Berner, L., Beck, P. S. A., Bunn, A. G., and Goetz, S. J. 2013. "Plant response to climate change along the forest-tundra ecotone in northeastern Siberia." *Glob. Change Biol.* 19: 3449–62.
- Berner, L., Jantz, P., Tape, K. D., and Goetz, S. J. 2018. "Tundra plant above-ground biomass and shrub dominance mapped across the North Slope of Alaska." *Environmental Research Letters*, 13.
- Chasmer, L., and C. Hopkinson. 2017. "Threshold Loss of Discontinuous Permafrost and Landscape Evolution." *Global Change Biology* 23 (7):2672–86.
- Connon, R. F., Quinton, W. L., Craig, J. R., Hanisch, J. and Sonntag, O. 2015. "The hydrology of interconnected bog complexes in discontinuous permafrost terrains." *Hydrological Processes* 29(18): 3831-3847.
- Epstein, H. E., Reynolds, M. K., Walker, D. A., Bhatt, U. S., Tucker, C. J., and Pinzon, J. E. 2012. "Dynamics of aboveground phytomass of the circumpolar Arctic tundra during the past three decades". *Environ. Res. Lett.* 7.
- Flannigan, M. D., Logan, K. A., Amiro, B. D., Skinner, W. R., and Stocks, B. J. 2005. "Future Area Burned in Canada." *Climatic Change*.
- Goetz, S. J., Bunn, A. G., Fiske, G. J., and Houghton, R. A. 2005. "Satellite-observed photosynthetic trends across boreal North America associated with climate and fire disturbance." *Proc. Natl. Acad. Sci. U.S.A.* 102 (38): 13521–13525.
- Goetz, S. J., Mack, M. C., Gurney, K. R., Randerson, J. T., and Houghton, R. A. 2007. "Ecosystem Responses to Recent Climate Change and Fire Disturbance at Northern High Latitudes: Observations and Model Results Contrasting Northern Eurasia and North America." *Environmental Research Letters* 2 (4).
- Hopkinson, C., Chasmer, L., Barr, A. G., Kljun, N., Black, T. A., and McCaughey, J. H. 2016. "Monitoring Boreal Forest Biomass and Carbon Storage Change by Integrating Airborne Laser Scanning, Biometry and Eddy Covariance Data." *Remote Sensing of Environment* 181: 82–95.
- Hopkinson, C., Chasmer, L., Colville, D., Fournier, R. A., Hall, R. J., and Luther, J. E. 2013. "Moving toward consistent ALS monitoring of forest attributes across Canada."

- Photogrammetric Engineering & Remote Sensing* 79(2): 159-173.
- Hopkinson, C., Chasmer, L., and Hall, R. J. 2008. "The uncertainty in conifer plantation growth prediction from multi-temporal lidar datasets." *Remote Sensing of Environment* 112(3): 1168–1180.
- Hopkinson, C., Lovell, J., Chasmer, L., Jupp, D., Kljun, N., and van Gorsel, E. 2013. "Integrating terrestrial and airborne lidar to calibrate a 3D canopy model of effective leaf area index." *Remote Sensing of Environment* 136: 301–314.
- IPCC 2013. "Climate Change 2013: The physical science basis Contribution of Working Group I to the Fifth Assessment Report of the Intergovernmental Panel on Climate Change ". Cambridge: Cambridge University Press.
- Johnston, D. C., Turetsky, M. R., Benscoter, B. W., and Wotton, B. M. 2015. "Fuel load, structure, and potential fire behaviour in black spruce bogs." *Canadian Journal of Forest Research* 45(7): 888–899.
- Larcher W. 1995. "Physiological Plant Ecology: Ecophysiology and Stress Physiology of Functional Groups." 3rd ed. Springer-Verlag, Berlin, Germany.
- Mahoney, C., Hall, R., Hopkinson, C., Filiatrault, M., Beaudoin, A., and Chen, Q. 2018. "A forest attribute mapping framework: a pilot study in a northern boreal forest, Northwest Territories, Canada." *Remote Sensing* 10(9):1338.
- Matasci, G., Hermosilla, T., Wulder, M. A., White, J. C., Coops, N. C., Hobart, G. W., and Zald, H. S. 2018. "Large-area mapping of Canadian boreal forest cover, height, biomass and other structural attributes using Landsat composites and lidar plots." *Remote Sensing of Environment*.
- Myers-Smith, I. H., Forbes, B. C., Wilmking, M., Hallinger, M., Lantz, T., Blok, D., Tape, K. D., et al. 2011. "Shrub Expansion in Tundra Ecosystems: Dynamics, Impacts and Research Priorities." *Environmental Research Letters* 6 (4).
- Quinton, W., Hayashi, M., and Chasmer, L. 2009. "Peatland Hydrology of Discontinuous Permafrost in the Northwest Territories: Overview and Synthesis." *Canadian Water Resources Journal* 34 (4):311–28.
- Shaver, G. R., Billings, W. D., Chapin, F. S., Giblin, L. F., Nadelhoffer, K. J., Oechel, W. C., and Rastetter, E. B. 1992. "Global change and the carbon balance of arctic ecosystems." *BioScience* 42: 433–441.
- Tucker, C. J., Slayback, D. A., Pinzon, J. E., Los, S. O., Myneni, R. B., and Taylor, M. G. 2001. "Higher northern latitude normalized difference vegetation index and growing season trends from 1982 to 1999." *Int. J. Biometeorol* 45: 184–190.
- Wulder, M. A., White, J. C., Alvarez, F., Han, T., Rogan, J., and Hawkes, B. 2009. "Characterizing boreal forest wildfire with multi-temporal Landsat and LIDAR data. *Remote Sensing of Environment*." 113(7): 1540–1555.
- Wulder, M. A., White, J. C., Bater, C. W. Coops, N. C., Hopkinson, C., and Chen, G. 2012. "Lidar plots - A new large-area data collection option: Context, concepts, and case study." *Canadian Journal of Remote Sensing*. 38(5): 600-618.

A snow quality assessment tool based on new techniques and Sámi knowledge for Northern Sweden

David Gustafsson¹

¹*Swedish Meteorological and Hydrological Institute, Norrköping SWEDEN*

**Corresponding author's email address: david.gustafsson@smhi.se*

ABSTRACT

Climate change impacts are already seen in Northern Sweden, where snow is an important resource for many sectors of the society including reindeer herding, tourism, hydropower, and transportation. Yet a coordinated information service for providing information on relevant snow conditions is missing in Sweden (snow depth, water equivalent, density, temperature, ice layering, and new snow depth). The objective of this study is to develop tools for assessing snow quality relevant for reindeer husbandry combining Sámi knowledge and observations of current snow conditions made by reindeer herders, with numerical modelling and data from satellite and drone based remote sensing and national monitoring programs. A pilot web-service will be developed providing analyses of current snow conditions, and short-term and seasonal forecasts to assist reindeer herders to follow and plan for the movement of the animals in relation to the snow and food access conditions in different areas during winter as well as in summer. The project is collaboration between researchers, reindeer herders and technical developers.

Reindeer herders are monitoring snow conditions on a daily basis while following the reindeer in the field to ensure that reindeers have access to grazing beneath the snow. Major changes in the snow conditions and corresponding reactions of the reindeer is also documented and summarized on a seasonal basis and used for evaluation and improvement of the assessment tools. Satellite data from passive and active microwave sensors will be assimilated in combination with available data from meteorological stations and Sámi observers to improve the simulation of the spatial distribution of snow depth, snow water equivalent, and ice layering. The modelling of the spatial distribution of the snow will be further supported by high resolution snow depth mapping using drone based techniques.

KEYWORDS

Arctic environments; Climate change; Snow; Indigenous knowledge;

Hydrological implications of permafrost thaw-induced landscape transition in the discontinuous permafrost zone at Scotty Creek, NWT, Canada

Kristine M. Haynes^{1*}, Ryan F. Connon², and William L. Quinton¹

¹*Cold Regions Research Centre, Wilfrid Laurier University, Waterloo, Ontario, N2L 3C5, CANADA*

²*Environment and Natural Resources, Water Resources Division, Government of the Northwest Territories, Yellowknife, Northwest Territories, X1A 2L9, CANADA*

**Corresponding author's email address: khaynes@wlu.ca*

ABSTRACT

Permafrost thaw resulting from increasing temperatures with climate change has induced a significant transition in land cover across the discontinuous permafrost zone of northwestern Canada. As permafrost degrades and is ultimately lost, elevated peat-dominated permafrost plateaus subside and become inundated by adjacent wetland features. The loss of intervening permafrost barriers facilitates hydraulic connections between isolated collapse scar bogs and the drainage network, effectively draining these newly-connected bogs. Given the contrast in hydrological function of peat plateaus, which generate runoff, as compared to collapse scar bogs and fens, which store and convey water, respectively, a change in the relative proportion of these land form types will affect the storage and routing of water across this mosaicked landscape. To better understand how the hydrology of these different land form types is changing with thaw-induced landscape transition, water levels on a permafrost plateau, channel fen, and isolated and connected bogs were monitored from 2003 to 2017 in the Scotty Creek watershed, Northwest Territories. The character of water level recessions in each of these land form types was examined to gain insight into the event response of individual features over time and reconcile such changes to the basin-scale runoff response. Bogs connected to the drainage network contribute stored water to basin runoff, with a water level decline of 40 to 220 mm over this period. Perched water tables on peat plateaus lower to coincide with those of adjacent wetlands, and exhibit an increasingly similar recession response to these wetlands over time as the underlying permafrost degrades. Understanding the hydrological implications of landscape change in the discontinuous permafrost zone will aid in forecasting the sustainability of water resources in this region.

KEYWORDS

permafrost thaw; peatlands; hydrological flowpaths; water level recession; wetland drainage; landscape change

1. INTRODUCTION

The landscape of the discontinuous permafrost zone is rapidly changing due to accelerated rates of permafrost thaw (Beilman and Robinson 2003; Quinton et al. 2011; Lara et al. 2016). Air temperatures in northwestern Canada are rising at nearly twice the global average rate resulting from anthropogenic climate change (Cohen et al. 2014; Richter-Menge et al. 2017), making this region one of the most rapidly warming on Earth (Vincent et al. 2015). This increase in temperature is catalysing large-scale changes in land form and function throughout the discontinuous to

sporadic permafrost zones with the thaw, degradation and ultimate loss of underlying permafrost (Rowland et al. 2010; Connon et al. 2014).

Peat plateaus have shallow perched water tables above the permafrost table, facilitating quick conversion of precipitation to runoff with minimal water storage capacity in the suprapermafrost layer (Wright et al. 2009). As permafrost thaws vertically, permafrost-cored, forested peat plateaus, which are elevated above the surrounding wetlands, subside. As the plateau surface subsides, the area becomes inundated by adjacent wetlands leading to black spruce mortality and canopy loss. In addition to vertical permafrost loss, lateral degradation of peat plateaus results in the expansion of wetland area including channel fens and collapse scar bogs (Connon et al. 2014). Treeless, permafrost-free channel fens in this region act as water conveyance features, directing water received from precipitation and surrounding peat plateaus (Hayashi et al. 2004). Water in this landscape is typically stored in permafrost-free collapse scar bogs isolated from the channel fen drainage network.

Loss of permafrost barriers significantly impacts the hydrology of the landscape; enhancing contributing areas to basin runoff and facilitating drainage of formerly isolated bog features (Connon et al. 2014; Haynes et al. 2018). The process of ‘bog capture’ incrementally connects formerly isolated collapse scar bogs to the basin drainage network (Connon et al. 2014), resulting in the contribution of stored water to basin runoff and expanding the area with the potential to contribute to basin drainage (Haynes et al. 2018). However, once the maximum contributing area is reached, when all bogs have developed a connection to the drainage network, a threshold of peak potential runoff will be achieved, which is higher than previously observed due to the significant expansion of the runoff contributing area (Haynes et al. 2018; Haynes et al. 2019). Given the rapid change to the features in this transitioning landscape, the future availability and sustainability of freshwater resources in this region will be impacted.

The overall objective of this study is to examine the effects of landscape transition on the hydrology of the land cover types that comprise the discontinuous permafrost zone. Given that permafrost thaw, the removal of permafrost barriers and the subsequent transition to wetland all affect the distribution and routing of water in the discontinuous permafrost landscape, it is important to understand the impacts of the associated climate change-induced shifts in hydrology and water resource availability. This study examines characteristics of event-based recession over the long-term water level records monitored in the land cover types of the Scotty Creek basin, Northwest Territories (NWT), representative of the discontinuous permafrost zone.

2. METHODS

2.1 Study Site

The Scotty Creek Research Station is located within the sporadic to discontinuous permafrost zone (61.44°N, 121.25°W; Figures 1a and 1b). The Water Survey of Canada gauged portion of the watershed covers 152 km² (Quinton et al. 2003) of heterogeneous upland moraines (48%), raised permafrost plateaus (20%), ombrotrophic bogs (19%), channel fens (12%), and lakes (2%) (Chasmer et al. 2014). The forested peat plateaus are dominated by an overstory of black spruce (*Picea mariana*) trees, with an understory of ericaceous shrubs (e.g. *Rhododendron groenlandicum*), lichens (*Cladonia* spp.), and mosses (*Sphagnum* spp.). Channel fens are dominated by floating vegetative mats of predominantly sedges (*Carex* and *Eriophorum*) with individual tamarack (*Larix laricina*) and birch (*Betula glandulosa*) trees scattered throughout the

fens (Garon-Labreque et al. 2015). Bogs in this basin are vegetated with ericaceous shrubs including leatherleaf (*Chamaedaphne calyculata*), bog rosemary (*Andromeda polifolia*), and small cranberry (*Vaccinium oxycoccos*) (Garon-Labreque et al. 2015). The dominant bryophyte species in the bogs include *Sphagnum balticum* and *S. magellanicum* (Garon-Labreque et al. 2015). Bogs that have developed a connection to the drainage network due to a breach in the surrounding permafrost and are actively undergoing drainage of stored water consist of primarily *S. fuscum* in the drying centre of the bogs, while *S. riparium* is confined mainly to the consistently saturated bog perimeter at the front of active permafrost loss and plateau subsidence (Gibson et al. 2018). Peat deposits in the basin range from 2 to 8 m deep (McClymont et al. 2013).

This study was conducted in the headwaters of the basin. The headwaters area, located in the southern portion of the basin, is entirely composed of peatland land cover types including permafrost plateaus, bogs and fens. Water levels were monitored from 2003 to 2017 in seven locations representing the dominant land cover types in the sub-basin including one peat plateau, one channel fen, and five bogs of varying degrees of connection (Figure 1c). The level of connection of each bog to the drainage network was assessed both visually using LiDAR imagery (Figure 1c) and through field observations. The monitored peat plateau is underlain by permafrost, which has rapidly degraded both vertically and laterally over time (Quinton et al. 2011), through which a talik has developed, providing a subsurface connection between the adjacent bog and channel fen (Connon et al. 2018). The average permafrost thickness was determined to be 9 ± 3 m in 2011 (McClymont et al. 2013) and is rapidly thawing over time. As the permafrost beneath the plateau has degraded, the plateau surface has subsided and become increasingly inundated as it transitions to a wetland feature (Quinton et al. 2011). Since measurements of this plateau began in 1999, the width of the plateau has decreased by more than half (Connon et al. 2018). Flanking the plateau are a channel fen to the west (Fen), which conveys water to the basin outlet, and a connected bog to the east (C-Bog 1), which is directly connected to the fen at the surface as well as the subsurface via a talik through the plateau (Figure 1c). C-Bog 2, adjacent to C-Bog 1, is also a connected bog (Figure 1c). C-Bog 3 has a partial direct connection to the fen, which became visible on aerial imagery between 1977 and 2000 (Quinton et al. 2011). The connection between the channel fen and C-Bog 3 has subsequently expanded as captured by the aerial image of 2008 (Quinton et al. 2011) and the LiDAR image of 2010 (Figure 1c). C-Bog 4 has a connection to the adjacent bog located to the east, apparent both on the digital elevation model (Figure 1c) and confirmed by field observations. This bog may form part of a bog cascade draining into a channel fen to the east of C-Bog 4. I-Bog 1 is an isolated collapse-scar bog formed as a result of localized permafrost thaw and ground subsidence (Figure 1c).

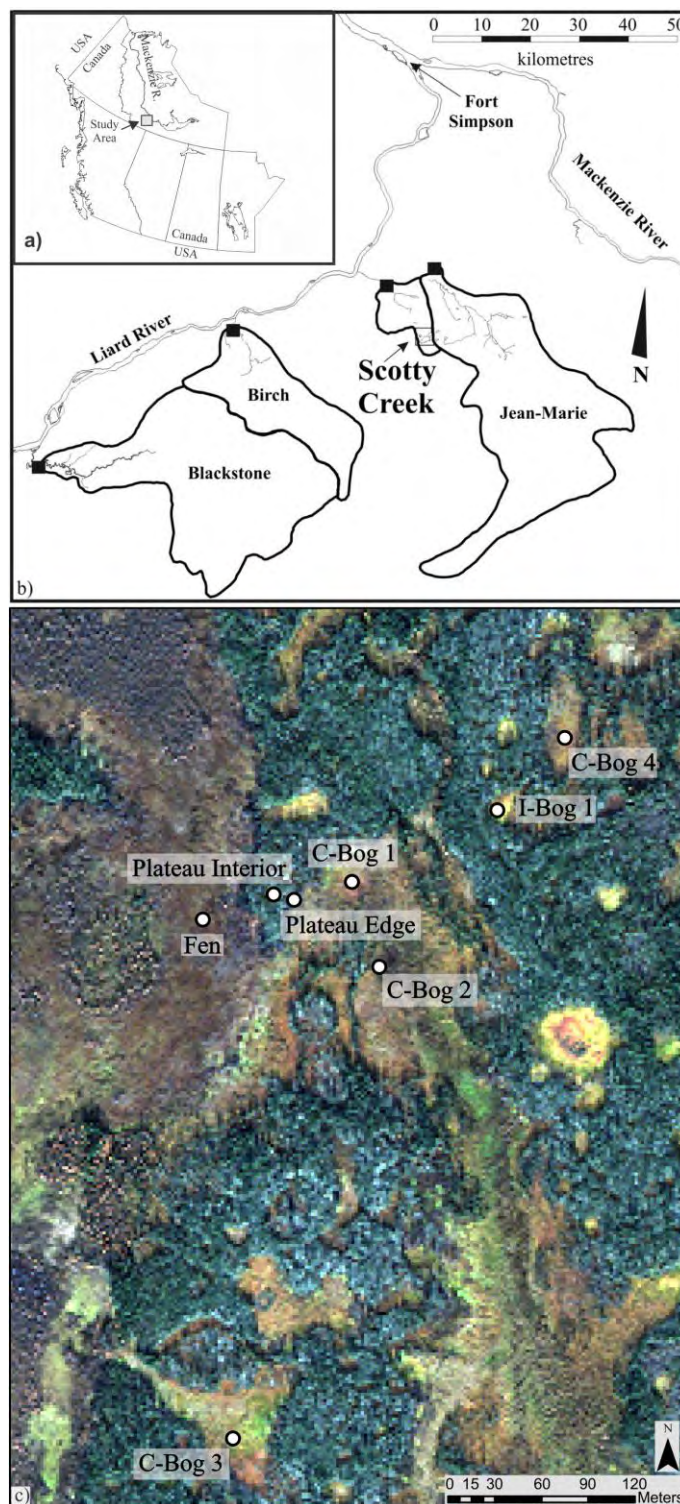


Figure 1. Location of study region in Canada (a), map of Scotty Creek, NWT (b), and a 2010 WorldView2 image of the 0.25 km² area of study within Scotty Creek (c). White dots represent the locations of wells in each of the monitored connected bogs (C-Bog), isolated bog (I-Bog), as well as channel fen and peat plateau sites.

2.2 Hydrometric Measurements

A single slotted stilling well was located at each site. Two wells were installed on the peat plateau, the first of which was located centrally on the plateau (referred to as Plateau Interior) and the other was installed approximately 5 m nearer to the plateau edge (referred to as Plateau Edge). Each well was equipped with a vented pressure transducer (Global Water WL15x and WL16s, Gold River, CA, USA). These vented transducers were used from 2003 to 2012, and in 2013 were replaced with total pressure transducers with internal data loggers (Levellogger Gold F15/M5, Solinst Canada Ltd, Georgetown, ON, Canada, and HOBO U20 Water Level Data Logger, Onset Computer Corporation, Bourne, MA, USA). To correct for barometric pressure, a barometric pressure transducer (Solinst Barologger Gold) was installed in the study area. During all study years, water level measurements were recorded at 30-minute intervals. From 2003 to 2013, water level loggers were installed in the wells each year either during or immediately following the spring freshet and removed prior to freeze-up in the late summer or early fall. Beginning in 2014 for C-Bog 1 and the channel fen and in 2015 for all other wetland wells, the pressure transducers were lowered within each well at the end of the growing season and remained in the wells over the winter season. To convert the pressure transducer measurements to actual water level depths, manual measurements from the top of the well casing to the water level were recorded typically at both sensor installation and removal. Absolute elevation, expressed in metres above sea level (m asl), for the top of each well casing was measured in May 2015 using a differential global positioning system (dGPS; SR530 RTK, Leica Geosystems Inc., Norcross, USA; system accuracy ± 0.02 m).

2.3 Water Level Recession Characteristics

2.3.1 Recession slope

Water level recession slopes were manually determined for a single mid-growing season event for a connected bog (C-Bog-2), a channel fen and the two wells located on the thawing peat plateau, one located centrally on the plateau (referred to as Plateau Interior) and the other located approximately 5 m nearer the plateau edge (Plateau Edge). One precipitation event, greater than 5 mm, was selected each year from 2003 to 2017, for years in which water level records were available, to assess the water level recession slope for each of these land cover types. Slopes of water level recession were determined from peak water level to the approximate water level prior to the precipitation event, but were stopped prior to considerable evaporative losses as evidenced by diurnal cycles in water level. To assess trends in recession slope for the sub-set of land cover types, the recession slope values were plotted over time for each site.

2.3.2 Recession constant

To expand the analysis of the character of water level recession in the different thermokarst land cover types representative of the discontinuous permafrost zone to incorporate a greater number of rainfall events, the Matlab-based toolbox known as HydRun was used (Tang and Carey 2017). HydRun is a hydrograph analysis package that objectively computes hydrometric indices for event-based rainfall-runoff analysis (Tang and Carey 2017). Given the ability of HydRun to associate rainfall events to the corresponding hydrograph response and determine hydrometric parameters based upon the user-selected values of key variables including peak threshold and return ratio, use of this tool reduces the subjectivity of manually calculating hydrograph characteristics (Tang and Carey 2017). Although designed for streamflow hydrograph analysis, HydRun was successfully parameterized to isolate recession characteristics using the water level data collected in the

dominant thermokarst landscape types in the Scotty Creek watershed over the period of record up to and including 2017.

Water level responses to rainfall events were extracted using HydRun from the long-term water level records collected in four connected bogs, one bog isolated from the drainage network, one channel fen and the two wells located on the monitored thawing plateau (Plateau Interior and Plateau Edge as described above) (Figure 1c). To compare responses to events of similar magnitude across sites, recession events isolated using HydRun were then filtered to include only those in response to a precipitation event with a depth of between 1 to 15 mm occurring 2 days antecedent to the water level recession. Recession constants were subsequently filtered so that only those with a normalized root mean square error (NRMSE) of less than or equal to 0.15 were selected, indicative of recession limbs that have a reasonable fit with an exponential function. This threshold value was selected to be greater than the NRMSE of 0.05 used by Tang and Carey (2017) to account for the likelihood that water level recession may not exhibit the same exponential trend as a streamflow hydrograph response.

Trends in recession constants (expressed in hours) were examined over the period of water level record according to land cover type. Recession constants were plotted for the connected bogs ($n = 4$), the isolated bog ($n = 1$), the channel fen ($n = 1$), as well as the edge ($n = 1$) and interior ($n = 1$) of a rapidly thawing plateau.

3. RESULTS AND DISCUSSION

3.1 Water Level Recession Slopes

Recession slopes for the connected bog (C-Bog-2) and adjacent channel fen were similar throughout the period of water level record (Figure 2). These recession slopes were low as compared to those recorded on the degrading plateau early in the long-term record. Due to destabilization of the well at the Plateau Edge site, the water level record ends in 2010. However, as time progresses, the recession slopes recorded at the Plateau Interior location became increasingly similar to those observed in the connected bog and channel fen.

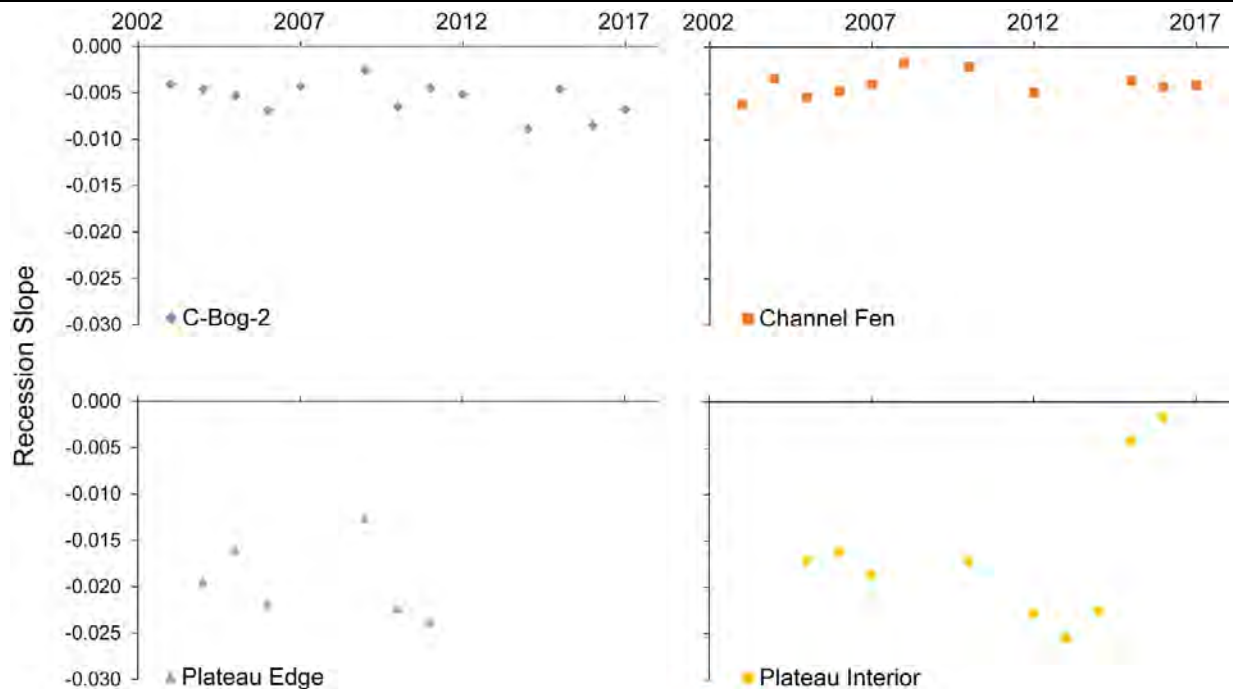


Figure 2. Annual recession slopes in response to one precipitation event each year for a connected bog (C-Bog-2), a channel fen as well as at the edge and interior of a rapidly thawing permafrost plateau (Plateau Edge and Plateau Interior, respectively).

Peat plateaus are known runoff generators, with precipitation being quickly converted to runoff due to the limited storage capacity of these landscape features (Wright et al. 2009). The perched water table located above the permafrost underlying elevated peat plateaus reacts quickly with the input of precipitation. Subsequently, the water level on these elevated features recedes quickly as water is shed to surrounding low-lying wetlands. As the peat plateau degrades over time, the perimeter of the plateau retreats due to lateral permafrost thaw resulting in a significant loss of plateau area. Additionally, vertical permafrost thaw induces significant subsidence of the plateau ground surface, leading ultimately to the transition from relatively dry permafrost plateau to saturated wetland. This transition is evident in the trend of annual recession slopes for the Plateau Interior site. As the peat plateau subsides throughout the course of the water level record, the recession slope for this interior site becomes similar to those measured in both the adjacent channel fen and connected bog at the end of the period (Figure 2). This suggests that the hydrological response of peat plateaus will transition to that of wetlands including channel fens and connected bogs as the landscape becomes increasingly connected due to the loss of impeding permafrost barriers.

3.2 Water Level Recession Constants

Over the course of the water level records, the mean annual recession constants generally decrease with time across the varied landscape features (Figure 3). The mean recession constants across the four monitored connected bogs decline slightly from 2005 to 2017 and are similar to those recorded in the channel fen. However, the recession constants of the connected bogs become variable in the latter years of the measurement period from 2013 to 2017, whereas the recession constants for the channel fen are quite variable throughout the water level measurement record (Figure 3). The response of the channel fen to precipitation events in this landscape is governed not only by the

magnitude of the event but also by the antecedent moisture condition prior to the input of precipitation. As permafrost barriers that act to hydrologically isolate wetland features from the drainage network are lost due to thaw, these wetlands develop the potential to contribute to basin runoff (Connon et al. 2014). However, the ability of individual wetlands to hydrologically connect to the basin drainage network is dependent upon the level of antecedent moisture, with connections forming only in periods of sufficient moisture supply in order to exceed the storage capacity of these wetlands (Connon et al. 2014). Therefore, the variability in the recession constants for the channel fen throughout the water level record may be a function of antecedent moisture conditions, controlling the establishment of hydrological connections to these drainage networks, and thereby influencing the length of time for this feature to return to pre-event water levels.

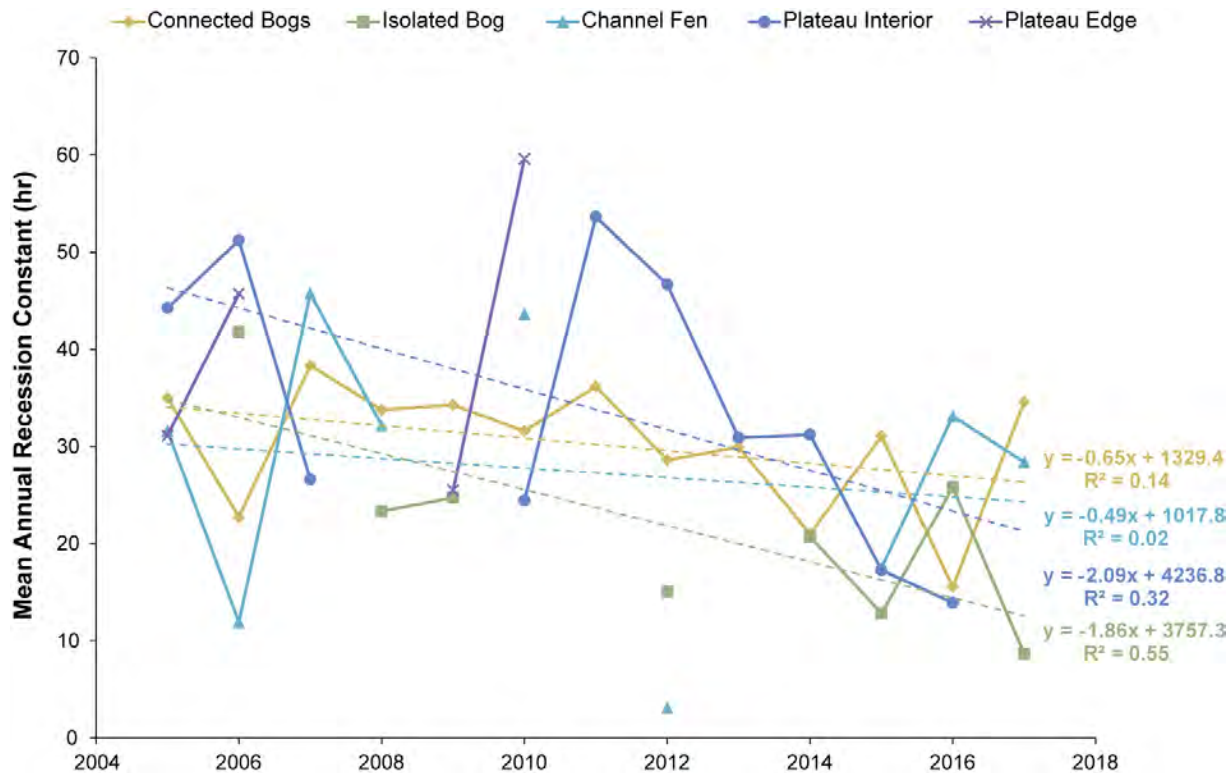


Figure 3. Mean annual recession constants (in hours) for events of 1-15 mm determined in connected bogs (n = 4), isolated bog (n = 1), channel fen (n = 1), peat plateau interior (n = 1) and peat plateau edge (n = 1).

Additionally, the variability in mean annual recession constants across the four monitored connected bogs may be a function of landscape change occurring in these bogs over time. Loss of permafrost barriers facilitates the hydrological connection of formerly isolated bogs to the drainage network, which in turn leads to drainage of the water stored within these bogs (Haynes et al. 2018). Permafrost thaw-induced drying of the bogs connected to the drainage network catalyses further landscape transition including the formation of hummock microtopography. The increased variability in recession constants may be a function of the increased area of hummocks in connected bogs, acting to increase the path length of the hydrological flow paths and subsequently increase

the recession time following precipitation events. The potential increase in flow path tortuosity may function in a similar manner as mineral earth hummocks in the continuous permafrost zone, which significantly influence subsurface drainage (Quinton and Marsh 1998; Quinton and Marsh 1999). Further research is required to examine the influence of hummock formation on the hydrology of this rapidly changing landscape.

4. CONCLUSIONS

Climate change-induced permafrost thaw is catalysing significant landscape change in the discontinuous permafrost zone. Vertical and lateral degradation of permafrost results in the considerable loss of plateau area and the inundation of subsiding plateaus by adjacent wetlands. Expansion of the wetland area contributing to the basin drainage network has enhanced runoff generation from the Scotty Creek basin with a concomitant decline in water stored in bogs due to the permafrost thaw-induced process of ‘bog capture’ (Connon et al. 2014; Haynes et al. 2018; Haynes et al. 2019). This study illustrates that the water level recession slope of peat plateaus in response to precipitation events have become increasingly similar to those of connected bogs and channel fens as the landscape changes. Examination of water level recession constants also indicates the potential for further landscape change such as the formation of hummocks to influence the hydrological response of this changing landscape. Further investigation of factors that may influence the hydrological response of this environment, including the perimeter-to-area ratio, flow path tortuosity and water table displacement, is warranted to understand the likely impacts associated with the future trajectory of landscape change in the discontinuous permafrost zone.

ACKNOWLEDGEMENTS

We acknowledge the contributions of all those involved in data collection at Scotty Creek. We also wish to thank the Dehcho First Nations for their support and acknowledge that the Scotty Creek Research Station is located on Treaty 11 land. We acknowledge funding support from a Natural Sciences and Engineering Research Council of Canada (NSERC) Discovery Grant.

REFERENCES

- Beilman D. & Robinson S. 2003. Peatland permafrost thaw and landform type along a climate gradient. In Proc. Eighth International Conference on Permafrost, vol. 1, Phillips M, Springman SM, Arenson LU (eds). A.A. Balkema: Zurich, Switzerland; 61–65.
- Chasmer, L., Hopkinson, C., Quinton, W., Veness, T. & Baltzer, J. 2014. A decision-tree classification for low-lying complex land cover types within the zone of discontinuous permafrost. *Remote Sens. Environ.* 143, 73–84.
- Cohen, J., Screen, J.A., Furtado, J.C., Barlow, M., Whittleston, D., Coumou, D., Francis, J., Dethloff, K., Entekhabi, D., Overland, J. & Jones, J. 2014. Recent Arctic amplification and extreme mid-latitude weather, *Nat. Geosci.* 7, 627–637.
- Connon, R.F., Devoie, É., Hayashi, M., Veness, T. & Quinton, W.L. 2018. The influence of shallow taliks on permafrost thaw and active layer dynamics in subarctic Canada. *J. Geophys. Res.: Earth Surf.* 123, 281–97.
- Connon, R.F., Quinton, W.L., Craig, J.R. & Hayashi, M. 2014. Changing hydrologic connectivity due to permafrost thaw in the lower Liard River valley, NWT, Canada. *Hydrol. Proc.* 28(14), 4163-4178.

- Garon-Labrecque, M.É., Léveillé-Bourret É., Higgins, K. & Sonnentag, O. 2015. Additions to the boreal flora of the Northwest Territories with a preliminary vascular flora of Scotty creek *Can. Field-Nat.* 129, 349–67.
- Gibson, C.M., Chasmer, L.E., Thompson, D.K., Quinton, W.L., Flannigan, M.D., & Olefeldt, D. 2018. Wildfire as a major driver of recent permafrost thaw in boreal peatlands. *Nature Communications* 9, 3041.
- Hayashi, M., Quinton, W.L., Pietroniro, A. & Gibson, J.J. 2004. Hydrologic functions of wetlands in a discontinuous permafrost basin indicated by isotopic and chemical signatures. *Journal of Hydrology* 296(1), 81-97.
- Haynes, K.M., Connon, R.F. & Quinton, W.L. 2018. Permafrost thaw induced drying of wetlands at Scotty Creek, NWT, Canada, *Environmental Research Letters* 13, 114001.
- Haynes, K.M., Carpino, O.A., Connon, R.F., Devoie, É. & Quinton, W.L. 2019. Thaw-induced land-cover change in the southern margin of discontinuous permafrost, northeastern British Columbia and southwestern Northwest Territories; in Geoscience BC Summary of Activities 2018: Energy and Water, Geoscience BC, Report 2019-2, p. 123–132.
- Lara, M.J., Genet, H., McGuire, A.D., Euskirchen, E.S., Zhang, Y., Brown, D.R.N., Jorgenson, M.T., Romanovsky, V., Breen, A. & Bolton, W.R. 2016. Thermokarst rates intensify due to climate change and forest fragmentation in an Alaskan boreal forest lowland. *Glob. Change Biol.* 22, 816–29.
- McClymont, A.F., Hayashi, M., Bentley, L.R. & Christensen, B.S. 2013. Geophysical imaging and thermal modeling of subsurface morphology and thaw evolution of discontinuous permafrost. *J. Geophys. Res.* 118, 1826–37.
- Quinton W.L., Hayashi, M. & Chasmer L. 2011. Permafrost-thaw-induced land-cover change in the Canadian subarctic: implications for water resources. *Hydrol. Proc.* 25, 152–158.
- Quinton, W.L., Hayashi, M. & Pietroniro, A. 2003. Connectivity and storage functions of channel fens and flat bogs in northern basins. *Hydrol. Process.* 17, 3665–84.
- Quinton, W.L. & Marsh, P. 1998. The influence of mineral earth hummocks on subsurface drainage in the continuous permafrost zone. *Permafrost Periglac.* 9, 213-228.
- Quinton, W.L. & Marsh, P. 1999. A conceptual framework for runoff generation in a permafrost environment. *Hydrological Processes* 13, 2563-2581
- Richter-Menge, J., Overland, J.E., Mathis, J.T. & Osborne, E. (Eds.): Arctic Report Card 2017, available at: <http://www.arctic.noaa.gov/Report-Card>, last access: 14 December 2017.
- Rowland, J.C. *et al.* 2010. Arctic landscapes in transition: responses to thawing permafrost. *EOS, Trans. Am. Geophys. Union* 91, 229–30.
- Tang, W. & Carey, S.K. 2017. HydRun: A MATLAB toolbox for rainfall–runoff analysis. *Hydrological Processes* 31, 2670–2682.
- Vincent, L., Zhang, X., Brown, R., Feng, Y., Mekis, E., Milewska, E., Wan, H. & Wang, X. 2015. Observed trends in Canada’s climate and influence of low-frequency variability modes, *J. Climate*, 28, 4545–4560.
- Wright, N., Hayashi, M. & Quinton, W.L. 2009. Spatial and temporal variations in active layer thawing and their implication on runoff generation in peat-covered permafrost terrain. *Water Resources Research* 45, W05414.

Assessing snowpack water equivalent in the Snare River watershed, NWT

J. Hickman¹, M. English², N. Wilson², S. Kokelj³, R. Judas⁴, M. Richardson⁵, P. Aukes⁶
D. Tokarski⁵

¹*Environmental Stewardship and Climate Change Division, Environment and Natural Resources
Government of the Northwest Territories, Yellowknife, NT, X1A 2L9, CANADA*

²*Cold Regions Research Centre, Wilfrid Laurier University, Waterloo, ON, N2L 3C5, CANADA*

³*Water Resources Division, Environment & Natural Resources, Government of Northwest Territories,
Yellowknife, NT, X1A 2L9, CANADA*

⁴*Wildlife Division, Environment and Natural Resources Government of the Northwest Territories,
Yellowknife, NT, X1A 2L9, CANADA*

⁵*Geography and Environmental Studies, Carleton University, Ottawa, ON, K19 5B6, CANADA*

⁶*Earth and Environmental Science, University of Waterloo, Waterloo, ON, N2L 3G1, CANADA*

*Corresponding author's email address: menglish@wlu.ca

ABSTRACT

Sampling snowpack water equivalent (SWE) in large basins remains a challenge. In some situations where hydroelectric production relies significantly on the annual recharge by the snowpack, assessing SWE as accurately as possible has significant economic implications to both providers and consumers. In this study we assess the effectiveness of the annual end-of-winter survey in the Snare River catchment which has been on-going for several decades. To provide a means of assessing the probability of achieving a reasonable approximation of basin SWE we established an intensive study site south of Wekweeti, within the catchment. To provide as accurate as possible an estimate of SWE within a 300km² area of the Snare system south of Wekweeti we divided the landscape into 9 terrain units (TUs) and sampled them proportionately to their areal coverage. The intensive site was located in portions of two EASE-Grid pixels. The spatial sampling was divided into four large blocks of land each 75km² in area covering representative portions of the two pixels. The topographic similarity of this site was compared with the sites used for the 'annual' survey by mapping the TUs in a 120km² area surrounding each of the specific sampling sites. Comparing the TU composition from each 'annual' site with the TUs sampled at that site provided an indication of how representative the 'annual' SWE survey was. The number of TUs sampled ranged from 6 to 3 out of 9 possible TUs. Given the number of sites chosen to sample in specified TUs at the annual sites it was possible using the larger data set at the intensive site the probabilities of accurate SWE assessment at the 'annual' sites. The mean SWE at the intensive site aligned quite nicely (difference of ~6%) with the Globsnow value. It is unclear whether this was coincidence or resulted from a structured sampling directed at proportional representation of the landscape. If the comparison is valid, there are meaningful implications for future assessment of SWE within the Snare River catchment.

1. INTRODUCTION

Power for over 50% of the Northwest Territories population is generated by hydroelectric installations along the Snare River which drains a 14,000 km² catchment. Storage potential within the catchment to retain economically efficient hydraulic head in the reservoirs to drive the turbines can be as short as a few months. Consequently drought usually results in periods when Northwest Territories Power Corporation (NTPC) relies upon diesel generators to provide power. The costs of relying on diesel fuel can be very significant. Determining the hydrological sensitivities of this system to year to year changes in both precipitation, and evapotranspiration is the primary objective of this research project. As snowmelt is always the major recharge event of the year estimations of catchment SWE are hydrologically and economically important. To address this, this paper examines the distribution of snow within the catchment prior to melt to determine if the current spatial grid sampling approach within each sampling site (hereafter referred to as the ‘annual’ sites) used in assessing catchment snowpack water equivalent (SWE) by NTPC is representative of both catchment and individual site SWE.

Figure 1 illustrates changing basin efficiencies in the Snare River basin from 1999 to 2015. The pattern illustrated here underlines the relative changes in basin storage through this 17 year period. The two declining portions of the curve result in significant fire years for the NWT especially in 2014. Inclusion of this figure serves to underline the idea that when these basins are undergoing prolonged drought the need for accurate snow surveys is important as the implications of significantly overestimating SWE would be more significant than during periods when basin efficiencies were high.

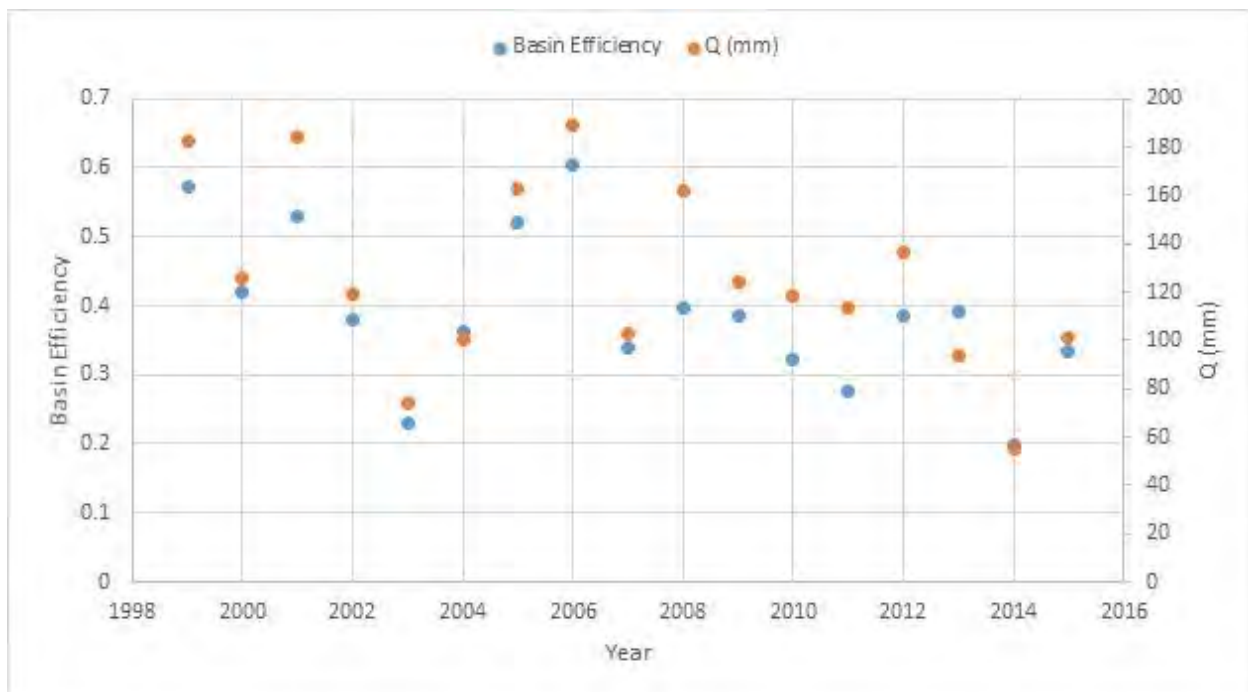


Figure 1. Snare River catchment estimated hydrological efficiencies and total discharge (1999-2015)

2. METHODOLOGY

Our study focused on a 300km² area in the Snare system south of the Tlicho community of Wekweeti, where during a four day period near the end of March 2018 we conducted a snow survey of 200+ sites. Prior to the survey the 5 m Arctic DEM was used to delineate the study site into 9 terrain units; 8 of the terrain units were based on the four primary cardinal directions which were further subdivided into shallow slopes (< 6°) and steeper slopes (>6°) acknowledging that topography and aspect plays a major role in snow accumulation (ref). The remaining terrain unit was lake surface. Site selection was proportional to the total area covered by each terrain unit. Specific site selection within each terrain unit avoided specific boundaries separating terrain units so that edge effect was not an issue. Edge effect was only visibly apparent along the lake perimeters. Sampling was performed by a team of five people using either an EC30 or a larger snow tube constructed at a metal shop in Kitchener to specifications. Environment Canada protocol was followed at each site which involved taking a single snow core to determine snowpack density; snowpack stratigraphy with respect to changes in snow grain size was recorded where the snow core was extracted. In addition at each site 30 depth measurements using a metre stick were randomly taken within an area of approximately 100m². All measurements taken by the larger core tube were corrected to EC30 values by a 10 core comparison of snow density taken side by side on a lake where snow crust and ice lenses were not present.

One of the primary objectives of this work is to determine whether the sampling technique employed annually to determine SWE in the Snare River catchment is reasonably accurate. Estimating SWE from fieldwork for large river catchments poses significant logistical problems tied intimately with economic realities. The latter may be offset by recognizing the issues associated with over-or-under estimating SWE prior to springmelt especially when maintaining sufficient hydraulic head in reservoirs is necessary for generation of hydroelectric power. The long term costs of not estimating the major recharge event of the year may outweigh the costs of additional fieldwork.

The first step in this process involved assessing if the terrain units sampled in the individual sites are representative of the area they are situated in. A terrain unit map was constructed (as described above for our intensive site) for an area of 121.1 km² around each of the *annual* sites. The areal coverage of terrain units was then compared with the terrain units sampled to determine if the terrain units sampled were reflective of the terrain.

At the annual sites the number of sites selected within individual terrain units was typically no more than 4 and often less than this. To put some perspective on this we examined three of the terrain units (Shallow North, Shallow South and Shallow East) sampled at the intensive site where the number of individual SWE sites was large to moderate (n = 42, 34, and 13 respectively). The objective of this exercise was to determine the probability, when selecting 4 sites, of obtaining a SWE value that was representative of the mean SWE of the terrain unit. Random selection of 4 SWE data points from the population of SWE data from these two sites 50 times each provided probability of obtaining a SWE value within 10-25% of the TU mean value.

A minor objective of this work was to determine if we have any evidence that Globsnow could be used with confidence to estimate SWE in the Snare River catchment. The strength of Globsnow is its temporal and spatial availability. The study is limited by the fact that our survey, though relatively intensive in terms of sampling density, was conducted in an area of 300km² less than half the spatial resolution of a single EASE-Grid pixel SSM/I. The strength of the survey is that is representative of the terrain within the EASE-Grid pixel and by association therefore we assume representative of SWE in the pixel. As well the survey was divided into 4 x 75km² areas located throughout the EASE-Grid pixel area.

3. RESULTS

Indications of sampling representativeness of the Snare River catchment terrain are indicated in Table 1. The specific areas sampled at each of the annual sites are compared with the larger terrain unit maps created for each of these sites. Including ‘lakes’ as a ‘terrestrial’ unit the annual survey at the nine long term ‘annual’ sites includes between 33% and 66% of available ‘terrain’ units which spatially represent between 60 and 90% of the terrain. If lakes are excluded as they represent between 28-35% of the surface areas of the site terrain unit maps only 27 to 58% of the remaining terrain units are sampled.

Table 1. Representativeness of ‘Annual’ sampling sites with respect to the surrounding terrain

Column1	Ghost	Castor	Mattberry	Christison	Indin	White Wolf	Snare	Winter	Mesa
A.	6	5	4	6	6	4	4	3	6
B	57.52	49.89	26.9	57.76	62.06	56.88	54.72	56.71	27.2
C	86.52	84.89	60.9	89.76	93.06	90.88	91.72	89.71	55.2
A. Terrain units sampled out of possible 9									
B.% of surface area sampled excluding lakes									
C. % of surface area sampled including lakes									

One objective of this work was to determine how the number of sites within any of the terrain units sampled during the annual snow survey might impact the probability of arriving at a representative SWE value. Assessing the probability of using a small number of sample sites to obtain a reasonable estimate of SWE within a sample site is accomplished by utilizing the ‘intensive’ site data set and specifically focusing on the terrain units that have been used to determine SWE at the ‘annual’ sampling sites. The two most often sampled terrain units in the ‘annual’ survey are ‘Shallow North’ and ‘Shallow South’. Typically, during the ‘annual’ SWE survey when one of these TUs are sampled 4 SWE data points are produced. Accordingly a test was run on both the ‘intensive site’ Shallow North (n=42) and Shallow South (n=34) terrain unit data sets wherein we randomly selected four of the number of sites in both TUs 50 times and compiled the data so that we could discern the percentage of times that we produced a SWE value within 10%, 15%, 20%

and 25% of the true mean for that TU. In similar fashion we calculated the same probabilities for the Shallow East TU (n = 16) that produced two SWE data points on average when it was sampled during the ‘annual’ survey. Again probabilities of producing a SWE value within 10%, 15%, 20% and 25% of the true mean for that TU was determined. Table 2 illustrates these probabilities. As the annual spring recharge to hydroelectric reservoirs is important for maintaining enough hydraulic head to drive the turbines efficiently accurate assessment of catchment SWE becomes an important factor in predicting operating efficiency. Table 1 and 2 illustrate two opportunities for the annual survey to increase predictive accuracy by increasing: 1. representativeness in site selection and, 2. number of sample sites within each terrain unit.

Table 2. Predicted probabilities of determining SWE within a specified percentage of the mean

	A	B	C	D
Site				
Shallow North	38%	54	70	84
Shallow South	36	46	54	58
Shallow East	34	46	66	78

A: +/- 10% of the mean value; B: +/- 15% of the mean value; C: +/- 20% of the mean value; D: +/- 25% of the mean value

The Globsnow data base provides an economically efficient means of ascertaining changes in SWE across large spatial scales on a daily time step. The algorithm converting brightness temperature (from the SSM/I satellite series) into meaningful SWE values is a case of ‘one size fits all’ in that the algorithm not only stays the same for boreal forest regardless of changes in the structure of the landscape, vegetation or the surface area ratio of lake:terrain but it remains the same for every biome (Derksen, Pers, comm 2019). It is understood that Globsnow will produce errors in SWE and these errors will be variable across a heterogeneous landscape (Derksen, pers. comm 2018). To build confidence in the Globsnow data, ground-truthing of the snowpack in areas of concern is done for verification. Typically the comparative errors may range between 15 and 30% (Larue et al, 2017, Langlois, pers. comm. 2019; Derksen, pers. comm., 2019). A problem relating Globsnow data to field data is generally tied into how representative the snow survey is of the landscape. A field sampling design aligned with the differences in terrain surface area and proportionally sampled will produce a mean SWE value that is closer to reality.

For the intensive site we assumed the methodological approach specifically designed to be representative of proportional areal coverage of each terrain unit, enabled us to produce a mean SWE estimate strongly reflective of the snowpack on the ground. The mean SWE at the intensive site was 7.92 cm while the corresponding Globsnow value was 8.43 cm, a 6.43% difference, much lower than the reported values noted above. Figure 1 illustrates a comparison of the Globsnow SWE value temporally appropriate for the intensive site and the range of SWE values recorded at the intensive site. The diagonal line is the 1:1 relationship. One of the factors at play when larger errors are reported between ground-truthing values and Globsnow is that the ground-truthing estimates in certain cases are based on a small number of data points located in areas

convenient to sample but perhaps not representative of the local topography. There is the possibility that the small difference we have found when comparing Globsnow SWE to the intensive site SWE is coincidental.

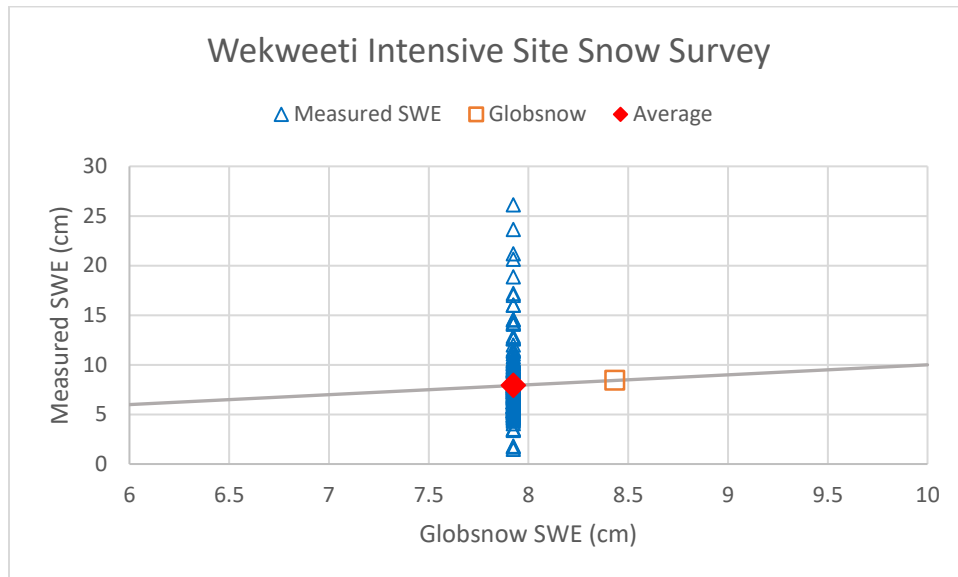


Figure 2. Intensive site measure SWE value and Globsnow value for 26-30 March 2018

Figure 3 illustrates the difference between the real and corrected Globsnow (using the intensive site correction factor of 6.43%) values for the EASE-Grid Pixels within which each NTPC-ENR sampling site is located and the relevant SWE values derived from the actual snow surveys in 2018. The comparisons indicate that in four cases there is not a great difference between the actual data collected in the field and the Globsnow value while the remaining data illustrate a range of differences from moderate to significant.

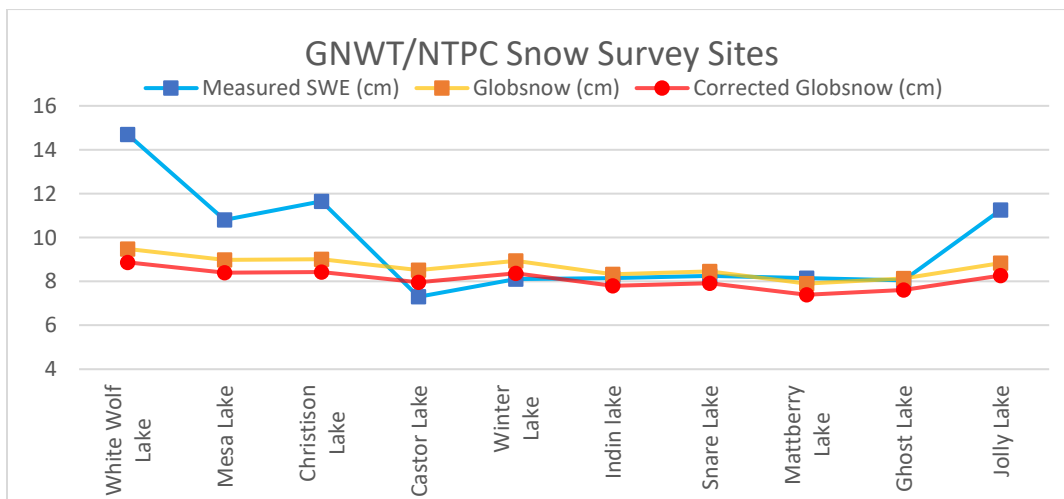


Figure 3. Globsnow and ‘Annual’ site SWE for 26-30 March 2018

Accepting these SWE values at face value means the difference between Globsnow and measured SWE at the ‘annual’ sites would result in an overestimation of SWE by the field measurements by 17.4%. Keeping in mind that small sample numbers in terrain units can be misleading the similarities between Globsnow and measured SWE at the ‘annual’ sites may be misleading. Confidence in SWE values more closely representing real SWE might be higher if there are structural similarities between the ‘intensive’ site and the ‘annual’ sites. To quantify structural similarities the terrain unit map for both the intensive and annual sites were compared. The ratios of areal coverage of each terrain unit between the intensive site and each ‘annual’ site were calculated and the average value determined (Figure 4).

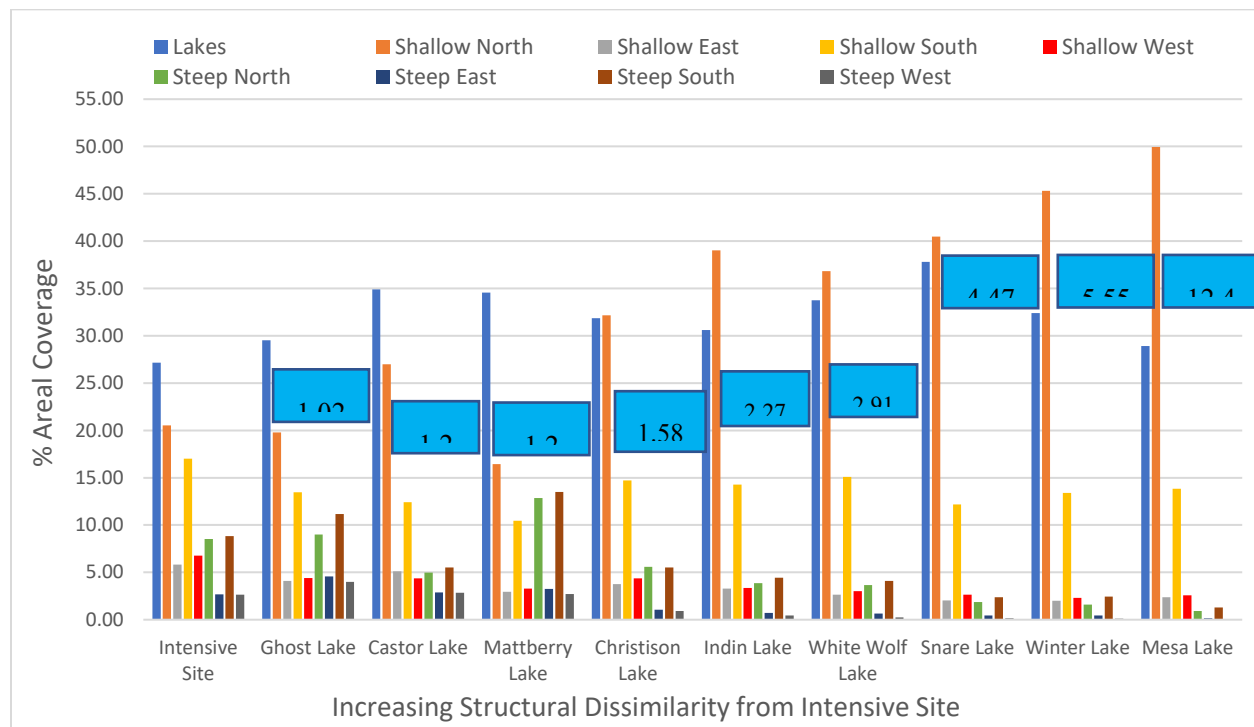


Figure 4. Illustration of areal coverage of terrain units in Intensive site and GNWT-NTPC sites

The mean site ratio of Intensive to Annual site is shown in the blue rectangles. In Figure 4 there is reasonably strong topographic similarity between the intensive site and Ghost, Castor, Mattberry and Christinson Lake NPTC-ENR sampling sites with a ratio of 1.02 to 1.58 whereas there is strong dissimilarity between the intensive site and Snare (4.47), Winter Lake (5.5) and Mesa Lake (12.31). As landscape structure plays a strong role in snowpack accumulation patterns it is assumed where there are notable differences in landscape similarity that extrapolation of a correction factor is probably not warranted.

4. CONCLUSIONS

This study examined the probability that the ‘annual’ snowpack survey in the Snare River catchment provides an appropriate level of accuracy to assess the quantity of snowmelt water recharging the system in spring. From this study it is apparent that the sample numbers in the terrain units used to estimate SWE could benefit from increasing in order to provide more confidence in estimating basin SWE. Though conclusions regarding the applicability of Globsnow to provide reasonable estimates of SWE in this basin are questionable given the fact we can only compare with confidence one EASE-Grid pixel it may point out that snow surveys accounting for proportional sampling on representative terrain units is important both for determining a reasonable estimate of SWE and a means to compare Globsnow values to with a reasonable degree of confidence. Small numbers of samples taken in terrain that may or may not be representative of the larger area it is intending to represent leads to a probable conclusion of inaccuracy.

Terrain and permafrost thaw controls on biomass trajectories across a Taiga Plains watershed; comparing lidar models with satellite optical vegetation indices

Chris Hopkinson¹, Laura Chasmer¹, William Quinton², Linda Flade¹, Guillermo Castilla³

¹*Department of Geography, University of Lethbridge, Lethbridge Alberta, T1J 3M4, CANADA*

²*Cold Regions Research Centre, Wilfrid Laurier University, Waterloo, ON, N2L3C5, CANADA*

³*Northern Forestry Centre, Natural Resources Canada, Edmonton, Alberta, T6H 3S5 CANADA*

**Corresponding author's email address: c.hopkinson@uleth.ca*

ABSTRACT

There is uncertainty over the nature of ecosystem processes and trajectories that underlie 'greening and browning' trends in sub Arctic environments. While there may be some justification for equating 'greening' (increasing NDVI) to an increase in biomass, and 'browning' (decreasing NDVI) to a loss of biomass, the actual processes occurring are complex and not well understood. At the Scotty Creek Watershed (~100km²) south of Ft Simpson, NWT, we have embarked on a time series field and airborne lidar campaign to monitor biomass changes from 2007 to 2018. This has allowed us to map changes in vegetation height and cover, diminution of individual permafrost plateaus and scale up to the watershed. We have compared biomass change to trends in MODIS NDVI to identify correlations across the watershed and with land surface types. No strong correlations between biomass and NDVI change were established at watershed-scale. However, spatial correlation between biomass loss (mortality) and terrain uplands and riparian zones around permafrost plateaus were established and rates of loss mapped across the watershed. Meanwhile, biomass accumulation was found to correlate primarily with fens and marshes. While mortality of vegetation due to upland drying and riparian thaw-induced saturation is widespread, the changes in canopy height indicate that biomass accumulation (expressed as canopy volume) could exceed loss by ~ up to 50%. This work does little to reconcile optical vegetation indices with ecosystem level processes in the Taiga Plains ecozone but it indicates that we cannot simply assume a change in VI correlates with a change in biomass.

KEYWORDS

Biomass model, change detection, permafrost thaw, lidar, vegetation index, NDVI, Scotty Creek.

Recent changes of the winter and spring season hydrological regime in Finland

Johanna Korhonen¹

¹Freshwater Centre, Finnish Environment Institute SYKE, Helsinki, 00790, FINLAND

*Corresponding author's email address: johanna.korhonen@ymparisto.fi

ABSTRACT

In a boreal snow-driven region, such as Finland, changes in the winter and spring climatic seasonal conditions have a large effect on the hydrology. Recently, winter and spring air temperatures in northern latitudes have increased remarkably – more than annual temperatures and more than in other regions. Ice cover and river discharge observations are among the oldest hydrological records in Finland and in some locations records cover 150–300 years. In this study, the recent 21st century changes of the winter and spring season hydrological regime are investigated and compared to long-term ice phenology and river discharge trends in Finland.

The analyses show statistically significant changes in both ice cover and discharge regime until the recent years. The ice freeze-up has become later, and the break-up is earlier, while the duration of the ice cover has shortened. In recent decades, changes have become even more apparent and the number of extremely early break-ups and late freeze-ups has increased (Fig. 1). In ice phenology, new records have been set in the 21st century. When comparing the break-ups and freeze-ups of the 2001–2018 winters to the averages of those from 1961–2000 of these longest time series, the winters of the 21st century have been extremely mild. The results of the updated data until the 2017–2018 winter, prove that 16–17 out of 18 (89–94%) break-ups have been earlier and 14–16 out of 17 (82–94%) freeze-ups have been later than the 1961–2000 average for each time series. Until 2002, there were both increasing and decreasing trends in the maximum lake ice thickness. Updated data until the winter 2017–2018 still show decreasing trends in the south, but no longer increasing trends in Central or Northern Finland.

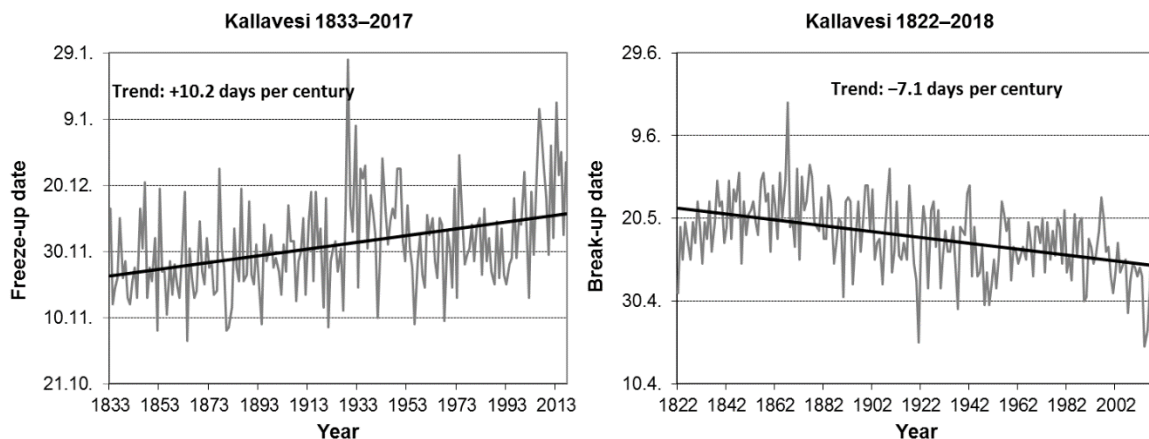


Figure 1. Lake Kallavesi freeze-up and break-up time series updated until the winter 2017–2018.

In the discharge regime, the seasonal winter and spring discharges have increased, and the spring peak has moved earlier. Similar tendencies as earlier have even continued with updated data until the year 2017 (Fig. 2). Trends have become stronger. These seasonal winter and spring hydrological trends are in line with findings of annual and seasonal air temperature and precipitation changes and also with projected climate change scenarios until the late 21st century. Results shown here are based on Doctoral dissertation of Korhonen (2019).

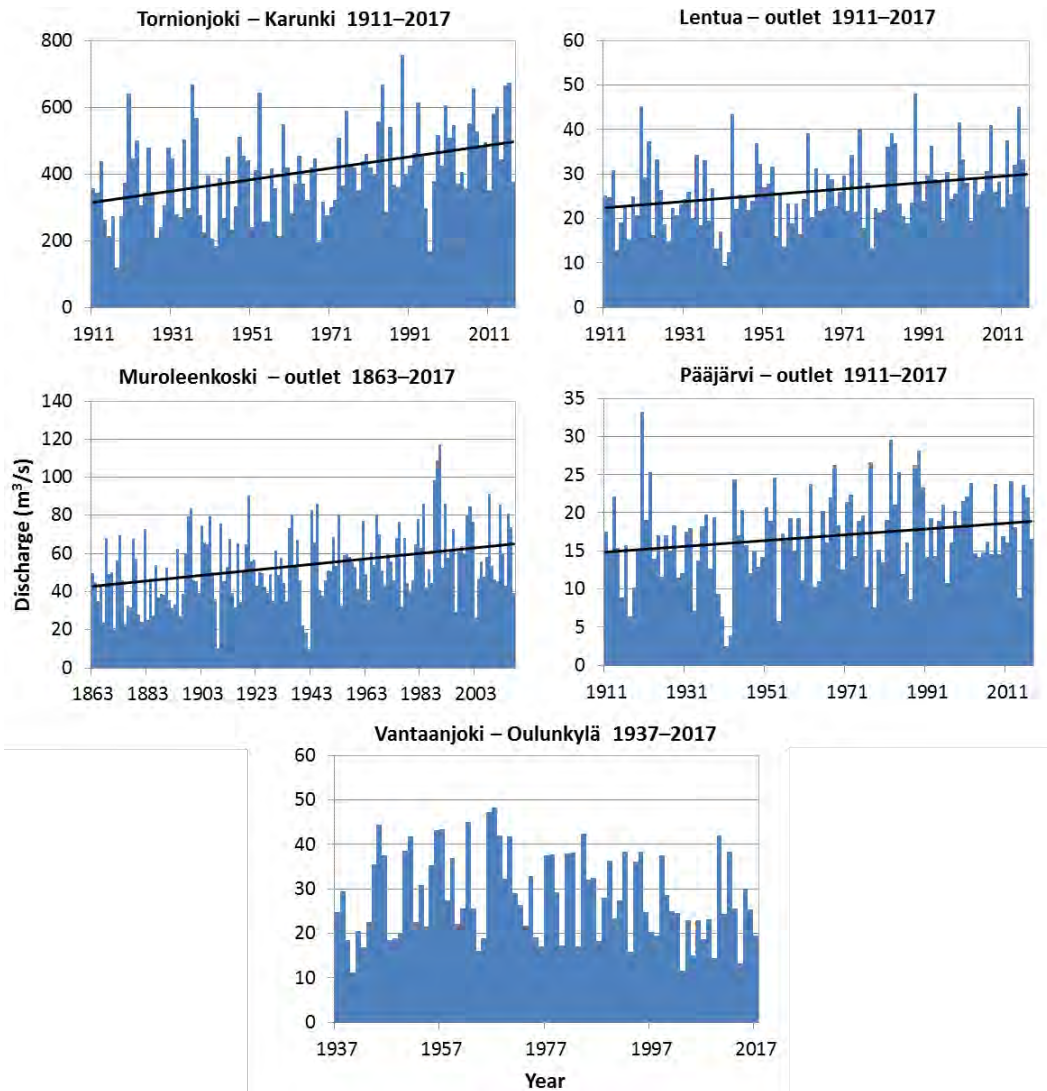


Figure 2. Updated spring season time series and their trends for selected five discharge time series.

KEYWORDS

Climate change; Finland; Ice cover; River discharge; Trends

REFERENCES

Korhonen, J. 2019 Long-term changes and variability of the winter and spring season hydrological regime in Finland. *Report Series in Geophysics*, 79. University of Helsinki.

Climate change impacts on mercury accumulation in northern lake sediments

Jennifer Korosi¹

¹*Department of Geography, York University, Toronto, Ontario, M3J1P3, CANADA*

**Corresponding author's email address: jkorosi@yorku.ca*

ABSTRACT

Climate warming has the potential to intensify the transport of mercury to high latitude lakes through a variety of mechanisms. For example, permafrost thaw and associated hydrological changes may accelerate the release of mercury from soils to surface waters, while increases in lake organic carbon can enhance the sequestration of mercury in the sediments. Lake sediment cores are commonly used to reconstruct the history of atmospheric mercury deposition, providing a critical long-term context for understanding present-day mercury dynamics in lakes. Using examples from the Canadian High Arctic (Ellesmere Island, Nunavut) and the Taiga Plains (Northwest Territories), I will discuss how multi-proxy paleolimnological techniques that pair mercury deposition histories with reconstructions of environmental change in strategically selected lakes can provide insights into the future of mercury cycling in high latitude lakes under a warming climate.

KEYWORDS

Mercury; Paleolimnology; Arctic; Permafrost thaw; Organic carbon

1. INTRODUCTION

The dramatic changes occurring in Arctic and subarctic landscapes in response to anthropogenic climate change have substantial implications for the transport of potentially toxic mercury to lakes. For example, the world's largest reservoir of mercury is contained within the permafrost (Schuster et al. 2018), and the subsequent thawing of permafrost can increase the flux of mercury to freshwater ecosystems (St. Pierre et al. 2018). Glacial melt may similarly release previously sequestered mercury to downstream freshwater ecosystems (St. Pierre et al. 2019). Increases in lake primary productivity that have been reported from across the Arctic (Michelutti et al. 2005) can enhance the retention of mercury in lakes by scavenging mercury from the water column (Outridge et al. 2019). Chromophoric dissolved organic carbon concentrations have been increasing in some high latitude lakes (Creed et al. 2018), and decreasing in others (Kokelj et al. 2009), which will impact mercury transport and bioaccumulation (Lavoie et al. 2019).

Mercury sequestered in lake sediments exhibits minimal diagenesis and porewater mobility, and consequently lake sediment cores can be used to reconstruct the history of mercury deposition in lakes. Lake sediment cores have played an integral role in documenting the long-range transport of mercury and other airborne pollutants to remote Arctic landscapes since the Industrial Revolution (Muir et al. 2009). Lake sediment cores also archive a wealth of information on various aspects of environmental change that have implications for mercury cycling in lakes, including changes in lake primary productivity (Outridge et al. 2019), forest fire regime (Sigler et al. 2003), and organic matter cycling (Bravo et al. 2017; Lavoie et al. 2019). Thus, paleolimnological studies can provide novel insights into the myriad of potential effects of climate change on mercury biogeochemical

cycling in high latitude lakes. In order to demonstrate the types of insights that can be gleaned from lake sediment records, this paper synthesizes paleolimnological studies on climate change impacts on lake mercury concentrations in two different climatic settings: (1) High Arctic lakes in bedrock-dominated catchments with minimal soil development (Korosi et al. 2018); and (2) subarctic lakes situated in boreal peatland complexes (Korosi et al. 2015).

2. STUDY SITE DESCRIPTIONS

2.1 Ellesmere Island, Nunavut

Ellesmere Island is the northernmost island in the Canadian High Arctic archipelago (Figure 1). Mean annual air temperatures are -19°C , and maximum daytime summer temperatures are $5-9^{\circ}\text{C}$. Paleolimnological reconstructions of mercury in the Canadian High Arctic have shown that mercury concentrations in lakes continue to increase despite stable or decreasing anthropogenic emissions since 1990 (Goodsite et al. 2013). This has led researchers to postulate that climate change may be enhancing mercury fluxes to Arctic lakes (Chetelat et al. 2015). The temporal overlap between Arctic climate warming and long-range mercury transport, both of which began ~ 1850 following the Industrial Revolution, makes it challenging to tease apart the influence of climate on mercury accumulation in lakes. Microclimatic gradients that have been identified on Ellesmere Island can be used to disentangle the effects of climate change and anthropogenic mercury emissions. Lakes and ponds at Ellesmere Island have been categorized into four *a priori* assigned climatic groups based on observational data on seasonal ice-cover patterns collected over thirty years, and diatom-based (siliceous algae) paleolimnological reconstructions of changes in lake ice-cover regime and primary production (Griffiths et al., 2017). This paper reports total mercury histories for four of these lakes, one in each of the four *a priori* assigned categories, described below:

Col Pond (“warm”) is among the first to lose ice cover in the summer, and exhibited early (~ 1850) limnological responses to anthropogenic climate warming. Moraine Pond (“cool”) is among the last to lose its ice cover in the summer, and exhibited a later response to anthropogenic climate warming (~ 1960). Both are located at Cape Herschel (Figure 1), where bedrock is Archean granites with outcrops of calcareous glacial tills, and shoreline vegetation is sparse. “Oasis” pond SV8 is located at Sverdrup Pass (Figure 1) on central Ellesmere Island, a low-lying valley bordered by high cliffs resulting in warmer temperatures and a longer growing season. “Oasis” ponds lose ice cover early in the season, but have had historically elongated seasonal ice-free periods prior to the onset of anthropogenic climate warming (Griffiths et al. 2017). SV8 is mesotrophic, with 100% vegetated shoreline and abundant submerged macrophyte growth. West Lake (“cold”) is located at high elevation (300-500m a.s.l.) on Pim Island (Figure 1), is rarely ice-free, and has not exhibited a biotic response to anthropogenic climate warming thus far (Griffiths et al. 2017).

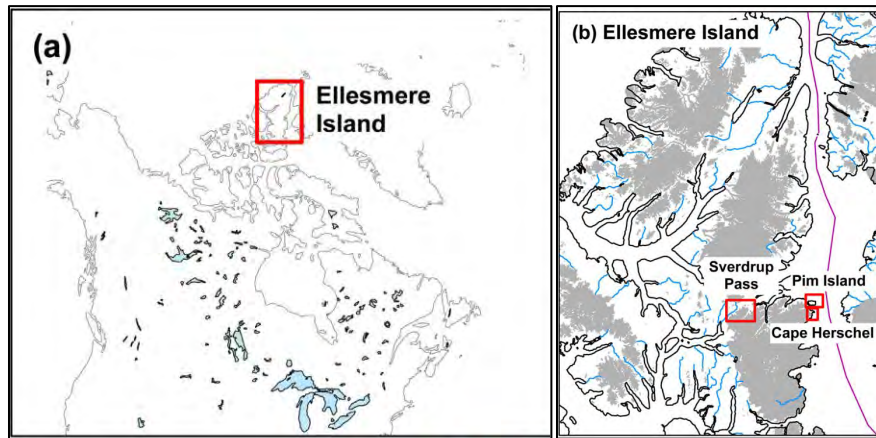


Figure 1. A map of the study site locations on or near Ellesmere Island, Nunavut, Canada. a) Location of Ellesmere Island in the Canadian High Arctic; b) Inset showing the three main regions of study, including Sverdrup Pass, Cape Herschel, and Pim Island. Figure modified from Korosi et al. (2018).

2.2 Taiga Plains, Northwest Territories

Lake “TAH-7” (unofficial name) is a small (<4 ha), shallow (<2 m) lake located east of Tathlina Lake, in the Taiga Plains Mid-Boreal Ecozone southwest of Great Slave Lake (Figure 2). It is a eutrophic (TP=44 µg/L), high DOC (DOC=47mg/L, colour=91 TCU) lake. Mean annual air temperatures recorded at the nearby Hay River Climate Station have increased from -6°C in 1900 to -2°C in 2010 (Coleman et al. 2015). Permafrost in the region is sporadic discontinuous, and is generally restricted to peat plateaus. The landscape is a mosaic of permafrost-supported peat plateaus dominated by black spruce, collapsed peat plateaus, and non-permafrost bogs and fens. Permafrost thaw has been occurring in this region since 1850 (Halsey et al. 1995), and has been accelerating in recent decades (Quinton et al. 2010).

A 44% increase in collapsed peat plateau features was inferred for a 1-km² study area centered on Lake TAH-7 using remotely sensed image analyses between 1970 and 2012 (Coleman et al. 2015). Peat subsidence can enhance the connectivity of drainage networks (Quinton et al. 2009) and may increase the export of DOC to downstream aquatic ecosystems (Olefeldt and Roulet 2014). Mercury transport and bioaccumulation in lake food webs is highly influenced by the quantity and quality of organic matter (French et al. 2014; Bravo et al. 2017; Lavoie et al. 2019). Consequently, changes in terrestrial organic matter run-off into lakes has important implications for lake mercury cycling.

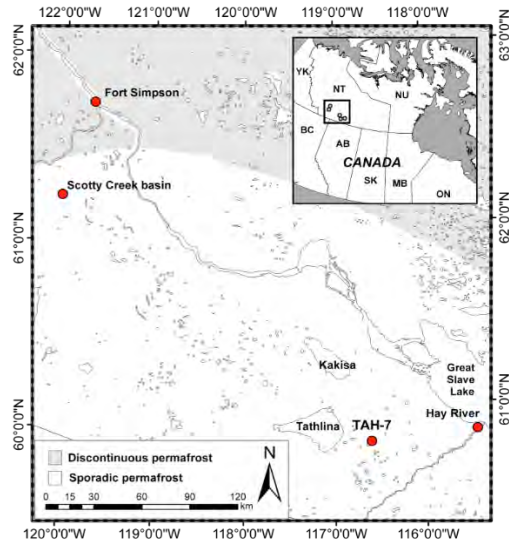


Figure 2. Map showing the location of study lake TAH-7 in the sporadic discontinuous permafrost zone of the Taiga Plains mid-boreal ecozone, southern Northwest Territories. Inset shows the location of the study region within Canada. Figure modified from Korosi et al. (2015).

3. METHODS

Sediment cores were taken from the centre of each lake/pond using gravity corers, sectioned into 0.25-0.5 cm intervals, and kept frozen until analysis. Sediments were freeze-dried and dated using ^{210}Pb gamma spectrometry and the constant rate of supply method (Appleby, 2001; Appleby and Oldfield, 1978). Freeze-dried sediments were analysed for total mercury via dual step gold amalgamation and detection via cold-vapor atomic absorption on a Nippon Sp-3D mercury analyser. For QA/QC, Marine Sediment Certified Reference Materials from the National Research Council of Canada (MESS-3) were used, and select intervals from each sediment core were run in triplicate. In order to correct sediment mercury concentrations for organic carbon, freeze-dried sediments were acid-fumigated in concentrated HCL for 48 hours in an acid desiccator to remove inorganic carbon, and analysed for organic carbon using an Elementar Micro Cube Elemental Analyzer at the G.G. Hatch Stable Isotope Laboratory (University of Ottawa, Canada).

Subfossil diatom assemblages were analysed to infer the nature and timing of limnological responses to climate warming (Griffiths et al. 2017; Coleman et al. 2015). The visual reflectance spectroscopy (VRS) method was used to infer chlorophyll *a* to reconstruct trends in lake primary productivity (Michelutti et al. 2005). For lake TAH-7, sediment organic matter sources were inferred using the carbon to nitrogen ratio (C/N), $\delta^{13}\text{C}$ and $\delta^{15}\text{N}$ stable isotope analysis, and organic matter biomarkers (Meyers 2003). Stable isotope analysis was conducted using an elemental analyzer interfaced to the DeltaPlus XP Isotope Ratio Mass Spectrometer at the G.G. Hatch Stable Isotope Laboratory. Solvent extraction (for n-alkanes and other lipid biomarkers) followed by cupric oxide (CuO) oxidation (for lignin-derived phenols) was conducted on 0.5 g of freeze-dried sediment in duplicate (for quality assurance) at the University of Toronto Scarborough (Korosi et al. 2015). Macroscopic charcoal was analysed using standard methods to reconstruct past forest fire events (Coleman et al. 2015).

4. RESULTS AND DISCUSSION

4.1 Ellesmere Island, Nunavut

Long-term increases in total mercury were observed in all four sediment cores for the post-industrial period (Figure 3), consistent with previous observations from high latitude lake sediments (Muir et al. 2009). When mercury was normalized to sediment organic carbon, the post-industrial increasing trend for mercury was no longer evident in Col Pond (“warm”), and a recent, declining trend was observed for SV8 (“oasis”). This suggests that mercury deposition in these lakes is strongly influenced by organic carbon dynamics related to the export of organic carbon from the catchment and/or internal primary production. West Lake (“cold”), which typically maintains 90-100% ice cover in the summer and has not experienced any increases in primary production or shifts in diatom assemblages (Griffiths et al. 2017), exhibited a clear post-industrial increase in mercury with an enrichment factor of 4.4, comparable with Col Pond (EF=5.4) and Moraine Pond (EF=5.6), which have been simultaneously impacted by both anthropogenic mercury emissions and climate warming. This indicates that, while organic carbon is important for mercury cycling in High Arctic lakes, lakes that have experienced substantial warming and increases in primary productivity are not necessarily more susceptible to post-industrial mercury loadings. This is consistent with a Holocene sediment mercury record collected from Lake CF3 on Baffin Island, where increases in mercury concentration and flux in the post-industrial period also occurred in the absence of any increase in inferred primary production (Cooke et al. 2012).

Moraine Pond presents an interesting case study for disentangling the potential effects of climate warming from long-range transport of airborne pollutants in the postindustrial period. Based on analysis of diatom subfossil assemblages and VRS-inferred chl *a*, Moraine Pond did not exhibit a limnological response to regional warming until ~1960 (Griffiths et al. 2017), while anthropogenic mercury emissions began ~1850. Moraine Pond exhibited a two-stage pattern of total mercury enrichment, with post-industrial enrichment followed by a later intensification of mercury enrichment at the time of diatom-inferred limnological response to climate warming. The Moraine Pond sediment core supports a potential effect of climate warming and algal scavenging on sedimentary mercury. The identification and down-core sedimentary mercury analysis of additional lakes that responded later to climate warming, similar to Moraine Pond, would be an interesting avenue for further research to determine whether Moraine Pond is indicative of a wider trend.

Our results suggest that climate warming has the potential to enhance mercury sequestration to lake sediments in certain cases (as observed in Moraine Pond), but is not a necessary precondition for substantial post-industrial mercury enrichment (as observed in West Lake).

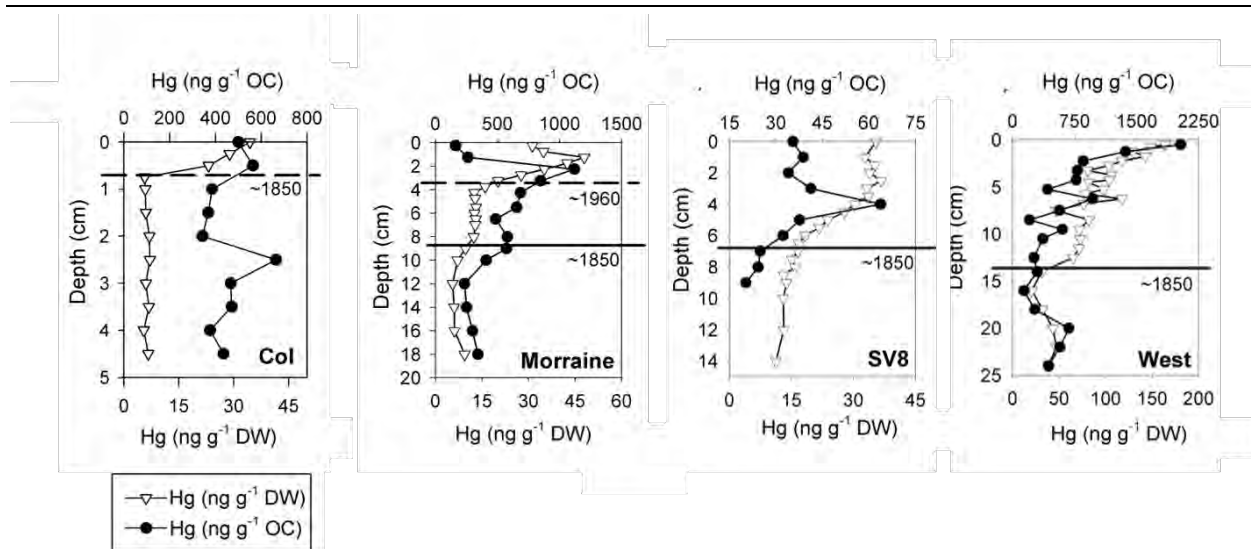


Figure 3. Down-core sediment profiles of total mercury for Ellesmere Island lakes across a microclimatic gradient. Dashed lines represent the timing of the change in diatom communities indicating a shift in lake ice cover regime occurring in response to climate warming (Griffiths et al. 2017). Where different from the diatom-inferred lake ice cover regime, the onset of the post-industrial period, ~1850, is denoted with a solid black line. Mercury enrichment factors (per gram dry weight): Col Pond = 5.4; Moraine Pond = 5.6; SV8 = 2.4; West = 4.4. Figure modified from Korosi et al. (2018).

4.2 Taiga Plains, Northwest Territories

A steady increase in total mercury (THg) concentrations was observed between core depth of 40 cm and 10 cm (Figure 4). No further increases in mercury were evident between ~1940 to present day. The increase in THg began in the preindustrial period, suggesting that increased anthropogenic mercury emissions are not the primary driver. Total mercury concentrations were positively correlated to lignin-derived phenols, a biomarker for terrestrial organic matter inputs, and negatively correlated to $\delta^{13}\text{C}$ (Figure 4). This indicates that the increase in lake sediment mercury concentrations is the result of increased allochthonous carbon inputs.

The beginning of the long-term increase in mercury and lignin-derived phenols, and the decrease in $\delta^{13}\text{C}$, occurred immediately following a forest fire event inferred from the sedimentary macroscopic charcoal record (Figure 5). Forest fires can cause rapid permafrost degradation (Gibson et al. 2018), and the fire event recorded at 40 cm may have initiated thawing of permafrost peat plateaus, resulting in an alteration of catchment vegetation and drainage patterns that enhanced the run-off of mercury, adsorbed onto terrestrial organic matter, into Lake TAH-7. This is further supported by n-alkane biomarker analysis that showed a shift in organic matter sources from higher plants (e.g. trees) to semi-aquatic plants (e.g. mosses) (Figure 5). Diatom assemblages changes indicative of reduced light penetration occurred after ~1940 (Figure 5), suggesting an ecological threshold for DOC was crossed at this time; however, no further increases in sediment mercury concentrations were evident.

Our findings suggest that landscape changes occurring in response to thawing permafrost have the potential to increase mercury concentrations in aquatic environments through changes in the quantity and source of terrestrial organic matter run-off.

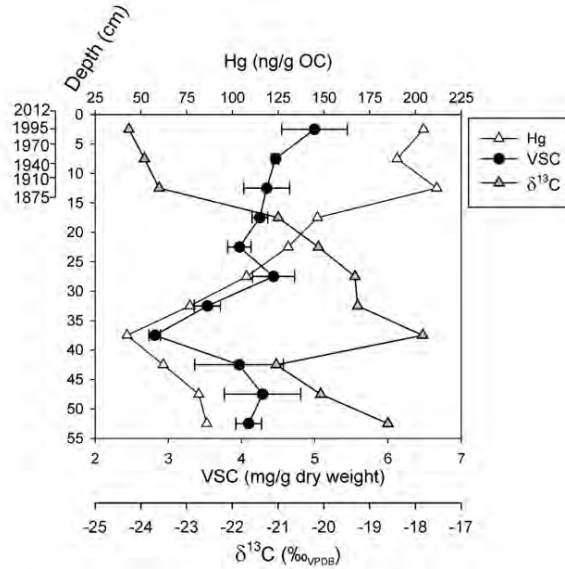


Figure 4. TOC-normalized total mercury concentrations (THg) vs. total concentration (mg/g dry weight) of lignin-derived phenols (vanillyls+syringyls+cinnamyls; VSC) and $\delta^{13}\text{C}$ in TAH-7 by depth. ^{210}Pb dates are shown on the left. Figure modified from Korosi et al. (2015).

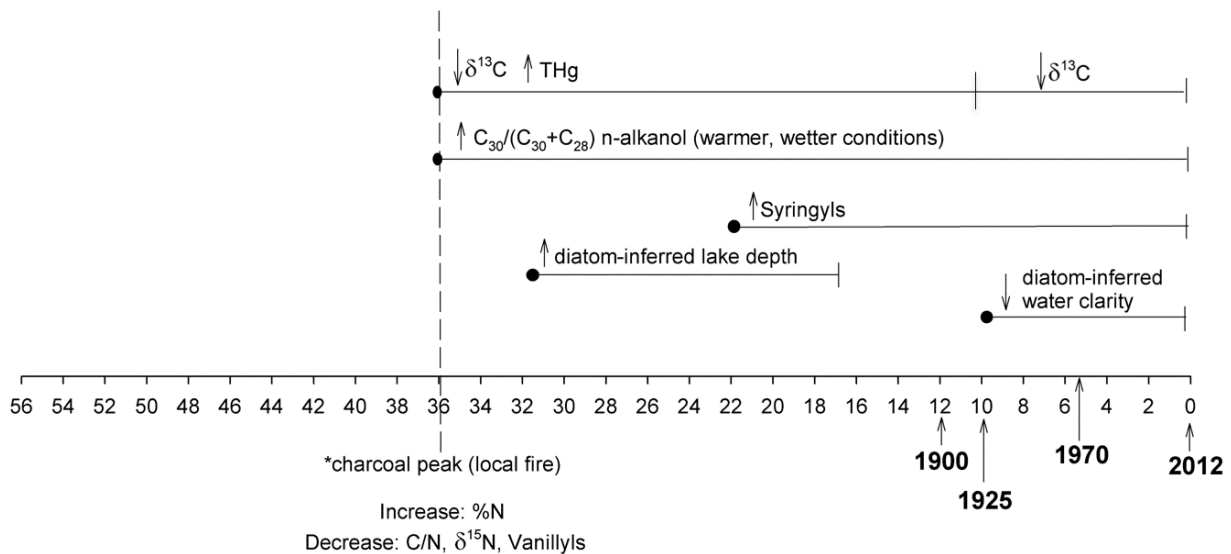


Figure 5. A visual representation of the main changes in mercury, organic matter proxies, and subfossil diatom assemblages through time in Lake TAH-7. Abbreviations: %N, percent nitrogen; C/N, organic carbon: nitrogen; THg, total mercury. Figure modified from Korosi et al. (2015).

5. CONCLUSIONS

Increases in terrestrial organic matter run-off and internal lake primary production are linked to increases in sedimentary mercury concentrations over time for High Arctic and subarctic lakes, providing further evidence that predicted changes in organic carbon cycling in lakes may enhance the accumulation of mercury in high latitude lakes, and confound recent efforts to reduce global mercury emissions under the Minamata Convention. Empirical evidence for climate change impacts on lake ecological and biogeochemical functions are typically based on short-term observations due to a lack of long-term monitoring. Paleolimnological records offer opportunities for examining the influence of limnological processes (e.g. organic carbon cycling) on mercury deposition in lakes over decadal, centennial, and millennial timescales. This long-term perspective can be useful for identifying high latitude lakes at greater risk of mercury contamination due to anthropogenic climate change.

ACKNOWLEDGMENTS

These projects were funded by the Natural Sciences and Engineering Research Council of Canada (NSERC) and the Government of the Northwest Territories Cumulative Impact Monitoring Program. Logistical fieldwork support was provided by the Polar Continental Shelf Program and the Ka'a'gee Tu First Nation in Kakisa (Northwest Territories). The research presented is the result of collaborative work with Dr. Jules Blais (University of Ottawa), Dr. John Smol (Queen's University), Dr. Katharine Griffiths (McGill University), Dr. Myrna Simpson (University of Toronto at Scarborough), Dr. Michael Pisaric (Brock University), and Michael Palmer (Carleton University). Dr. Joshua Kurek (Mount Allison University), Dr. Joshua Thienpont (York University), Dr. Marianne Douglas (Queen's University), Dr. Ellen Bielawski (University of Alberta), Dr. Emily Stewart (Queen's University), and Chris Grooms (Queen's University) assisted with fieldwork.

REFERENCES

- Appleby, P. G. 2001. Chronostratigraphic techniques in recent sediments. In: Last, WM & Smol, J.P. (eds). *Tracking Environmental Change Using Lake Sediments*. Springer, Netherlands. pp. 171-203.
- Appleby, P.G. & Oldfield, F. 1978. The calculation of lead-210 dates assuming a constant rate of supply of unsupported ²¹⁰Pb to the sediment. *Catena* 5, 1-8.
- Bravo, A.G., Bouchet, S., Tolu, J., Björn, E., Mateos-Rivera, A. & Bertilsson, S. 2017. Molecular composition of organic matter controls methylmercury formation in boreal lakes. *Nature Comm.* 8, 14255.
- Chetelat, J., Amyot, M., Arp, P., Blais, J.M., Depew, D., Emmerton, C.A., Evans, M., Gamberg, M., Gantner, N., Girard, C. & Graydon, J. 2015. Mercury in freshwater ecosystems of the Canadian Arctic: recent advances on its cycling and fate. *Sci. Total Environ.* 509, 41-66.
- Coleman, K.A., Palmer, M.J., Korosi, J.B., Kokelj, S.V., Jackson, K., Hargan, K., Courtney Mustaphi, C., Thienpont, J.R., Kimpe, L.E., Blais, J.M., Pisaric, M.F.J. & Smol, J.P. 2015 Tracking the impacts of recent warming and thaw of permafrost peatlands on aquatic ecosystems: a multi-proxy approach using remote sensing and lake sediments. *Boreal Environ. Res.* 20, 363–377.

- Cooke, C.A., Wolfe, A.P., Michelutti, N., Balcom, P.H. & Briner, J.P. 2012. A Holocene perspective on algal mercury scavenging to sediments of an Arctic lake. *Environ. Sci. Technol.* 46, 7135-7141.
- Creed, I.F., Bergström, A.K., Trick, C.G., Grimm, N.B., Hessen, D.O., Karlsson, J., Kidd, K.A., Kritzberg, E., McKnight, D.M., Freeman, E.C. & Senar, O.E. 2018. Global change-driven effects on dissolved organic matter composition: Implications for food webs of northern lakes. *Glob. Change Biol.* 24(8), 3692-3714.
- French, T.D., Houben, A.J., Desforges, J.P.W., Kimpe, L.E., Kokelj, S.V., Poulain, A.J., Smol, J.P., Wang, X. & Blais, J.M. 2014. Dissolved organic carbon thresholds affect mercury bioaccumulation in Arctic lakes. *Environ. Sci. Technol.* 48(6), 3162-3168.
- Gibson, C.M., Chasmer, L.E., Thompson, D.K., Quinton, W.L., Flannigan, M.D. & Olefeldt, D. 2018. Wildfire as a major driver of recent permafrost thaw in boreal peatlands. *Nature Comm.* 9(1), 3041.
- Goodsite, M.E., Outridge, P.M., Christensen, J.H., Dastoor, A., Muir, D., Travnikov, O., et al. 2013. How well do environmental archives of atmospheric mercury deposition in the Arctic reproduce rates and trends depicted by atmospheric models and measurements? *Sci. Total Environ.* 452-453.
- Griffiths, K., Michelutti, N., Sugar, M., Douglas, M.S. & Smol, J.P. 2017. Ice-cover is the principal driver of ecological change in High Arctic lakes and ponds. *PLoS One* 12(3), e0172989.
- Halsey, A., Vitt, D.H. & Zoltai, S.C.. 1995. Disequilibrium response of permafrost in Boreal continental Western Canada to climate change. *Clim. Change* 30, 57-73.
- Kokelj, S.V., Zajdlík, B. & Thompson, M.S. 2009. The impacts of thawing permafrost on the chemistry of lakes across the subarctic boreal-tundra transition, Mackenzie Delta region, Canada. *Permafrost Periglac.* 20(2), 185-199.
- Korosi, J.B., Griffiths, K., Smol, J.P. & Blais, J.M. 2018. Trends in historical mercury deposition inferred from lake sediment cores across a climate gradient in the Canadian High Arctic. *Environ. Pollut.* 241, 459-467.
- Korosi, J.B., McDonald, J., Coleman, K.A., Palmer, M.J., Smol, J.P., Simpson, M.J. & Blais, J.M. 2015. Long-term changes in organic matter and mercury transport to lakes in the sporadic discontinuous permafrost zone related to peat subsidence. *Limnol. Oceanogr.* 60(5), 1550-1561.
- Lavoie, R.A., Amyot, M. & Lapierre, J.F. 2019. Global meta-analysis on the relationship between mercury and dissolved organic carbon in freshwater environments. *J. Geophys. Res.: Biogeosci.* <https://doi.org/10.1029/2018JG004896>.
- Meyers, P.A. 2003. Applications of organic geochemistry to paleolimnological reconstructions: A summary of examples from the Laurentian Great Lakes. *Org. Geochem.* 34, 261-289.
- Michelutti, N., Wolfe, A.P., Vinebrooke, R.D., Rivard, B. & Briner, J.P. 2005. Recent primary production increases in Arctic lakes. *Geophys. Res. Lett.* 32(19), L19715.
- Muir, D.C.G., Wang, X., Yang, F., Nguyen, N., Jackson, T.A., Evans, M.S., Douglas, M., Köck, G., Lamoureux, S., Pienitz, R., Smol, J.P., Vincent, W.F. & Dastoor, A. 2009. Spatial trends

and historical deposition of mercury in eastern and northern Canada inferred from lake sediment cores. *Environ. Sci. Technol.* 43, 4802-4809.

- Olefeldt, D. & Roulet, N.T. 2014. Permafrost conditions in peatlands regulate magnitude, timing, and chemical composition of catchment dissolved organic carbon export. *Glob. Chang. Biol.* 20, 3122-3136
- Outridge, P.M., Stern, G.A., Hamilton, P.B. & Sanei, H. 2019. Algal scavenging of mercury in preindustrial Arctic lakes. *Limnol. Oceanogr.* <https://doi.org/10.1002/lno.11135>
- Quinton, W.L., Hayashi, M. & Chasmer, L.E. 2009. Peatland hydrology of discontinuous permafrost in the Northwest Territories: Overview and synthesis. *Can. Water Resour. J.* 34, 311-328.
- Quinton, W. L., Hayashi, M. & Chasmer, L.E. 2010. Permafrost-thaw-induced land-cover change in the Canadian subarctic: implications for water resources. *Hydrol. Process.* 25, 152-158.
- Schuster, P.F., Schaefer, K.M., Aiken, G.R., Antweiler, R.C., Dewild, J.F., Gryziec, J.D., Gusmeroli, A., Hugelius, G., Jafarov, E., Krabbenhoft, D.P. & Liu, L. 2018. Permafrost stores a globally significant amount of mercury. *Geophys. Res. Lett.* 45, 1463-1471.
- Sigler, J.M., Lee, X. & Munger, W. 2003. Emission and long-range transport of gaseous mercury from a large-scale Canadian boreal forest fire. *Environ. Sci. Technol.* 37(19), 4343-4347.
- St Pierre, K.P., St. Louis, V.L., Lehnher, I., Gardner, A.S., Serbu, J.A., Mortimer, C.A., Muir, D.C.G., Wiklund, J.A., Lemire, D., Szostek, L. & Talbot, C. 2019. Drivers of mercury cycling in the rapidly changing glacierized watershed of the High Arctic's largest lake by volume (Lake Hazen, Nunavut, Canada). *Environ. Sci. Technol.* 53(3), 1175-1185.
- St. Pierre, K.A., Zolkos, S., Shakil, S., Tank, S.E., St. Louis, V.L. & Kokelj, S.V. 2018. Unprecedented increases in total and methyl mercury concentrations downstream of retrogressive thaw slumps in the western Canadian Arctic. *Environ. Sci. Technol.* 52(24), 14099-14109.

Rapid increase in recent permafrost temperatures and upland groundwater, Interior Alaska

Anna Liljedahl¹, David Barnes¹, Heather Best, Uma Bhatt², Ronald Daanen³, Vladimir Romanovsky², Richard Thoman⁴, and Emily Youcha¹

¹ *Water and Environmental Research Center, University of Alaska Fairbanks, Alaska, USA*

² *Geophysical Institute, Center, University of Alaska Fairbanks, Alaska, USA*

³ *Alaska Division of Geological and Geophysical Surveys, Alaska Department of Natural Resources, Fairbanks, Alaska, USA*

⁴ *International Arctic Research Centre, University of Alaska Fairbanks, Alaska, USA*

**Corresponding author's email address: akliljedahl@alaska.edu*

ABSTRACT

Gradual increases in permafrost temperatures and winter river discharge are well documented across the Arctic and sub-Arctic in past decades. Interior Alaska rivers and permafrost follow the same gradual increasing trend, with typically large interannual variability in winter river runoff.

However, in the last ~5 years, Interior Alaska permafrost temperatures and upland groundwater well data show unprecedented increases resulting in record high values since observations began in the early 1980s. Only one long-term upland groundwater well has been maintained nearly 40 years in Interior Alaska, but this Fairbanks well shows similar variations over time as winter runoff from the Chena and Salcha Rivers. Winter river runoff in the non-glacierfed Chena, Salcha, and Kobuk Rivers also shows record highs since the observations began in the late 1940s. Only six months in the past six years have seen mean monthly air temperatures below normal, while 64% (46 months) have been above normal. Cumulative 60-month running accumulated precipitation results in unprecedented high values in the last few years, while total annual snowfall includes two above and two below normal years in the last five years. Two of the ten wettest summers since 1912 occurred in the last five years, with large late summer rainfall.

A visual comparison suggests a similar timing of sub-decadal periods of increased/decreased well groundwater levels, winter river discharge, and permafrost temperatures. The recent dramatic increase in groundwater storage and permafrost temperatures coincides with many reports of difficulties with river ice travel, record low Bering Sea ice cover, and long periods of warmer winter air temperatures associated with an irregular jet-stream. Gradual change, occurring over multiple decades, may have reached a threshold where positive feedbacks in the regional land-ocean and global atmospheric systems result in strong responses from local thermal and hydrological regimes.

KEYWORDS

Arctic environments; Northern research basins; Permafrost; Groundwater storage.

Challenges and Opportunities of Implementing the National Water Model in Alaska

Scott Lindsey¹, Dave Streubel¹, David Gochis², and Brian Cosgrove³

¹ National Weather Service Alaska-Pacific River Forecast Center, Anchorage, Alaska, USA

² National Center for Atmospheric Research, Boulder, Colorado, USA

³ National Weather Service Office of Water Prediction, Silver Spring, Maryland, USA

*Corresponding author's email address: scott.lindsey@noaa.gov

ABSTRACT

Current water level and river discharge forecasting in Alaska is confined to a limited number of forecast locations, most of which correspond to a stream gage operated by the US Geological Survey. A suite of lumped parameter conceptual models for snowmelt, rainfall-runoff and routing are calibrated using historical datasets. The models are utilized by staff at the Alaska-Pacific River Forecast Center (APRFC) to create river forecasts for the monitoring and when flood conditions manifest, warning of affected communities for the protection of life and property. The National Water Model (NWM) simulates observed and forecast streamflow along with all of the variables that fully define the water cycle over the entire continental United States. Based on the stream reaches defined in the National Hydrography Dataset, the NWM uses mathematical representations of the various processes that track water as it moves through the atmosphere, falls to the surface of the earth as snow or rainfall, accumulates through the stream network and evaporates or transpires back into the atmosphere.

The suite of computer models necessary is so complex that it runs on a high performance computer in order to complete the calculations in the time frame that decision makers require. The spatial density of information from this physical based forecast model is several orders of magnitude greater than the current modeling approach used by River Forecast Centers. Currently only the contiguous US is represented by the NWM. This presentation will explore the challenges of implementation in Alaska.

KEYWORDS

Arctic environments; Northern research basins; National Water Model, Arctic Hydrology, Sparse observational datasets, Water Budget information, High Performance Computing, Real-time Operational River Forecasting.

Aufeis of the North-East of Russia in changing climate

Olga Makarieva^{1,2*}, Andrey Shikhov³, Nataliia Nesterova^{2,4}, Andrey Ostashov²

¹Melmikov Permafrost Institute, Yakutsk, 677010, RUSSIA

²St.Petersburg State University, St. Petersburg, 199034, RUSSIA

³Perm State University, Perm, 614990, RUSSIA

⁴State Hydrological Institute, St. Petersburg, 199053, RUSSIA

*Corresponding author's email address: omakarieva@gmail.com

ABSTRACT

The distribution of aufeis in the North-East of Russia in current climate is being studied and compared to the period of 70 years ago. Landsat images for the period of 2013-2017, topographic maps and historical Cadastre of aufeis (1958) have been used to compile spatial geodatabase of aufeis in the basins of three large rivers of permafrost – the Yana, Indigirka and Kolyma (total area more than 1.2 mln. km²). The satellite-derived total area of aufeis is 2167 km² of 3429 aufeis fields, while historical Cadastre (1958) contains data of 2561 aufeis fields with total area of 4009 km². The comparison of recent and historical data has shown that aufeis conditions have changed since the mid-20th century indicating the changes of hydrological regime and permafrost conditions in studied area.

KEYWORDS

taryn-aufeis; the North-East of Russia; climate change; groundwater; streamflow; surface and ground water interactions

1. INTRODUCTION

Giant aufeis are ice fields that occur annually in the river valleys as a result of layer-by-layer freezing of streambed groundwater (Figure 1). According to rough estimates, the area of groundwater aufeis in Siberia and the Far East is more than 42, 000 km² (Alekseev 1987).

The changes of streamflow are observed in the permafrost domain. Recent studies presented the rates of streamflow changes but the reasons of hydrological regime transformation are still discussed (Tananaev et al. 2016; Makarieva et al. 2019a). Hydrological role of aufeis is the seasonal redistribution of groundwater component of river streamflow. Aufeis dynamic can be traced by remote-sensing data and used as the indicator of the changes of the surface and groundwater interactions in poorly-gauged permafrost basins (Yoshikawa et al. 2007; Makarieva et al. 2019a). Aufeis is the important element of water balance in cold regions (Ensom et al. in preparation).

The aim of the study was to develop the GIS database of recent aufeis fields in three basins of large Arctic rivers of the North-East of Russia – the Yana, Indigirka and Kolyma with total area of more than 1.2 mln km² and compare it with historical Cadastre of aufeis published in 1958.

2. STUDY AREA

North-East of Russia is famous for the vast distribution of aufeis. The region includes Chukotka and the Verkhoyansk-Kolyma mountainous system.

Assessed water storage in aufeis of Chukotka in spring is about 1.4-1.6 km³. Approximately 50% of aufeis fields do not fully melt during the summer and about 1-5% of their volume remains for the following year. The number of aufeis fields per unit area increases with higher elevation; at the same time, there is a pronounced tendency of growth of the average thickness of aufeis deposits from 1.5 m on the coastal plains to 3.0 m high in the mountains (Alekseev et al. 2011).

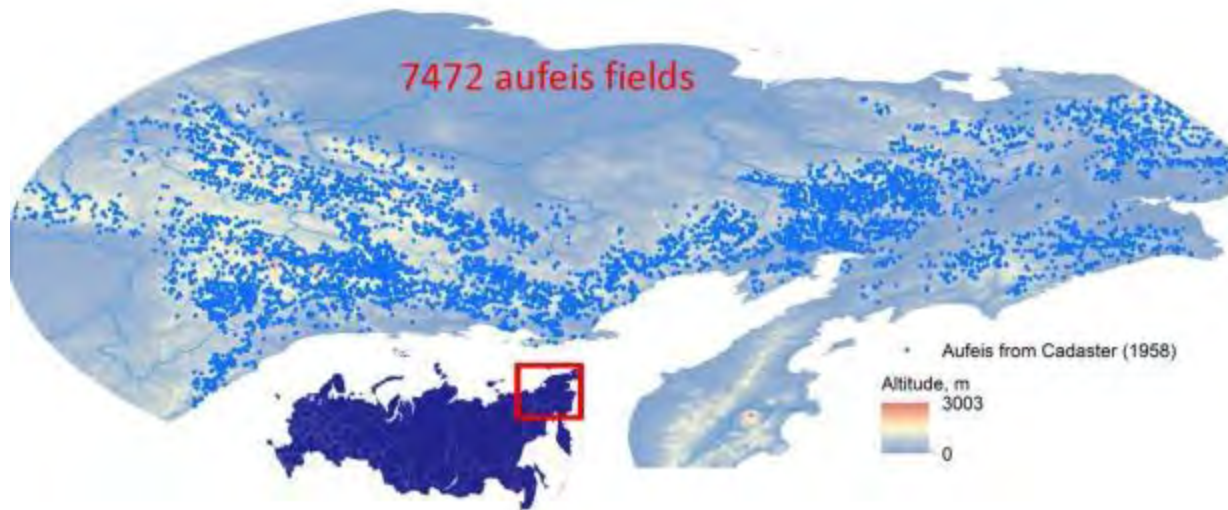


Figure 1. General overview of study area including the distribution of aufeis fields in the North-East of Russia according to the Cadastre (1958)

The Verkhoyansk-Kolyma highland is characterized by the most severe climate in Asia. The thickness of continuous permafrost in the watershed divides reaches 500-600 m, and in the bottoms of the river valleys it ranges from 150 to 200 m. The water-bearing taliks are located mainly in depressions of the relief along tectonic faults, under the river beds and large lakes of glacial origin. Aufeis on average occupy 1.0-1.2% of the territory, while a significant part of them belongs to the category of giant.

Simakov and Shilnikovskaya (1958) developed the Cadastre of aufeis of this region based on air-photo interpretation data and field geological surveys which contains the data on 7,472 aufeis fields with total area 10,445 km² and the areas of individual aufeis fields varying from 0.01 to 82 km². 10% of the largest aufeis fields make up about 60% of their total area in the Cadastre. Most aufeis is located in the elevation band of 1000–1200 m (Makarieva et al. 2019b). The elevation band of 200–300 m is characterized by the location of giant aufeis fields (Figure 2), including the largest in the world, the Bolshaya Morskaya naled (aufeis), which length is about 26 km, maximum width reaching 10 km and the area amounting up to 82 km².



Figure 2. The example of aufeis field in the upstreams of the Kolyma River. Stratified ice of about 0.5 m depth can be seen at the right photo. The photo is taken by O. Makarieva on the 24th of July, 2016.

3. METHODS

The methods applied in this study are in detail described by Makarieva et al. (2019a). The Normalized Difference Snow Index (NDSI) was used to detect aufeis. It was calculated according to the formula (Hall et al. 1995):

$$\text{NDSI} = (\text{GREEN} - \text{SWIR1}) / (\text{GREEN} + \text{SWIR1})$$

where SWIR1 is reflectance in the mid-infrared band (1.56–1.66 μm for the Landsat-8 images), and GREEN is reflectance in the green band (0.525–0.6 μm for the Landsat-8 images). Following Hall et al. (1995), the threshold value for snow and ice has been set at 0.4.

Aufeis detection in the basin of the Yana, Indigirka and Kolyma River basins was conducted based on the Landsat-8 OLI satellite images, from 2013 to 2017, downloaded from the United States Geological Survey web-service. We selected late spring images (between 15 May and 18 June) to detect the maximum possible number of aufeis fields and their maximum area, since in June they melt intensively. There was between 1% and 20% of cloudiness in some images.

Apart from the Landsat images, the digital terrain model with a spatial resolution of 250m was used to build a network of thalwegs within the study basin. This is essential for semi-automated separation of the aufeis from snow-covered areas in late spring Landsat images. Based on the preliminary analysis of aufeis location in relation to the network of thalwegs created, a 1.5 km wide buffer zone was used.

4. RESULTS

The results of the comparison of the historical and modern data collection are presented in Table 1 and at Figures 3-4. In total for three basins, 1803 aufeis fields from the Cadastre (1958) were found by the Landsat images and 1043 aufeis fields from the Cadastre (1958) with total area 620 km² were missing in recent images. 2066 new aufeis fields with total area of 522 km² were discovered on recent images in the study area.

The main sources of uncertainty in both datasets are the following. The Cadaster (1958) provides an area of aufeis glades but not the aufeis itself. Late Landsat images may underestimate the area of aufeis fields due to its ablation in comparison with the maximum values.

Table 3. Data correlation of aufeis based on the Cadastre (1958) and the Landsat images

River Basin	Data source	Matching aufeis	Not matching aufeis
Yana	Cadaster (1958)	68 (616 km ²)	117 (122 km ²)
	Landsat	262 (320 km ²)	321 (107 km ²)
Indigirka	Cadaster (1958)	634 (1905 km ²)	262 (159 km ²)
	Landsat	611 (1037 km ²)	602 (250 km ²)
Kolyma	Cadaster (1958)	1101 (1606 km ²)	664 (339 km ²)
	Landsat	1073 (714 km ²)	1143 (165 km ²)

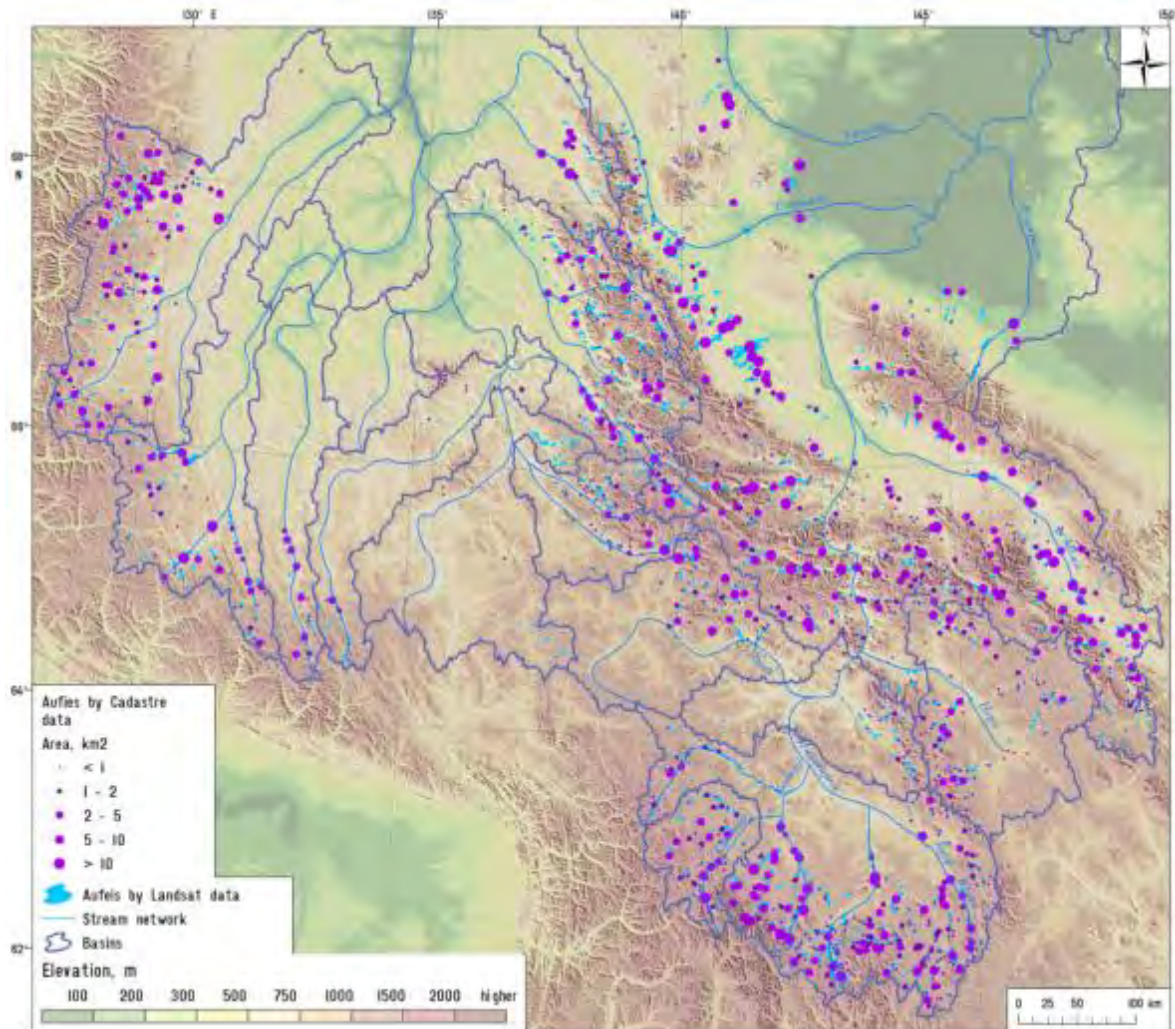


Figure 3. Aufeis in the Yana and Indigirka River basins according to the Cadastre (1958) and recent Landsat images

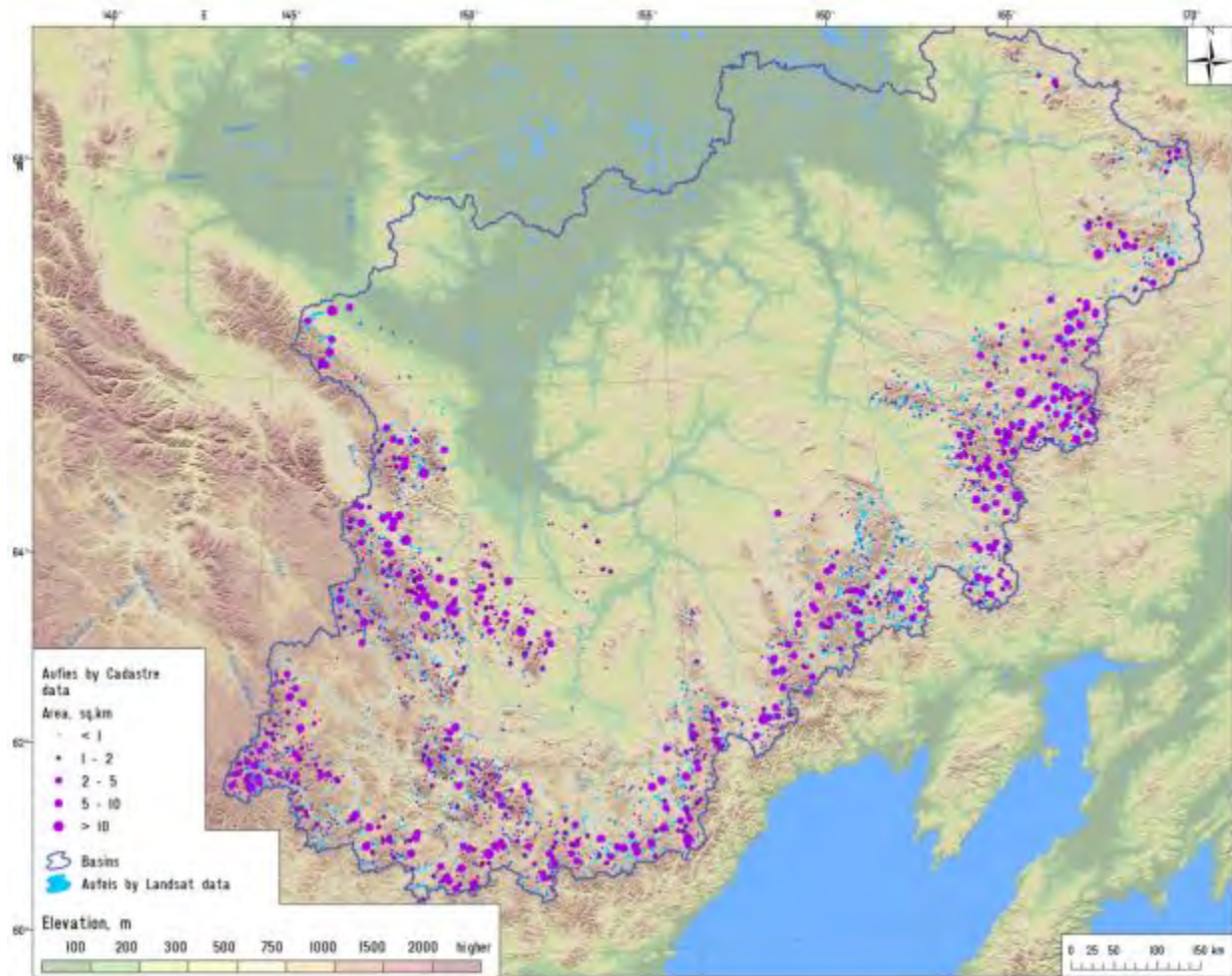


Figure 4. Aufeis in the Kolyma River basins according to the Cadastre (1958) and recent Landsat images

5. CONCLUSIONS

Developed database contains the coordinates and characteristics of 896 aufeises with total area of 2064 km² at the Indigirka River basin, 385 aufeises with total area 738 km² at the Yana River basin and 1765 aufeises with total area 1945 km² at the Kolyma River basin. Recent satellite-derived total aufeis area is 1.6 - 2.2 times smaller than stated in the Cadastre (1958).

Simultaneously, the historical Cadastre archive is lacking data on over 2050 aufeises that were identified using satellite images. This suggests that the Cadastre data is incomplete, while there may also have been significant change in aufeis formation conditions in the last half century.

ACKNOWLEDGMENT

The study was funded by the Russian Geographical Society.

REFERENCES

- Alekseev, V. R. 1987 *Naledi*. Novosibirsk, Nauka, Moscow
- Alekseyev, V.R., Gorin, V.V., Kotov, S.V. 2011 Taryn aufeis in the Northern Chukotka. *Lyod i Sneg (Ice and Snow)* (4) 85–93
- Cadastre to the map of the naleds of the North-East of the USSR: Scale 1 : 2 000 000, 1958 Edited by Shilnikovskaya, Z. G. Central complex thematic expedition of the North-Eastern Geological Survey, Magadan, 398 pp., 1958 (in Russian)
- Ensom, T., Alekseev, V.R., Kane, D.L., Makarieva, O.M., Marsh, P, Morse, P.D. 2019 The Distribution and Dynamics of Aufeis in Permafrost Regions, *Permafrost and Periglacial Processes*, in preparation.
- Hall, D. K., Riggs, G. A., Salomonson, V. V. 1995 Development of methods for mapping global snow cover using Moderate Resolution Imaging Spectroradiometer (MODIS) data, *Remote Sens. Environ.*, 54, 127–140
- Makarieva, O., Nesterova, N., Post, D. A., Sherstyukov, A., and Lebedeva, L. 2019a Warming temperatures are impacting the hydrometeorological regime of Russian rivers in the zone of continuous permafrost, *The Cryosphere*, 13, 1635-1659, <https://doi.org/10.5194/tc-13-1635-2019>
- Makarieva, O., Shikhov, A., Nesterova, N., and Ostashov, A. 2019b Historical and recent aufeis in the Indigirka River basin (Russia), *Earth Syst. Sci. Data*, 11, 409-420, <https://doi.org/10.5194/essd-11-409-2019>
- Simakov, A. S., Shilnikovskaya, Z. G. 1958 *Map of the naleds of the North-East of the USSR Scale 1 : 2 000 000*, The North-Eastern Geological Survey of the Main Directorate of Geology and Subsoil Protection, Central complex thematic expedition, Magadan, 1958 (in Russian)
- Tananaev, N. I., Makarieva, O.M., Lebedeva, L.S. 2016 Trends in annual and extreme flows in the Lena River basin, Northern Eurasia, *Geophys. Res. Lett.*, 43, 10,764–10,772, doi:10.1002/2016GL070796
- US Geological Survey Server: available at: <http://earthexplorer.usgs.gov>, last access: 15 July 2019.
- Yoshikawa, K., Hinzman, L. D., and Kane, D. L. 2007 Spring and aufeis (icing) hydrology in Brooks Range, Alaska, *J. Geophys. Res.-Biogeosci.*, 112, 1–14

Operational Snow Measurements with Ground Penetrating Radar – A Case Study from Överuman, Sweden

Wolf-Dietrich Marchand^{1*} and Björn Norell²

¹*Sweco Norge AS, Sluppenveien 19, 7037 Trondheim, NORWAY*

**Corresponding author's email address: wolf.marchand@sweco.no*

²*Vattenregleringsföretagen, Kyrkgatan 21, 831 31 Östersund, NORWAY*

ABSTRACT

A method for designing effective snow measurement systems for hydropower plants has been applied to several catchments in Norway and Sweden over the past 16 years. The method establishes representative snow measurement survey lines which reflect the physical characteristics for the entire catchment. The method is based on GIS analysis of the following seven terrain parameters: elevation, slope, aspect, curvature, location (x- and y coordinates), and vegetation.

Snow measurements are performed by towing a "snow radar" (ground penetrating radar) behind a snowmobile along the determined snow survey lines. Measurements of the two-way travel time (TWT) of the radar signal are then used to calculate snow depth. Density measurements are used to convert snow depth to snow water equivalent (SWE).

The presented study is based on 74 km of snow courses measured during March 2017 in the Swedish basin Överuman. Överuman is located in the upper part of a hydropower system along the Umeälven River. The mean snow depth in the catchment was approximately 179 cm, with values ranging from 0 to 923 cm. Based on measured SWE and measured or calculated runoff, a water balance study was performed after the end of the snow melting season. The snow data were also used for updating the model state in the hydrological Hydrologiska Byråns Vattenbalansavdelning (HBV) model. Without any correction the simulated (modelled) runoff showed a deviation of 25 % to the observed runoff. Incorporating snow measurements resulted in a 1 % deviation between simulated and observed runoff. The use of good quality snow data provides a better estimation of hydropower production and helps to avoid flood spill.

KEYWORDS

Snow measurements, snow measurement system, snow distribution, snow depth, terrain characteristics, terrain parameters, snow radar, ground penetrating radar, Överuman, water balance, snow water equivalent, hydropower

1. INTRODUCTION

Runoff from the Swedish catchment Överuman is used in several hydropower plants along the river Umeälv. Since Överuman is both high up in the hydropower system and at a high elevation, the water from that catchment has both a huge potential for power production and receives a large amount of precipitation, especially snow. This means the snow storage in the catchment is important for the benefit of the hydropower producer.

Initiated by large flood spill in 2015, with the accompanying economic losses, a snow measurement system has been established and used since 2017. The theory behind the development of the measurement system is described in detail in Marchand (2003). In short,

snow measurement courses are distributed over the whole catchment in a way that snow distribution variations are accounted for at different scales: micro-, meso- and macroscale. This is obtained by comparing seven terrain characteristic parameters for the entire catchment with the same parameters measured at the snow courses. The terrain characteristics used for comparison based on GIS analysis are elevation, X and Y location, aspect, curvature, slope, and vegetation (forest or no forest). The idea behind the developed snow measuring system is that if the terrain characteristics are equal for both catchment and snow survey courses, the wind and weather will influence the snow distribution for both catchment and snow survey courses in the same way. Hence the snow measurements will be representative for the catchment.

The presented study aims to assess how the hydrological modelling of the catchment is improved by using the results from the snow measurements. Based on 18 years of hydrologic modelling with the *Hydrologiska Byråns Vattenbalansavdelning* (HBV) model and Ground Penetrating Radar (GPR) measurements along 74 km of snow courses, measured during March 2017 and April 2018, a water balance calculation was performed.

Figure 7 shows the location of the Överuman catchment. Most of the catchment area is in Sweden, with the remaining portion in Norway. The outflow from the catchment drains into the river Umeälven, which runs through Sweden to the Baltic Sea. The catchment has an area of 652 km². The elevation ranges from 524 to 1575 masl, and large parts of the area have an alpine character with little vegetation.



Figure 7. Overview of the location of the Överuman basin in Scandinavia



Figure 8. Map of the Överuman catchment and the resulting snow courses (blue lines). Steep slopes are indicated in the map with yellow, orange and red color, for snow avalanche awareness.

2. METHODS

Snow measurements are performed by towing a “snow radar” (ground penetrating radar, GPR, Sensor & Software with a Noggin 500 Plus antenna) behind a snowmobile, along the determined snow survey lines. Radar data are then analysed with the software Sirdas (Albrektsen Innovation) to find the snow-ground interface. The time that the radar signal needs from the antenna to the snow-ground interface and back is the two-way travel time (TWT). The travel speed of the radar signal is determined with manual calibration measurements in the field. Based on the radar signal speed and the TWT, the snow depth is calculated. Density measurements are used to convert snow depth to snow water equivalent (SWE).

Runoff from the catchment is calculated from continuous reservoir level measurements. This is here called the measured runoff.

In this study the average SWE for the whole catchment was calculated based on the snow measurements. The following simulations were performed with the HBV model:

1. Model run where the snow in the model every year was corrected to give a spring flood volume corresponding to the measured runoff, 18 years.
2. Model run with updating of the modelled SWE, based on the value of modelled SWE used in the operational forecasts, two years.
3. Model run with updating the modelled SWE based on the result from the snow measurements, two years.

To investigate the quality of the snow measurement results, and benefit from using it for model updating, an analysis for the whole winter season was performed for the years with snow measurements (2017 and 2018). Based on the simulated snow storage in the model and observations in the field, August 31st was defined as the date where the catchment is snow free. Simulated and measured SWE at date of snow measurements were compared, as well as accumulated runoff at the end of the snow melting season.

3. RESULTS AND DISCUSSION

Without any correction, the SWE value in the model needed a correction of -28 to 8 %, during the 18 years, to make the accumulated model runoff equal to the accumulated observed runoff at May 1st. When using the results from the snow measurements in the model the correction factor was reduced to -3 and -6 % for the years 2017 and 2018 respectively, see **Figure 9**.

The analysis of the results for 18 years of hydrological modelling shows that the performance of the model is not good for many of the years. This might indicate that the model needs improvement or better calibration. A significant change in the trend is shown after the year 2012 where the modelled SWE has been far too overestimated. Especially large deviations between observed and simulated runoff is shown for the last three years. When updating the model with measured SWE the modelling results are much closer to the measured values.

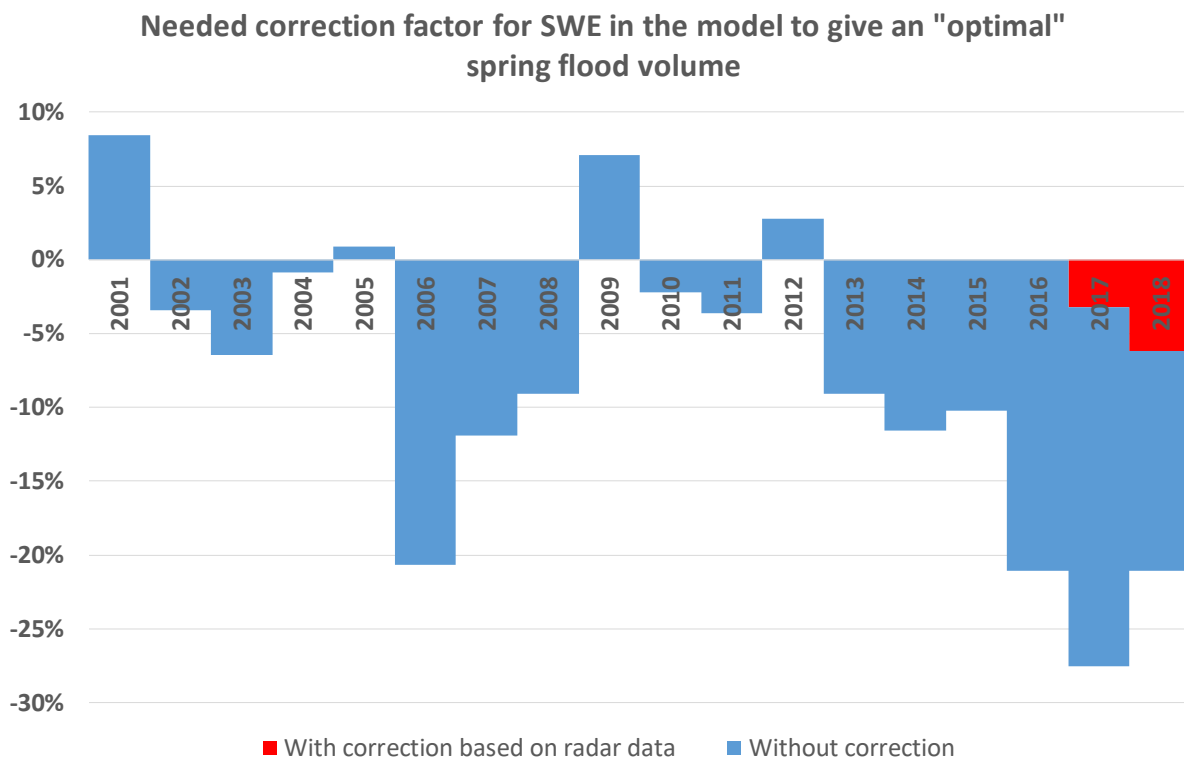


Figure 9. Correction factors for SWE in the model to make accumulated simulated runoff corresponding to accumulated “optimal runoff”. The “optimal runoff” is defined by the measured runoff with a correction factor applied, since the measurements at the reservoir are known to underestimate the runoff, due to some inaccuracies, probably an inaccurate rating curve.

The analysis of the two years with snow measurements shows that the model corrected with the radar measurements give a result very close to the optimal value, see **Figure 10**. By the end of

snowmelt, August 31st, the comparison of simulated and “optimal runoff” shows that the uncorrected model overestimates the accumulated runoff with 26 and 20 % in the years 2017 and 2018. The “optimal runoff” is defined by the measured runoff with a correction factor applied, since the measurements at the reservoir are known to underestimate the runoff, due to some inaccuracies, probably an inaccurate rating curve.

When updating the model at the date of snow measurement, with the measured SWE, the deviation between simulated and measured runoff is 2 and 4 %, for the years 2017 and 2018 respectively.

Model run	SWE (mm) At date of snow measurements		Sum Runoff (mm) From date of snow measurement to August 31rd				Year
	mm	difference mm	simulated mm	"optimal" mm	difference mm	difference %	
No correction	1085	0	1393	1102	291	26 %	2017
Corrected based on measured runoff	748	-337	1102	1102	0	0 %	
Corrected based on radardata	777	-309	1126	1102	24	2 %	
No correction	649	0	887	739	148	20 %	2018
Corrected based on measured runoff	487	-162	739	739	0	0 %	
Corrected based on radardata	518	-131	767	739	28	4 %	

Figure 10. Results from the analysis for the two years with snow measurements

4. CONCLUSION

The overall performance of the hydrological model shows large variations during the analysed period of 18 years. A significant change in the trend is shown after the year 2012 where the modelled SWE has been far too overestimated. This might indicate a need for improvement of the model.

The comparison of simulated and measured runoff during the two years of measurement shows that the use of measured snow data for model updating has given a great improvement of the model results. Thus, the measured data for the snow storage in the catchment show to have good quality and closely resemble the real snow storage. It also indicates that the system for snow measurements is functioning well and that GPR is a useful tool for precise snow measurements for in relatively large catchments.

It can be concluded further that good quality snow data provide an important input for better hydropower production planning and improved preparedness flood spill.

REFERENCES

Marchand, W-D. 2003 *Application and improvement of a georadar system to assess areal snow distribution for advances in hydrological modeling*. PhD thesis, NTNU, ISBN 82-471-5616-4, Trondheim, Norway

Changing snowfall and snow cover in the western Canadian Arctic

P. Marsh¹, P. Mann¹, and B. Walker¹

¹*Cold Regions Research Centre, Wilfrid Laurier University, Waterloo, Ontario, CANADA*

**Corresponding author's email address: pmarsh@wlu.ca*

ABSTRACT

Snowfall and snow cover have been shown to be changing across the Arctic, but there are few details on these changes at the local scale due to limited data. In this paper we will use a 60-year snow record from sites in the Inuvik, NWT region. In this region, the general changes are decreases in: snowfall, snow depth in forested sites near Inuvik, and decreases in snow depth and snow water equivalent at tundra, shrub and forest patches at tundra research site 50 km north of Inuvik. However, due to large measurement errors in many aspects of the snow environment, it is still difficult to understand the details of these changes and it is not possible to balance the incoming vs. outgoing components of the snow system with the accuracy needed to consider changes to all aspects of the snow environment, or to develop robust snow models. Although these problems are well known, until very recently there have been few advances in our snow measurement technologies. With recent technological advances, we are implementing an Integrated Arctic Snow Observing System (IASOS) across the treeline in the western Canadian Arctic near Inuvik, NWT. Manual observations of snow depth and density will be carried out at key times over the winter and spring. ISOS will provide new insights into the snow environment, data sets to allow the development of a modern snow prediction system and remote sensing sensors and methods.

KEYWORDS

Snow; climate change; Arctic; research needs; Arctic observing network

1. INTRODUCTION

Snow is a keystone component of the Arctic environment, with implications to, and interactions between vegetation, permafrost, hydrology and ecology (Quinton and Marsh, 1998; Pomeroy et al., 1999), as well as feedbacks to the climate (Sturm et al., 2001a). Changes in snow cover are primarily due to the combined effects of changes in air temperature and in precipitation, but also a combination of changes in wind, blowing snow, and vegetation for example (Sturm et al., 2001a; Lantz et al., 2012; Loranty and Goetz, 2012). Recent studies have showed significant changes in snow across the Arctic with increasing/decreasing snowfall and decreases in the spring snow cover area (Brown and Robinson, 2011) and snow water equivalent (SWE) (Liston and Hiemstra, 2011). However, there are few if any studies that have looked at local scale changes in snowfall, snow depth, snow density and SWE over the last few decades.

Our understanding of changes in Arctic snow is limited by two significant issues. First, observations of Arctic snow are limited to a small number of locations and typically for less than 60 years of record. Second, there are large errors in measurements of snowfall (Woo et al., 1983; Pan et al., 2016); sublimation during blowing snow events (Pomeroy et al., 1999); water vapour flux from frozen soil to snowpack (Santeford, 1978; Woo, 1982); continuous measurement of snow

erosion and accumulation at a range of upland and drift sites; and mapping snow water equivalent (SWE) at the watershed scale (Woo and Marsh, 1978). These limitations severely constrain our ability to close the snow balance over a watershed, and to develop and test appropriate models at the spatial scales needed. Given these significant deficiencies, the objectives of this short paper are: 1. characterize changes in snowfall and snow on the ground over the 60-year period of record in the Inuvik, NWT region (Inuvik-A), and 2: over a subset of this 60-year period, compare snowfall with traditional snow surveys of snow depth, density and SWE for a research site north of Inuvik.

2. STUDY SITES

Field observations were carried out in the Trail Valley Creek (TVC) watershed located 49 km north of Inuvik (Mike Zubko) Airport in the Northwest Territories (NWT) (Figure 1) where hydrological research has been carried out continuously since 1991 (Marsh et al., 2008). The watershed is characterized by rolling hills with deeply carved river valleys and elevations ranging from 45 to 190 meters above sea level (Marsh et al., 2010). TVC climate is best described by climate data from the Inuvik-Airport station, what shows a climate marked by short summers and long cold winters, with about 8 to 9 months of snow on the ground. The mean annual air temperature, rainfall and snowfall are -8.2°C , 114 mm and 159 cm (snowfall is uncorrected for wind undercatch) respectively, for a total of 241 mm of precipitation (Canadian Climate Normals 1981-2010, 2016). TVC is at the northern edge of the tundra-taiga ecotone and is underlain by continuous permafrost with an active layer ranging from 0.3 to 1.0 m (Endrizzi et al., 2011; Wilcox et al., 2019). TVC snow cover is typical of the Arctic (Sturm, 2015), varying greatly in depth, density and SWE over small spatial scales. The tundra is comprised of grasses, lichens and mosses, while shrub patches consist of alder, willow and birch. These shrub patches primarily occupy stream edges, lake edges, hill slopes and some upland area. Forest patches are comprised of white spruce and occur in a range of environments from valley bottoms to upland plateaus in the lower reaches of TVC. End of winter spatial variability in snow depth at TVC is very high, with typical upland snow cover averaging 40 cm in depth, while drifts in tall vegetation patches and on steep slopes is often 300 cm in depth (Marsh and Pomeroy, 1996), but can be up to 600 cm. Detailed field work was carried out in TVC from April and May of 2015 and 2016, and focused on Siksik Creek (Figure 1), a representative sub-basin of TVC that is approximately 1 km².

3. METHODS

Precipitation and related meteorological data are available from Inuvik Airport (Inuvik-A; YEV, 2202570) for the period 1958 to present (climate.weather.gc.ca). This is one of the longest, continuous, data records of snowfall and snow on the ground data in the Canadian Arctic and provides a unique opportunity to consider changes in winter snowfall in this region of the Arctic. Snowfall data includes estimates from ruler measurements, SR50 ultrasonic ranging sensors and a variety of manual and weighing precipitation gauges. There are limitations to each of these data sets and after careful consideration, it was decided to use the total precipitation data from Inuvik-A during the period of October to May as this record was the most complete. We will use the climate.weather.gc.ca data set that has a relatively full period of record for total precipitation, but is uncorrected for wind undercatch. As nearly all winter precipitation falls as snow, we will estimate snowfall at Inuvik-A as occurring on days with precipitation as days with mean air temperatures below 0°C from October 1st to May 30th. In addition to snowfall, we will use ruler and SR50 measurements of snow on the ground from Inuvik-A to compare to the snowfall for trends, as well

as snow on the ground measurements from 20-point snow surveys from a natural open forest site near to Inuvik-A.

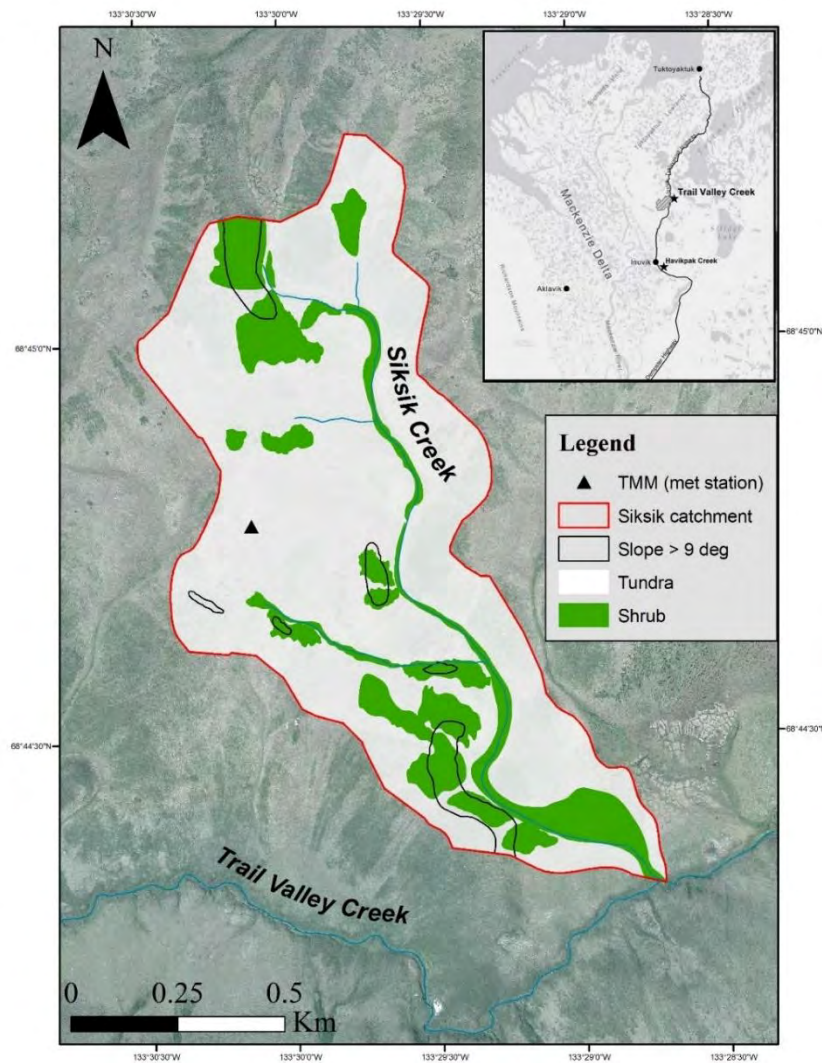


Figure 11. Land classification of Siksik Creek watershed, showing slopes where terrain dominated rifts typically form; shrub patches (green) with vegetation heights > 0.5 m, and tundra (white) with vegetation heights ≤ 0.5 m. Inset map shows the location of TVC, as well as the Inuvik to Tuktoyaktuk Highway.

We will also use snowfall and related meteorological observations from TVC, including the Main “Meteorological” station (TMM) (Figure 1), and a Forest Site (TFS) located 2.5 km south of TMM. TMM has two weather stations, the Wilfrid Laurier weather station (TMM-W) that was installed in 1991 and a Meteorological Service of Canada weather station (TMM-M; 220N005) installed in 1998 during the Mackenzie GEWEX Study (MAGS). TFS was installed in 2009. TMM-W and TMM-M are located approximately 20 meters apart. Due to a variety of instruments used over the period of record, we will concentrate on the 2008 to 2016 period when all sites measure snowfall using a single alter shielded T-200B Geonor weighing gauge, and other measurements include: air temperature and relative humidity, wind speed and direction and snow depth. TFS is also equipped with a 7.5 m² snow scale measure SWE accumulation over an area of 0.84 m². Pomeroy et al. (1997)

suggested that due to little blowing snow at TFS, and minimal canopy interception due to the widely separated trees, snow on the ground at this site approximates total winter snowfall.

To correct undercatch errors due to wind for single-alter shielded Geonors, solid precipitation is adjusted for wind speed using the methods of Pan et al. (2016). Using a minimum threshold of 1.2 m/s and a maximum threshold of 9 m/s for the wind speed, results in catch efficiencies of 1 and 0.23 for winds below 1.2 m/s and above 9 m/s respectively. Daily images, from a time lapse camera installed at TMM, were used to determine the onset of snow accumulation for winters of 2014/15 and 2015/16.

To complement TMM and TFS snowfall and snow on the ground data, we used spatially distributed snow survey data from TVC from 1991 to 2017 at the same locations reported by Marsh and Pomeroy (1996). These included: tundra (low vegetation less than 0.5 m; 70% of watershed area), shrub (tall shrub vegetation greater than 0.5 m, but less than 3 m; 22%), forest (tree vegetation greater than 3 m; 0.5%) and drift (slopes greater than 9°; 8%). A total of 6808 snow depths and 854 snow density measurements were obtained over this period. Additional snow surveys were conducted in Siksik during April of 2015 and 2016 study period. These were conducted along transects selected to be representative of the catchment's land classification and well distributed throughout the catchment. Total basin SWE for Siksik Creek were calculated using weighted averages of SWE for each landcover type similarly done for the past snow surveys at TVC.

4. RESULTS

4.1 Inuvik-A snowfall and snow on the ground: 1958 to 2017

Comparing the two 30-year periods of record at Inuvik-A, 1958 to 1987 and 1988 to 2017 (Table 1), the mean winter air temperature was 2.7°C warmer during the second period, with an impact on all aspects of the winter snow regime. Specifically, average snowfall (Table 1), maximum and minimum snowfall, mean snow depth, and snow as a percentage of total annual precipitation all decreased, while standard deviation was similar during both periods. Figure 2 shows data for each year over the 60-year period of record. Using Mann-Kendall trend test, we see significant decline in snowfall ($p = 0.0002$) and maximum snow on the ground ($p = 0.003$) at Inuvik-A. Recent snowfall has been very low, with 2010 and 2014 recording the lowest snowfall on record, and the 2015 and 2016 study winters also being extremely low.

4.2 TVC snow on the ground: 1990 to 2017

Figure 3 illustrates 1991 to 2017 end of winter snow cover data for TVC. Over this period, average snow depths show that snow depth and SWE have shown slight decreases for each of the TVC

Table 1. Inuvik-Airport 30-year snow and air temperature averages

	1958-1987	1988-2017	Difference
Mean snowfall (mm SWE)	131	111	-20
Maximum snowfall (mm)	192	179	-13
Minimum snowfall (mm)	80	63	-17
Standard deviation of snowfall (mm)	32	31	-1
Mean snow depth (cm)	71	61	-10
Mean snow percentage of total precipitation (%)	52	45	-7
Mean air temperature (°C)	-9.6	-7.2	-2.7

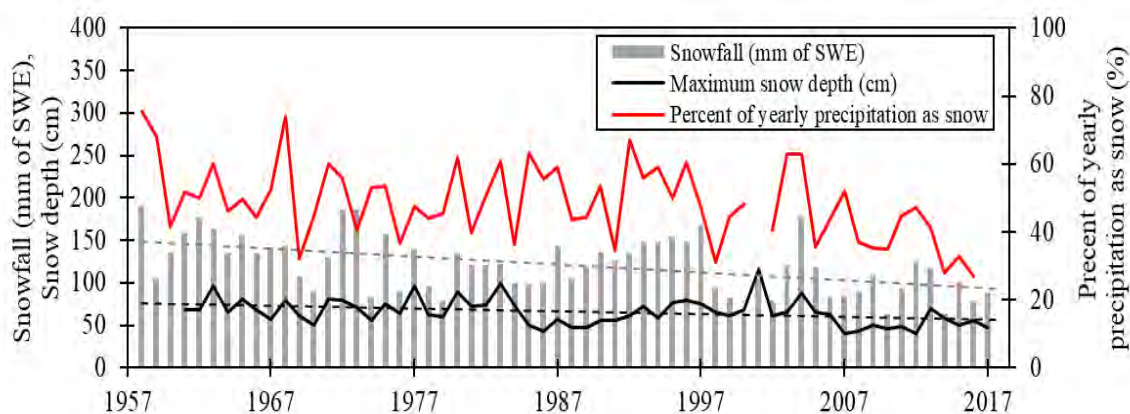


Figure 2. Inuvik-A yearly snowfall, maximum snow depth and percent of yearly precipitation as snow from 1958 to 2017. The dashed lines are the trendlines for snowfall and maximum snow depth respectively.

landcover types, but also large annual variability. While density shows no change. Average snow depth for the terrain types (tundra, shrub, forest and drift) was 37, 69, 73 and 185 cm respectively over the entire period of record. For the first half of the period of record (1991 to 2004), depths averaged 43, 80, 77 and 197 cm respectively, and for the second half (2005 to 2017) depths averaged 39, 63, 69 and 183 cm. End of winter SWE for tundra, shrubs, forest and drifts respectively ranged from: 60 to 170 mm, 80 to 340 mm, 80 to 290 mm and 33 to 1270 mm, with basin average end of winter SWE ranging from 108 to 253 mm. There is greater inter-annual snow

depth and SWE variability in the drift landcover. Figure d illustrates that over the past 26 years (1991 to 2017), the TVC end of winter snow cover has averaged 167 mm of SWE, with a maximum of 253 mm in 1991/92, a minimum of 108 mm in 2006/07 and a standard deviation of 38 mm.

End of winter snow cover is sensitive to both the rate of precipitation during the below freezing winter period, and to the length of the snowfall period. For Inuvik, the length of winter (as indicated by the period between the first and last three consecutive daily mean air temperatures below the 0°C isotherm, Shi et al. (2015)) are becoming shorter. Changes in fall and spring temperature show a reduction of total winter length by approximately 14 days over the 60-year period. With the of the Mann-Kendall trend test the total winter length shows a significant ($p = 0.04$) trend.

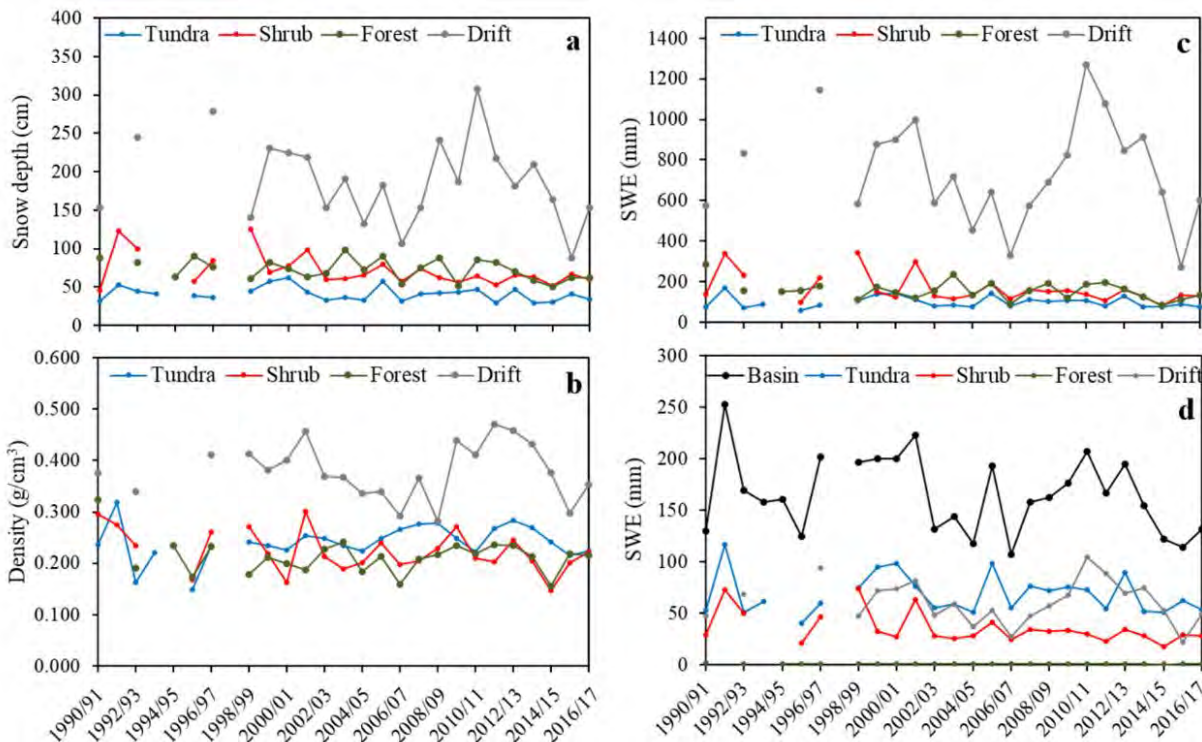


Figure 3. End of winter snow cover at TVC, showing snow depth, density and SWE for tundra, shrub, forest and drift are shown in **a**, **b** and **c** respectively. Basin mean SWE (black) and aerial weighted SWE for each landcover type shown in **d**.

4.3 Trail Valley snowfall: 2008 to 2016

Over the period 2008 to 2016, Inuvik-A uncorrected snowfall is typically larger than the TMM-W uncorrected snowfall, but corrected TMM-W snowfall (Figure 4) is always larger than the Inuvik-A uncorrected winter precipitation. Over this period, the mean winter uncorrected snowfall at TVC was 71 mm and the mean corrected snowfall was 137 mm, compared to the uncorrected snowfall at Inuvik-A of 94 mm for this period. Although Inuvik-A wind speed is less than at TMM-W, it is unclear if the difference in snowfall is due to using uncorrected snowfall at Inuvik, or due to an actual difference in snowfall between the two stations. It should be noted that the long term MSC snowfall records show that Tuktoyaktuk, 80 km north of TVC on the Beaufort Sea coast has average winter snowfall of 103 mm compared to 159 mm at Inuvik (Canadian Climate Normals 1981-2010, 2016). This suggests that TVC would normally receive less snowfall than Inuvik on average.

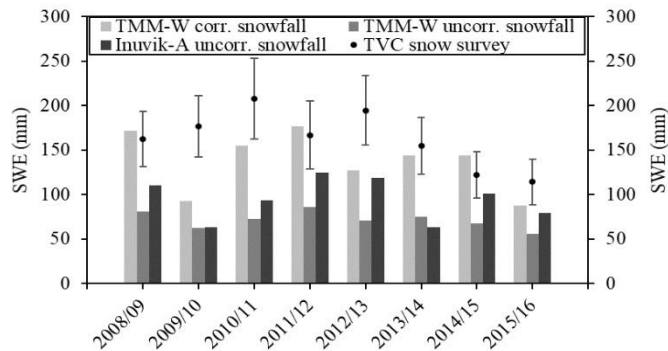


Figure 4. Comparison of TVC end of winter SWE from snow surveys (points) (also shown in Figure 3d), TMM-W corrected snowfall (light grey columns), TMM-W uncorrected snowfall (dark grey columns) and Inuvik-A uncorrected snowfall (black columns). Error bars on the snow surveys represent ± 1 standard deviation. Snowfall at TMM-W was measured using Geonor gauges with alter shields since 2008.

Pan et al. (2016) ran bias corrections for yearly precipitation (including rainfall, mixed precipitation and snowfall) at TVC for the years 2008 to 2014, and they found that the annual mean corrected precipitation at TMM was 251 mm, while we attained a mean corrected snowfall of 137 mm of SWE at TMM for the years 2008 to 2016. This suggests that snowfall accounts for 55% of the yearly precipitation at TVC, slightly higher than the average of 49% for the Inuvik region.

Figure 5 shows a selection of the metrics collected in the two detailed study winters (2014/15 and 2015/16) at TMM and TFS. Winter of 2015/16 saw colder temperatures, lighter winds and less uncorrected and corrected precipitation than the previous winter. Furthermore, the winds at TFS are lighter than those at TMM-W, suggesting that the gauge undercatch may be lower, that the forest cover hinders blowing snow events within the forest patch and hence the forest snow cover may be closer in magnitude to the winter snowfall. Differences between snowfall measurements at TMM-W and TMM-M are 25 mm for 2014/15 and 22 mm for 2015/16. Therefore, we see less precipitation in 2015/16 at TMM-W than TMM-M. Much larger differences are present between the TFS gauge and the other two gauges due to lower wind speeds in the forest cover resulting in a lower wind-induced undercatch correction. SWE from snow surveys and from snowfall are compared in Figure 4 for the period 2008-2016 at TVC. Over this period, end of winter basin average SWE has been, on average, 24% greater than corrected snowfall and only four out of eight of the winters snowfall has been within 1 standard deviation of the snow surveys. This difference is not due to the effect of blowing snow sublimation, as sublimation would reduce basin SWE compared to snowfall. Note that Pomeroy et al. (1997) have estimated winter sublimation at TVC to be 20% of total snowfall. Larger SWE than corrected snowfall could be the result of two possibilities: i) the TVC basin may be a sink for blowing snow or ii) that true snowfall is actually larger than our estimate from snow gauges at TVC. Figure 4 shows that there doesn't seem to be a year to year relationship between end of winter SWE on the ground and corrected snowfall.

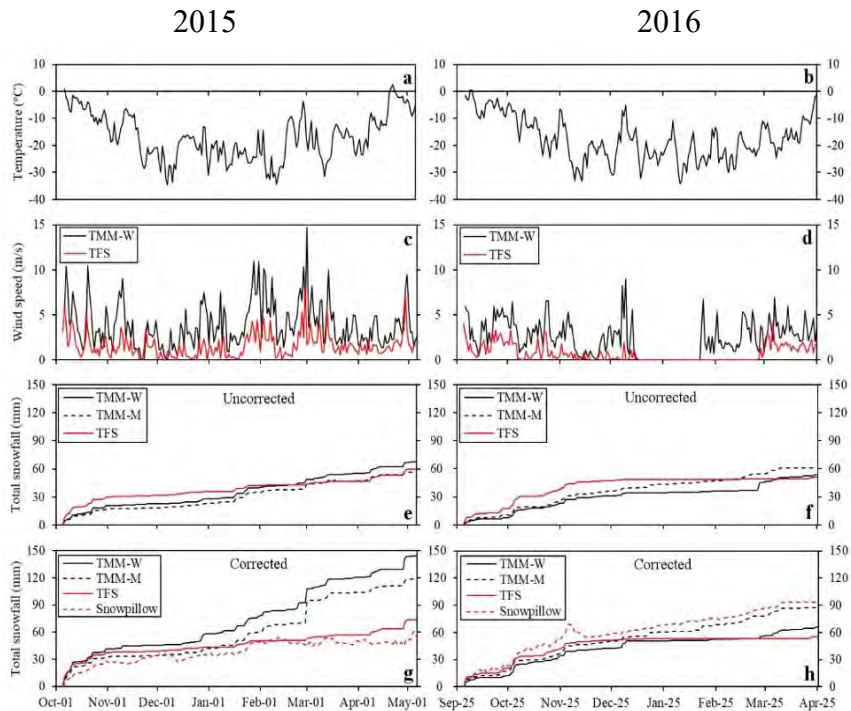


Figure 5. Daily time series of meteorological data for the winters of 2014/2015 (left; 1-Oct-2014 to 6-May-2015) and 2015/2016 (right; 25-Sept-2015 to 25-April-2016). 2-meter air temperature at TMM-W (**a**, **b**), 10-meter wind speed at TMM-W and TFS (**c**, **d**) and total snowfall at TMM-W, TMM-M and TFS (**e**, **f**, **g**, **h**) in mm of SWE. For total snowfall, a comparison of the three Geonor gauges is shown for uncorrected snowfall (**e**, **f**) and for corrected snowfall for wind-induced undercatch (**g**, **h**). The red dashed line in **g** and **h** is the snow scale located at TFS, meters away from the Geonor gauge.

5. INTEGRATED ARCTIC SNOW OBSERVING SYSTEM

Observations from the Inuvik region show complex changes in snowfall and snow on the ground and Shi et al., (2015) show resulting complex changes in snowmelt runoff at TVC. However, Figure 5 shows the difficulty in measuring snowfall, with large errors very common. Not discussed in this paper are the errors also in measuring sublimation during blowing snow events, fluxes of water from the ground into the snowpack over the winter, continuous snow accumulation or the difficulty in mapping snow depth, density and SWE over Arctic watersheds. These limitations in our observing ability, and limited Arctic snow data sets, means that it has been difficult to develop, test, and use snow models in the Arctic. Existing models are likely insufficient to guide our understanding of future changes in the Arctic snowcover at the scale required by local communities and decision makers. To solve these limitations, we are developing an Integrated Arctic Snow Observing System (IASOS) in the tundra-taiga zone near Inuvik (TVC and HPC, Figure 1). We have installed (underlined below) or will soon install: 1) a network of traditional meteorological stations, including snowfall gauges, 2) a micro rain radar system to improve observations of snowfall, 3) a blowing snow particle detector, 4) a network of cosmic ray snow sensors and GNSS snow sensors to allow the continuous observations of snow erosion at upland sites and snow deposition at accumulation sites over the winter, and snow melt, 5) eddy covariance towers to measure sensible and latent heat flux over the entire snowcovered period, 6) unmanned aerial

vehicles and structure from motion methods to map snow depth at high resolution, 7) a combination of measurements and modelling to estimate snow density across the watershed, 8) combining #6 and #7 allows mapping of SWE at high resolution, 9) streamflow gauges at TVC in collaboration with Water Survey of Canada and 2 sub-watersheds of TVC, and 10) a solar/wind/diesel generator system to allow powering and heating this instrument network over the entire winter. This unique snow observing system will allow balancing the snow budget over a watershed with greater accuracy than previously possible and will allow testing and development of next generation snow models.

6. CONCLUSION

During the period of 1958 to 2017 at Inuvik-A, snowfall, snow on the ground and percentage of total precipitation as snowfall have declined, and the lengths of winters have become shorter. Although it is expected that most of the Arctic will experience greater precipitation, the western Canadian Arctic is not experiencing an increase in winter precipitation as snow. The IPCC AR5 states that decreases in snowfall are due to a shift in precipitation phase from solid to liquid and an earlier melt onset from consequent warming in the Arctic and that increases in snowfall are as a result of higher moisture content available from a reduced Arctic sea ice extent. Both scenarios are likely the case for the Inuvik region.

At TVC, the total corrected snowfall is consistently less than the watershed SWE at the end of winter. This is similar to Woo et al. (1983) who also found that snowfall was smaller than snow on the ground at the end of the accumulation period in the Canadian high Arctic. For various hydrological and ecological needs, this clearly indicates that there are still significant unknowns in our understanding of the Arctic snow regime. These may include the following. Firstly, the catch efficiency equation used to correct for wind induced undercatch may be underestimating the precipitation, and therefore a new equation for Arctic landscapes would be necessary. Secondly, throughout winter there may be a significant water vapour flux from the soil to the snowpack. Such vapour fluxes are dependent on soil characteristics and fall soil moisture, in interior Alaska, Santeford (1978) measured 30 mm of SWE transferred from the soil to the snowpack representing 25 to 30% of the moisture already in the snowpack. In Resolute, NU, Woo (1982) measured an upward flux of 2 to 3 mm of SWE for a 0.5 m snowpack. This phenomenon adds additional SWE to the snowpack without a snowfall source and needs further monitoring. Thirdly, sublimation occurs throughout winter, in greater amounts during blowing snow events, reducing the quantity of snow on the ground by approximately 20% (Pomeroy et al., 1997). Fourthly, snow surveys may over/under estimate snow on the ground. Unfortunately, our understanding of the magnitude, and in some cases direction of the errors, of each of the above is poorly understood. This is a significant problem greatly limiting both our understanding of the current snow environment of the Arctic and ability to predict future changes to the snow environment.

REFERENCES

- Brown, R. D., & Robinson, D. A. 2011. Northern Hemisphere spring snow cover variability and change over 1922-2010 including an assessment of uncertainty. *Cryosphere*, 5(1), 219–229.
- Endrizzi, S., Quinton, W. L., & Marsh, P. 2011. Modelling the spatial pattern of ground thaw in a small basin in the arctic tundra. *The Cryosphere Discussion*, 5, 367–400.
- Lantz, T. C., Marsh, P., & Kokelj, S. V. 2012. Recent shrub proliferation across the boreal-arctic transition and microclimate implications. *Ecosystems*.

- Liston, G. E., & Hiemstra, C. a. 2011. The Changing Cryosphere: Pan-Arctic Snow Trends (1979–2009). *Journal of Climate*, 24(21), 5691–5712.
- Loranty, M. M., & Goetz, S. J. 2012. Shrub expansion and climate feedbacks in Arctic tundra. *Environmental Research Letters*, 7(1), 011005.
- Marsh, P., & Pomeroy, J. W. 1996. Meltwater fluxes at an arctic forest-tundra site. *Hydrological Processes*, 10(10), 1383–1400.
- Marsh, P., J. Pomeroy, S. Pohl, W. Quinton, C. Onclin, M. Russell, ... S. McCartney. 2008. Snowmelt processes and runoff at the Arctic treeline: Ten years of MAGS research. In Ming-ko Woo (Ed.), *Cold Region Atmospheric and Hydrologic Studies, The Mackenzie GEWEX Experience. Volume 2: Hydrologic Processes* (pp. 97–124). Berlin: Springer.
- Marsh, P., Bartlett, P., MacKay, M., Pohl, S., & Lantz, T. 2010. Snowmelt energetics at a shrub tundra site in the western Canadian Arctic. *Hydrological Processes*, 24(25), 3603–3620/.
- Pan, X., Yang, D., Li, Y., Barr, A., Helgason, W., Hayashi, M., ... Li, Y. 2016. Bias Corrections of Precipitation Measurements across Experimental Sites in Different Ecoclimatic Regions of Western Canada. *The Cryosphere*, 10, 2347–2360.
- Pomeroy, J. W., Marsh, P., & D.M. Gray. 1997. Application of a distributed blowing snow model to the Arctic. *Hydrological Processes*, 11(11), 1451–1464.
- Pomeroy, J. W., Davies, T. D., Jones, H. G., Marsh, P., Peters, N. E., & Tranter, M. 1999. Transformations of snow chemistry in the boreal forest: accumulation and volatilization. *Hydrological Processes*, 13(14–15), 2257–2273.
- Quinton, W. L., & Marsh, P. 1998. The Influence of Mineral Earth Hummocks on Subsurface Drainage in the Continuous Permafrost Zone. 228(May).
- Santeford, H.S. 1978. Snow soil interactions in interior Alaska. In: Modeling of Snow Cover Runoff, S.C. Colbeck and M. Ray (Eds), U.S. Army, Cold Regions Research and Engineering Laboratory, Hanover, New Hampshire, pp. 311- 318.
- Shi, X., Marsh, P., & Yang, D. (2015). Warming spring air temperatures, but delayed spring streamflow in an Arctic headwater basin. *Environmental Research Letters*, 10(6), 064003. <https://doi.org/10.1088/1748-9326/10/6/064003>
- Sturm, M., McFadden, J. P., Liston, G. E., Chapin III, F. S., Racine, C. H., & Holmgren, J. 2001. Snow–shrub interactions in Arctic tundra: a hypothesis with climatic implications. *Journal of Climate*, 14(3), 336–344.
- Sturm, M. 2015. White water: fifty years of snow research in WRR and the outlook for the future. *Water Resources Research*, 51, 4948–4965.
- Wilcox, E., D. Keim, T. de Jong, B. Walker, O. Sonnentag, A. Sniderhan, P. Mann and P. Marsh. 2019. Tundra shrub expansion may amplify permafrost thaw by advancing snow-free timing. *Arctic Science*, under review.
- Woo, M. K., Heron, R., Marsh, P., & Steer, P. 1983. Comparison of weather station snowfall with winter snow accumulation in high Arctic basins.
- Woo, M. 1982. Upward flux of vapor from frozen materials in the high Arctic. *Cold Regions Science and Technology*, 5(3), 269–274.
- Woo, M.-K., & Marsh, P. 1978. Analysis of Error in the Determination of Snow Storage for Small High Arctic Basins. *Journal of Applied Meteorology*, 17(10), 1537–1541.

River idealization for identification of critical locations in steep rivers using 2D hydrodynamic modelling and GIS

Adina Moraru^{1*}, Kh Rahat Usman¹, Oddbjørn Bruland¹, and Knut Alfredsen¹

¹Department of Civil and Environmental Engineering, Norwegian University of Science and Technology (NTNU), Trondheim, 7049, NORWAY

*Corresponding author's email address: adina.moraru@ntnu.no

ABSTRACT

Planform variation and hydrodynamics in steep rivers were characterized based on the combination of 2D hydrodynamic simulations and GIS tools. The idealization of topography (*i.e.* slope) and hydrology (*i.e.* discharge) permitted analysing their relevance and effect in river's response to identify critical locations in case of flooding. A total of 24 scenarios were idealized. Slope idealization was achieved by means of modifying the slope of the river bed while keeping the terrain constant outside of it. Slope ranged from 4% to 5.5%. Discharge idealization was implemented as constant steady flow from $Q = 30 \text{ m}^3/\text{s}$ ($>Q_{\text{Mean}}$) to $Q = 105 \text{ m}^3/\text{s}$ ($>Q_{200}$). Hydrodynamics at channel bends with a curvature of 35° to 95° along 1125 m of reach and their correlation with topography were analysed. Both river banks and channel's centre points were analysed; the left bank generally presented higher values and higher variability. Results show that discharge has a stronger influence in river's response than slope when $s \leq 4.5\%$ and $Q \geq 60 \text{ m}^3/\text{s}$. For slopes higher than 4.5%, discharge shows poorer correlation with hydraulic forces than slope gradient's influence. The same trend is observed for $Q < 60 \text{ m}^3/\text{s}$, where slope presents stronger correlations than discharge with river's response. However, the difference in river response decreases and shows a stabilizing tendency with increasing slope. Bend curvature influenced hydraulic response together with channel narrowing in subsequent cross-sections. Water surface elevation was usually lower at the convex side of bends, which presented higher hydraulic forces.

KEYWORDS

Steep rivers; Morphometric indicators; Critical locations; 2D hydrodynamic modelling; GIS; Flood risk assessment

1. INTRODUCTION

Floods are the most widespread type of natural disaster and cause the highest damages (UNISDR, 2019). Flood frequency is increasing as a result of highly unpredictable climate changes: higher snow melt, changes in precipitation patterns and its spatiotemporal distribution, as well as locally reduced precipitation in the form of snow (Schumann *et al.*, 2018). Human actions have become a dominant influence on fluvial systems and, together with potential effects of climate change on flood regime (*e.g.* spatially restricted extreme rainfalls affecting more severely steep and ungauged rivers), predicting where major geomorphic changes may occur is very challenging. Associated geomorphic processes cause a significant amount of the damages related to floods and river planform variation during floods can vary significantly. Considering controlling factors to streambank erosion during high-magnitude floods affecting steep rivers would contribute to sound land use management and the reduction of damages and economic loss due to floods (Moraru *et*

al., 2018). Recent environmental changes introduce new and more complex scenarios that translate into expertise demands, such as detecting these changes promptly and increasing social awareness of the problem at hand (Moraru *et al.*, *in press*).

Flash flood dynamics are controlled by factors that could be differentiated at two levels: i) catchment-intrinsic factors, which do not vary significantly at the human scale, and ii) factors that vary in time and are perceived at such scale (Furdada *et al.*, 2018). The first type includes, for example, topographic data, whereas the second type includes hydrologic data. Hydraulic forces are topography- and hydrology-dependent, hence, simulating scenarios where these factors are constant will underscore the influence of other parameters. Keeping track of changes in topographic and hydrologic parameters allows to identify how river's response is determined by them and helps discerning whether other factors act complementarily to them or show some interdependence. For instance, the analysis of geomorphic indicators controlling morphological changes during flood events affecting 54 European watercourses (Moraru, 2017) showed that rivers incised in the bedrock (*i.e.* with a high Lateral Confinement Index, LCI) and with a steep slope presented low changes in channel width during extreme rainfalls, which suggests that slope might not be the most relevant factor determining planform changes when certain conditions (*e.g.* high LCI) are given.

Geographic Information Systems (GIS) allow us to virtually modify land use, topographic information, river morphology and information regarding infrastructure near studied rivers. Combining such information with river hydro- and morphodynamic modelling, we may highlight which factors influence steep rivers' eroding potential as well as changes in the river bed. Mapping these will result in the representation of critical locations (*i.e.* combining the inherent damage potential and added damage potential with elements of risk results in the vulnerability assessment) in case of flood events. By shaping artificial rivers (*i.e.* idealized rivers, Kvočka *et al.*, 2017), the different parameters can be isolated, changed, modelled and their effect studied more independently of the rest of the factors playing part in river's response (Figure 1). Characterizing rivers in such fashion and transposing the methodology into a GIS application allows identifying critical locations in selected cases and then extrapolate to real scenarios in order to validate the method.

In this paper we intend to define and generate morphometric measures relevant to flood risk assessment in steep rivers and combine them with river hydrodynamic models in GIS. Idealized rivers have been modelled under various idealized rainfall scenarios, and the water level, forces and velocity have been mapped for further analysis. The aim was to identify relationships between river hydraulics and river geometry in a simplified manner, which contributes to a more rapid and more effective preliminary risk assessment.

2. METHODS

The study was carried out in a steep idealized river, where the river response was analysed in hydrologic and topographic changing conditions. River response was characterised in terms of channel width (W), relative section ratio (W_{xs}), water depth (D), flow velocity (V), shear stress (SS) and total stream power (SP). Special attention was set on monitoring these parameters in channel bends (B). Figure 1 shows the general methodology, where bathymetry-idealization was carried out on the 1x1 m resolution DEM of an originally steep and locally sinuous river. Geographic information was retrieved from hoydedata.no and nibio.no.

Byrteåi river drains into lake Byrtevatn, in the region of Telemark, Norway (Figure 2A), and has a length of approx. 20 km, and an average slope of 6.5 %. The original slope was modified to a constant gradient (Figure 3, left) using HEC-RAS v.5.0.6's terrain modification tools (see further information in HEC-RAS user's manual), although the cross-section shape was preserved (Figure 3, right). This was performed on a systematic fashion on a river length of 2600 m (Figure 2B), where average slope was 4.5% and 100 m-long cross-sections (X-S) were established every 50 m in ArcGIS v.10.6 and later imported to RAS Mapper.

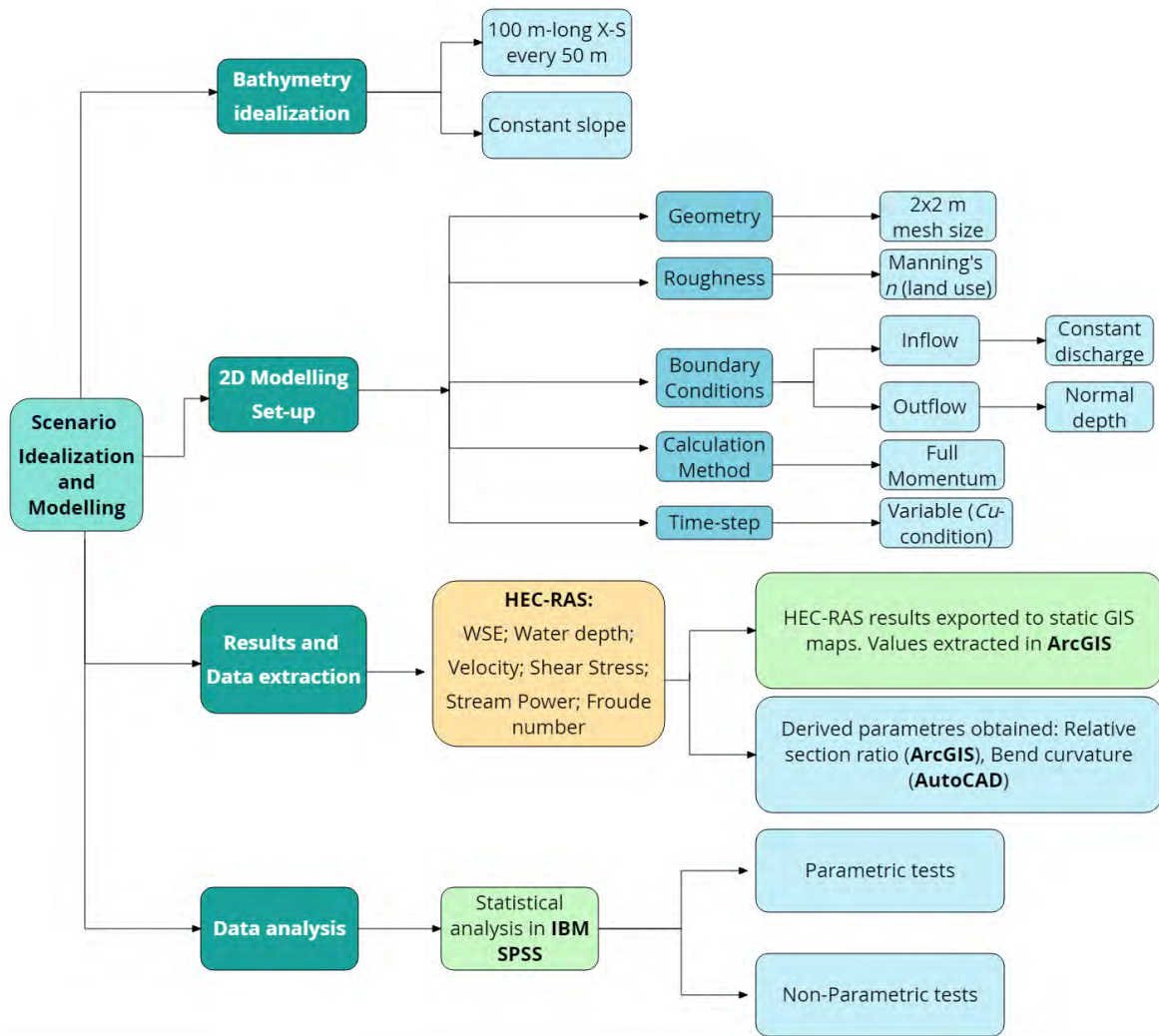


Figure 1. Workflow diagram followed for the scenario idealization and hydrodynamic modelling, as well as for the data analysis performed in the present study. Further information is available in the text.

Two-dimensional hydrodynamic simulations were carried out in HEC-RAS v.5.0.7. An overview of the fluid simulations set-up is presented in Figure 1. The roughness coefficients (*i.e.* Manning's n) were set based on the land use information for the aforementioned catchment as follows: roads and cultivated land 0.04, river channel 0.05, swamp and open land 0.06, forest 0.12, buildings 10 (Figure 2C). Idealized constant flow hydrographs were set as the inflow boundary condition (BC),

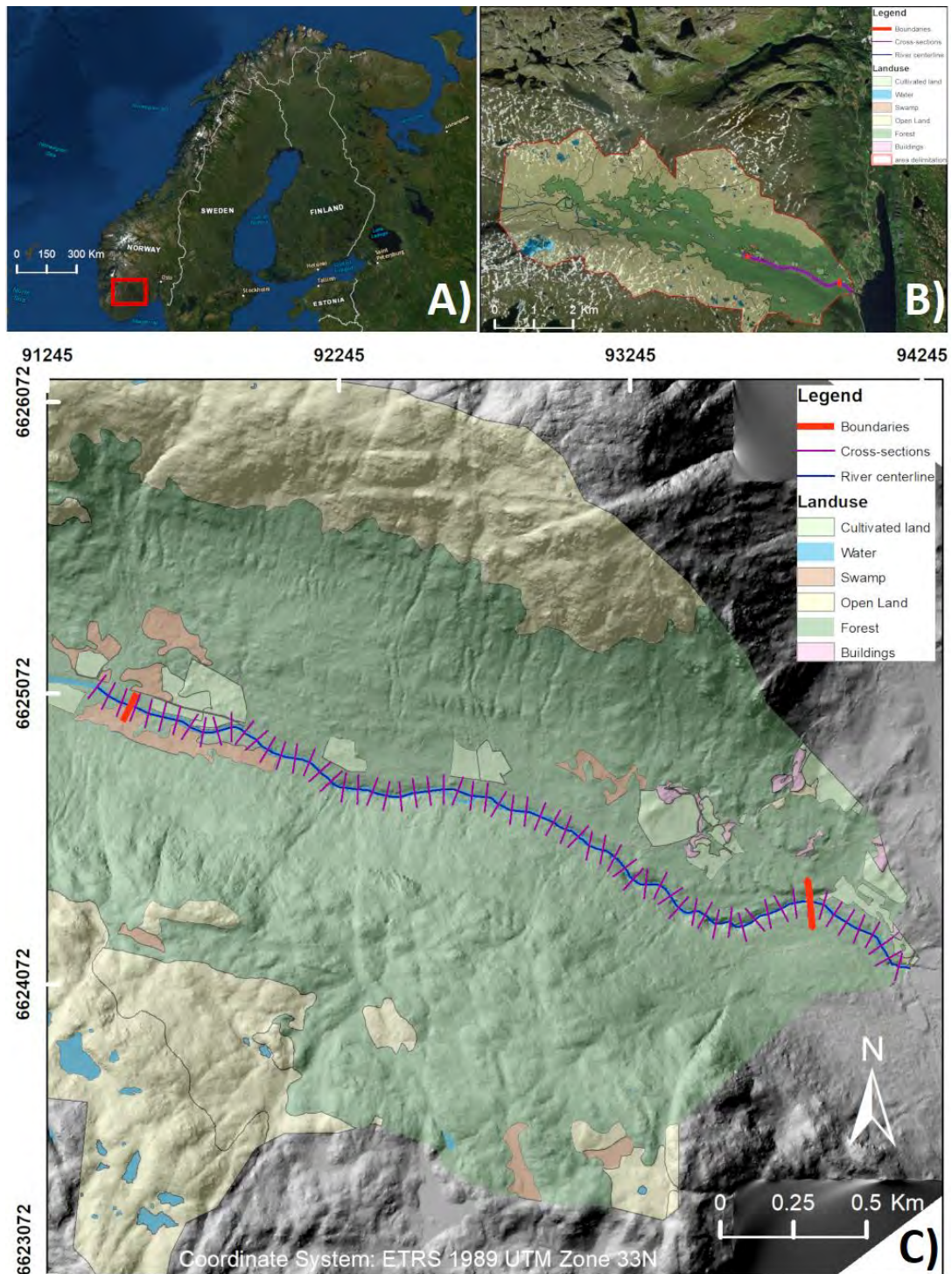


Figure 2. A) Context map of selected study case (Byrteåi river in Telemark, Norway). Scale is 300 km. B) River catchment with over imposed land use cover. Scale is 2 km. C) Close up of the reach used for 2D hydrodynamic simulations, with land use cover over imposed to the DEM hill shade. BCs in red; water flows NW-SE.

and the outflow BC was set as the Normal water depth estimated based on the rating curve and the idealized input slope. Solving the 2D Full Momentum equation seemed to give more accurate

results than Diffusion Wave, hence, this calculation method was preferred. The computational time-step was set variable and based on the defined Courant (Cu) condition; computational time-step was set to 15 seconds and $Cu = 1$.

2.1 Idealized scenarios

Slope was considered steep when equal or higher than 0.040 m/m. For the simulated idealized scenarios, the slope was set at constant increasing intervals, from 0.040 to 0.055 m/m, with an interval spacing of 0.5% (*i.e.* 0.005 m/m). The discharge was set at constant increasing intervals, from 30 m³/s to 105 m³/s, with an interval spacing of 15 m³/s. The combination of slope and discharge resulted in a total of 24 simulated scenarios (Table 1).

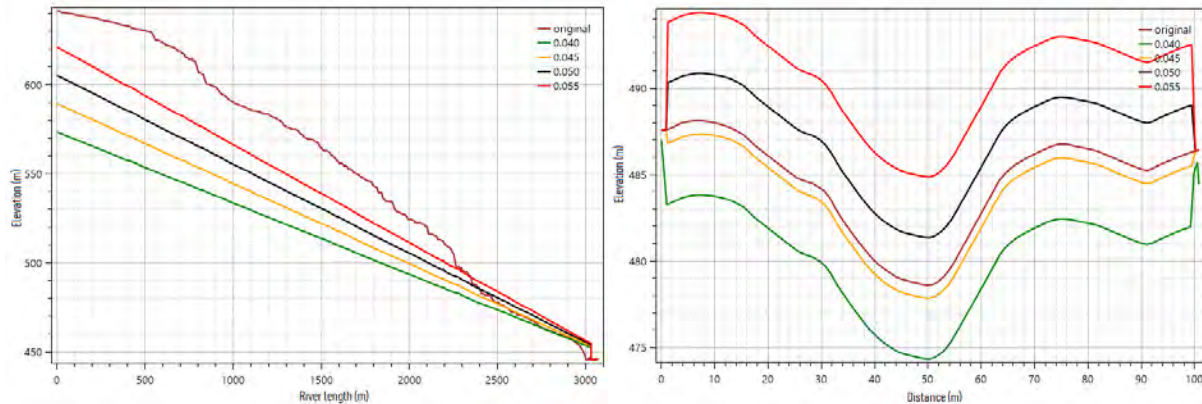


Figure 3. Left: terrain profile of the original (brown) and idealized scenarios from the inflow BC to the tailwaters into lake Byrtevatn. Right: cross-sectional profile shows that the original shape has been preserved. Slope of idealized scenarios: green 0.040, yellow 0.045, black 0.050, red 0.055 m/m.

2.2 Data extraction and analysis

Each simulated scenario resulted in static maps of Water Surface Elevation (WSE), D , V , SS , SP and Froude number (Fr) at each computed time-step. Data obtained in HEC-RAS v.5.0.7 was imported to ArcGIS v.10.7 for further processing.

Table 1. Combinations of simulated scenarios (*i.e.* 24), where idealized slope and discharge were set constant.

Slope (m/m)	Discharge (m ³ /s)					
	30	45	60	75	90	105
0.040	1	2	3	4	5	6
0.045	7	8	9	10	11	12
0.050	13	14	15	16	17	18
0.055	19	20	21	22	23	24

Data regarding these parameters was extracted in the centre of the channel, and in both river banks (Figure 4, right). Channel bends (see description, for example, in Sin *et al.*, 2012) were analysed

in AutoCAD v.2018 and then converted to GIS files for post-processing; the bend was expressed in terms of outside bend-curvature in degrees (Figure 4, left). Only bends with a curvature greater than 35° were considered in this study, as hydrodynamics seemed rather complex in such cases. This resulted in a total of 14 bends affecting 1125 m of reach.

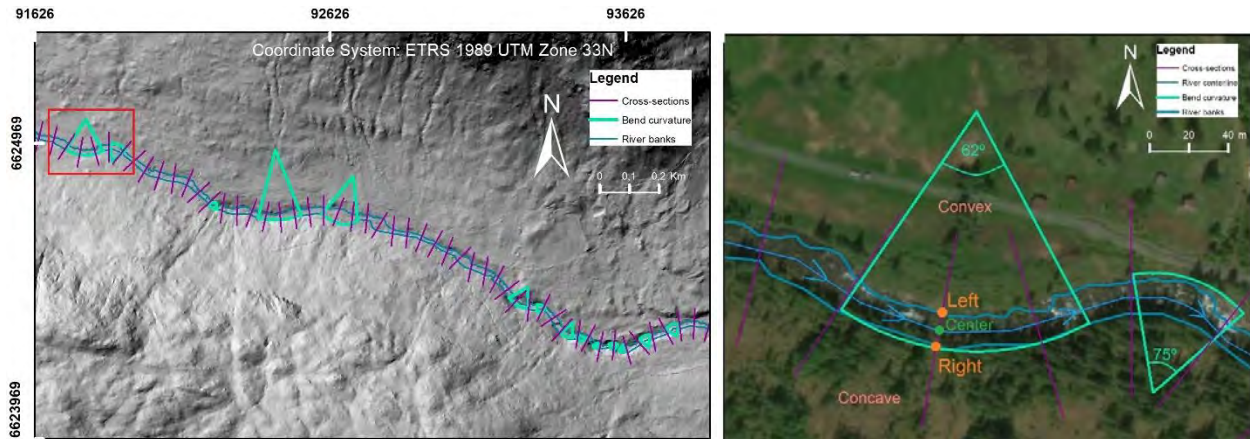


Figure 4. Left: bend curvature analysis over the DEM hill shade. The outside-bend arc is measured in degrees, ranging from 35 to 95 degrees. Scale is 0.2 km. Right: zoom in to area in red rectangle in the left-hand side figure; characterization of bend arc and localization of data extraction points. Blue arrows indicate flow direction.

Further information, such as W and W_x s were calculated based on GIS data; the dataset was analysed statistically with IBM SPSS Statistics v.25.0. Frequency histograms were used to define breakpoints and classes (Table 2) for the different parameters. Boxplots showed the variation of the results for the centre points and riverbanks, as well as the dispersion in the data. Pearson’s correlation test identified linear linkages between the hydraulic and topographic parameters. Linear multivariate analysis was performed to identify the parameters that have the highest correlations with river’s response once discharge and slope were idealised. Level of significance was set at p -value ≤ 0.05 .

Table 2. Classification of discharge and bend curvature in statistical analysis.

<i>Parameter</i>	<i>Range</i>	<i>Class</i>
<i>Discharge</i> (m^3/s)	30–45	moderate
	60–75	extraordinary
	90–105	extreme
<i>Bend</i> <i>curvature</i> (degrees)	35–55	soft
	56–75	intermediate
	76–95	tight

3. RESULTS

Discharge (Q) is positively correlated to all the hydraulic parameters (Figure 5). Slope (s) correlates positively with SP , Fr and SS , and negatively with water depth, although not strongly. Discharge has a stronger correlation with hydraulic forces than s ; slope correlates more with Fr than Q .

D	0.689						
V	0.905	0.781					
SS	0.897	0.593	0.777				
Fr	0.693	0.333	0.798	0.593			
W_{xs}	-0.026	-0.141	-0.068	-0.064	-0.023		
s	0.124	-0.068	0.065	0.135	0.151	0.001	
Q	0.347	0.482	0.298	0.406	0.013	-0.004	0
	SP	D	V	SS	Fr	W_{xs}	s

Figure 5. Correlation matrix based on Pearson’s coefficients for constant discharge and slope (Pearson’s $r = 0$ for Q and s). N= 7200; outliers are included.

It was observed that the highest values for different hydraulic parameters appeared generally close to channel bends, which indicated their influence on river response once discharge and slope were idealized. This influence differs based on the curvature and orientation (*i.e.* concave or convex, Figure 6). Recirculation of flow is observed within and right after bends. Higher values of WSE are observed on the bank at the concave side of a bend. This trend is opposite for V, SP and SS (*i.e.* higher values at convex bend sides).

The trend is very similar for velocity, total stream power and shear stress, with increasing values right after a bend and oftentimes with channel narrowing ($W_{xs} < 0.9$; Figure 7). Tight curvatures show higher increases of these hydraulic parameters than soft bends. However, shear stress seems to be more influenced by sudden narrowing/widening of the channel rather than by bend curvature when both criteria are present.

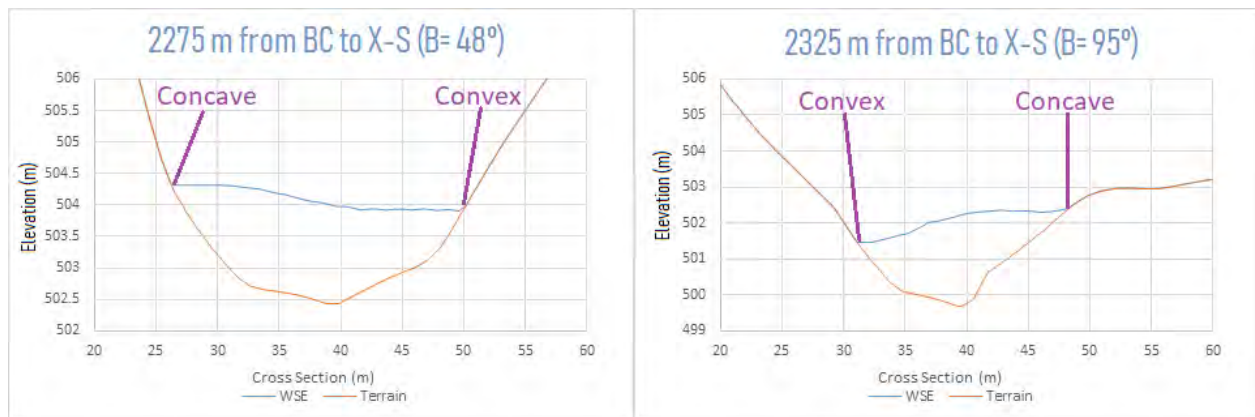


Figure 6. Water surface elevation at two different bend angles, a soft bend curvature on the left-hand side compared to a tight bend curvature on the right-hand side. It is noteworthy that there is an elevation difference between convex and concave sides of the bend; this difference is higher on tighter curvatures.

Setting slope constant allowed evaluating discharge effect in river’s response. River banks showed larger variations than center points (linear multivariate regressions; see Usman, 2019). Slope influence was rather notorious for scenarios with moderate discharges (*i.e.* $Q < 60 \text{ m}^3/\text{s}$). For extraordinary and extreme discharges (Table 2), however, hydraulic parameters seemed to be controlled by the hydrology instead. Steeper scenarios showed the same trend, for instance,

discharge seemed less influencing for $s \geq 0.050$ m/m. The left bank presents, in general, higher values and variability than the right bank and centerline data. It is noteworthy, nevertheless, that the difference in river response decreases and shows a stabilizing tendency with increasing slope. The gradient does not show a significant effect on total stream power in the river center points at any simulated discharge. This effect, however, is evident on the banks for moderate Q . When $Q > 90$ m³/s, shear stress experiences a sudden increase with increasing slope no matter where the observation is done.

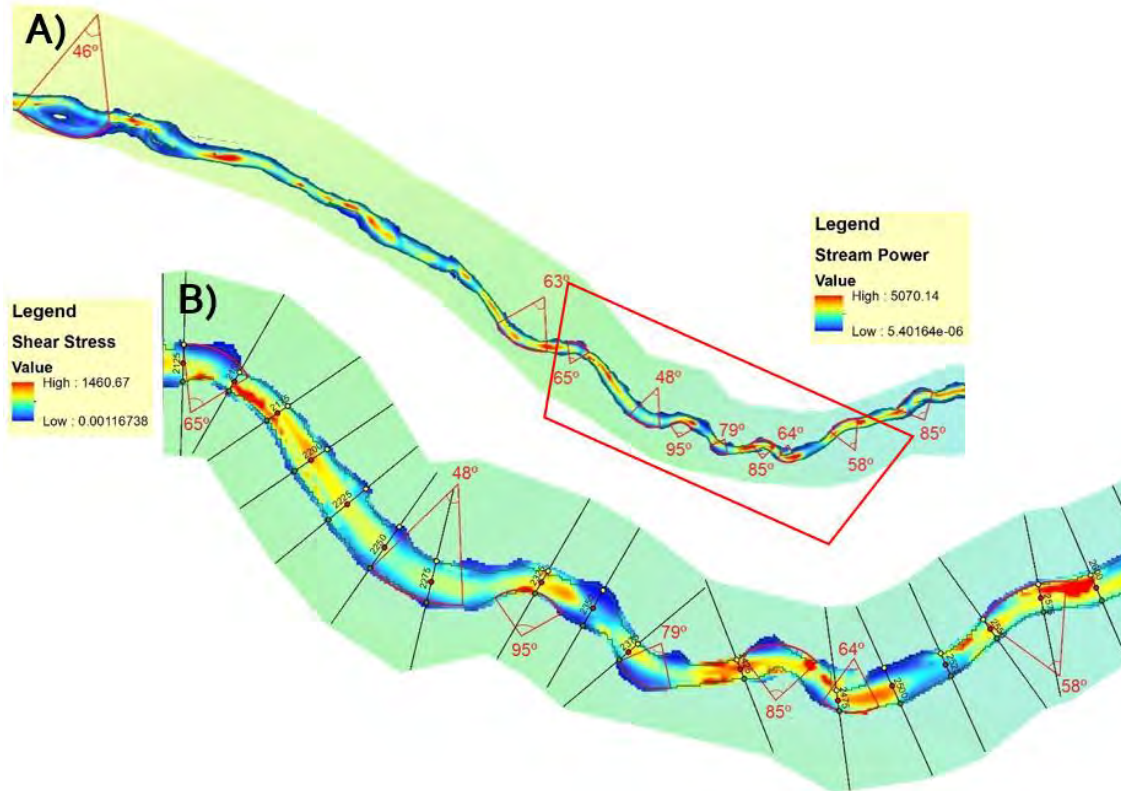


Figure 7. A) total stream power along the modelled reach. B) shear stress in red trapezoidal area marked in A). Results from scenario 23 ($s = 0.055$ m/m and $Q = 90$ m³/s).

4. DISCUSSION

Slope idealization was achieved by means of modifying only the slope in the river bed while keeping the terrain constant outside of it. Simulated slopes went above the mean slope for the selected sub-reach (*i.e.* 4.5%). Discharge idealization was implemented by setting the fluid simulation inflow BC to constant steady flows similar to floods of return period above Q_{200} , as reported by the Norwegian Water Resources and Energy Directorate (NVE) for the selected idealized catchment. Correlation coefficient analysis (Figure 5) shows that, generally, hydraulic forces have a stronger relation with discharge than slope but, exceptionally, Froude number relates more with slope than with discharge, although moderately. This is because Froude number highlights sudden change in water level (*i.e.* hydraulic jumps), which are originated when topography presents step-pool geometries. Shear stress' relation to discharge is stronger than that to total stream power because HEC-RAS approximates SP as a product of SS and V . As velocity's relation to Q is lower than that of SS, SP's value and, consequently, its relation to Q , are diminished.

River banks seemed to be more sensitive to varying conditions than the centre of the channel, especially regarding hydraulic forces. This can be explained by higher roughness at the banks; oftentimes different land uses were set very closely, especially near the tailwaters, where anthropic activity was more extended. The left bank was largely more sensitive to both slope and discharge increase, and further analysis of bend curvature showed that when the concave side of the bend was positioned on the left bank, the curvature was usually tight (*i.e.* approx. 70% of these cases presented $B > 75^\circ$). This side of the bend presented larger WSE and water depth, which are strongly related to Q, V and SS (Figure 5). The tight bends with the concave side oriented to the left bank also presented lower W_{xs} , hence, narrowing and increasing depth after the bend. This results in increasing hydraulic forces after the water flow has gone down the bend.

The terrain idealization method used in this study is tedious and time-consuming when performed manually for long watercourses. This induced to limit the studied reach length to the most interesting 10% sub-reach sections; channel morphology and hydraulics seemed rather interesting where the stream was more sinuous, and the concentration of bends was higher. The original topography presented step-pool geometry and the slope was non-uniform, which results in hydraulic jumps and complex hydrodynamics (Chartrand *et al.*, 2011). When modifying the slope, the original terrain was “flattened” (Figure 3, left), which resulted in elevation difference that needed to be compensated (*i.e.* the new river reach was longer, although the X-S location and points of data extraction was kept constant) either before or after the BCs, by including initial and final X-S that were not part of the 2D modelling. Simulating higher idealized slopes results in higher elevation difference that needs to be compensated by adding an initial (or final) elevation drop, hence, this should be performed in shorter reaches, which will eventually be lengthened when modifying the river bed slope.

5. CONCLUDING REMARKS

A total of 24 idealized scenarios were used to characterize planform variation and hydrodynamics in steep water courses based on the combination of 2D hydrodynamic simulations and GIS tools. The idealization of topography and hydrology permitted analysing their relevance as well as the interdependency of two of the most influencing factors, effect in river’s response and identification of critical locations if flooding occurred. Discharge has a stronger influence in river’s response than slope when $s \leq 4.5\%$ and $Q \geq 60 \text{ m}^3/\text{s}$. For slopes higher than 4.5%, hydraulic forces show poorer relation with discharge than slope gradient’s influence. Bend curvature influenced hydraulic response together with channel narrowing in subsequent cross-sections. The left bank generally presented higher susceptibility to Q and s. When the concave side of the bend was positioned on the left bank, the curvature was usually $B > 75^\circ$. Such bends also presented narrowing channel and increasing depth after the bend. This resulted in increasing hydraulic forces once the flow had gone down the bend. Two-dimensional hydrodynamic simulations of few kilometres-long reaches is computationally intensive, hence, running time can be reduced by increasing the spacing between X-S (*e.g.* initially X-S were spaced every 25 m, and later increased to 50 m, as the aim of the study required general observations rather than local phenomena). Slope was simulated every 0.5% increase, and differences were at time not significant between scenarios. Future work will aim at 1% slope intervals instead. Furthermore, other terrain modification methods will be explored and compared.

ACKNOWLEDGEMENTS

The authors wish to thank Katherine Aurand (SWECO) for fruitful discussion regarding the selected approach. We thank Bartłomiej Wyżga for comments that helped improve the manuscript. We also thank Ana Juárez and Michal Pavlíček for their insightful guidance on hydrodynamic simulations. This publication is part of the World of Wild Waters (WoWW) project, which falls under the umbrella of Norwegian University of Science and Technology (NTNU)'s Digital Transformation initiative.

REFERENCES

- Chartrand, S. M., Jellinek, M., Whiting, P. J., & Stamm, J. (2011). Geometric scaling of step-pools in mountain streams: Observations and implications. *Geomorphology*, 129, 141–151. DOI:10.1016/j.geomorph.2011.01.020
- Furdada, G., Guinau, M., Subiela, G. B., & Moraru, A. (2018). Las cuencas de Portainé y Romadriu: susceptibilidad al cambio y factores de control antrópicos y naturales. In: Garcia, C., Gómez-Pujol, L., Morán-Tejeda, E., Batalla, R. J. (Eds.), *Geomorfología del Antropoceno: efectos del cambio global sobre los procesos geomorfológicos* (pp. 335–338). Palma de Mallorca, Balearic Islands: Universitat de les Illes Balears, Sociedad Española de Geomorfología.
- Kvočka, D., Ahmadian, R., & Falconer, R. A. (2017). Flood inundation modelling of flash floods in steep river basins and catchments. *Water (Switzerland)*, 9(9), 705. DOI: 10.3390/w9090705
- Moraru, A. (2017). *Streambank erosion and channel widening: implications for flood hazard*. MSc Thesis, Universitat de Barcelona – Universitat Autònoma de Barcelona, Barcelona, Spain, 25pp. + Electronic Appendix (Last access: 10 June 2019; available at: <http://hdl.handle.net/2445/115638>).
- Moraru, A., Ruiz-Villanueva, V., & Furdada, G. (2018). Factors controlling streambank erosion and channel widening: implications for flood hazard. In: Garcia, C., Gómez-Pujol, L., Morán-Tejeda, E., Batalla, R. J. (Eds.), *Geomorfología del Antropoceno: efectos del cambio global sobre los procesos geomorfológicos* (pp. 247–252). Palma de Mallorca, Balearic Islands: Universitat de les Illes Balears, Sociedad Española de Geomorfología.
- Moraru, A., Bruland, O., Perkis, A., & Rütter, N. (2019). Materializing natural hazards: is visualizing hydrodynamic fluid simulations relevant to create an immersive experience? In: Skallerud, B. & Andersson, H. I. (Eds.), *10th National Conference on Computational Mechanics - MekIT'19* (pp. 1–19). 3-4 June, Trondheim, Norway: CIMNE (International Center for Numerical Methods in Engineering). *In press*.
- Schumann, G. J., Bates, P. D., Apel, H., & Aronica, G. T. (Eds.) (2018). *Global Flood Hazard: Applications in Modeling, Mapping and Forecasting*. Geophysical Monograph Series, Wiley, 254pp. DOI:10.1002/9781119217886
- Sin, K.-S., Thornton, C. I., Cox, A. L., & Abt, S. R. (2012). *Methodology for Calculating Shear Stress in a Meandering Channel*. Fort Collins, Colorado, USA, Report, 168pp.
- UNISDR (United Nations Office for Disaster Risk Reduction) (2019). *United Nations Office for Disaster Risk Reduction: 2018 annual report*. 107pp. + annex I (24pp.).
- Usman, K. R. (2019). *Safe Rivers – Identification of critical locations along steep watercourses during flood events*. MSc Thesis, Norwegian University of Science and Technology, 119pp. *Unpublished*.

Impacts of wildfire and permafrost thaw on water quality and carbon cycling in peatland-rich catchments in western boreal Canada

David Olefeldt¹, Suzanne Tank², Ryan Hutchins², Katheryn Burd¹, McKenzie Kuhn¹,
Lauren Thompson¹

¹*Department of Renewable Resources, University of Alberta, Edmonton, Alberta, T6G 2G7, CANADA*

²*Department of Biological Sciences, University of Alberta, Edmonton, Alberta, T6G 2G7, CANADA*

**Corresponding author's email address: olefeldt@ualberta.ca*

ABSTRACT

Northern peatlands are widespread in boreal permafrost regions, and are located where the most rapid climate change is observed. Two disturbances that are likely to strongly influence the future water quality in catchments with extensive peatlands are permafrost thaw and wildfire. Both of these disturbances are common and likely increasing in occurrence in the western boreal forest in Canada. These disturbances have the potential to alter the export of dissolved organic matter, nutrients, and contaminants from peatland rich catchments, with implications for landscape carbon cycling, aquatic health, and water quality from a drinking water perspective. Our research in boreal western Canada is carried out along a latitudinal gradient from south of the permafrost boundary to the continuous permafrost zone. Using synoptic studies we have investigated latitudinal trends in chemical characteristics of dissolved organic matter and mercury export, while also choosing sampling sites to reflect differences in fire histories. More detailed work has been done at paired catchments in the discontinuous permafrost zone, where thaw is occurring rapidly. Here we have monitored seasonal changes in solute export from burned and unburned peatland catchments, with focus on nutrient and mercury transport. Within the study catchments, we have studied the peat profiles to assess the potentials for carbon, nutrient, and contaminant mobilization after thaw. Our findings show that not all solute transport is vulnerable to disturbances such as permafrost thaw or wildfire, but also identify settings where vulnerabilities to climate change is great.

KEYWORDS

Arctic environments; Northern research basins; permafrost thaw; wildfire; peatlands; dissolved organic matter;

The Dehcho Collaborative on Permafrost: working with communities to manage permafrost thaw

W. Quinton^{1*}, R. Connon², J. Craig³, K. Haynes¹, and M. Sioui¹

¹*Cold Regions Research Centre, Wilfrid Laurier University, Waterloo, ON, N2L3C5, CANADA*

²*Water Resources Division, Government of Northwest Territories, Yellowknife, NT, X1A2L9, CANADA*

³*Civil and Environmental Engineering, University of Waterloo, Waterloo, ON, N2L3G1, CANADA*

*Corresponding author's email address: wquinton@wlu.ca

ABSTRACT

Climate warming and human disturbance in the Dehcho region of the Northwest Territories (NWT), Canada, has led to widespread permafrost thaw and land cover change that has disrupted the hydrological cycle and the ecosystems and human activities that depend on it. There is a growing awareness in the Dehcho that permafrost thaw is negatively affecting the region's economy, and the health, well-being and livelihoods of its residents. However, there is lack of information on permafrost distribution, evolution, and resultant landscape change trajectory in this region. As a result, the ability to manage and respond to this new and growing threat to the Dehcho is extremely limited. There is therefore an urgent need to develop and mobilise knowledge on permafrost thaw in the Dehcho and elsewhere in the subarctic, develop new, practical and customised predictive tools and strategies to adapt to permafrost thaw, and to provide interactive training to decision makers and other users. In direct response to this need, the Scotty Creek Research Station (SCRS) and the Dehcho First Nations (DFN), co-propose the Dehcho Collaborative on Permafrost (DCoP), a Dehcho-wide initiative whose overall objective is to generate a fusion of leading-edge scientific and Indigenous knowledge on permafrost, and to use it as a basis to co-develop new predictive decision support tools and innovative risk management strategies to inventory and manage permafrost and adapt to permafrost thaw.

KEYWORDS

Permafrost thaw; water resources; community engagement; collaborative; Dehcho

1. INTRODUCTION

In the Northwest Territories (NWT), Canada, it is widely recognised by all levels of government that the success of management plans and policies intended to guide the long-term stewardship of resources (e.g. *NWT Water Stewardship Strategy: Northern Voices, Northern Waters*) depends on a resource of trained-in-the-north expertise. It is also widely recognised that developing and maintaining such an expertise requires long-term engagement and collaboration with Indigenous communities in all aspects of knowledge development and application (Frantz and Howitt, 2012). This emphasis on sustained engagement is a departure from the previous norm that focussed instead on irregular “events”, and is an underlying theme of the NWT’s new Knowledge Agenda document. It also aligns with the vision of international environmental organisations and initiatives in regards to sustainable development (UNSDG, UNESCO), sustainable land use (IUCN), and Indigenous rights to manage resources (UNDRIP). In recent years, the emphasis on Indigenous community engagement has grown and is now a central theme guiding the activities of researchers and research programmes. This is the case in the Dehcho region of the NWT where researchers and communities

recently initiated a collaboration focussed on responding to the growing challenge of widespread permafrost thaw. This paper describes this collaborative as an example of Indigenous community engagement and leadership in research.

The ~150,000 km² Dehcho region in the southern NWT is one of the most rapidly warming on Earth (Vincent et al., 2015). It is also experiencing an increase in direct human disturbance due to expanding industrial activity. Permafrost thaw in the Dehcho is widespread and occurring at unprecedented rates, evidence that this region is particularly sensitive to climate warming and disturbance due to thaw. Permafrost thaw is transforming the Dehcho's land (Chasmer and C Hopkinson, 2016; Helbig et al., 2016), changing the distribution and routing of its water (St. Jacques and Sauchyn, 2009; Connon et al., 2014) and damaging its roads, air strips, ferry crossings, pipelines, buildings and other key infrastructure (GNWT, 2018). Permafrost thaw is one of the most dramatic manifestations of climate warming. However, how it will transform the Dehcho's land and water resources over the coming decades, and what can be done about it, is unclear. Given that permafrost is the foundation of much of the Dehcho's land cover, and that it exerts a primary control on surface and subsurface hydrological processes, its thinning and disappearance has profound implications to both land-cover stability and the water cycle from local to regional scales. Although it is widely acknowledged that permafrost thaw is disrupting the Dehcho's land, water and therefore human activities, the patterns, rates, controls and mechanisms of permafrost thaw, and associated feedbacks and land cover transformations across the region remain poorly understood. As a result, there is an urgent need to investigate thaw-induced changes to the Dehcho's land and water, develop and mobilise knowledge on these changes, develop predictive modelling tools, and provide interactive training to decision makers and other stakeholders. Although there is a growing awareness throughout the Dehcho that permafrost thaw is negatively affecting the region, regulatory authorities, resource management boards, and communities are ill-equipped to respond effectively to this new and growing challenge because there exists little or no permafrost thaw monitoring, adaptation or predictive capacity in the region, and therefore no appropriate basis for decision support.

2. DEVELOPEMNT OF A NEW COLLABORATIVE

In direct response to the serious shortcoming described above, the Dehcho First Nations (DFN) and the Scotty Creek Research Station (SCRS) co-proposed the Dehcho Collaborative on Permafrost (*DCoP*) to improve the understanding of and ability to predict and adapt to permafrost thaw. Because livelihoods in the Dehcho are so tightly connected to “the land”, *DCoP*'s close collaborative approach that places Indigenous communities in leadership positions, is required to generate the new knowledge, predictive capacity and decision-support tools needed to manage the land and water resources that support Dene ways of life (Louis, 2007; McGregor, 2004).

Close consultations with Indigenous communities throughout the Dehcho, identified the urgent need for sustained community engagement based on two-way knowledge exchange to guide specific needs for improved permafrost thaw monitoring, adaptation, process understanding, and prediction. These needs collectively formed *DCoP*'s “five themes”, each with specific objectives. *DCoP* researchers and community members are also co-developing a number of knowledge-based (*i.e.* founded upon scientific and/or Indigenous knowledge) resources for permafrost adaption, including novel and affordable devices for monitoring permafrost and inhibiting ground thaw, new probabilistic methods for determining permafrost presence and thaw susceptibility, knowledge-based evaluation of adaptation strategies, and new means of determining future permafrost

conditions and resultant land cover and hydrological changes. Other resources will be accessible from a web portal, including real-time data, data archives from the *DCoP* research and monitoring sites, remote sensing data layers and synthesis products including interactive maps of permafrost distribution, thaw susceptibility, and permafrost thaw-induced land-cover changes. The latest hydrological modelling output demonstrating rates and patterns of permafrost thaw, land-cover change and hydrograph response for different scenarios of warming will also be accessible through the data portal. These knowledge-based tools and devices, collectively referred to as *DCoP*'s "Permafrost Resources", will be integrated into all *DCoP* themes, and will be continually updated and improved as *DCoP* evolves. *DCoP* will draw upon these resources to inform the development / improvement of knowledge-based adaptation and decision support tools and strategies which can be extended throughout much of the circum-polar subarctic region.

3. CO-DEVELOPED THEMES AND OBJECTIVES

Close consultation with Indigenous communities throughout the Dehcho identified six broad research questions:

Q1: Where is permafrost located within the Dehcho and where is it thawing?

Q2: What is the rate and pattern of permafrost thaw?

Q3: How is permafrost thaw changing land?

Q4: What adaptation and mitigation measures can or should be taken?

Q5: How is permafrost thaw changing the flow and storage of water on the land?

Q6: What is the long-term trajectory of thaw-induced change to the land and water?

It was clearly evident from these consultations that the concerns over permafrost thaw and its effect on the land, water and livelihoods are shared throughout the Dehcho. Consultation also provided clear guidance to *DCoP* through specific recommendations for improved community engagement focussed on two-way knowledge exchange between scientists and Indigenous communities so that permafrost thaw can be better monitored, adapted to, understood and predicted. From this guidance, *DCoP* has placed community engagement at the centre of all of its activities. For each theme, the *DCoP* project objectives (O) are stated below. The research question(s) addressed by each objective are given in brackets.

Theme 1: Co-develop with Indigenous communities, new initiatives for improving the monitoring (Theme 2), adaptation (Theme 3), understanding (Theme 4), and prediction (Theme 5) of permafrost thaw and its impacts in the Dehcho. O1: Gather and synthesise the Indigenous Knowledge pertaining to permafrost and permafrost thaw in the Dehcho, and compile this information into the Permafrost Resources. O2: Gather and synthesise all new knowledge arising from Themes 2-5, and add it to the Permafrost Resources. O3: Mobilise throughout the Dehcho the Permafrost Resources assembled in O1 and O2 through the community engagement in support of themes 2-5.

Theme 2: Monitoring. O4: *DCoP* will produce permafrost probability maps as a first step toward defining the current distribution of permafrost in the Dehcho, and establish an Indigenous community-led network to monitor changes to permafrost (Q1, Q2, Q3) using both conventional temperature-based and new (*DCoP*-developed) ice-content monitoring probes. O5: *DCoP* will use

2018 imagery to map the current spatial distribution of permafrost, and archived photos (1970) to assess the change in permafrost distribution over the intervening 48 year period (Q2, Q3).

Theme 3: Adaptation. O6: DCoP will develop and test new knowledge-based permafrost thaw adaptation strategies designed to lessen the impacts of such thaw, improve safety on the land and in communities, and safeguard infrastructure (Q4).

Theme 4: Process Understanding. O7: Develop new knowledge on the permafrost thaw processes, rates and patterns causing the changes observed in Theme 2 with a focus on critical (and understudied) lateral thaw of discontinuous permafrost (Q5).

Theme 5: Prediction. O8: Share, apply and interpret new methods for predicting the rate, pattern and impact of permafrost thaw customised for specific conditions within the Dehcho (Q6).

4. IMPLEMENTATION

Since 1999, the SCRS (www.scottycreek.com) has served the Dehcho as an “outdoor laboratory” for the observation and study of warming-induced change for a land cover type that dominates much of the Dehcho. The SCRS is now in the process of transforming into a regional Research Park for the Dehcho, a state-of-the-art, inter-disciplinary scientific observatory and centre of community engagement for researchers and community members to come together as “partners in learning” to exchange experiences and ideas, to co-develop new knowledge, and to nurture the next generation of collaborations between western scientists and Indigenous knowledge holders. Co-development of new knowledge is empowering to communities and solidifies researcher-community collaborations (Frantz and Howitt, 2012.). DCoP will deepen the existing relationship between the SCRS and the First Nations of the Dehcho region, and thereby increase the likelihood of new knowledge leading to effective community uptake and response (Coombes et al., 2014; Shaw et al., 2006).

The new knowledge arising from DCoP on permafrost thaw rates, controls, patterns, processes and impacts will be used to co-develop knowledge-based, community-informed strategies for permafrost thaw monitoring, adaptation, process understanding, and prediction. This will include new baseline monitoring and decision support tools for permafrost management, and for permafrost thaw response and prevention strategies, leading to prudent investment and knowledge-based community adaptation. Data from the SCRS will be available to Dehcho communities in real time, and DCoP will compile and synthesise existing and new datasets into high-quality data archives and GIS spatial data layers which will be housed and managed by the DFN on behalf of all Dehcho communities. Making the SCRS a place for researcher-community collaboration, brings community decision makers closer into the process of generating new knowledge and knowledge-based predictive tools, and provides them with a deeper understanding of their meaning, application and limitations. This will increase the likelihood that management and policy decisions will be well-informed so that they can be more confidently applied, reducing the level of uncertainty and risk. As such, transforming the SCRS into a regional Research Park is an investment in the Dehcho’s knowledge economy.

Although the SCRS will play a central role in the engagement, educational and research aspects of DCoP, other sites in the Dehcho will also be used for DCoP field activities. This will include 1) 100 sites for calibration and validation of probabilistic permafrost mapping, 2) a subset of 40 (of the 100) biophysically-representative permafrost monitoring sites, 3) a subset of 10 (of the 40)

monitoring sites for application and evaluation of permafrost thaw adaptation strategies, 4) 12 remote sensing areas of interest (each “AOI” is 36 km²) located along a 200 km transect extending southward from Scotty Creek through the NWT's southern fringe of discontinuous permafrost, 5) 3 study basins along the 200 km transect, and 6) 10 permafrost slope failure locations along the Mackenzie River.

5. MILESTONES

The researchers and community members within *DCoP* identified and described specific milestones to accomplish over the next 3 to 5 years. These are summarised below.

5.1 New Regional Research Park

Over the next 3 years, the SCRS will transform into a regional “Research Park” for the Dehcho, a state-of-the-art, inter-disciplinary scientific observatory and centre of community engagement for researchers and community members to come together as “partners in learning” to exchange experiences and ideas, to co-develop new knowledge, and to nurture the next generation of collaborations between scientists and Indigenous knowledge holders. A regional research park led by an Indigenous community will be the first of its kind in Canada and novel throughout the circumpolar region, and will be a flagship for scientific-Indigenous collaboration in Canada’s North.

5.2 Coordinated permafrost monitoring

DCoP will monitor permafrost at a) extensive sites covering the range of major land-covers throughout the Dehcho, including a subset of sites for testing of adaptation methodologies, b) a north-to-south transect extending over the southern margin of thawing discontinuous permafrost along which will be the AOIs for examination of rates and patterns of permafrost thaw-induced land cover change, and c) intensive study basins located along the transect for examination of thaw processes and their impacts on water. Monitoring will be supported by novel frost-probe technology developed by DCoP for over-winter monitoring of ice content.

5.3 New High-Quality Data Sets

High quality datasets are the foundation for all policy and management decisions as noted in the “Knowledge Agenda” (2018) of the GNWT. DCoP’s monitoring network will generate new and unique data sets, which will include the historical data of the three study basins, including the extensive archives (1999-present) of the SCRS, and aerial and satellite remotely sensed data, including extensive and high-quality data sets from the NASA/ABOVE programme. DCoP is well connected to ABOVE data resources as the DCoP PI is a member of the NASA/ABOVE Science Team (<https://above.nasa.gov/>), and Scotty Creek and the 200 km transect are designated as “Super Sites” by NASA/ABOVE. DCoP will manage, process and archive the new high quality datasets according to ArcticNet protocols, and will assist the DFN in developing its regional data portal so that community members have access to all DCoP archives. Novel permafrost probability and thaw susceptibility mapping techniques will be developed, tested, validated against field data, and deployed across the Dehcho region. These techniques will also apply to the wetland-dominated areas of discontinuous permafrost that dominate much of subarctic.

5.4 New Adaptation Strategies

DCoP researchers and community members will co-develop, co-assess, and co-implement new knowledge-based, strategies for management of permafrost, and for prediction and adaptation to permafrost thaw. The new strategies will be supported by permafrost monitoring (Theme 2), process field studies (Theme 4) and new predictive tools (Theme 5) as called for by the Pan-Territorial Climate Change Adaptation Strategy (e.g. pp. 22, 25). New strategies will include both changes to land-use practises to minimise negative impacts, and the application of new methods and technologies to reduce or offset permafrost thaw and/or its impacts.

5.5 New Predictive Tools and Capacity

The GNWT's Knowledge Agenda, Climate Change Adaptation Framework, Water Strategy Action Plan, and trans-boundary water agreements each explicitly call for "new decision support tools". In direct response, DCoP will share, apply, interpret and provide training on new methods developed in Theme 5 for predicting the rate and pattern of permafrost thaw for permafrost conditions unique to the Dehcho. On-going interactive training, incorporation of feedback from communities, and model application in support of end-user decision making ensures that DCoP places into the hands of Indigenous communities, customised knowledge-based predictive tools designed to meet their specialised decision needs so that environmental and resource management strategies can be confidently applied. Improved predictive capacity will become increasingly important in the Dehcho as resource development increases.

6. LEGACY

Unprecedented climate warming has compelled the Government of the Northwest Territories (GNWT) and regulatory authorities to take action, although management and policy decisions often have to be made without sufficient information. DCoP will directly address this urgent need for new knowledge, and will leave a legacy of benefits for residents of the Dehcho, the NWT and for all Canadians including new high-quality public datasets; practical predictive tools; and new knowledge to guide management, adaptation and policy. A significant catalyst for DCoP is the Partnership Agreement between Wilfrid Laurier University (hereafter "Laurier") and the GNWT (<http://nwtwlu.com>) which aims to expand the NWT's capacity for environmental monitoring and research, and which has allowed Laurier's researchers to cultivate strong connections to NWT policy-makers. DCoP also helps to ensure that future policy development is knowledge-based through its training initiatives in which trainees not only gain skills, but direct linkages to decision makers. DCoP will also leave a lasting legacy of research infrastructure, world-class data sets, and well-informed, community-led decision making. These benefits will improve the assessment of scenario outcomes and reduce uncertainties and risk in land and water resource planning / co-management. This is a highly relevant return on investment considering that climate warming is the most significant challenge to northern Canada's economic and environmental security. Finally, DCoP will set a new precedent for collaboration between scientific and Indigenous communities focussed on the challenges arising from rapid permafrost thaw. As such, it will therefore lead by example and provide a lasting legacy and example of scientific-Indigenous collaboration.

REFERENCES

- Chasmer, L, and C Hopkinson, 2016. Threshold loss of discontinuous permafrost and landscape evolution, *Glob. Change Biol.*, 1-15.
- Connon, R.F., W.L. Quinton, J.R. Craig, and M. Hayashi, 2014. Changing hydrologic connectivity due to permafrost thaw in the lower Liard River valley, NWT, Canada, *Hydrol. Process.*, 28, 4163-4178.
- Coombes, B, JT Johnson, R Howitt, 2014. Indigenous geographies III: Methodological innovation and the unsettling of participatory research. *Progress in Human Geography*, Vol. 38(6) 845–854. DOI: 10.1177/0309132513514723.
- Frantz, K and R Howitt, 2012. Geography for and with indigenous peoples: indigenous geographies as challenge and invitation. *GeoJournal*, 77:727–731. DOI: 10.1007/s10708-010-9378-2.
- Government of the Northwest Territories (GNWT), 2018. Northern Voices, Northern Waters: NWT Water Stewardship Strategy, Government of the Northwest Territories, Yellowknife, NT, 54 pp.
- Helbig, M, LE Chasmer, N Kljun, WL Quinton, CC Treat, and O Sonnentag, 2016. The positive net radiative greenhouse gas forcing of increasing methane emissions from a thawing boreal forest-wetland landscape, *Glob. Change Biol.*, 1-15.
- Louis, RP, 2007. Can You Hear us Now? Voices from the Margin: Using Indigenous Methodologies in Geographic Research. *Geographical Research*, 45(2):130–139. DOI: 10.1111/j.1745-5871.2007.00443.x
- McGregor, D, 2004. Coming Full Circle: Indigenous Knowledge, Environment, and Our Future. *The American Indian Quarterly*, Volume 28, Number 3&4, Summer/Fall, pp. 385-410. DOI: 10.1353/aiq.2004.0101.
- Shaw, WS, RDK Herman, and GR Dobbs, 2006. Encountering Indigeneity: Re-imagining and Decolonizing geography. *Geogr. Ann.*, 88 B (3): 267–276.
- St. Jacques, JM, and DJ Sauchyn, 2009. Increasing winter baseflow and mean annual streamflow from possible permafrost thawing in the Northwest Territories, Canada, *Geophys. Res. Lett.*, 36, L01401.
- Vincent, L, X Zhang, R Brown, Y Feng, E Mekis, E Milewska, H Wan, and X Wang, 2015. Observed trends in Canada's climate and influence of low-frequency variability modes, *J. Climate*, 28, 4545-4560.

Spatial and temporal trends in end-of-winter snow cover properties north and south of treeline in a large sub-Arctic river basin

Derek Tokarski¹, Murray Richardson^{1*} and Shawne Kokelj²

¹*Department of Geography and Environmental Studies, Carleton University, Ottawa, Ontario, K1S 5B6, CANADA*

²*Environment and Natural Resources, Government of the Northwest Territories, Yellowknife, Northwest Territories, X1A 2L9, Canada*

**Corresponding author's email address: murray.richardson@carleton.ca*

ABSTRACT

Historical snow surveys conducted at 11 sites across the ~13,700 km² sub-Arctic, Snare River basin near Yellowknife, NWT, were analyzed to characterize snow regimes in the southern forested vs northern tundra regions of the basin and to identify spatial and temporal trends in snow cover properties at local and regional scales. Tundra snow cover was typically shallower but significantly denser than snow cover in the southern forested region, resulting in higher SWE in the areas north of treeline. The snowpack properties also exhibited significantly higher variability in the tundra region compared to the forested areas of the basin, at local and regional scales. Over the full historical record (1978-2018), no significant temporal trends in snow cover properties were detected at any scale. Over the more recent timeframe of 1995-2018, statistically significant trends in SWE, snow depth, and snow density were detected at local and regional scales. Snow density is declining strongly and significantly in the south, with corresponding declines in SWE despite no changes in snow depth. In the northern region, snow density is also in decline whereas snow depth is apparently increasing, with no detectable trends in SWE. The relative contributions of depth and density to the spatial variability of SWE in the north are trending towards the conditions found in the south. The observed changes in snow cover are consistent with the expected impacts of regional warming and ecosystem change in subarctic landscapes, including a shorter snow accumulation season and increasing vegetation biomass.

KEYWORDS

SWE; snow density; snow depth; snow surveys; temporal; spatial; variability; hydrology; forest; tundra; climate change

1. INTRODUCTION

An understanding of the spatial and temporal distribution of snow water equivalent (SWE) is important for a wide variety of practical and environmental research reasons. In northern watersheds, where snow represents a significant percentage of annual precipitation, an estimate of the total SWE before the spring melt begins is a critical input for hydrologic models used for short- to medium-term water supply. SWE at a point is estimated from the product of snow depth and snow bulk density, both of which vary spatially across a landscape and temporally over the course of a year. The variation is due to a wide variety of factors including initial differences in deposition, landscape features, redistribution after deposition, and different rates and types of metamorphism on the ground (Goodison 1981). Despite its importance, SWE remains difficult to measure over

large areas (McCreight, *et al.* 2014) and up-scaling point measurements of SWE to the basin-scale remains a fundamental problem in snow hydrology (Blöschl 1999, Steppuhn 1976). As a result, there is considerable interest in understanding statistical properties of snow cover properties to help optimize sampling strategies (Blöschl 1999, Watson, *et al.* 2006).

As arctic regions transition towards a rain dominated environment with shorter snow accumulation seasons (Bintanja and Andry 2017) and increasing vegetation biomass (Myers-Smith, *et al.* 2011), statistical properties of snow cover are also changing rapidly and non-uniformly (Bokhorst, *et al.* 2016), and/or may be used themselves as an indicator of climate change impacts in northern river basins. Arctic surface air temperatures have risen by a factor of close to 2 times the global mean (Serreze and Barry 2011). Wider-spread declines in northern snow cover extent and/or SWE associated with climate change have also been reported (Serreze and Barry 2011, Sturm, *et al.* 2017) and quantification of temporal trends in snow cover using available records is important for northern water managers and communities that rely on finite water supplies for municipal water or hydropower production. It is therefore opportunistic to use available datasets, wherever possible, to simultaneously characterize spatial and temporal trends in snow-cover over large northern regions, particularly in the context of operational hydrology where such information may guide short and long-term planning for resource deployment and infrastructure development.

Accordingly, this study focuses on the analysis of historical snow survey data that has been collected since 1978 by the Northwest Territories Power Company (NTPC) for operational monitoring purposes. The availability of this long-term dataset presents the opportunity to examine spatial and temporal trends in snow cover properties along a physiographic and climatic gradient. The specific objectives of this study were to; (1) statistically analyze snow survey observations taken across the Snare River basin to identify local and regional-scale differences in snow cover properties found north and south of treeline, and; (2) analyze and describe the temporal variability and trends in snow cover properties at the basin, region, and site scale. For these analyses, we employed a multi-scale, multi-temporal approach to empirically characterize fundamental differences in snow regimes of forested *vs* tundra regions of this large sub-Arctic basin, including long-term trends in snow depth, density or SWE, north and/or south of treeline.

2. METHODS

2.1 Study Site

The Snare basin is located within the North Slave region of the NWT and is part of the larger Mackenzie River basin. The area's primary terrestrial zone is the Taiga Shield which is characterized by shallow, coarse soils as well as numerous lakes and streams. Vegetation is sparse, open forest and open shrub tundra. Mean annual daily temperature in Yellowknife is -4.3 °C and mean annual precipitation is 289 mm. A large proportion of the annual precipitation is stored as snow resulting in spring melt being the most significant hydrologic event of the year (subarctic nival regime). The basin can be broadly categorized into two regions, northeast and southwest of treeline, hereafter simplified to "north" and "south" of treeline for brevity. The treeline is not a distinct boundary but an ecotone running along the northwest to the southeast axis. The area of the basin is approximately 13,700 km² with roughly 52% north of treeline and 48% to the south. It lies within the remote traditional territory of the Tłı̨chǫ First Nation and travel for operational snow surveys, often conducted in early April, is only feasible by helicopter or ski plane.

2.2 Snow Survey Data

NTPC began conducting snow surveys in 1978 at eight sites. Three additional sites (Big, Christison, Whitewolf) were added in 1995. All eleven sites, with minor exceptions, were surveyed from 1995 to 2017. Of the eleven sites, six are located south of treeline and five to the north. The three sites added in 1995 are all located north of treeline. Previous to that year the survey was heavily biased towards the southern region. Ten of the NTPC sites were visited by Twin Otter over the course of a typical survey day. The use of a ski-plane necessitates the sites being near relatively large lakes. At each site the surveyors walk off the lake into the uplands and take 10 SWE measurements along a looped transect that varies in length from 130 m to 275 m. Measurements were taken using an ESC-30 snow tube. At each location where a SWE measurement was taken the snow depth was also recorded. Snow density was calculated from the recorded SWE and depth. Complete records of those mean SWE observations were available for 354 observations yielding 3540 individual SWE measurements.

2.3 Analysis

The historical snow survey dataset was analyzed at the site, region, and basin scales. Mean and coefficient of variation (C_v) values were calculated for each site and region between both 1978 - 2017 and 1995 - 2017. The addition of three new northern sites in 1995 makes the period 1995 – 2017 more suitable for comparing the regions. Stratification by landscape was at the regional scale (north and south of treeline) only. The coefficient of determination (R^2) between SWE and depth were calculated for each site over the historical record. Correlation matrices between site-scale means over the complete historical record for SWE, depth, and density were produced. Paired, one sample t-tests (Welch's) were performed between the two regions for snow depth, snow density, and SWE data to determine if regional differences were significant. Linear trend analysis was conducted on the mean depth, density, and SWE values at the site, region, and basin scales. Linear trend analysis was also conducted on the annual R^2 value between SWE and depth for each site and for each region, to determine any long-term changes in the relative variability of depth and density, which would manifest as a change in the SWE vs depth relation. These analyses were conducted for the two time-frames mentioned above.

3. RESULTS

3.1 Spatial Patterns

Over the entire historical record, the mean SWE in the northern half of the basin was 18% higher than in the southern half (Table 1). Higher SWE in the north was associated with 25% higher snow density in that region, whereas snow depth tended to be lower than the south by an average of 8% (Table 1). These patterns were consistent from year to year and the differences were found to be statistically significant in all years based on paired, one-tailed t-tests ($p < 0.0001$). Mean SWE values for individual sites in the southern region ranged from 9.5 cm to 11.2 cm, and northern sites fell within the range of 11.4 cm to 13.4 cm, with the exception of the Winter lake site (7.7 cm). Similarly, snow depth in each region fell into two separate but close ranges (South: 51.4 cm – 58.5; North: 44.5 cm – 51.4 cm), again with the exception of the Winter lake site (35 cm).

The spatial variability of all three snow cover properties was greater in the northern region, as indicated by the coefficient of variations (C_v) (Table 1). This large difference in C_v of SWE was most attributable to high spatial variability of snow depth in the northern region: 0.55 vs 0.22 in

the south, a difference of 155%. Comparatively, the C_v of density for northern sites was only 13% greater than the southern sites (30% without the Big Spruce site). The C_v of density at the Big Spruce site had a value greater than at any other site in the north or south. Without the Big Spruce Lake site, the C_v of density in each region fell into two narrow, non-overlapping ranges (South: 0.18 – 0.21; North: 0.23 - 0.28). In the south, C_v of density was approximately equal to C_v of depth, whereas in the north, C_v of density was less than half the C_v of depth.

Table 1: Statistical summary of bulk snow property observations by site. R^2 is the coefficient of determination for the relationship between snow depth and SWE.

Site	R^2	SWE (cm)		Depth (cm)		Density (kg m^{-3})		
		Mean	C_v	Mean	C_v	Mean	C_v	
South	Big Spruce	0.33	10.3	0.28	51.8	0.28	0.21	0.36
	Ghost	0.52	10.3	0.28	52.6	0.22	0.2	0.21
	Mattberry	0.51	9.5	0.29	51.4	0.23	0.19	0.21
	Snare	0.50	11.0	0.26	53.5	0.19	0.21	0.20
	Indin	0.58	10.8	0.29	58.5	0.21	0.18	0.20
	Castor	0.61	11.2	0.27	57.4	0.2	0.2	0.18
	Mean	0.51	10.49	0.28	54.19	0.22	0.20	0.23
North	Winter	0.89	7.7	0.77	35.0	0.6	0.21	0.27
	Christison	0.88	11.4	0.73	44.5	0.52	0.24	0.27
	Big	0.92	12.2	0.86	44.5	0.71	0.26	0.28
	Mesa	0.88	12.5	0.67	51.4	0.51	0.23	0.25
	Whitewolf	0.87	13.4	0.65	48.7	0.49	0.27	0.23
	Mean	0.89	12.37	0.73	47.29	0.56	0.25	0.26
% Difference (North vs South)		75%	18%	160%	-8%	155%	25%	13%

The R^2 of the relation between SWE vs depth was calculated for individual sites and by region (Table 1). Over the entire historical records, there was a significant difference in the annual R^2 for SWE vs depth between the regions based on a two-sample different of means test ($p < 0.001$). Among the northern sites, the R^2 was high and varied across a narrow range from 0.87 to 0.92, while R^2 values for southern sites were lower and varied through a wider range of 0.33 to 0.61. The Big Spruce site was again a potential outlier, in this case manifesting as the site with categorically lower R^2 (0.33) than any of the others. With Big Spruce removed, the mean R^2 in the north was 66% greater than in the south.

Spatial variability of snow cover at the regional scale was assessed by comparing inter-site correlations (year to year) over the historical record. These correlations are shown for SWE and depth in the form of a correlation matrix, for the period 1978-2018 (Figure 1). Overall, SWE at southern sites (shown with the solid black line) were highly correlated with one another (mean $r = 0.83$) (Figure 1a). Correlations in SWE among the northern sites were much lower (mean $r = 0.36$)

(Figure 1a). Correlations in snow depth showed a very similar pattern to snow density between regions (Figure 1b). The mean correlation of snow density among southern sites was 0.58 and among northern sites it was 0.59.

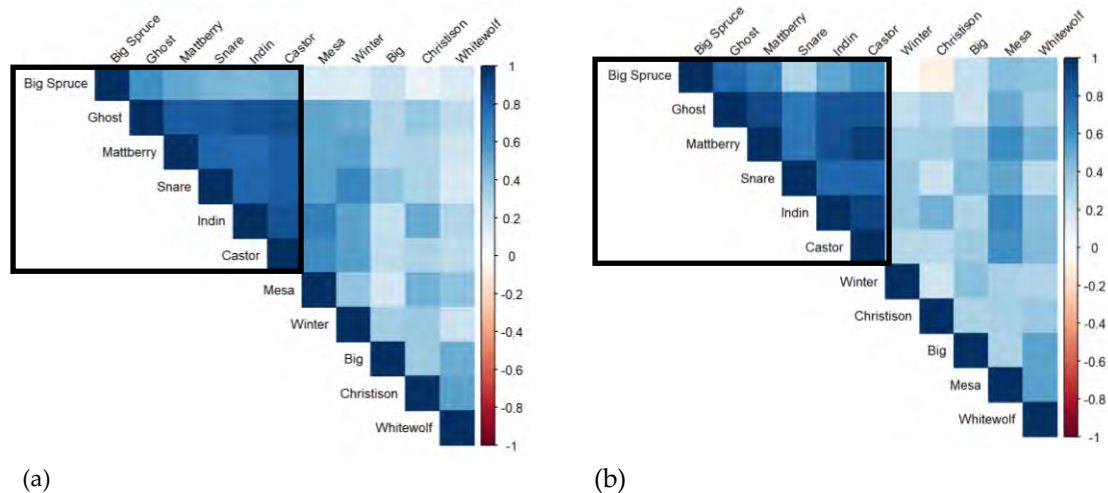


Figure 1. Correlation matrices of mean SWE (a) and depth (b) among snow survey sites for the period 1978-2018. Solid black box highlights correlations among the southern sites only. Density results are not shown since there was no distinct geographic difference.

3.2 Temporal Trends

There was no significant increase or decrease in basin-wide SWE, depth or density over the full historical record. Stratifying the trend analysis by region, only snow density was found to be decreasing among the southern sites (weakly significant, $p < 0.1$). These trend analyses were repeated using the timeframe 1995 – 2018 which coincides with the period when a more balanced snow survey design was used. Figure 2 shows the time series of annual mean SWE, snow depth, and snow density for the period 1995 – 2018, stratified by region. Of the six trend lines shown, five are weakly significant ($p < 0.1$), with the exception of SWE north of treeline (Figure 2 caption). Two of the regional trends were found to be significant at the 95% confidence level or higher. Specifically, SWE and density in the southern region were identified to be decreasing at a rate of 0.13 cm yr^{-1} ($p < 0.05$) and $-0.0028 \text{ kg m}^{-3} \text{ yr}^{-1}$ ($p < 0.001$), respectively.

Trend analyses were also conducted for each individual site, north and south of treeline. Table 2 summarizes these results and illustrates that in many cases, local-scale temporal trends are more pronounced (i.e. more significant) compared to weakly the mostly significant ($p < 0.1$) trends detected at the regional scale, since some sites with non-significant trends reduce the trend effect size when pooled by region. For example, three of six sites in the southern basin exhibited statistically significant declines in SWE ($p < 0.05$), and a fourth site showed a weakly significant decline ($p < 0.1$).

Figure 3 illustrates statistical non-stationarity in the strength of the relation between snow depth and SWE in the northern half of the basin, including increasing interannual variability and

decreasing goodness of fit. The R^2 of the southern sites varies through a much greater range than in the northern sites. The overall mean is 0.55 for the southern sites and 0.90 for the northern sites.

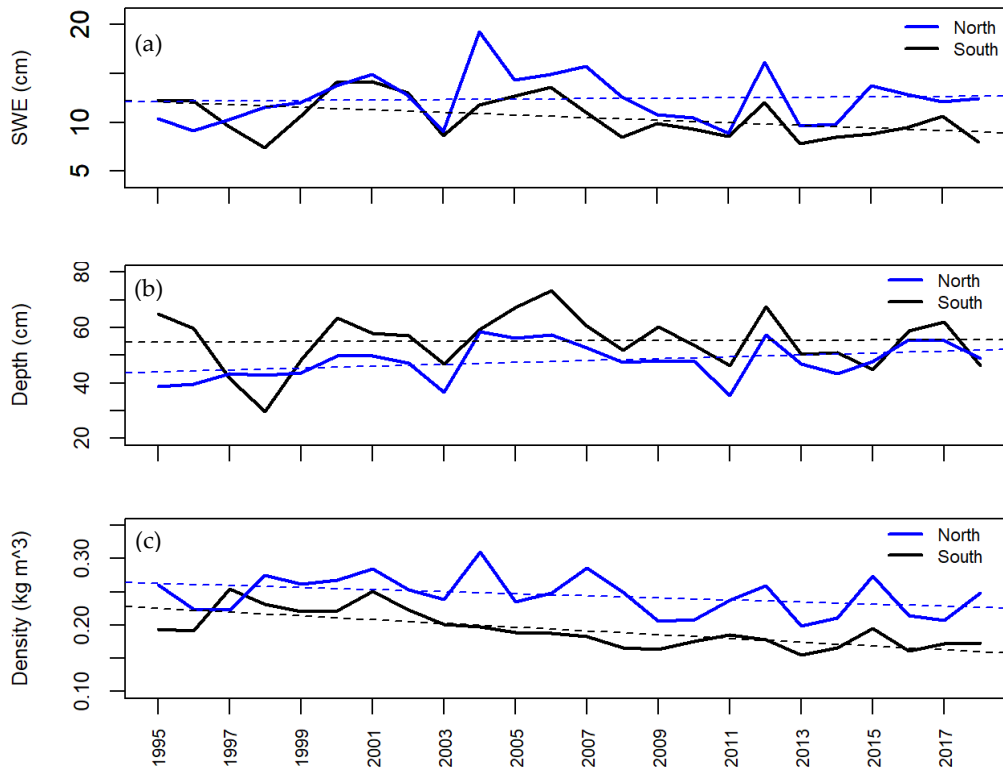


Figure 2. Linear trend analysis of SWE, snow depth, and snow density broken down by region (north and south of treeline) for the period of 1995-2018. At significance threshold of $p < 0.1$ the following trendlines above were significant: South SWE: $p=0.08$, slope= -0.13 cm yr^{-1} ; South depth: $p=0.09$, slope = 0.03 cm yr^{-1} ; North depth: $p=0.07$, slope = 0.35 cm yr^{-1} ; South density: $p < 0.001$, $-0.0028 \text{ kg m}^{-3} \text{ yr}^{-1}$; North density: $p=0.07$, $-0.0015 \text{ kg m}^{-3} \text{ yr}^{-1}$.

4. DISCUSSION

4.1 Spatial Patterns

Higher SWE in the northern half of the Snare basin may be attributable to a longer accumulation season and/or reduced canopy interception and sublimation associated with lack of tree cover. Many studies have compared the accumulation of snow in adjacent open and forested areas. In forested landscapes a large portion of falling snow (up to 60%) is intercepted by the trees and then a portion of that (up to 40% of original snow fall) sublimates back to the atmosphere rather than unloading to the ground (Pomeroy, *et al.* 2002). Rees, *et al.* (2007) reported a mean density of 0.293 g cm^{-3} at Daring Lake, a site located at a similar latitude to the northern part of the Snare basin but further north of treeline. Sturm, *et al.* (2010) report average densities of 0.28 g cm^{-3} and

0.21 g cm⁻³ for Tundra and Taiga ecozones in North America, respectively. The band of high shrub area in the northern half of the Snare River basin could be a zone of transitional density (0.25 g cm⁻³) between the lower densities of the southern forest covered region (0.19 g cm⁻³) and the higher densities normally found in the northern tundra (~0.29 g cm⁻³).

Table 2. Trends in SWE, snow depth, and snow density at the site level for time periods 1978 – 2018 and 1995-2018. p and s represent the p-value and slope of a linear regression model. Slopes for SWE, depth, and density are measure in cm yr⁻¹, cm yr⁻¹ and kg m⁻³ yr⁻¹ respectively. Significant trends with p-values less than 0.1 and 0.05 are highlighted in light and dark shades, respectively. Negative slopes are bolded, for significant cases.

Site	1978 - 2018						1995 - 2018						
	SWE		Depth		Density (x 10 ⁻³)		SWE		Depth		Density (x 10 ⁻³)		
	p	s	p	s	p	s	p	s	p	s	p	s	
South	Big Spruce	0.67	0.01	0.15	0.34	0.12	-1.9	0.04	-0.15	0.61	0.25	0.03	-5.7
	Ghost	0.36	-0.03	0.30	0.15	0.05	-0.80	0.08	-0.13	0.78	0.09	0.00	-3.1
	Mattberry	0.32	-0.03	0.58	0.09	0.37	-0.40	0.16	-0.08	0.44	0.28	0.00	-3.0
	Snare	0.02	-0.08	0.52	-0.09	0.06	-0.77	0.14	-0.10	0.80	0.08	0.01	-2.1
	Indin	0.47	-0.03	0.31	0.15	0.24	-0.41	0.03	-0.18	0.79	-0.09	0.00	-2.9
	Castor	0.11	-0.06	0.93	0.03	0.03	-0.78	0.04	-0.16	0.77	-0.09	0.00	-2.5
North	Winter	0.45	-0.03	0.03	0.27	0.00	-1.4	0.58	0.03	0.10	0.46	0.06	-1.7
	Christison	-	-	-	-	-	-	0.91	-0.01	0.45	0.17	0.38	-0.9
	Big	-	-	-	-	-	-	0.33	0.13	0.03	0.71	0.05	-2.6
	Mesa	0.30	-0.04	0.13	0.18	0.00	-1.6	0.17	-0.13	0.74	0.09	0.00	-2.7
	Whitewolf	-	-	-	-	-	-	0.29	0.012	0.04	0.60	0.49	-0.8

Higher local scale (intra-site) spatial variability in the northern tundra region of the Snare supports previous studies that have reported higher Cv's of SWE in open areas than within forested areas (Pomeroy, *et al.* 2008). Many studies have also shown that snow depth varies more than density. For example, Derksen, *et al.* (2014), working at Daring Lake, found Cv's of depth and density of 0.50 and 0.16 respectively. The Cv's found in the northern part of the Snare were similar to those

found at Daring Lake, with the C_V of depth (0.56), much greater than the C_V of density (0.26) (Table 1). In the southern region, however, CV of depth and density were 0.22 and 0.23, respectively. The C_V of depth for the southern region is at the high range of what has been reported for forested areas in previous studies (e.g. Hannula, *et al.* 2016). The similarity in spatial variability of snow depth and density in the southern part of the Snare basin contrasts the findings of many other studies. Most of these studies, however, have been conducted at alpine, prairie, tundra, or more southern boreal forest sites, rather than the relatively open canopy forests found at the northern edge of treeline.

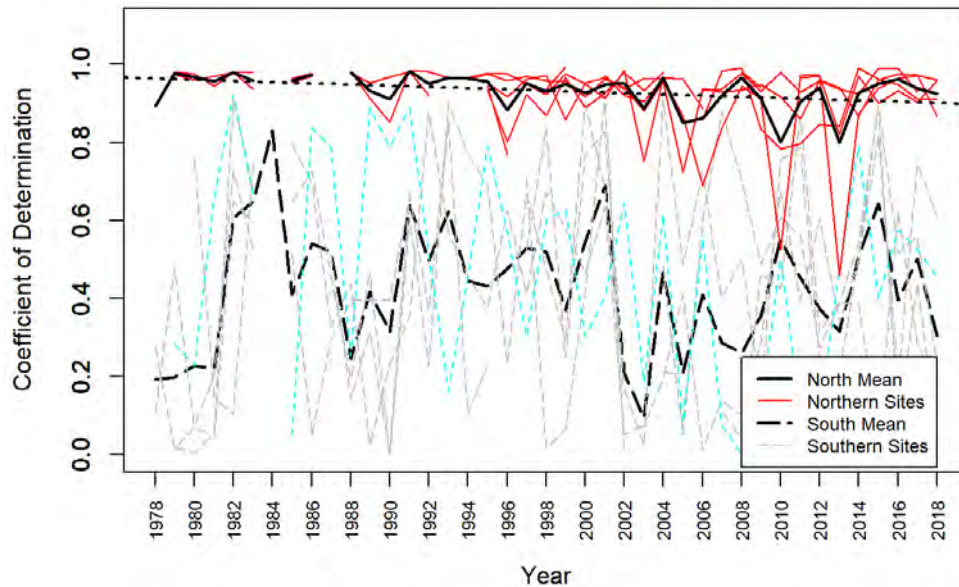


Figure 3: Coefficient of determination (R^2) between SWE and snow depth (1978-2018). Red lines show individual northern sites with the solid black line showing the mean of all northern sites. Linear trend analysis performed on the northern means indicated a declining trend with a slope of 0.002 yr^{-1} ($p = 0.01$). Gray dashed lines show individual southern sites with the black dashed line showing the mean of the southern sites. Southern sites vary through a much greater range than northern sites. The variability of R^2 for northern sites appears to be increasing with time.

At the regional scale (inter-site), the higher variability of the snow cover north of treeline observed in this study also supports previous findings that forest covered landscapes exhibit more large-scale homogeneity in snow properties than open areas, which are prone to greater wind distribution (e.g. Derksen, *et al.* 2014, Hannula, *et al.* 2016). The high R^2 between SWE and depth is similar to other studies (e.g. Sturm, *et al.* 2010). The low R^2 value found for the southern region is uncharacteristic of previous studies. High R^2 values imply that SWE is well predicted by snow depth whereas lower values imply that density varies considerably and also contributes appreciably to spatial variability of SWE.

4.2 Temporal Trends

Remote sensing data from several studies have shown a general decline in Northern Hemisphere SWE over the period roughly coinciding with NTPC historical snow survey (e.g. Jeong, *et al.* 2017). The magnitude of the decline in SWE and the applicability of the studies at a smaller scale

is uncertain (Sturm, *et al.* 2017). In the Snare basin, no statistically significant ($p < 0.1$) linear trends of increasing or decreasing SWE were detected at the basin or region scale over the full historical record. A weakly significant ($p < 0.1$) decline in SWE was detected in the southern part of the basin over the period 1995 – 2017, and three southern sites showed more significant declines in SWE ($p < 0.05$).

Compared to SWE, temporal trends in annual snow *depth* and *density* were more consistently observed at the basin, region and site scales. The most notable trend is the decline in snow density among the southern sites, which was strongly significant at regional scale ($p < 0.001$) and local ($p < 0.001$ to $p < 0.05$) scales. Significant albeit lower magnitude declines in density were also observed in the northern tundra region. Snow density varies strong along climatic gradients and increases seasonally up until the end-of-winter snowmelt period (Sturm, *et al.* 2010). Mean annual temperature at Yellowknife has increased since the 1960s (Laing and Binyamin 2013) and systematic declines in snow density across the Snare basin likely reflect a resulting shortening of the snow accumulation season. Moreover, vegetation in Arctic and subarctic shrub lands has been increasing in response to climate change (Sturm, *et al.* 2017). Since vegetation has a significant effect on snow, changes in shrub height, complexity, or species could have an effect on how the snow collects and is redistributed. For example, an increase in shrub growth will tend to increase snow accumulation by increasing snow deposition (Sturm, *et al.* 2017). The increase in snow depth is typically accompanied by a decrease in density due to a greater portion of the snowpack being depth hoar rather than tightly packed wind slab. In the northern tundra region, increasing shrub biomass has plausibly led to the observed increase in snow depth and associated decrease in density.

5. CONCLUSION

Our analysis of snow cover properties in the Snare River basin over the historical period of record illustrates that there are consistent, statistically significant differences in snow depth, density and SWE between the northern (tundra) and southern (forested) regions of the watershed. Over the historical record northern snow cover was, on average, shallower by approximately 8%, denser by approximately 25%, and contained approximately 18% more water, than the southern region. These two different snow regimes are also characterized by differences in spatial variability of snow cover properties at local and regional scales. Local and regional scale variability of all snow cover properties, particularly SWE and depth, was higher in the northern region. Systematic declines in snow density are now underway, particularly among sites in the southern forested half of the basin where SWE is also in decline. At several of the northern tundra sites, snow density is in decline, with small detectable increases in snow depth. All of these changes in snow properties are consistent climate change impacts that are now underway in this region including increasing mean annual temperatures, decreasing length of the snow accumulation season, and increasing vegetation biomass. The Snare River basin contains four hydro-electric power generation facilities and supplies electricity to approximately half of the population in Canada's Northwest Territories. The findings of the study not only have implications for understanding and monitoring snow properties in the Snare basin for the purpose of short-term hydrological forecasting, but also demonstrate a clear need to improve understanding of how the emerging snow regime will impact annual runoff and hydropower potential in the coming decades.

REFERENCES

- Bintanja, R. & Andry, O. 2017. Towards a rain-dominated Arctic. *Nature Climate Change* **7**(4): 263.
- Blöschl, G. 1999. Scaling issues in snow hydrology. *Hydrological processes* **13**(14-15): 2149-2175.
- Bokhorst, S., Pedersen, S. H., Brucker, L., Anisimov, O., Bjerke, J. W., Brown, R. D., Ehrich, D., Essery, R. L., Heilig, A. & Ingvander, S. 2016. Changing Arctic snow cover: A review of recent developments and assessment of future needs for observations, modelling, and impacts. *Ambio* **45**(5): 516-537.
- Derksen, C., Lemmetyinen, J., Toose, P., Silis, A., Pulliainen, J. & Sturm, M. 2014. Physical properties of Arctic versus subarctic snow: Implications for high latitude passive microwave snow water equivalent retrievals. *Journal of Geophysical Research: Atmospheres* **119**(12): 7254-7270.
- Goodison, B. 1981. Compatibility of Canadian snowfall and snow cover data. *Water Resources Research* **17**(4): 893-900.
- Hannula, H.-R., Lemmetyinen, J., Kontu, A., Derksen, C. & Pulliainen, J. 2016. Spatial and temporal variation of bulk snow properties in northern boreal and tundra environments based on extensive field measurements. *Geoscientific Instrumentation, Methods and Data Systems* **5**(2): 347-363.
- Jeong, D. I., Sushama, L. & Khaliq, M. N. 2017. Attribution of spring snow water equivalent (SWE) changes over the northern hemisphere to anthropogenic effects. *Climate dynamics* **48**(11-12): 3645-3658.
- Laing, J. & Binyamin, J. 2013. Climate change effect on winter temperature and precipitation of Yellowknife, Northwest Territories, Canada from 1943 to 2011. *American Journal of Climate Change* **2**(04): 275.
- McCreight, J. L., Small, E. E. & Larson, K. M. 2014. Snow depth, density, and SWE estimates derived from GPS reflection data: Validation in the western US. *Water Resources Research* **50**(8): 6892-6909.
- Myers-Smith, I. H., Forbes, B. C., Wilking, M., Hallinger, M., Lantz, T., Blok, D., Tape, K. D., Macias-Fauria, M., Sass-Klaassen, U. & Lévesque, E. 2011. Shrub expansion in tundra ecosystems: dynamics, impacts and research priorities. *Environmental Research Letters* **6**(4): 045509.
- Pomeroy, J., Gray, D., Hedstrom, N. & Janowicz, J. 2002. Prediction of seasonal snow accumulation in cold climate forests. *Hydrological Processes* **16**(18): 3543-3558.
- Serreze, M. C. & Barry, R. G. 2011. Processes and impacts of Arctic amplification: A research synthesis. *Global and planetary change* **77**(1-2): 85-96.
- Sturm, M., Goldstein, M. A. & Parr, C. 2017. Water and life from snow: A trillion dollar science question. *Water Resources Research* **53**(5): 3534-3544.
- Sturm, M., Taras, B., Liston, G. E., Derksen, C., Jonas, T. & Lea, J. 2010. Estimating snow water equivalent using snow depth data and climate classes. *Journal of Hydrometeorology* **11**(6): 1380-1394.
- Watson, F. G., Anderson, T. N., Newman, W. B., Alexander, S. E. & Garrott, R. A. 2006. Optimal sampling schemes for estimating mean snow water equivalents in stratified heterogeneous landscapes. *Journal of Hydrology* **328**(3-4): 432-452.

Carbon cycling in the Central Subarctic Boreal Shield, Canada

Sherry Schiff¹, Pieter Aukes², Michael English², Richard Elgood¹, Paul Dainard³, Jason Venkiteswaran²

¹*Department of Earth & Environmental Sciences, University of Waterloo, Waterloo, Ontario, CANADA*

²*Department Geography and Environmental Studies, Wilfrid Laurier University, Waterloo, Ontario, CANADA*

³*Department of Environmental Geochemistry, University of Waterloo, Waterloo, Ontario, CANADA*

**Corresponding author's email address: sschiff@uwaterloo.ca*

ABSTRACT

Lakes and ponds in the Boreal Shield of northern Canada store large amounts of carbon (C) in their sediments. This C largely originates in terrestrial catchments where soils, particularly in wetlands, have high organic C content. Decomposition produces high levels of dissolved organic carbon (DOC) in porewaters and shallow groundwaters that can be transported to surface waters when hydrologic flow is active. DOC is a key determinant of trace metal concentrations and mobility including Arsenic through metal complexation and effects on the redox conditions and stratification in lakes. DOC is also a key factor in provision of drinking water supplies governing the disinfectant demand and the production of harmful disinfection by-products. In open water bodies, DOC is transformed, producing both organic C particles that accumulate in lake sediments and greenhouse gases (CO₂ and CH₄) that are released to the atmosphere.

The subarctic shield (taiga and tundra) covers a wide area in Canada but is poorly studied, although it is known that the subarctic climate is changing and permafrost is degrading, affecting both water levels and C pathways. Partitioning of C between C sediment sinks and GHG emissions is also disrupted by human activities including building of infrastructure (dams, communities, roads, mining activities), and forest fire and wildlife management (particularly beaver populations). The subarctic is particularly sensitive to human actions because of shallow active layer depths and low rates of microbial processing limited by temperature. In general, lakes and ponds in the subarctic Boreal Shield have the highest DOC levels in Canada but the fate of DOC under changing conditions is uncertain. We present carbon concentration and stable isotopic data for a suite of lakes near Yellowknife where we plan to couple hydrology, landscape unit analysis, biogeochemistry to: 1) quantify rates of and controls on processes dictating partitioning of C between C storage and CO₂ and CH₄ fluxes, 2) quantify the relative role of the important processes that modify the composition of DOC.

KEYWORDS

Arctic environments; carbon storage; permafrost.

Performance of a blowing snow model for characterizing the spring snow distribution in an arctic tundra landscape

Keegan Smith^{1*} and Murray Richardson¹

¹*Department of Geography and Environmental Studies, Carleton University, Ottawa, Ontario, K1S 5B6, CANADA*

**Corresponding author's email address: smithk53@mcmaster.ca*

ABSTRACT

The objective of this study was to quantify and characterize the 2016 spring snow distribution in the 52 km² Niaqunguk River watershed (NRW) near Iqaluit, Nunavut on South Baffin Island. This watershed is now being used as an emergency supplemental water supply for the City of Iqaluit, where population growth is rapidly outpacing the natural recharge of the municipal surface water reservoir. Extensive snow depth and density data were collected during pre-melt surveys, with a mean snow water equivalent depth of 242 mm in the NRW. These data were used to assess the performance of a distributed, physically based snow transport and evolution model (SnowModel). The model used an hourly time step and 10 m grid to simulate processes over the entire winter. The model was assessed based on its ability to replicate spatial patterns of snowdrift development and estimate watershed average accumulation. Qualitatively, SnowModel replicated spatial patterns of drifting effectively. However, quantitative point-wise comparisons to field data showed that the model underestimated depths of drifts, and overestimated depths in open tundra. The model also overestimated watershed average accumulation by 12%. These findings suggest that the model simulates too little snow transport, and possibly underestimates the blowing snow sublimation flux as a result. This is likely due to SnowModel's handling of non-equilibrium snow transport, which may be inappropriate for the highly dissected fetch distances over Baffin Island's rugged terrain. Therefore, while the model shows some promise in simulating winter snow processes, we conclude that its transport processes may require closer analysis for application in this landscape.

KEYWORDS SWE; snow density; snow depth; snow surveys; SnowModel; hydrologic modelling; sublimation

1. INTRODUCTION

The amount of water stored as snow on the landscape at the end of winter is a critical variable for Arctic hydrology. Snowmelt is the dominant input to Arctic systems, accounting for the majority of annual precipitation. Estimation of this important seasonal input must account for the complex spatial pattern of snow depth resulting from extensive redistribution and sublimation by strong winds over open tundra. By spring, flat areas retain a shallow snowpack whereas topographic depressions and leeward slopes accumulate deep snowdrifts (Woo, *et al.* 1983). Drifts cover a small area but contain a large fraction of the total snow mass, requiring careful sampling design to account for them.

Modeling techniques are available to simulate snow transport and thus replicate these complex snow accumulation patterns. However, they require snowfall measurements as an input, and the snowfall gauges typically suffer from large wind-induced biases during winter in

open environments (Goodison, *et al.* 1998, Wolff, *et al.* 2015, Woo, *et al.* 1983). Ground-based survey measurements are therefore commonly used to validate model results (Prasad, *et al.* 2001) or remotely sensed snow cover products (Derksen, *et al.* 2010).

Snow transport occurs when wind shear stress exceeds the snow surface's strength. Shear stress increases proportionally to wind speed (Pomeroy and Male 1988), whereas snow strength results from bonds between particles in the snowpack. These bonds form during snowpack metamorphosis, and the degree of bonding is mainly dependent on snow temperature and age (Colbeck and Anderson 1982). In general, fresh cold snow is easily moved at even low wind speeds, whereas older snow that has partially melted and refrozen requires higher wind speeds (Li and Pomeroy 1997). At lower wind speeds most snow is transported by saltation, the temporary flight of snow particles in parabolic trajectories 10-20 cm above the surface (Mellor 1965). As wind speeds increase, turbulent suspension becomes an increasingly important transport mode relative to saltation (Pomeroy and Gray 1990).

During transport, suspended particles can rapidly lose mass to sublimation due to the strong vapour gradient between the saturated particle surface and surrounding air. The sublimation rate increases with wind speed, air temperature, and incoming radiation (Pomeroy and Gray 1995). Seasonal water losses from blowing snow can be significant in open environments; 15-41% of annual SWE on the Canadian Prairies (Pomeroy and Gray 1995), 20-47% from the western Canadian Arctic tundra (Pomeroy, *et al.* 1997), and up to 50% of pan-Arctic precipitation according to (Liston and Sturm 2004).

SnowModel is a fully-distributed physically-based snow process modeling software system. The system consists of 4 coupled sub-models: (1) MicroMet, which distributes meteorological forcing data from one or more meteorological stations to the whole domain using empirical relationships between meteorological variables and terrain, (2) EnBal, which calculates the snow surface energy budget, (3) SnowPack, which simulates snowpack density evolution, and (4) SnowTran-3D, which actually simulates snow transport processes. Snow accumulation per time step is determined by SnowTran-3D's mass balance equation:

$$\frac{d\zeta}{dt} = \frac{1}{\rho_s} \left[\rho_w P - \left(\frac{dQ_s}{dx} + \frac{dQ_t}{dx} + \frac{dQ_s}{dy} + \frac{dQ_t}{dy} \right) - Q_{vb} \right]$$

where ζ is snow depth, t is time, x and y are the horizontal spatial coordinates, ρ_s and ρ_w are the densities of snow and water, Q_s and Q_t are the horizontal mass transport rates by saltation and turbulent suspension, Q_{vb} is the blowing snow sublimation rate, and P is the water-equivalent precipitation rate. The snowpack water balance is closed with the calculation of *in-situ* snow sublimation (Q_{vs}) and melt (M) by the EnBal sub-model.

The objective of this study was to quantify and characterize the 2016 spring snow distribution in the 52 km² Niaqunguk River watershed (NRW) near Iqaluit, Nunavut. Extensive snow depth and density data were collected during pre-melt surveys. Field data was then used to characterize the snowpack and to provide validation data for SnowModel. In a similar approach to Prasad *et al.* (2001), three assessment techniques were used: (1) qualitative visual comparison of snow distribution patterns, (2) quantitative comparison of watershed average SWE derived from field measurement and SnowModel, and (3) point comparison between measured and modeled SWE, yielding spatially relevant comparison information.

2. METHODS

2.1 Study Site

The Niaqunguk River Watershed (NRW) is a small (52 km²) watershed on southern Baffin Island, near the city of Iqaluit, Nunavut, Canada (Figure 1). The river's nival flow regime is typical for an Arctic River. Summer and autumn baseflow is limited, with occasional large rainfall peaks, and no flow in winter. Elevations range from 0 - 363 masl and the rugged terrain is dominated by parallel valleys dipping to the southeast, and is underlain by continuous permafrost. Vegetation is limited to tundra grasses, dwarf shrubs, and forbs less than 10 cm tall, with little blowing snow interception capacity (unlike shrub tundra or taiga).

Regional climate is cold and arid, with annual precipitation of 404 mm, 57% as snow (ECCC, 2018). The snowfall fraction may be much greater, as snowfall is underestimated by standard gauges and precipitation type has not been recorded at Iqaluit since 1997. Snowfall can occur throughout the year, with accumulation from October to May. Most (96.5%) snowfalls are less than 10 cm, though daily accumulations up to 32 cm have been recorded. Rainfall predominates when the average air temperature rises above 0°C in June to September. Prevailing winds are from the NNW, and winds can exceed 100 km h⁻¹ during winter storms. Frequent blowing snow events redistribute the winter snow cover, resulting in a variable snow depth distribution in spring and causing a patchy snow cover pattern during melt.

2.2 Field Measurements

Snow surveys were conducted by snowmobile and on foot in April-May of 2016, with 193 sites sampled. At each site, a central SWE measurement was made using a Federal coring tube, with 3 supporting depth measurements made 2m from the central measurement at random angles. The depth measurements (including the depth in the centre) were averaged to give a site depth, and the snow density from the central point was assumed to apply to the entire site, allowing SWE calculation. The total sample size was limited compared to surveys in the NRW in other years due to the presence of heavy ice layers, which had to be punched through, slowing the procedure and requiring more frequent equipment repairs.

Sampling sites were predetermined; random points were selected along six parallel transects running the length of the watershed. Some opportunistic random samples were also added as time became available later in the season. All sites were separated by at least 100m, as an autocorrelation range of 80m had been identified based on survey data from 2015. Samples taken within this range cannot be considered statistically independent, so this survey was designed to avoid this problem entirely.

2.3 Spatial Data

A 1 m DEM was provided by Natural Resources Canada, derived from WorldView-1 stereo-optical data collected in August 2008 (Short, *et al.* 2013) and resampled to a 10 m grid spacing to improve computational speed. Test runs on a small area indicated that snow distributions from runs with a 1 m or 5 m spacing were not substantially different from the 10m simulations but required significantly greater computational resources. The DEM was clipped to a 12.65 x 18.20 km area, leaving a buffer on each side of the watershed to prevent boundary effects from causing errors in the simulated NRW accumulations.

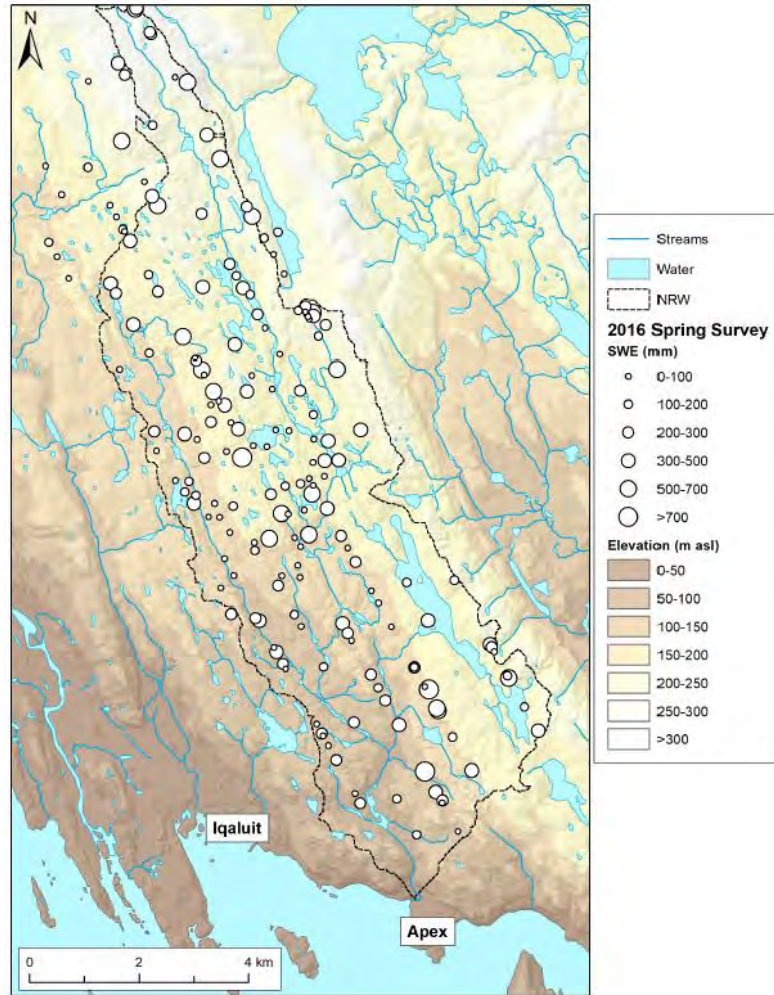


Figure 12. Map of the 53 km² Niaqunguk (Apex) River watershed near Iqaluit NU, showing 2016 snow survey locations and SWE magnitudes.

SnowModel also requires a grid of vegetation heights to define surface snow holding capacity (SHC). For this study, two SHC classes were defined: tundra and ice. Tundra SHC was 5 cm, which is Liston and Sturm’s (2002) value for “barrens” and seems reasonable given the low-lying vegetation in the watershed, as well as the hummocky microtopography, which can catch varying depths of snow below the 10 m grid scale. Ice SHC was set to 1 cm, as lake ice was rough and granular in 2016, with enough friction to hold some snow. Ice cells were delineated using a hillshade of the DEM and satellite imagery from GoogleEarth (2017), visually scanned at 1:10,000 scale. Overall, ice comprises 7.6% of the total area of the NRW.

2.4 Meteorological Data

Hourly measurements of air temperature, humidity, and wind speed and direction at 2m were drawn from the Iqaluit airport XFB climate station (ECCC, 2018). Standard precipitation measurements at XFB are taken from an Alter-shielded Geonor T-200B gauge. Snowfall measurements from these gauges suffer from extreme wind bias in open environments such as tundra, so snowfall measurements for this study were instead drawn from a double-fence automatic reference (DFAR)

OTT Pluvio² gauge located nearby. The DFAR data was quality-checked and aggregated from a 6s measurement interval to an hourly interval.

All meteorological data were examined for missing data. Since most gaps were less than 3 hours in length, all data except wind direction were gap-filled by linear interpolation, while wind direction was filled using angular interpolation. Over the accumulation period, precipitation was registered almost twice as often by the DFAR compared to the standard gauge, with twice as much total precipitation logged, justifying the decision to use the DFAR data. The user-defined parameters passed to SnowModel for this study are given in **Table 2**. Selection of the wind field parameters η , γ_s , and γ_c is described in the section below.

2.5 Wind field parameter selection

Micromet distributes wind speed and direction over the domain, modifying the station-measured wind speed and direction over the terrain through relationships to slope, aspect, and curvature. For this study, two steps were used to determine reasonable values for the wind field parameters (η , γ_s , and γ_c). First, terrain curvature maps were produced for a reasonable range of η values and compared to survey data; since snow should accumulate in a concave area and erode from a convex area, a negative correlation should be found between SWE and curvature. Second, the selected curvature value was used to calculate wind-weighting factors from a range of slope-curvature weighting ratios and a wind direction of 340° (typical for the watershed in winter). As with η , higher wind-weighting factors should be associated with shallower snow, resulting in negative correlations. Simulation outputs resulting from different wind field parameter combinations were then mapped and quantitatively compared to survey measurements. For the purposes of this paper, only SnowModel results for the best-case scenario parameters shown in Table 1 above, are presented.

2.6 Model assessment

SnowModel's ability to simulate the correct amounts of snow accumulation or erosion at the correct locations was assessed using three techniques. First, the model's ability to capture general spatial patterns was tested by qualitative visual comparison between maps of the simulated snow surface with field photos and data. This allowed researchers to determine whether SnowModel was placing drifts on leeward slopes and concavities, for example. Second, the model's ability to simulate the correct amounts of erosion and deposition was tested by comparison against survey data at measurement sites. This provided an estimate of goodness-of-fit between observed and simulated accumulation. Finally, the model's ability to capture overall watershed accumulation was assessed by comparing mean values from survey and simulation data. This allowed the simulated winter water balance to be calculated, allowing researchers to benchmark the magnitude of modeled fluxes against typical values from the literature.

3. RESULTS

3.1 Field Observations

Watershed-averaged statistics from the 2016 spring snow survey are given in Table 2. Snow depth was extremely variable between sites, with a standard deviation close to the mean. Exposed areas such as ridges and outcrops were often scoured clear of snow, whereas open tundra retained a thin snow cover, and large drifts could be several metres deep. Spatial variability within sites (2 m radius) was significantly lower than between sites but was non-negligible due to the rough surface

of hummocky tundra or boulderfields. This indicates that there is some degree of random spatial variability below the grid resolution of the SnowModel simulation, so some noise in the relationship between surveyed and simulated data is to be expected.

Snow density was much less spatially variable than depth, so SWE patterns are mostly reflective of the snow depth distribution. The measured density is unusually high for Arctic tundra due to a large number of ice layers in the snow, which made sampling more difficult. Community members stated that these layers had formed during storms in April. The unusual snow densities are corroborated by (Dolant, *et al.* 2018), who determined that snow density rapidly increased to 425 – 520 kg m⁻³ in April 2016 on Prince Charles Island (550 km northeast of Iqaluit) due to high wind speeds.

Table 2. User-defined parameters passed to SnowModel.

SnowModel Parameter	Value
Grid Spacing (m)	10
Domain Size (x,y)	[1265, 1820]
Timestep (s)	3600
η (m)	30
γ_s	0.35
γ_c	0.65
Precipitation Adjustment Factor	0
Upwind Boundary Condition	Equilibrium flux
Snow-Holding Capacity (m)	0.05 (tundra) 0.01 (ice)

3.2 SnowModel outputs

Watershed averaged snow depth, SWE and density simulated by SnowModel are also provided in Table 2, including measures of variability (standard deviation and coefficient of variation or Cv). The simulated water balance components over the entire winter are summarized in Table 3. Sublimation was the largest loss of SWE from the domain at 68.9 mm (18% of total snowfall), 54.1 mm of which was lost during blowing snow events. There was net transport out of the domain over the winter, with the majority moved by turbulent suspension. Total transport loss was 54.2 mm, almost exactly equal to the amount lost to blowing snow sublimation. A small residual term (1.9 mm) is assumed to have been due to melt during warm periods in November and January, though some of this may also be cumulative truncation error by the software. Note that the mean SWE of 264.2 represents the whole domain, and therefore is slightly different from the watershed-only value given in Table 2.

3.3 Accuracy assessment

The accuracy of the simulation outputs was examined by (1) visually assessing spatial patterns of snow accumulation, (2) comparing survey measurements to corresponding SnowModel grid cell values, and (3) comparing watershed-averaged survey and simulation statistics.

SnowModel’s spring snow pattern (Figure 2) matches that observed in the field based on visual assessment - shallow snow in exposed locations and drifted snow in sheltered areas (concavities and leeward slopes). Large simulated drifts could be easily identified on maps, which match the locations of late-lying drifts during snowmelt in the field. These typically contain the most SWE and are thus last to melt out. Drift patterns around lakes were also well-captured, with drifts at the margins and limited accumulation at the open centre of the ice. In several cases on the maps

however, the model appeared to leave too much snow on the ground; shallow accumulation was simulated in many areas that were scoured to bare rock in the field.

This is supported by the point comparisons (Figure 2). The slope of the relationship between surveyed and SnowModel SWE is very low below 300 mm, indicating that the model is less accurate in shallow snow, where it tends to overestimate SWE depth. The slope of this relationship improves at greater depths, indicating that the model more successfully captures deeper snow, although model errors at greater depths are often very large. Most of the simulated values above 300 mm observed SWE fall below the 1:1 line, indicating that the model is underestimating at these greater depths. The model shows relatively poor quantitative spatial accuracy overall ($R^2 = 0.22$).

At the watershed scale level (Table), SnowModel appears reasonable, as it overestimates SWE by only 28 mm (12%). However, this is actually due to a cancellation of errors, as the model overestimated snow depth by 17.8 cm (31%) and underestimated density by 98 kg m^{-3} (21%). The model also underestimated the overall variability in snow depth, as the modelled standard deviation was 47 cm (63% of model mean), compared to the observed standard deviation of 54.4 cm (95% of survey mean).

Table 2. Watershed-averaged 2016 spring snow statistics ± 1 standard deviation (with Coefficient of Variation in brackets). Mean difference is calculated for SnowModel with respect to the survey-derived means.

	Depth (cm)	SWE (mm)	Density (kg m^{-3})
Survey (n = 193)	57 \pm 54 (0.94)	242 \pm 232 (0.96)	460 \pm 109 (0.23)
SnowModel	75 \pm 47 (0.63)	270 \pm 189 (0.70)	362 \pm 38 (0.10)
Difference of Means	17.8 (31%)	28 (12%)	-98 (-21%)

Table 3. SnowModel water balance fluxes by year (all in mm water equivalent), where P = precipitation, Q_s = saltation transport, Q_t = suspension transport, Q_{vs} = *in-situ* sublimation, Q_{vb} = blowing snow sublimation, M = melt, SWE = snow water equivalent on the ground by end of simulation.

P	Q_s	Q_t	Q_{vs}	Q_{vb}	M	SWE
389.2	-23.1	-31.1	-14.8	-54.1	-1.9	264.2

4. DISCUSSION

This is the first reported study to simulate snow accumulation and distribution on Baffin Island in Canada’s eastern Arctic using a physically-based blowing snow model and high spatial resolution terrain representation. This environment is characterized by long winters and very high wind speeds, resulting in a very dense and spatially heterogeneous snowpack including large areas of thin snowpack and very deep drifts within leeward slopes, stream channels and valley bottoms, typical of areas with extensive blowing snow (e.g. Pomeroy and Gray 1995).

The 2016 snowpack was deeper than usual for the NRW, with remarkably high density. This was due to thick ice layers, which formed during storms in March and April when wet snow fell and

refroze on the snow surface. Similar conditions were observed around the same time elsewhere in the Eastern Arctic (Dolant, *et al.* 2018), suggesting that synoptic weather conditions may have been responsible. These layers made sampling difficult, reducing the total number of survey points in 2016. SnowModel was unable to replicate this unusually high density, perhaps because ground-based meteorological measurements did not show air temperatures above 0 °C, and thus the model did not predict surface melting and ice formation. Severe storms with higher proportions of liquid precipitation are increasing at polar latitudes (Ye 2008), suggesting that modeling techniques capable of handling such events will be needed in the future.

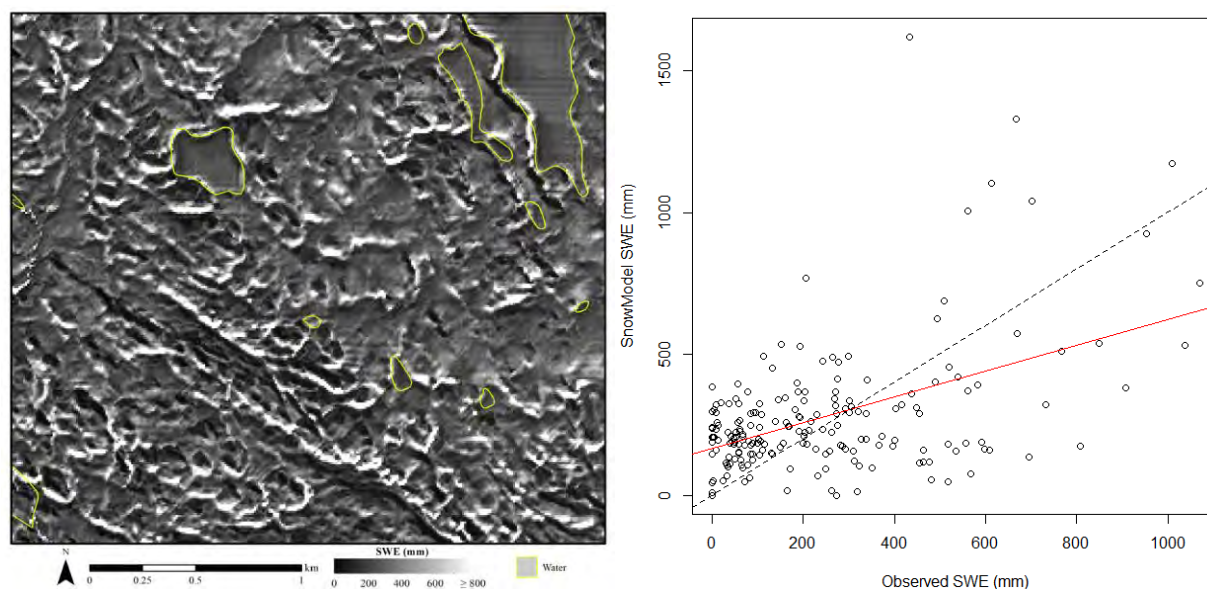


Figure 2. (Left) SnowModel output for the Lake 1 sub-domain; (Right) Scatterplot of Simulated vs Observed SWE across the NRW domain with line of best fit (solid red) and one to one line (dashed black).

4.1 Model water balance and comparison to other studies

SnowModel overestimated average snow depth and underestimated its spatial variability. Combined with the model's tendency to overestimate the depth of shallow snow and underestimate the depth of deep snow, this suggests that the model is underestimating total transport; not enough SWE is being moved from exposed to deep areas. However, the magnitudes of the transport and sublimation fluxes in the NRW seem reasonable when compared to studies in similar areas. In the present study, transport accounted for 13.8% of total winter snowfall, and sublimation accounted for 17.7%, most of which was blowing-snow sublimation. In Arctic Alaska, Liston and Sturm (2002) ran SnowTran-3D and found that 15 – 34% of precipitation was lost to blowing snow sublimation. Pomeroy and Gray (1995) found that transport fluxes from fallow fields on the Canadian Prairies accounted for the removal of 13 – 36% of annual precipitation and blowing snow sublimation fluxes accounted for 23 – 41%. At Trail Valley Creek in the Western Canadian Arctic, Pomeroy, *et al.* (1997) found that 11 mm (5.8% of snowfall) were transported out of the study area and 37 mm (19.5% of snowfall) were sublimated.

The performance metrics in this study are in good agreement with the findings of Prasad, *et al.* (2001) who applied SnowTran-3D to a small Alpine catchment in the Idaho Rockies. Their basin-averaged simulated SWE overestimated measured SWE by 51 mm, whereas our simulation

overestimated by only 28 mm. Similar to our results, Prasad *et al.* (2001) concluded that the simulated drift patterns corresponded to observed drifting patterns, but comparisons against observed SWE were poor ($R^2 = 0.19$), similar to our findings ($R^2 = 0.22$). Applying SnowTran-3D at Libby Flats, an Alpine ridge in Wyoming, Hiemstra, *et al.* (2006) found that the simulated spatial patterns of accumulation appeared correct from field experience, but in point comparisons against surveyed SWE, the R^2 ranged from 0.14 – 0.18. As in our study, they found that SnowModel overestimated shallow snow depths and underestimated drift depths. An earlier study of the area by Hiemstra, *et al.* (2002) resulted similar conclusions, with R^2 for the relationship between predicted and observed SWE ranging from 0.13 – 0.33.

Compared to other studies using SnowModel, the domain used for this study falls within the range of typical sizes (from $<1 \text{ km}^2$ to $>20,000 \text{ km}^2$), grid spacings (5 to 100 m), and regional meteorological conditions used for other Arctic regions. The main difference is in topography - the rugged tundra of the NRW occupies a “middle ground” between the complex Alpine terrain and low-relief tundra that account for most past model applications. In low-relief tundra, wind flow is less spatially variable than in Alpine terrain and the NRW. During their original paper documenting SnowTran-3D, Liston and Sturm (1998) stated that the wind model “may be inadequate for many topographic profiles”, and that “a more sophisticated model, that could handle flow over a range of topographic configurations”, would improve the model’s performance. These statements, combined with our comparison of observed *vs* simulated SWE for the NRW domain, suggest that SnowModel’s handling of non-equilibrium snow transport, which may be inappropriate for the highly dissected fetch distances over Baffin Island’s rugged terrain SnowModel, may be inappropriate for the highly dissected fetch distances over the rugged terrain of Baffin Island.

5. CONCLUSION

The objective of this study was to quantify and characterize the 2016 spring snow distribution in the NRW and to test a physically based blowing snow model for its ability to replicate complex spatial heterogeneity of snow accumulation in this rugged, windy landscape on South Baffin Island. The field data collected in this study represent the first systematic collection of snow data for this region. From survey observations, the snow distribution in the NRW can be characterized as a predominantly shallow snowpack, with exposed areas often scoured to bare ground, and sheltered areas accumulating very large drifts. Qualitatively, SnowModel performed well with snowdrift development generally matching observed drift locations. The model underestimated the depth of drifts, and overestimated depth of shallow snowpack. The watershed-scale mean SWE was slightly overestimated but was within reasonable limits. However, the model significantly underestimated snow density and overestimated snow depth, resulting in a cancellation of errors. These findings suggest that the model simulates too little snow transport, and possibly underestimates the blowing snow sublimation flux as a result. Therefore, while the model shows promise in simulating winter snow processes, we conclude that its transport processes may require closer analysis and refinement for application in this landscape.

REFERENCES

- Colbeck, S. & Anderson, E. A. 1982. The permeability of a melting snow cover. *Water Resources Research* **18**(4): 904-908.
- Derksen, C., Toose, P., Rees, A., Wang, L., English, M., Walker, A. & Sturm, M. 2010. Development of a tundra-specific snow water equivalent retrieval algorithm for satellite passive microwave data. *Remote Sensing of Environment* **114**(8): 1699-1709.
- Dolant, C., Langlois, A., Brucker, L., Royer, A., Roy, A. & Montpetit, B. 2018. Meteorological inventory of rain-on-snow events in the Canadian Arctic Archipelago and satellite detection assessment using passive microwave data. *Physical Geography* **39**(5): 428-444.
- Hiemstra, C. A., Liston, G. E. & Reiners, W. A. 2006. Observing, modelling, and validating snow redistribution by wind in a Wyoming upper treeline landscape. *Ecological Modelling* **197**(1-2): 35-51.
- Hiemstra, C. A., Liston, G. E. & Reiners, W. A. 2002. Snow redistribution by wind and interactions with vegetation at upper treeline in the Medicine Bow Mountains, Wyoming, USA. *Arctic, Antarctic, and Alpine Research* **34**(3): 262-273.
- Li, L. & Pomeroy, J. W. 1997. Probability of occurrence of blowing snow. *Journal of Geophysical Research: Atmospheres* **102**(D18): 21955-21964.
- Liston, G. & Sturm, M. 2004. The role of winter sublimation in the Arctic moisture budget. *Hydrology Research* **35**(4-5): 325-334.
- Liston, G. E. & Sturm, M. 2002. Winter precipitation patterns in arctic Alaska determined from a blowing-snow model and snow-depth observations. *Journal of hydrometeorology* **3**(6): 646-659.
- Pomeroy, J. & Gray, D. 1990. Saltation of snow. *Water resources research* **26**(7): 1583-1594.
- Pomeroy, J. & Gray, D. 1995. Snowcover accumulation, relocation and management. *Bulletin of the International Society of Soil Science* no **88**(2).
- Pomeroy, J. & Male, D. 1988. Optical properties of blowing snow. *Journal of Glaciology* **34**(116): 3-10.
- Pomeroy, J., Marsh, P. & Gray, D. 1997. Application of a distributed blowing snow model to the Arctic. *Hydrological processes* **11**(11): 1451-1464.
- Prasad, R., Tarboton, D. G., Liston, G. E., Luce, C. H. & Seyfried, M. S. 2001. Testing a blowing snow model against distributed snow measurements at Upper Sheep Creek, Idaho, United States of America. *Water Resources Research* **37**(5): 1341-1356.
- Wolff, M., Isaksen, K., Petersen-Øverleir, A., Ødemark, K., Reitan, T. & Brækkan, R. 2015. Derivation of a new continuous adjustment function for correcting wind-induced loss of solid precipitation: results of a Norwegian field study. *Hydrology and Earth System Sciences* **19**(2): 951-967.
- Woo, M. k., Heron, R., Marsh, P. & Steer, P. 1983. Comparison of weather station snowfall with winter snow accumulation in High Arctic basins. *Atmosphere-Ocean* **21**(3): 312-325.
- Ye, H. 2008. Changes in frequency of precipitation types associated with surface air temperature over northern Eurasia during 1936–90. *Journal of climate* **21**(22): 5807-5819.

Freshwater flux to the Beaufort Sea from Northern Alaska

Svetlana Stuefer¹, Kelsey Dean¹, Michael Rawlins²

¹*Water and Environmental Research Center, University of Alaska Fairbanks, Alaska, USA.*

²*Climate System Research Center, University of Massachusetts, Amherst, Massachusetts, USA. .*

**Corresponding author's email address: sveta.stuefer@alaska.edu*

ABSTRACT

Estimates of freshwater flux (Q) to the Beaufort Sea from northern Alaska are often solely based on water delivered by relatively large rivers such as Colville (35,820 km²) and Kuparuk (8,107 km²) Rivers. These two rivers annually deliver $8.9 \hat{\pm} 1.5$ km³/yr and $1.3 \hat{\pm} 0.4$ km³/yr of fresh water to the Beaufort Sea, respectively. Our study shows that Q increases by approximately a factor of two when runoff from the entire contributing area is accounted for in total Q estimates. We evaluate Q using available long-term hydrologic observations collected by the Water and Environmental Research Center at University of Alaska Fairbanks (WERC/UAF) and the United States Geological Survey (USGS). These observations include runoff from additional eight watersheds that represent the diverse hydrologic conditions of Arctic coastal plain, foothills, and mountains of the Brooks Range. We further compare observationally-based Q with modelling results simulated with the Pan-Arctic Water Balance Model (PWBM) for years 1981-2010. This presentation discusses hydrologic processes and feedbacks that account for the large range of variability and trends in freshwater input to the Beaufort Sea.

KEYWORDS

Rivers; fresh water; measurements; rural Alaska; Arctic.

Hydrological Changes in the Four Largest Siberian Arctic River Basins

Kazuyoshi Suzuki^{1*}, Tetsuya Hiyama², Kazuhito Ichii³, Yoshihiro Iijima⁴, Koji Matsuo⁵, Dai Yamazaki⁶

¹*Institute for Arctic Climate and Environment, Japan Agency for Marine-Earth Science and Technology, Yokohama, Kanagawa, 236-0001, JAPAN*

²*Institute for Space-Earth Environmental Research, Nagoya University, Nagoya, Aichi, 464-8601, JAPAN*

³*Center for Environmental Remote Sensing (CEReS), Chiba University, Chiba, 263-8522, JAPAN*

⁴*Graduate School of Bioresources, Mie University, Tsu, Mie, 514-8507, JAPAN*

⁵*Geospatial Information Authority of Japan, Tsukuba, Ibaraki, 305-0816, JAPAN*

⁶*Institute of Industrial Science, The University of Tokyo, Meguro-ku, Tokyo, 153-8505, JAPAN*

*Corresponding author's email address: skazu@jamstec.go.jp

ABSTRACT

The Arctic freshwater budget is critical for understanding climate in the northern regions and affects global climate. However, the hydrology of the largest Eurasian Arctic rivers is still not well understood, and the largest Siberian basins and the Arctic circumpolar regions are experiencing rapid hydrological change (Suzuki et al., 2018). In this study, we analyzed the spatiotemporal variations of the hydro-climatological factors of four of the largest Siberian Arctic river basins (the Ob, Yenisey, Lena, and Kolyma) from 2000 to 2016. To examine the recent hydro-climatological changes of the river basins, we utilized monthly observation-based gridded meteorological and evapotranspiration data, MODIS-based products such as the snow area fraction (SAF), Normalized Difference Vegetation Index (NDVI), and Enhanced Vegetation Index (EVI), Global Land Data Assimilation System products, and Gravity Recovery and Climate Experiment (GRACE) data from 2000 to 2016. Using these products together with river runoff data, we identified river runoff change from June to May in the analysis period. River runoff in May of the largest four basins increased significantly, although annual discharge had no trend. In addition, the SAF in April decreased drastically, which provides evidence that spring snow coverage in the Siberian basins has been shrinking. Additionally, we found a positive trend in NDVI in summer. Through our research, we intend to evaluate the temporal lag correlation between the water cycle and vegetation activity. In addition, we will provide a case study of the hydrological changes in the Kolyma River Basin.

KEYWORDS

Arctic hydrological cycle; River discharge; Snow cover fraction; Vegetation activity; Freshwater budget

REFERENCES

Suzuki, K., Yamazaki, D., Iijima, Y., Yanagi, Y., Hiyama, T., 2018. Hydrological variability and changes in the Arctic circumpolar tundra and the three largest pan-Arctic river basins from 2002 to 2016. *Remote Sensing* 10, 402. doi:10.3390/rs10030402

Recent summer low flows in two subarctic regions in Canada

Robin Thorne^{1*}, Ming-ko Woo¹, and Laura Brown²

¹*School of Geography and Earth Sciences, McMaster University, Hamilton, Ontario, L8S 4K1,*

²*Department of Geography, University of Toronto Mississauga, Mississauga, ON, L5L 1C6, CANADA,*

** Corresponding author's email address: thornerrf@hotmail.com*

ABSTRACT

The recent five years have been some of the warmest on global record. While most of the Canadian subarctic had experienced an increase in daily air temperatures during the summer (taken as July and August in the subarctic), trends in seasonal precipitation were spatially variable. The position of the polar jet stream has been shifting northward, and the position aloft will affect the distribution of frontal precipitation through the subarctic. Enhanced evaporation and lower than usual streamflow can result from warmer, and potentially drier, than usual summers. However, basin settings add complicity. Various factors influencing summer flows include localized rain events engendered by atmospheric moisture recycling that interrupt the declining summer flow; the nature of snowmelt freshet such that smaller and earlier spring peak were trailed by diminished flow recession in July; possible degradation of ground ice that adds runoff to augment river discharge; and water storage in wetlands and lakes that delayed and tempered low flow response to the atmospheric driver.

Two groups of hydrometric stations were chosen for this low flow investigation: one in northwestern Canada, the other in northern Manitoba/Ontario. Examples assembled from the 2014-2018 records confirmed that a number of the hydrometric stations experienced a summer flow shortage, but to varying degrees based on location and regional climate influences. Results from this study demonstrated that both atmospheric signals and land phase hydrology need to be considered in order to interpret the inter- and intra-regional variations in the summer flow of northern rivers.

KEYWORDS

Low flow; Subarctic; Jetstream; Temperature, Precipitation

1. INTRODUCTION

Most subarctic rivers experience recurrent low flow conditions in the summer, implying that the amount of flow falls below a certain level that is normally expected, or that is required to sustain human activities, or environmental wellbeing. In large river systems, summer low flows are hydrological hazards that reduce water supply, present problems for water-borne traffic, impact aquatic habitats and affect the entrainment of sediments and nutrients.

In recent years, the polar front and associated jet stream, a meandering band of strong westerly winds in the upper troposphere that forms the boundary between the polar air to the north and the warmer tropical air to the south, has been shifting north (Archer & Caldeira, 2008), influencing the subarctic basins. The formation process for mid-latitude cyclones is related to the jet stream, and therefore the position and strength of the jet stream will affect the location of precipitation events, as well as influence the regional climate.

Recent variability in the polar jet stream have led to a number of studies (Francis & Vavrus 2012; Mann et al., 2018; Kornhuber et al., 2019) that suggest that unusually persistent and amplified disturbances in the jet stream could be associated with persistent extreme summer weather events. The last five years (2014-2018) included extreme events such as 2014 and 2015 low flow events within the Mackenzie Basin, 2016 Alberta wildfires and the 2018 heatwave in North America.

In addition to synoptic precipitation (as dictated by the jet stream position and strength) contributing to subarctic streamflow, within-region sources of moisture, such as localized rainfall from moisture recycling, permafrost thaw, or sustained lake outflow, will also impact the summer flow regimes.

Effects of causative factors that induce low flow conditions would produce signals that are embedded in the flow and reflected in the hydrograph (Woo & Thorne 2016). Recent summers offer further opportunities, as case studies, to assess the below normal flow status that responded to the meteorological and hydrological forcing. The climatic and hydrological settings were expected to be not only spatially variable but would change during and between each summer. Both the annually variable basin-wide and site-specific conditions impact the flow at individual hydrometric stations.

This study investigated recent summer low flow events of select hydrometric stations from two different subarctic regions: northwestern Canada and northern Manitoba and Ontario. These regions were selected not only due to the warmer trends and increased variability in extreme weather events, but also to represent the western and eastern portions of the Canadian subarctic, as they were situated towards the upper reach of the jet stream (western portion), and where the jet stream had already passed across the continent (eastern portion). The goal of this study was to explore examples from the recent five years that highlight the complexity of the hydrologic response to the drivers of low flow. Understanding and quantifying temporal and spatial variations of summer low flow offers a sound hydrological basis for planning and decision making, the formulation of adaptation strategy and policy in response to natural and anthropogenic changes.

2. DATA SUPPORT AND METHOD OF ANALYSIS

Selected 80 hydrometric stations were distributed in two regions of the subarctic (a) North northwestern Canada, which includes the Cordilleras, Interior Plains and Canadian Shield, and (b) northern Manitoba and Ontario, which includes undulating Canadian Shield overlain in the north by sedimentary beds with flat topography (Figure 1). The diverse environments give rise to different streamflow regimes, the most prevalent being the nival regime in which winter low flow is terminated by snowmelt-generated freshet in the spring, which then recedes to low summer discharges (Woo & Thorne 2003). Modifications to this flow pattern include flow augmentation by glacier melt, intensified evaporative water loss from wetlands and lakes, and the effect of large lakes in smoothening outflow except where the flow pattern is complicated by reservoir operation (Woo & Thorne, 2016). Overall, summer usually contains low flow periods in the subarctic, a feature that applies to other major circumpolar rivers, both in North America and in Eurasia.

In view of the vastness of the region, the timing of summer flow varies in different parts of the subarctic. To give uniformity in the time frame, we confined summer to July and August. For low flow analyses, requisite streamflow data were obtained from HYDAT, the National Water Data Archive compiled by Water Survey of Canada (<http://wateroffice.ec.gc.ca/>), with recent data provided directly by the Ontario Region National Hydrological Service.

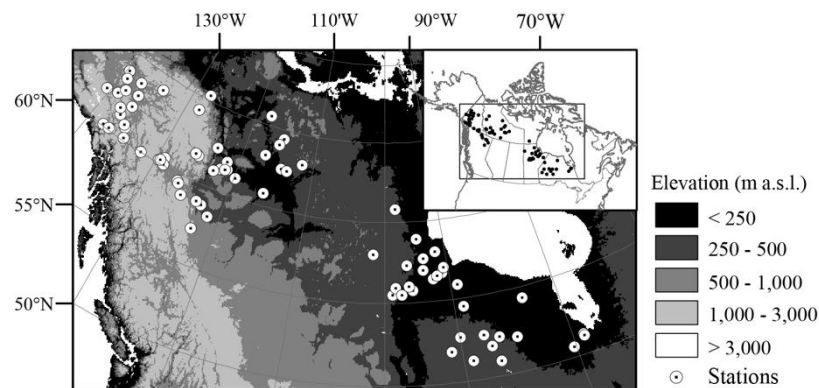


Figure 13. Locations of the selected hydrometric stations and the topography, highlighting the topographic differences between the north-western study region and the more eastern study region.

Low flow is a relative term, suggesting that river discharge falls below a particular level of expectation. For the investigation of the recent five years (2014 to 2018), we used the departure of the daily mean discharge (Q_i , m^3/s) from the long-term (1972 to 2018) daily median (Q_{Ni}), to calculate the net shortage or surplus for the summer (July and August) in each year using Equation 1:

$$\sum_{Jul\ 1}^{Aug\ 31} (Q_i - Q_{Ni}) \Delta t \quad (1)$$

where $(Q_i - Q_{Ni})$ is the net shortage or surplus values on day t (Δt is time interval, being 86 400 sec/day), for each hydrometric station, depending on if the total is negative or positive. These values were then divided by its basin area (km^2) to convert the values to runoff (mm).

To examine a continuous region across the country, reanalysis data was used to create comparison maps of temperature and precipitation and to develop a proxy for jet stream location. Monthly mean 2-m air temperature, monthly mean forecast precipitation accumulations (representing total precipitation), along with daily U and V component wind speed from the 300 hPa pressure level for 12:00 UTC were extracted from the ERA Interim data set for 1979 – 2018 (0.75° , available from: <https://www.ecmwf.int/>). Jet stream data was approximated by identifying where windspeeds at the 300 hPa pressure level exceeded $30\ \text{ms}^{-1}$ (e.g. Belmecheri et al, 2017). While the general jet stream position can be represented by identifying the latitude of greatest average windspeed for each month (e.g. Belmecheri et al., 2017; Barton & Ellis, 2009), our aim was to also highlight the positional variability of the jet stream within each month. To this end, the number of days where the windspeed aloft exceeded $30\ \text{ms}^{-1}$ was tallied for each grid cell, creating a monthly positional frequency dataset. Anomaly maps were created to compare the recent years (2014-2018) to a developed climatology (1981-2010) which highlight areas that experienced more, or less, days per month than ‘normal’ with winds $> 30\ \text{ms}^{-1}$. The latitude (for each longitude) that had the highest tally of days per month with windspeeds aloft exceeding $30\ \text{ms}^{-1}$, along with the ‘normal’ tally of days (1981-2010), are both presented to approximate the predominant jet stream position and highlight the monthly variability.

3. RESULTS

3.1 Jet Stream Variability

Mean jet stream position (1981-2010) showed a different pattern between July and August. In July, the mean jet stream pattern was more linear, flowing from lower West Coast, across the Canada/U.S.A. border into Central Ontario. While in August, the mean jet stream position flowed down to southern British Columbia, then up across Alberta to central Saskatchewan before flowing down to southern Manitoba and into Central Ontario. Over the recent five years, patterns have emerged that deviated from the mean positional pattern (Figure 2). For the month of July, most patterns generally followed the mean, with the exceptional deviation in portions of the jet stream that flowed more north or more south compared to the long-term mean. In 2015, the jet stream flowed just south of the subarctic before continuing heading south and into Central Ontario, while in 2018, the jet stream flowed into the eastern subarctic area in Northern Ontario. In August, recent jet stream patterns flowed through the subarctic regions, with the exception of 2016 and 2017.

Further to the most frequent location of the jet stream for each month (Figure 2), the within-month variability (Figure 3) highlighted how often the daily jet stream persisted above the subarctic regions compared to the monthly normal position.

Variability in summer flow can be attributed to two groups of factors: atmospheric and hydrologic. For atmospheric conditions, the jet stream can control the spatial patterns of both temperature and precipitation by changing the frontal position and dissipation of frontal precipitation zone. Additionally, it influences the persistence and lifespan over different subarctic regions.

3.2 Atmospheric Factors

In terms of atmospheric conditions, winter snowfall provides the initial amount of water available at the start of the open-water flow season, summer precipitation controls the supply while evaporation, indirectly indicated by air temperature, results in water loss. Trends were evaluated from 1979 – 2018 for air temperature and total monthly precipitation using the “zhang” method of climate trend analysis (Zhang et al., 2000).

3.2.1 Temperature

High temperature plays dual roles in affecting the water balance. It is a driver both for water loss through evaporation and paradoxically, for adding water to glacierized drainage basins through intensifying snow and ice melt.

Reanalysis climate data superimposed on top of the map of hydrometric stations showed that temperatures have increased in the subarctic over the past four decades by up to 5°C (Figure 4). Significant temperature increases were found near the stations close to Nunavut in July, and stations in the Yukon and along the Cordilleras in August.

Recent temperature anomalies in July show that the western subarctic region was warmer than normal in 2014 and cooler in 2015, with other years falling within the normal monthly temperature (Figure 5). In the East, recent July temperatures were closer to the normal. For August, the western subarctic experienced recent warmer temperatures for most years, particularly in 2017. In 2018, most of the subarctic had cooler than normal temperatures.

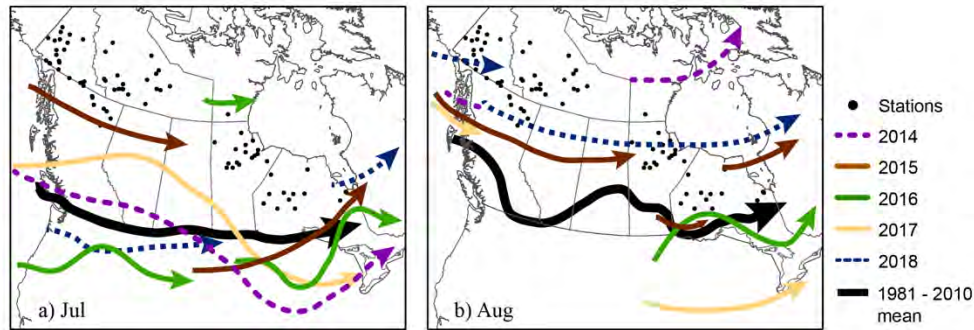


Figure 14. Most frequent position of the jet stream during a) July and b) August from 2014 to 2018, relative to the long-term monthly mean jet stream position averaged from 1981 to 2010.

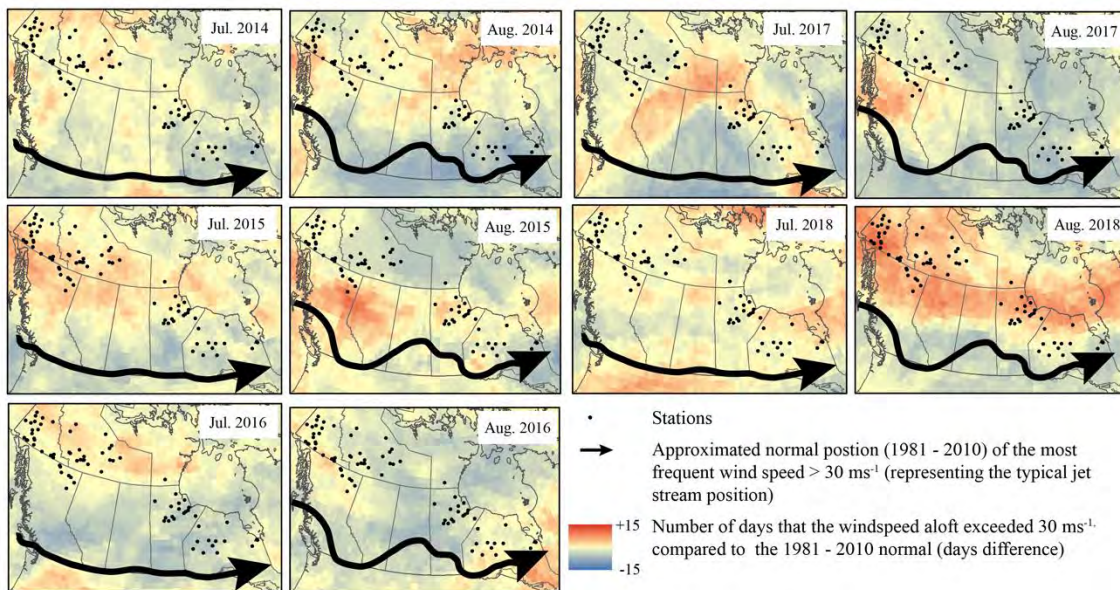


Figure 15. Within-month variability of the jet stream position for July and August in recent years (2014 to 2018), relative to the long-term monthly mean jet stream position averaged from 1981 to 2010.

3.2.2 Summer Precipitation

Summer precipitation controls the supply to rivers after the spring freshet, where localized rainstorms can terminate low events in small rivers. Across most of the subarctic summer precipitation has increased, except for a consistent decrease in Northern British Columbia. Significant increases were shown to be located over the Great Slave Lake area in both July and August and over select stations in the Yukon and Ontario in August (Figure 4).

Precipitation anomalies for the latest five years showed a spatial distribution of both wet and dry patches, even within the western and eastern subarctic regions (Figure 5). In July, the western subarctic was drier for 2014 and 2018, with more precipitation in 2015 and 2017 mostly.

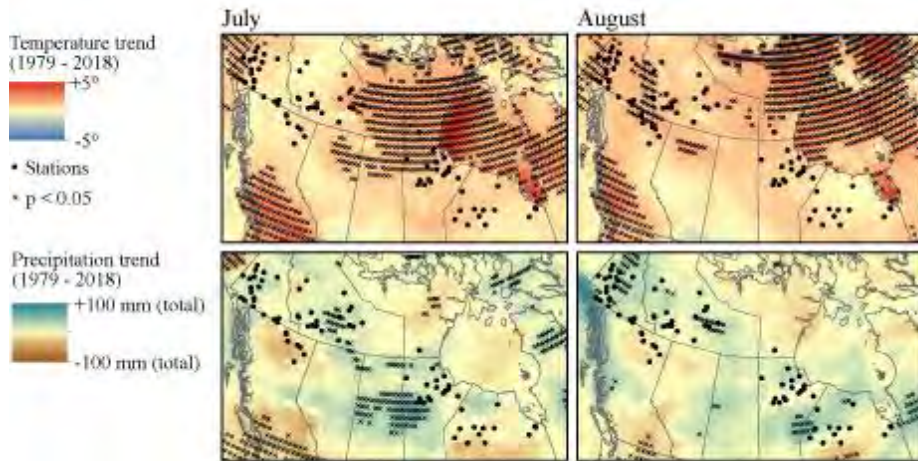


Figure 16. July and August temperature and precipitation trends from the ERA Interim data set, for 1979 – 2018. x denotes significance at the 95% confidence level.

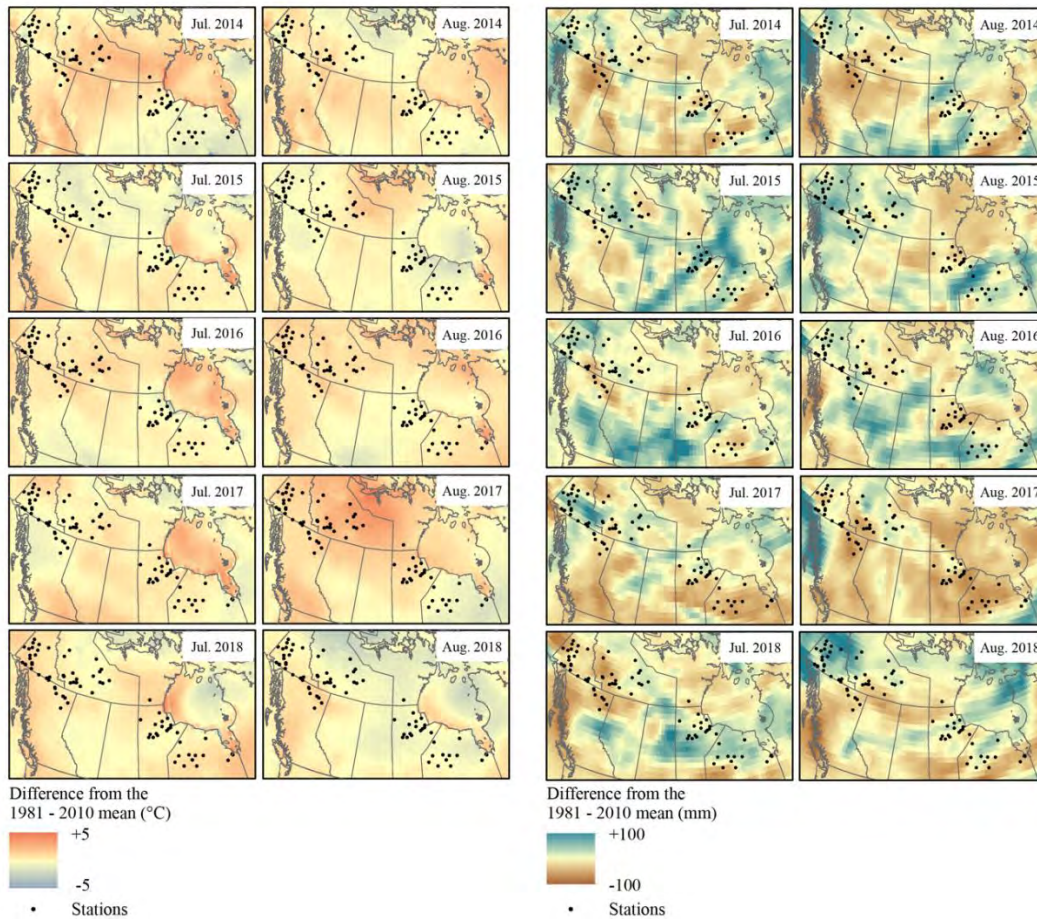


Figure 17. Left: monthly temperature difference to the 1981 - 2010 climatology and right: monthly precipitation totals compared to the climatology.

The eastern subarctic was below normal in 2014 and 2017, and above-normal precipitation levels for 2015 and 2018. Similar patterns were seen in August, except for 2017, which was drier for the majority of the subarctic region.

Comparing jet stream patterns of recent years to precipitation anomalies, instances appear where the two coincide. For example, in August 2017, when the majority of Canada had below normal precipitation, the monthly average jet stream position was below Canada, and flowed into Southern Ontario.

3.3 Regional Low Flow Analysis

Figure 6 presents the pattern of surplus, or deficit, for the select hydrometric stations within the subarctic over each of the recent five years, mapped using data from sub-basins with areas of < 50,000 km². Focusing on the net shortage (degree of red dots in Figure 6),

In 2014 and 2015, approximately a half of the western stations in 2014, and around two-thirds in 2015, experienced a shortage in flow greater than 500 mm over both July and August, with a few stations having experienced severe shortage in flow (>2000 mm). While in the East, only around 20 to 35% of the stations experienced this deficit. In 2016, both regions underwent episodes of low flow, with half of the western and eastern stations dropping below normal. The following year, low flow conditions were scarce in the west, with only one-third the stations affected, while half the stations in the east experienced low flow, particularly in northern Ontario. In 2018, more severe episodes of low flow events were observed across the whole subarctic region, with over half of all stations recording levels below the normal.

Compared to the spatial patterns of the atmospheric drivers, there were instances where low flow events correspond to warmer temperatures and below-average rain events, such as in 2014 for the western region, 2017 in the eastern subarctic, and 2018 for the whole subarctic. However, even when atmospheric factors encourage low flow events to occur, land phase factors, such as lakes and topography, can overwhelm atmospheric influence.

3.4 Basin Factors

Hydrological settings in different parts of a large basin exert varied influences on the gains and losses, storage and release of water to affect runoff and streamflow. As well, hydrological responses produced at one area can be transmitted downstream through river flow and can be detected elsewhere in the drainage system.

Lakes and wetlands provide storage by absorbing the influx of water and releasing it later at a more gradual rate. Resulting lake outflow, when compared to the inflow, showed that the short-term fluctuations are smoothed and the rhythm is attenuated. A comparison of two hydrometric stations along the Snare River (NWT) showed the resulting lake inflow and outflow, with a change in the hydrologic regime from a nival to a proglacial (Figure 7). This proglacial regime supplied sufficient discharge to reduce the occurrence of low flow events, thus complicating the spatial pattern results of the regional low flow analysis (Figure 6).

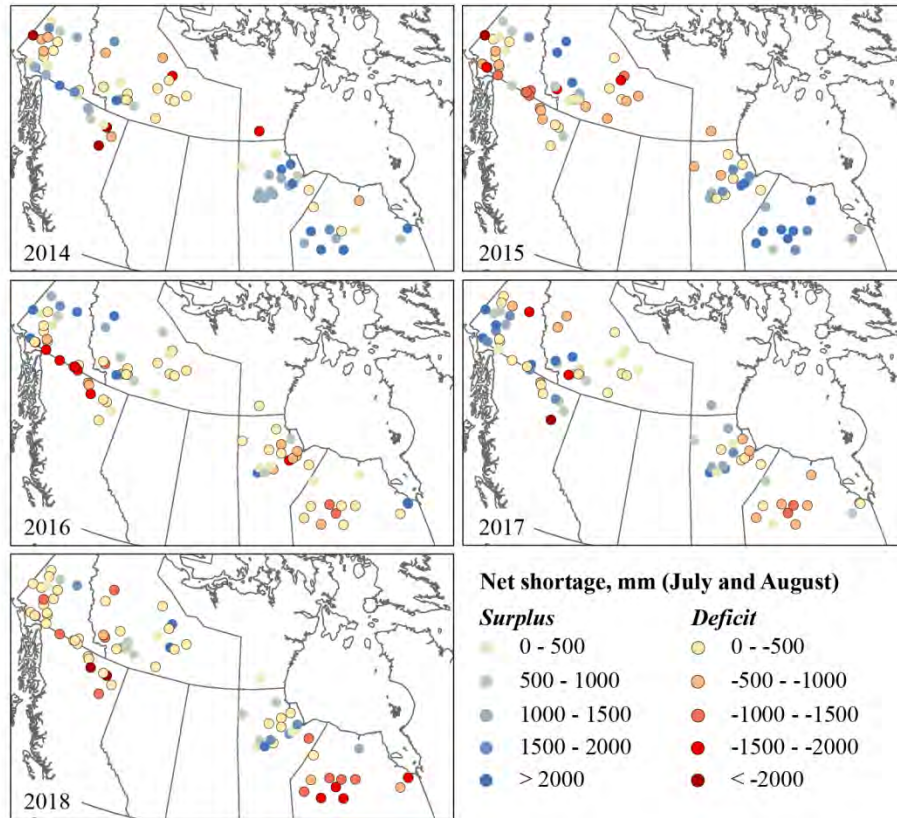


Figure 18. Total surplus (mm), or deficit (mm), for the months of July and August across the western and eastern regions of the subarctic.

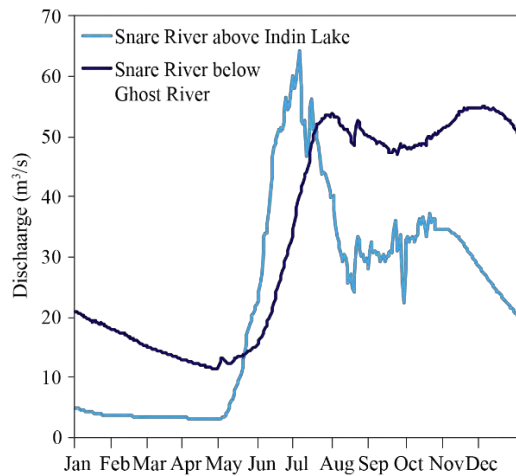


Figure 19. Hydrometric stations along the Snare River, NWT for 2015, above and below a series of lakes along the Canadian Shield, which modified the hydrologic regime and reduced the occurrence of low flow events.

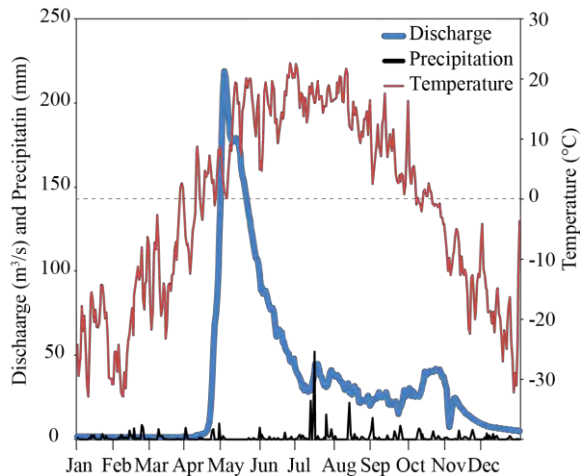


Figure 20. Summer low flow conditions for Trout River, NWT in 2015, with high temperatures, which strengthened the evapotranspiration rate; below normal summer precipitation; and a declining flow recession all contributing to the event.

Some land phase factors can create opposing types of response to climate (e.g. for the same temperature increase, the processes of permafrost thaw yields higher summer flow, while evaporation reduces runoff contribution). High air temperature tends to strengthen evaporation, especially the daily maximum, which was usually attained during daylight hours to accompany radiation input to drive the evaporative process (e.g. Trout River, NWT, Figure 8). High evaporation also leads to the lowering of lake levels, and consequently diminishing outflow. While land phase processes dominate the Trout River example, the peak in July precipitation coincided with a more frequent incursion of the jet stream aloft into that region.

After the passage of peak flow, discharge can recede to low values, unless interrupted by new sources of water input, such as snowmelt, rainfall or river inflow, leaving groundwater as the principal contributor to streamflow. A gradual reduction in the groundwater input, and a continued loss of water due to evapotranspiration, leads to a decline in river discharge, indicated by a recession from high flow to the baseflow (Figure 8). Late arrival of spring peak event delays the advent of low flows and a snowmelt peak of large, rather than lower magnitude, takes longer to decline to low discharges.

Localized rainstorms can terminate low flow events in small rivers. Much of the high discharge generated by intense rainfall in small catchments tends to run off quickly rather than be stored for later release, and this water would not be available to ameliorate subsequent low flow situations. Spatial patterns of precipitation anomalies are a combination of frontal precipitation from the jet stream and pockets of localized rainfall derived from moisture recycling within the region. Rain from this recycling would contribute to the temporary termination of summer low flow.

4. CONCLUSION

Most northern rivers experienced recurrent low flow conditions in the summer that can affect water supply, pose problems for river traffic, and can adversely affect aquatic ecology. Through the water balance, temperature and precipitation would have an impact on streamflow variability. Climatic variability was captured by the variations, intensity, and duration in the polar jet stream trajectory, which drive the spatial and temporal variability in both temperature and precipitation. The recent

five years have been some of the warmest on global record. Hotter than usual summers were expected to affect low flows through enhanced evaporation. Most northern locations have experienced rising daily air temperatures in the summer (taken as July and August in the subarctic) but there was a varied trend in seasonal precipitation regionally. Examples assembled from the 2014-18 records confirmed that most hydrometric stations underwent a reduction in summer flow, which appeared to be the continuation of a multi-year trend, and likely related to the summer temperature increase. However, individual rivers showed responses that varied on the sub-regional scale as the climate signal was complicated by land phase factors. In the subarctic regions, streamflow responded to the regional, or external, circulation leading to precipitation; local/within region evapotranspiration, which implied the interaction of temperature (external or internal) to available moisture; local recycling of moisture, which can be exaggerated by mountain plain circulation; and local-scale variations in flow due to land phase factors such as the storage function of large lakes, different timing of recession from peak discharges, basin size, topography, geology, peat, wetlands, vegetation and permafrost. Thus, both climate and land factors need to be taken into consideration when examining the regional year-to-year variations in summer streamflow.

REFERENCES

- Archer, C.L. & Caldeira, K. 2008. Historical trends in the jet streams. *Geophysical Research Letters* 35, L08803, doi:10.1029/2008GL033614.
- Barton, N.P., & A. W. Ellis. 2009. Variability in wintertime position and strength of the North Pacific jet stream as represented by re-analysis data. *Int. J. Climatol.* 29, 851–862.
- Belmecheria, S., Babst, F., Hudson, A., Betancourt, J., and Trouet, V. 2017. Northern Hemisphere Jet Stream Position Indices as Diagnostic Tools for Climate and Ecosystem Dynamics, *Earth Interactions* 21(Paper No. 8), 1-23.
- Francis, J.A., Vavrus, S.J. 2012. Evidence linking Arctic amplification to extreme weather in mid-latitudes. *Geophysical Research Letters* 39, L06801, doi: 10.1029/2012GL051000.
- Kornhuber, K., Osprey, S., Coumou, D., Petri, S., Petoukhov, V., Rahmstorf, S and Gray, L. 2019. Extreme weather events in early summer 2018 connected by a recurrent hemispheric wave-7 pattern. *Environmental Research Letters* 14 (5) 4002.
- Mann, M.E., Rahmstorf, S., Kornhuber, K., Steinman, B.A., Miller, S.K., Petri, S. and Coumou, D. 2018. Projected changes in persistent extreme summer weather events: The role of quasi-resonant amplification. *Science Advances* 4, 1-9.
- Zhang, X., Vincent, L.A., Hogg, W.D. & Niitsoo, A. 2000. Temperature and precipitation trends in Canada during the 20th century. *Atmosphere-Ocean*, 38, 395–429.
- Woo, MK., Thorne, R. 2003. Streamflow in the Mackenzie Basin, Canada. *Arctic* 56, 328-340.
- Woo, MK., Thorne, R. 2016. Summer low flow events in the Mackenzie River system. *Arctic* 69, 286-304.

Assessing Controls on Thermokarst Lake Water Balances using Stable Water Isotopes between Inuvik and Tuktoyaktuk, Northwest Territories, Canada

Evan Wilcox^{1*}, Gabriel Hould-Gosselin², Branden Walker¹, Philip Marsh¹, Brent Wolfe¹,
Oliver Sonntag²

¹*Cold Regions Research Centre, Wilfrid Laurier University, Waterloo, Ontario, N2L3C5, CANADA*

²*Département de Géographie & Centre d'Études Nordiques, Université de Montréal, Montréal Québec, H2V2B8, CANADA*

**Corresponding author's email address: wilc0150@mylaurier.ca*

ABSTRACT

A warming climate in permafrost regions has the potential to change thermokarst lake water fluxes, which cover a large portion of the Arctic. To predict how thermokarst lakes respond to these pressures, an overall understanding of the main influences on lake water balances is required. We comparatively assessed the water balance of 25 lakes between Inuvik and Tuktoyaktuk, Northwest Territories, Canada using stable water isotope tracer methods, which allowed us to calculate the ratio of evaporation to lake inflow (E/I) for the five dates we sampled these lakes between May 1 and September 3, 2018. Lakes isotopic signatures shifted away from the signature of snow, and towards the signature of lake ice after snowmelt, suggesting that snowmelt runoff is not the primary contributor to lake waters in spring. We determined through repeated isotopic measurements at two adjacent lakes that snowmelt runoff did not become hydrologically connected with lake waters beneath lake ice until over a week after discharge began at lake outlets. Overall, E/I was controlled by the relative area of the lake catchment, but was also potentially dependent on antecedent soil moisture conditions. This study highlights the strength in combining process-based knowledge with efficient isotopic sampling methods in an environment which is challenging to access.

KEYWORDS

Thermokarst lakes; water balance; isotope tracers; continuous permafrost

1. INTRODUCTION

Climate warming in permafrost regions is causing longer and warmer summers, longer ice-free periods on lakes, and shifting precipitation from snowfall to rainfall (Vaughan et al. 2013; Bintanja and Andry 2017). These changes have the potential to alter lake water balances and lake temperatures by changing the amount and timing of lake water balance inputs and outputs. Thermokarst lakes are one of the most prominent landscape features in the permafrost regions, covering 15 – 50% of the land surface area depending on the region (Burn and Kokelj 2009). Thermokarst lakes form in localized depressions where permafrost has already thawed and expand when permafrost surrounding the lake thaws. Carbon from thawing permafrost is carried into lakes by subsurface runoff or enters lakes directly when thermokarst lakes expand. Thermokarst lakes are productive environments for microbes which consume carbon and consequently, thermokarst lakes typically produce large amounts of greenhouse gas relative to the surrounding land (Kokelj and Jorgenson 2013). Microbes consume this carbon and release carbon dioxide or methane, creating a positive feedback loop between permafrost thaw and climate warming (Schuur et al. 2015). The strength of this feedback loop partially depends on how much of the carbon released from permafrost can be converted into greenhouse gasses.

Emissions of greenhouse gasses from thermokarst lakes are closely tied to the hydrological behavior of lakes (Serikova et al. 2019). The amount of carbon that enters a lake is partially dependent on the amount of permafrost thaw, and the area of the catchment that drains into the lake. Then, the amount of greenhouse gas released from the lake depends on the temperature of the lake water, and the length of time water spends in the lake, as these factors control the rate and amount of time microbes have to consume the carbon. Therefore, in order to understand how carbon delivery and processing in lakes will change as the climate changes, we need to understand the controls on lake water fluxes.

Many studies of lake water balances in areas of continuous permafrost are limited to direct measurements of water balance components at one to a few different lakes in a region, as making direct measurements of lake level, discharge, and inflow are time and resource intensive. We used stable water isotope samples to qualitatively compare water fluxes across a range of lakes in the region. The ratio of $^{18}\text{O}/^{16}\text{O}$ to $^2\text{H}/^1\text{H}$ in precipitation changes seasonally, causing different sources of water, such as snow and rain, to have different isotopic signatures (Craig and Gordon 1965). Additionally, the isotopic signature of waterbodies undergoing evaporation follow a trajectory towards an isotopic signature which is determined by the regional climate (Yi et al. 2008). We collected stable water isotope samples five times from 25 lakes from before snowmelt (April 29) until the end of summer (September 3) to quantify elements of lake water balance. While this method results in a poorer temporal measurement resolution and can only be used to assess lake water balances comparatively, the relatively small amount of time it takes to take isotope samples allows a larger assessment of a region's lakes. We hypothesized that the relative area of a lake to the area of its catchment ($\text{LACA} = \text{Area}_{\text{Catchment}} / \text{Area}_{\text{Lake}}$) would be a primary control on lake water balance. To test this, we selected a set of lakes with varying LACA along the Inuvik – Tuktoyaktuk Highway (ITH). We also took samples of lake waters, lake ice, and lake outflow at two adjacent lakes throughout the snowmelt period, to better understand the mixing of snowmelt waters with lake waters during the snowmelt period.

2. METHODS

2.1 Study Area

Water samples were collected five times from 25 lakes situated beside ITH, spanning ca. 75km from south to north (Figure 1). The entire region is underlain by ice-rich permafrost > 100 m deep, except beneath large water bodies (Burn and Kokelj 2009). Surface sediments consist of mostly fine-grained glacial deposits, with large areas affected by thermokarst (Rampton 1988). The tree-line extends ca. 50km north of Inuvik, while tundra areas north of the tree-line are characterized as erect low-shrub tundra (S2) (Walker et al. 2005; Lantz et al. 2013).

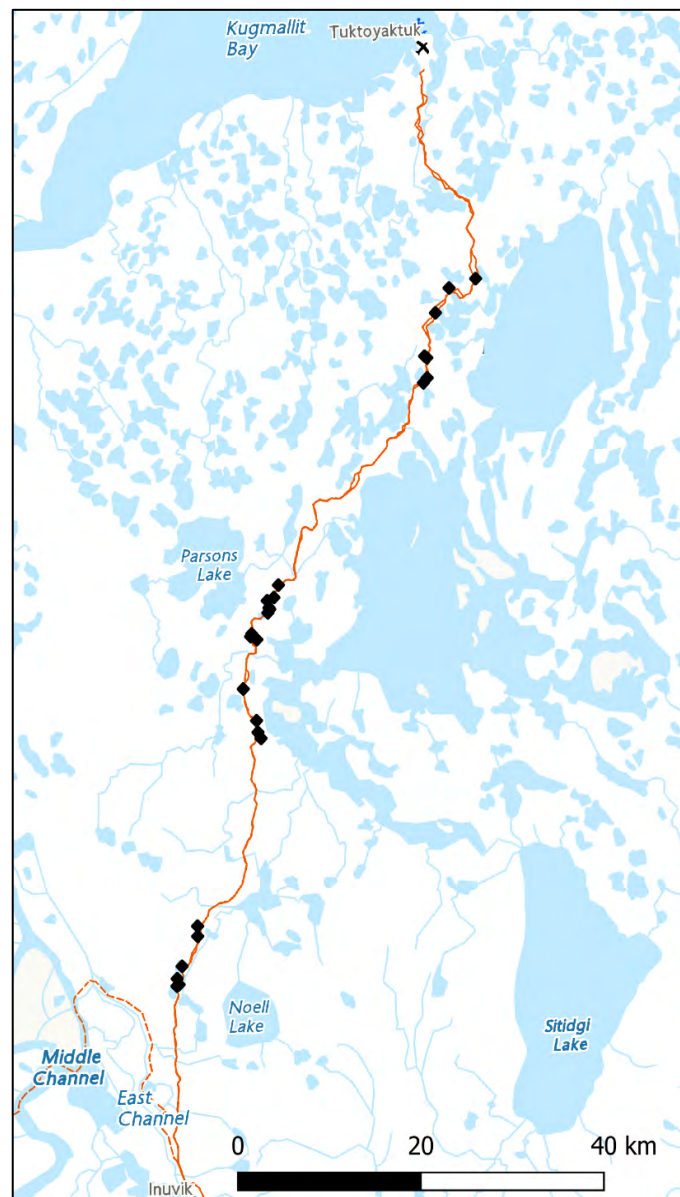


Figure 22. Map of study area. Sampled lakes are indicated with black diamonds, and the red line marks the ITH. Larger water bodies are shown in light blue.

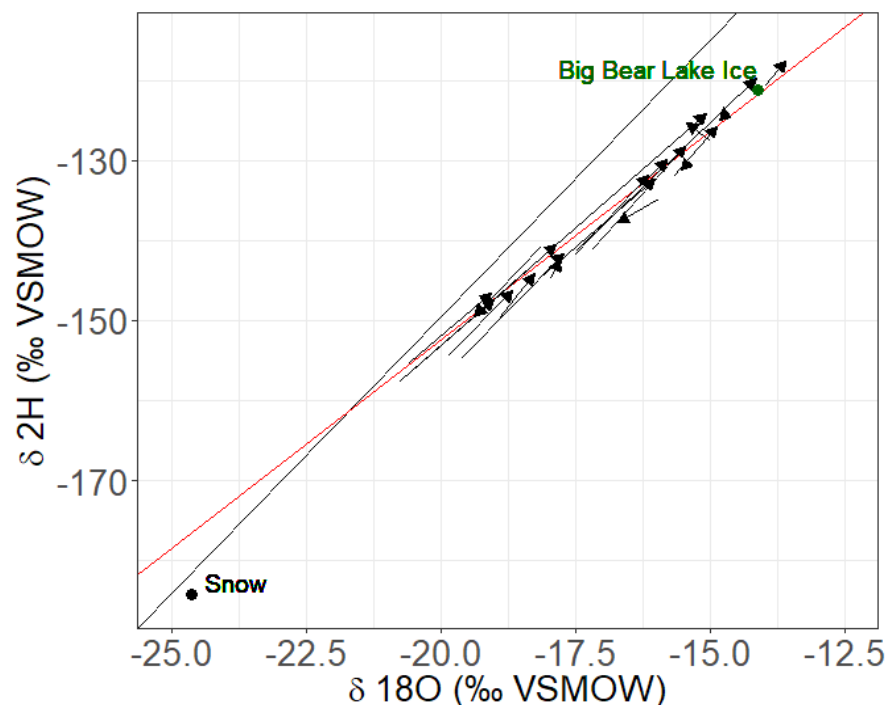


Figure 23. Trajectory of lake isotopic compositions from before to after snowmelt. The majority of lakes are pointed in the direction of lake ice, and not towards snow. Lake ice composition of each lake likely varied from the composition of Big Bear’s ice, depending on the isotopic composition of the lake at freeze-up. The black line represents the local meteoric water line, and the red line represents the local evaporation line, as determined by a linear regression through all lake water samples.

2.2 Isotope Sampling and Analysis

Before snowmelt from April 29 to May 1, 2018, 30 mL water samples were collected from holes drilled through the lake ice at the centre of the lake. Ice thickness, lake depth, and snow depth were also measured at this time. Samples of snow were taken around the study area in large plastic bags, which were then melted at the end of each day and put into 30 mL sample bottles. Samples of lake water, lake ice, water on top of lake ice, and lake outflow were made periodically during the snowmelt period from May 11 – June 3 at Big Bear and Little Bear Lake. From June 15 onward, samples were collected from the edge of the lakes, and liquid precipitation was collected in a bowl in Inuvik and placed into a sample bottle after precipitation ceased. Sample bottles were flushed three times with sample water before a sample was taken. Samples were analysed at University of Waterloo Environmental Isotope Laboratory. Results are denoted by δ , indicating deviation per mil (‰) from V-SMOW, where $\delta = (R_x / R_s - 1) \cdot 1000$, R_x is the ratio of $^{18}\text{O}/^{16}\text{O}$ or $^2\text{H}/^1\text{H}$ in the sample and R_s is the ratio of $^{18}\text{O}/^{16}\text{O}$ or $^2\text{H}/^1\text{H}$ in the standard (Kendall and McDonnell 1998). The ratio of evaporation to inflow (E/I) was calculated for each lake sample using a coupled isotope-tracer method developed by Yi et al. (2008). For example, when $E/I = 1$, the amount of water flowing into the lake and the amount of water evaporating from the lake are equal. The E/I ratio provides an integrated measure of overall lake water fluxes, and has been used to assess controls on lake water balance in other similar permafrost environments (Macdonald et al. 2017).

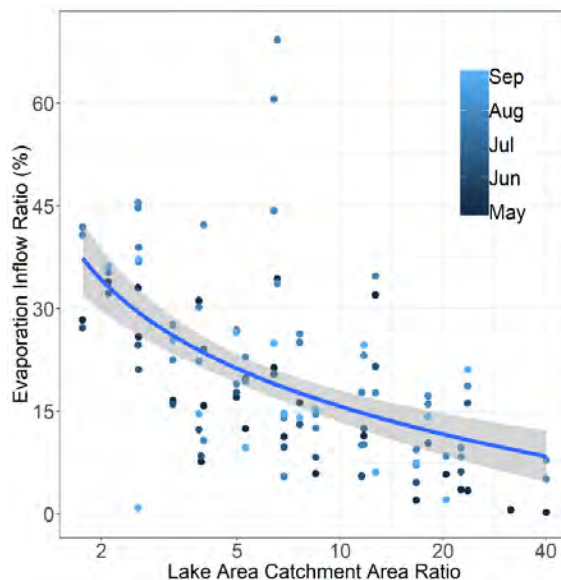


Figure 24. The relationship between the Lake Area Catchment Area Ratio and the Evaporation - Inflow Ratio. The blue line represents the relationship between EI and $\ln(\text{LACA})$, with an adjusted r^2 of 0.33.

3. RESULTS AND DISCUSSION

3.1 Snowmelt Period

As roughly 50% of precipitation in this region falls as snow (Environment and Climate Change Canada 2019), we hypothesized that lakes would experience a large influx of snowmelt water which would shift lake isotopic signatures towards that of snow. However, isotopic signatures shifted away from snow once lakes were resampled on June 15, days after they became ice-free (Figure 2). This was likely caused by the contribution of the melting lake ice, which had an enriched isotopic signature compared to the lake water under the ice. On average, ice thickness was 49% (1.0 m) of the lake depth at the 25 lakes we sampled. The composition of lake ice on Big Bear Lake and the water beneath the lake ice of Big Bear Lake was $\delta^{18}\text{O}$, $\delta^2\text{H} = -14.11\text{‰}$, -121.23 and -7.40‰ , -143.96‰ , respectively, before snowmelt began. Additionally, we saw evidence that snowmelt does not mix hydrologically with lake water beneath the ice for over a week after outflow begins at lake outlets. The difference isotopic signatures between Big Bear and Little Bear lake waters and the isotopic signature of water flowing from their outlets was greater than $\delta^{18}\text{O}$, $\delta^2\text{H} = 7\text{‰}$, 50‰ until May 25, meaning all earlier snowmelt runoff, which began on May 13, had flowed overtop of ice and out of the lake. The last previous set isotope samples which showed different isotopic signatures between lake and outlet waters were taken on May 20. The combination of high ice volume in the lake with snowmelt runoff bypass of the lake, contributed to relatively little apparent snowmelt signature in lake waters on June 15.

3.2 Summertime Evaporation, Recharge

Overall, LACA was a significant control on lake E/I ratio, with lakes with relatively smaller catchments experiencing significantly higher E/I ratios regardless of sampling date (Figure 3). This trend agrees with findings by Turner et al. (2014), who calculated the E/I ratio from water isotope samples from 57 study lakes in the Old Crow Flats, Yukon. The mean E/I ratio varied between the

sampling dates, giving insight into how lake water balance changed during the course of the summer (Table 1). The mean E/I ratio was highest for the July 26 samples, as only 26.0 mm of rain had fallen since the last sampling date (June 15). Between July 26 and August 2, 41.3 mm fell, however the dry antecedent conditions likely caused little runoff to be generated in soils, as evidenced by the minimal change in lake isotopic composition between the two sample dates (Figure 4). Lakes which were recharged by rainwater point in the direction of the isotopic composition of rain, however most lakes show relatively little movement. Between August 2 and September 3, 66 mm of rain fell, however the mean E/I ratio fell disproportionately more for the amount of rain which had fallen, with the mean E/I going from 0.24 to 0.14 by September 3. This is likely because soils were more saturated than the previous period, and were then able to generate runoff into lakes.

Table 3: Evaporation - inflow changes over the course of the year.

E/I	01-May	15-Jun	26-Jul	02-Aug	03-Sep
Mean	0.16	0.16	0.26	0.24	0.14
Std. Dev.	0.12	0.08	0.17	0.13	0.12

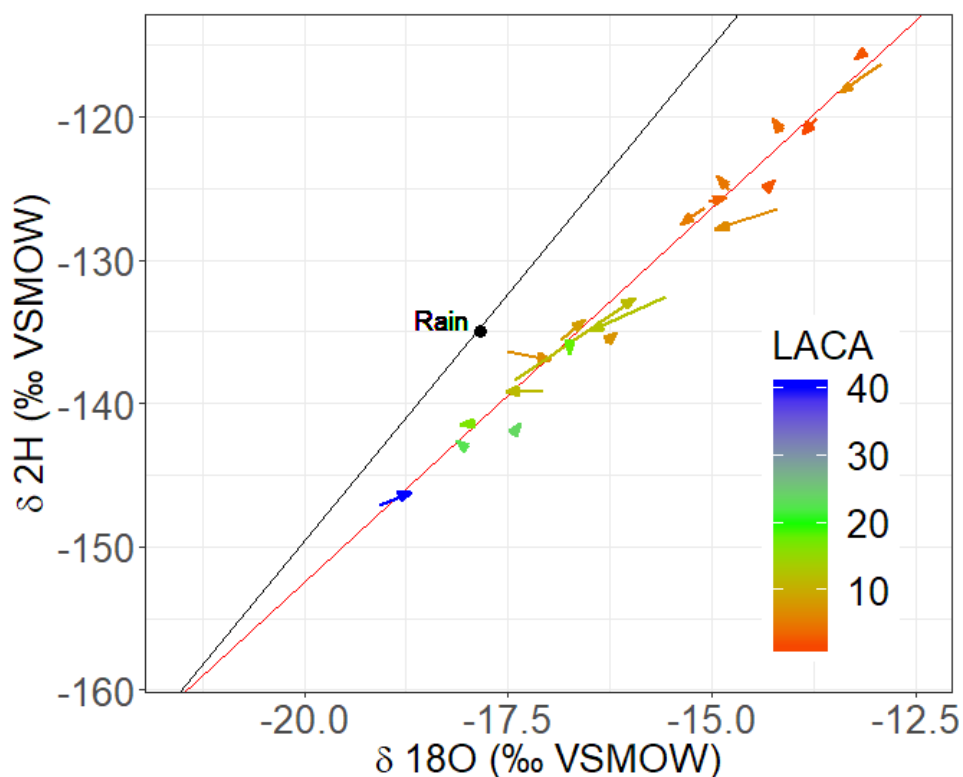


Figure 25. Change in lake isotopic composition from before to after a 41.3 mm of rainfall. Arrows represent the change in isotopic composition from before to after the event, and the black dot marks the isotopic composition of the rainfall from the event. The black line represents the local meteoric water line, and the red line represents the local evaporation line, as determined by a linear regression through all lake water samples.

4. CONCLUSION

Here we show that the hydrological regime of thermokarst lakes in the Inuvik – Tuktoyaktuk region is predominantly controlled by the relative area of a lake to its catchment. We also show that snowmelt runoff may contribute less than melting lake ice to recharging lake waters during freshet. These results were obtained using stable water isotope samples, which allowed us to sample more lakes than we could have using direct measurements of water balance components. However, it was necessary to have an understanding of the relevant physical processes which act on lake water fluxes, such as snowmelt bypass, in order to interpret results from isotope samples correctly. Future research can incorporate this fast and relatively inexpensive sampling method with other biogeochemical measurements of lakes to assess how lake water fluxes may impact lake carbon input and cycling.

ACKNOWLEDGEMENT

The authors wish to thank Kiyoo Campbell, Dilshan Kariyawasam, Barun Madjumder and Carolina Voigt for their assistance in collecting water samples. Evan Wilcox was funded by the Northern Scientific Training Programme and the W. Garfield Weston Foundation. We also acknowledge funding from Natural Sciences and Engineering Research Council of Canada, Polar Knowledge Canada, ArcticNet, and the Canada Research Chair programs.

REFERENCES

- Bintanja, R., and Andry, O. 2017. Towards a rain-dominated Arctic. *Nat. Clim. Chang.* **7**: 263–267. doi:10.1038/nclimate3240.
- Burn, C.R., and Kokelj, S.V. 2009. The Environment and Permafrost of the Mackenzie Delta Area. *Permafr. Periglac. Process.* **20**: 83–105. doi:10.1002/ppp.
- Craig, H., and Gordon, L. 1965. Deuterium and oxygen 18 variations in the ocean and the marine atmosphere. *Stable Isotopes in Oceanographic Studies and Paleotemperatures.*
- Environment and Climate Change Canada 2019. Canadian Climate Normals. [Online] Available: http://climate.weather.gc.ca/climate_normals/.
- Kendall, C., and McDonnell, J.J. 1998. *Isotope Tracers in Catchment Hydrology.* Elsevier, Amsterdam.
- Kokelj, S. V., and Jorgenson, M.T. 2013. Advances in thermokarst research. *Permafr. Periglac. Process.* **24**: 108–119. doi:10.1002/ppp.1779.
- Lantz, T.C., Marsh, P., and Kokelj, S. V. 2013. Recent Shrub Proliferation in the Mackenzie Delta Uplands and Microclimatic Implications. *Ecosystems* **16**: 47–59. doi:10.1007/s10021-012-9595-2.
- Macdonald, L.A., Wolfe, B.B., Turner, K.W., Anderson, L., Arp, C.D., Birks, S.J., Bouchard, F., Edwards, T.W.D., Farquharson, N., Hall, R.I., McDonald, I., Narancic, B., Ouimet, C., Pienitz, R., Tondou, J., and White, H. 2017. A synthesis of thermokarst lake water balance in high-latitude regions of North America from isotope tracers. *Arct. Sci.* **3**: 118–149.
- Rampton, V.N. 1988. *Quaternary Geology of the Tuktoyaktuk Coast-lands, Northwest Territories,* Geological Survey of Canada.
- Schuur, E.A.G., McGuire, A.D., Grosse, G., Harden, J.W., Hayes, D.J., Hugelius, G., Koven, C.D., and Kuhry, P. 2015. Climate change and the permafrost carbon feedback. *Nature* **520**: 171–179. doi:10.1038/nature14338.
- Serikova, S., Pokrovsky, O.S., Laudon, H., Krickov, I. V., Lim, A.G., Manasypov, R.M., and

- Karlsson, J. 2019. High carbon emissions from thermokarst lakes of Western Siberia. *Nat. Commun.* **10**: 1552. Springer US. doi:10.1038/s41467-019-09592-1.
- Turner, K.W., Wolfe, B.B., Edwards, T.W.D., Lantz, T.C., Hall, R.I., and Larocque, G. 2014. Controls on water balance of shallow thermokarst lakes and their relations with catchment characteristics: a multi-year, landscape-scale assessment based on water isotope tracers and remote sensing in Old Crow Flats, Yukon (Canada). *Glob. Chang. Biol.* **20**: 1585–1603. doi:10.1111/gcb.12465.
- Vaughan, D.G., Comiso, J.C., Allison, I., Carrasco, J., Kaser, G., Kwok, R., Mote, P., Murray, T., Paul, F., Ren, J., Rignot, E., Solomina, O., Steffen, K., and Zhang, T. 2013. Observations: Cryosphere. *Clim. Chang. 2013 Phys. Sci. Basis. Contrib. Work. Gr. I to Fifth Assess. Rep. Intergov. Panel Clim. Chang.*: 317–382. doi:10.1017/CBO9781107415324.012.
- Walker, D.A., Reynolds, M.K., Daniëls, F.J.A., Einarsson, E., Elvebakk, A., Gould, W.A., Katenin, A.E., Kholod, S.S., Markon, C.J., Melnikov, E.S., Moskalenko, N.G., Talbot, S.S., Yurtsev, B.A., Bliss, L.C., Edlund, S.A., Zoltai, S.C., Wilhelm, M., Bay, C., Gudjónsson, G., Moskalenko, N.G., Ananjeva, G. V., Drozdov, D.S., Konchenko, L.A., Korostelev, Y. V., Melnikov, E.S., Ponomareva, O.E., Matveyeva, N. V., Safranova, I.N., Shelkunova, R., Polezhaev, A.N., Johansen, B.E., Maier, H.A., Murray, D.F., Fleming, M.D., Trahan, N.G., Charron, T.M., Lauritzen, S.M., and Vairin, B.A. 2005. The Circumpolar Arctic vegetation map. *J. Veg. Sci.* **16**: 267–282. doi:10.1111/j.1654-1103.2005.tb02365.x.
- Yi, Y., Brock, B.E., Falcone, M.D., Wolfe, B.B., and Edwards, T.W.D. 2008. A coupled isotope tracer method to characterize input water to lakes. *J. Hydrol.* **350**: 1–13. doi:10.1016/j.jhydrol.2007.11.008.

A Brief History of Cryohydrology in Canada

Ming-ko Woo¹

¹*School of Geography and Earth Sciences, Hamilton, Ontario, L84K1, CANADA*

**Corresponding author's email address: woo@mcmaster.ca*

ABSTRACT

Cryohydrology studies the properties, distribution, movement and storage of water in both its solid and liquid phases at sub-zero temperatures. Thus, it concerns snow, ice, frozen ground and cold waters. As over 95 percent of Canada experiences at least one month with below-zero mean air temperatures, the cryohydrology of Canada is inexorably entwined with Canadian hydrology. Several periods of hydrologic development since the centennial year of Canada (1967) are recognized. Initially, hydrology was subsidiary to hydraulics and aspects of cryohydrology were mainly applied in nature. In the two decades that followed, cryohydrology flourished as a result of international impetus, national support, expanded hydrometric network, growing publications, and intensified field investigations that augmented the role of science. This period also witnessed the strengthening of statistical hydrology and the ascendancy of modelling. Next came economic recession that, together with government policy, resulted in the reductions in funding and research activities. Economic stringency eventually relaxed, accompanied by the emergence of large projects that crossed disciplines and embraced investigators from academic, government and private sectors. Cryohydrology, commonly labelled as cold regions hydrology, is now a branch of hydrology well established to address economic and environmental issues to meet societal needs.

KEYWORDS

Cryohydrology; cold regions hydrology; history; cold environment; Canada

1. INTRODUCTION

Cryohydrology, or hydrology at low temperatures, concerns snow, ice, frozen ground and cold waters. Canada, with a land surface area of approximately 10 million km², is a cold country. About half of Canada retains a snow cover for at least six months each year and only low elevation zones in its southwest coast have January mean temperature getting above 0°C (Fig. 1). With cold regions being dominant, cryohydrology permeates almost all aspects of Canadian hydrology. The history of cryohydrology is necessarily entwined with the general history of Canadian hydrology.

2. WHEN CANADA WAS 100 YEARS OLD

My course through the history of Canadian cryohydrology starts in 1967. When Canada was 100 years old then, hydrology was auxiliary to other subjects and practices. Large engineering ventures such as the Baie James hydroelectricity project used hydrology to supplement hydraulics; forestry and agriculture wanted hydrology for drainage and water supply purposes; floods were investigated as part of river ice studies; and snow was studied for avalanches, over-winter transportation and structural stability. This supporting role laid a good foundation for Canadian hydrology to enter a splendid period of development. There had been experts from other cold countries who worked in Canadian governments and universities, contributing to Canadian research and training on various cryological aspects. An important institution, the Canada Centre for Inland Waters, was set up by

the federal government in 1967, with Jim Bruce as its first Director, one year after he co-authored a book on “Introduction to Hydrometeorology” (Bruce & Clark 1966) that links hydrology with meteorology, possibly the first treatment of this subject for Canada. Foreign books such as Hydrology for Engineers (Linsley et al. 1958) and Handbook for Applied Hydrology (Chow 1966) had their influences, and the Handbook on the Principles of Hydrology (Gray 1970) became a comprehensive hydrology text with Canadian content. Nevertheless, as summarized by Gray (1970, p. 1.3), “hydrology is not entirely a pure science, for the object of study is usually directed to a practical application”.

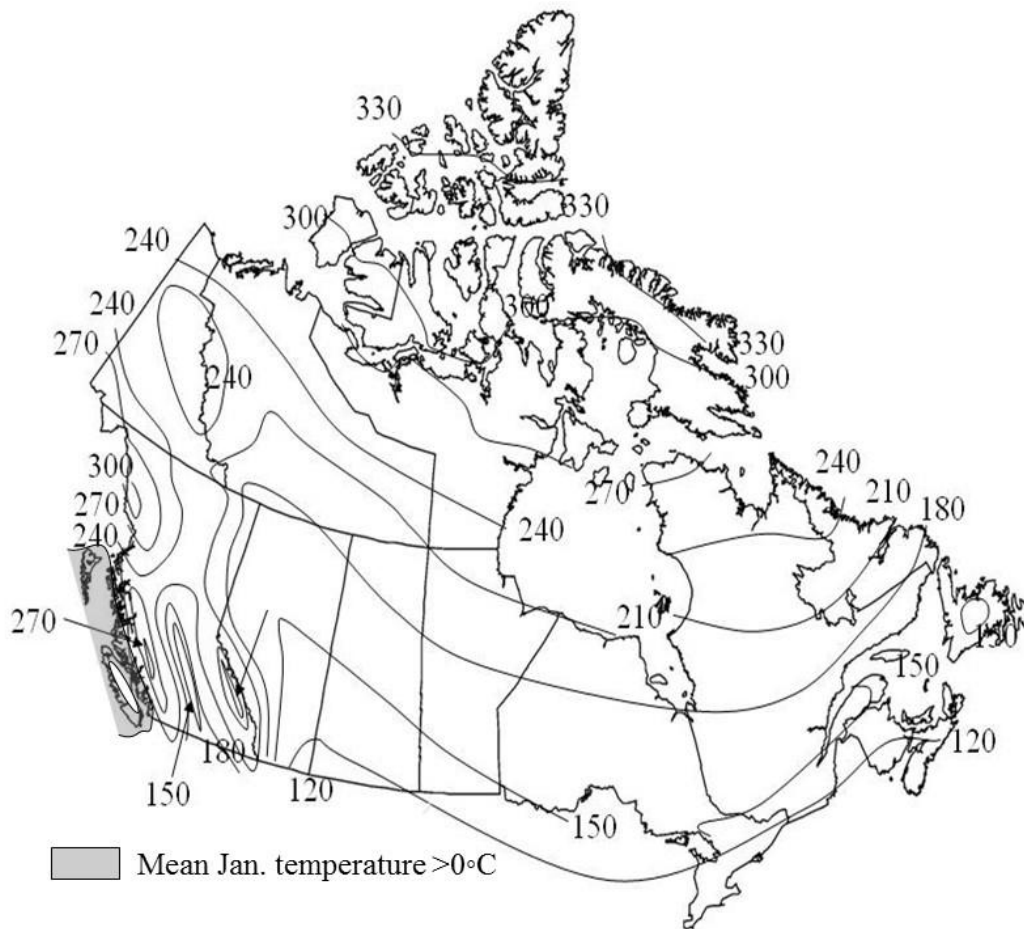


Figure 1. Map of Canada showing median number of days per year with ≥ 2.5 cm of snow on the ground; and areas where mean January air temperature is above 0°C .

3. RAPID GROWTH OF CRYDROLOGY

Science focuses on the question ‘why’. Scientific hydrology of cold region enables understanding of basic processes that improves applications. The growth of process research followed nationwide expansion in field investigations and was also a response to external impetus. Since around 1970, there was an increase of cold regions research participation by geoscientists and geographers who have a long tradition of conducting field work in far flung areas and under trying conditions. Curiosity-driven and applied research enriched knowledge on snow, river ice, glaciers and permafrost hydrology. Rapid growth in digital computer technology soon outstripped the usefulness

of analog computers. Hydrological models as well as statistical hydrology grew in tandem with scientific hydrology.

The International Hydrological Decade (IHD) under UNESCO already started in 1965, which led to the formation of the Canadian IHD and the creation of benchmark research basins in 1966. Other research basins also started, partly because they “were in vogue” in the U.S. (Swanson et al. 1988, p.5). The international initiative of IHD was followed by several International Hydrological Programs (IHP), beginning in 1975. One of the initiatives relevant to cryohydrology was the Northern Research Basin Symposium and Workshop (NRB) that provided a forum for researchers from circumpolar countries.

Both climatic and hydrometric station networks enlarged steadily. The Water Survey of Canada (since 1908) gradually switched from publishing streamflow, water level and sediment data in book form to CD and finally to HYDAT that allows online access. The Hydrological Atlas of Canada was published by Fisheries and Environment Canada in 1978 and remains as a major source of hydrological information to-day. Satellite imagery offers spatial information that is difficult to obtain for high latitudes and high altitudes where cryohydrological conditions prevail. The federal government also fostered science and engineering through its National Research Council. A Subcommittee on Hydrology was already formed in 1957, under the Associate Committee on Geodesy and Geophysics. The subcommittee status was elevated in mid-1970s, to become the Associate Committee on Hydrology (ACH), with membership comprising representatives from federal and provincial governments, professional societies, private companies, and academics of several universities. To promote hydrology, bi-annual symposia were held between 1959 and 1988, and “Hydrology of Floods in Canada” was published in 1989. The Committee on River Ice Processes and the Environment (CRIPE) was established in 1975, with strong support from the engineering community (Beltaos & Burrell 2015).

4. TROUBLED TIMES

One major event before the onset of hard times was the creation of the National Hydrology Research Institute in Saskatoon in 1986. Then, a stormy period came in early 1990s when years of government deficits and inflation culminated in economic recession, which affected government spending and engineering opportunities. National Research Council was restructured and no longer advocates basic scientific research. All Associate Committees were terminated and this deprive Canadian hydrology of its mooring. The situation was alleviated in 1993 when the Canadian Geophysical Union approved the creation of a Hydrology Section (HS). CRIPE followed as a committee of HS and continues to be active and highly successful. The networks of climatic and hydrometric stations had a different story. Many hydrometric and climatic stations were closed (Shiklomanov et al. 2002; Laudon et al. 2017) and some were contracted out to private business that lacked technical training. The loss of stations was particularly damaging in the far North where only a few stations served a vast domain. In addition to streamlining operations and personnel, government departments sought external funding by charging for the usage of data.

5. MATURING OF CRYOHYDROLOGY

Conditions improved after a decade. Upon arrival of the new millennium, cryohydrology was well established. A series of special issues in the *Hydrological Processes* journal traced the progress on topics related to, river ice, glaciers, frozen ground, wetlands, forests, floods, subsurface flow, statistics, and process-based modelling. Applied hydrology benefitted from northern resource development. Climate change and environmental challenges strengthened cryohydrological investigations. For a decade until 2016, however, a dark shadow fell upon many federal government scientists who were not able to freely express their views, especially those pertaining to climate change and its environmental and ecosystem impacts.

Funding for hydrological research, like other branches of science and engineering, began to support large collaborative projects, with partnership among universities and participation from government and private sectors. Projects with a significant cryohydrological component have been highly successful. They include the Mackenzie GEWEX Study (MAGS, 1996-2005; see Woo 2008), Improved Processes and Parameterization for Prediction in Cold Regions (IP3, 2006-10), and Changing Cold Regions Network (CCRN, 2013-18) and Global Water Futures (GWF, 2018-). Nevertheless, the principal granting council for university research, NSERC, has to balance between assisting collaborative and individual projects, the latter having provided the thrust for many cryohydrological investigations in the last 50 years.

6. FINAL REMARKS

In 1988, Vit Klemeš, a prominent Canadian hydrologist of international standing, lamented that “hydrology is regarded mostly as a technological discipline rather than a science; this attitude is responsible for much bad science in hydrology which, in turn, has led to much bad technology in applied disciplines”. By now, thirty years later, this situation is fortunately remedied in Canadian cryohydrology.

Advances in cryohydrology strengthens our understanding of fundamental cold region processes, which in turn enables us to better confront the growing societal needs for reliable and clean water, to provide improved knowledge in support of resource development in remote areas, and to enhance the assessment of hazards to the northern environment, its ecosystem and livelihood under climate change that is projected to be particularly intense in Canada and in other world northern regions.

In memory of my late friends for having contributed to Canadian cryohydrology:

Peter Adams, Graham Cogley, Sylvia Edlund, Larry Gerard, Don Gray, Ric Janowicz, Rolf Kellerhals, Fritz Koerner, Don Mackay, Ross Mackay, Brian McCann, Dave Milburn, Ric Soulis

REFERENCES

- Beltaos, S. & Burrell, B.C. 2015 Hydrotechnical advances in Canadian river ice and engineering during the past 35 years. *Can. J. Civil Engineering* 42, 583-591.
- Bruce, J.P. & Clark, R.H. 1966 *Introduction to Hydrometeorology*. Pergamon Pr., Oxford, 334 pp.
- Chow, V.T. 1964 *Handbook of Applied Hydrology*. McGraw-Hill, New York.
- Gray, D.M. 1970 *Handbook on the Principles of Hydrology*. Canadian National Committee for the International Hydrological Decade, National Research Council of Canada, Ottawa.

- Hardy, J.P., Pomeroy, J.W., Moore, R.D. & Woo, M.K. (Guest Editors) 2001 Special Issue: Eastern Snow Conference / CGU-Hydrology Section 2001 Meeting. *Hydrol. Proc.* 15, 3327-3327.
- Hydrological Atlas of Canada*. 1978 Ministry of Supply and Services, Ottawa.
- Klemeš, V. 1988 A hydrological perspective. *J. Hydrol.* 100, 3-28.
- Laudon, H., Spence, C., Buttle, J., Carey, S.K., McDonnell, J.J., McNamara, J.P., Soulsby, C. & Tetzlaff, D. 2017 Save northern high-latitude catchments. *Nature Geoscience* 10, 324-325.
- Linsley, R.K., Kohler, M.A. & Paulhus, J.L.H. 1958 *Hydrology for Engineers*. McGraw-Hill, New York, 482 pp.
- Shiklomanov, A.I., Lammers, R.B. & Vorosmarty, C.J. 2002. Widespread decline in hydrological monitoring threatens pan-arctic research. *EOS* 83(2), pp. 13, 16-17.
- Swanson, R.H., Dickinson, W.T. & Young, G.J. 1988 Canadian research basins, in review. *Proceedings Canadian Hydrology Symposium No. 17. Canadian Research Basins: Successes, Failures and Future*. Associate Committee on Hydrology, National Research Council of Canada, Ottawa. 3-12.
- Woo, M.K. 2008 *Cold Region Atmospheric and Hydrologic Studies: the Mackenzie GEWEX Experience, Vols. 1 and 2*. Springer, Berlin.
- Woo, M.K. 2012 *Permafrost Hydrology*. Springer, Heidelberg. 563 pp.

Impact of Dust on the Local Hydrology of Arctic Landscapes

Kathy L. Young^{1*}, Harold-A. Scheffel¹, and Elizabeth A. Perera¹

¹*Geography Department, York University, Toronto, Ontario, M3J 1P3, CANADA*

**Corresponding author's email address:klyoung@yorku.ca*

ABSTRACT

Studies have examined the role of dust on terrestrial and mountainous snowcovers, and glaciers through the melt-albedo feedback, while others have investigated the role of dust on vegetation growing along northern roads in Alaska. In this study we consider the impact of dust, including tephra, on the local hydrology of northern landscapes, drawing upon recent scientific literature and our high arctic field studies at Polar Bear Pass (PBP), Bathurst Island and from Iceland, a low arctic region. The paper will first highlight the source areas for dust and tephra for northern landscapes and its ensuing effects on snowmelt timing, groundwater recharge, and sandur-wetland water levels. We also examine how dust modifies surface temperature and infiltration across hillslope catchments, including small, drained patchy wetlands in Iceland. Glacial outwash plains continue to be critical sources for local dust. At PBP, sediment erosion from the plateau predominates during the spring-summer period (snowmelt season). In Iceland, presence of tephra (volcanic ash and dust) can modify infiltration rates and soil moisture levels, while dust storms can trigger small jökulhlaups raising water levels in glacial rivers, outwash plains, and adjoining wetlands. We were not able establish any definitive impact of dust on groundwater recharge in rising lava pits (depressions). This paper contributes to ongoing discussions of how northern landscapes and their hydrology are being transformed in response to triggers of climate change.

KEYWORDS

Dust; Infiltration; Sandur, Snow ablation; Streamflow, Volcanic ash, Wetlands

1. INTRODUCTION

Recently, there are several studies detailing the impacts of tephra (volcanic ash), including mineral dust (< 20 µm-Groot Zwaafink *et al.* 2016), on arctic landscapes (e.g., Arnalds, 2013; Ágústssdóttir, 2015; Arnalds *et al.* 2016a; Anderson *et al.* 2017; Bullard & Mockford, 2018; Skiles *et al.* 2018; Vincent, 2018). Due to climate warming, there will be a reduction in terrestrial ice masses and an increase in suitable sediment for the aeolian system. Aside from Iceland, there are few key studies that look at the long-term variation in the magnitude and frequency of dust events (Bullard & Mockford, 2018). In Iceland, the dire consequences of volcanic ash and dust on the environment were highlighted to the rest of the world during the eruption of Eyjafjallajökull in 2010, which lasted 39 days. Fine volcanic ash brought countless flights to a stand-still, stranding millions of people and impacting global economies to the tune of \$1.7 billion (Arnalds, 2013). Another volcano, Grimsvötn, erupted in spring, 2011, and it produced more European tephra fallout in the first 24 hours than occurred during the entire Eyjafjallajökull event. Overall the bulk volume of tephra was 2-3 times greater for the Grimsvötn eruption, but due to the shorter duration and absence of strong upper atmospheric winds, the dispersal of tephra at the global scale observed in 2010 was prevented (Ágústssdóttir, 2015). Its impact (coarser ash) was felt locally along the southern coast of Iceland and into the interior uplands. Arnalds (2010) and Arnalds *et al.* (2016a)

provide exceptional details on the distribution of tephra (volcanic ash and dust) across Iceland, its impact on soils, near-by glaciers, and the occurrence and reoccurrence of dust storms and clouds from sandy deserts including large gravelly, outwash plains (sandur-pl. sandar). For instance, Skeiðarásandur is the largest plain sandur in the world (1000 km² in area – Marren, 2002) and lies in SE Iceland. The occurrence and persistence of severe weather (especially strong winds in Iceland) due to frequent low-pressure systems help to continually erode and transfer sediments from these barren areas onto the surrounding landscape. Several studies indicate that this sediment can lower the albedo on Iceland glaciers, thereby enhancing snowmelt, which in turn affects their mass balance and leads to sea level rise (Whittmann *et al.* 2017; Skiles *et al.* 2018). Only 27% of Iceland remains vegetated and natural forests cover about 1.2% of the total areas. In addition to the hazards of volcanic ash and dust storms, large tracks of ground are devoid of vegetation, especially in the interior (the highlands. Presently, dust deposition in Iceland is estimated to have an influence over an area greater than 500,000 km² (Arnalds *et al.* 2013; Dagsson-Waldhauserova *et al.* 2013, 2014).

In Greenland, recent aeolian studies (Anderson *et al.* 2017) have documented how wind transfers dust from barren glacial flood plains onto the lower elevations of glacial margins. Dust storms can reach several hundred meters above the sandur plain, and dust deposited on the glacier surfaces serves to lower the surface albedo, enhancing ablation-cryoconite holes, dirty ice, and ice algae (biological hot spots) (Anderson *et al.* 2017). The wind threshold for erosion (saltation) to take place appears to be >5 m/s (Heldmann *et al.* 2012), though Bullard and Mockford (2018) indicate that the threshold for aeolian sediment transport is 6 m/s in Greenland.

In Arctic Canada, previous detailed aeolian studies have been conducted on a Baffin Island sandur near Pangnirtung (~ 66.2°N, 65.7°W). These studies by Church (1972), Gilbert (1983), McKenna-Neuman (1990a, b; 1993), and McKenna-Neuman & Gilbert (1986) indicated that, like Iceland and Greenland, strong seasonal winds together with little snow cover can loosen soil grains through sublimation and allow sediments to be eroded and carried. Occasionally, a single sediment layer can occur on the seasonal snowpack, and in other instances, the snowpack is characterized by layers of sediment, indicating strong winds and soil erosion throughout the long arctic winter, processes similar to those found in Antarctica in the Dry Valley (Heldmann *et al.* 2012). Other studies in Canada's High Arctic have observed similar processes (e.g., Lewkowicz & Young, 1991; Lewkowicz, 1998; Woo *et al.* 1991). Woo & Dubreuil (1985) examined the impact of dust on surface reflectivity. They showed that winter snowpacks near airports with gravel road-ways tended to have dark surfaces (low albedo) and the snowpacks disappear quite quickly in these areas compared to the surrounding watershed, a process documented by others (e.g., Heldmann *et al.* 2012-Dry Valley, Antarctica, Skiles *et al.* 2018-Alaskan glaciers). In fact, Skiles *et al.* (2018) indicated that dust is much more effective in enhancing absorption of solar radiation than black carbon in the visible range. Still others have shown that sediments blown onto spring snow surfaces can cause snow ramparts (an insulation effect), changing the surface roughness of the snowpack, thereby enhancing turbulent transfers and ablation (Lewkowicz & Young 1991). Melt-out of snow can leave sediment draped over arctic slopes, changing their slope micro-topography (small earth hummocks-Lewkowicz & Guðjonsson, 1992), or sediments can become incorporated into the vegetation or be replaced by new plants. Others have indicated that given time, large bodies of deep snow by aeolian material may become incorporated into permafrost (e.g., Woo *et al.* 1991; Heldmann *et al.* 2012).

In this paper, we contribute to our understanding of dust effects on northern hydrology by examining the role of dust on the local hydrology of two arctic locations where we have recently been conducting field studies – Polar Bear Pass (PBP), Bathurst Island, Canada and Southern Iceland. Specifically, these field studies together with relevant literature will explore the impact of tephra and dust on local snowcover melt patterns, groundwater resources, soil infiltration, surficial thermal conditions, and sandur-wetland water dynamics.

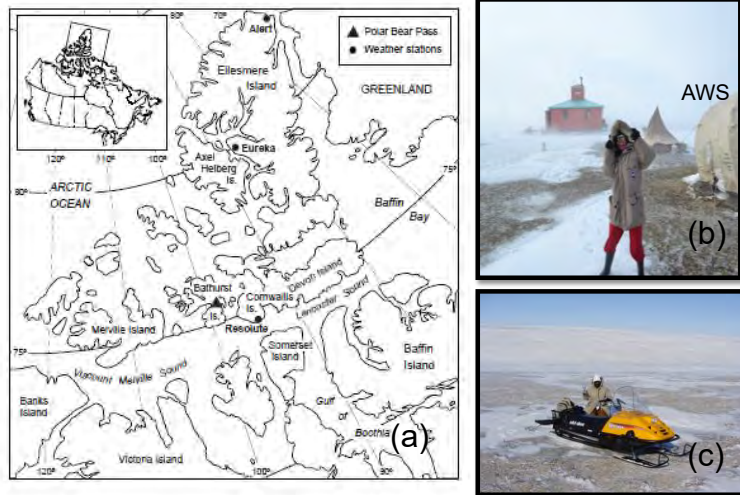


Figure 1. (a) Location of Polar Bear Pass (PBP) in the Canadian High Arctic; (b) the gravelly substrate, patchy snow cover, and windy conditions of the plateau June 18, 2013; and (c), the late-lying snowbed and dusty snowcover of the wetland, May 23, 2009. The location of the plateau AWS location is labeled

2. STUDY AREAS

2.1 Polar Bear Pass, Nunavut & South-East Iceland

Figure 1 indicates the location of Polar Bear Pass (PBP) in the Canadian High Arctic and study sites in Southern Iceland (Figure 2). PBP, a large, low-gradient wetland, is located in the middle of Bathurst Island (75° 40'N, 98° 30'W). The Pass is about 20 km long and 5 km wide and it is bordered by two large hills with elevations up to 250 meters above sea level. Extensive late-lying snowbeds often form in the lee of hillslopes, while polar-desert plateau areas are sparsely vegetated (Figures 1b, c). The area is underlain by continuous permafrost and active layers are generally shallow in the

wetland 0.5-0.75 m but can reach deeper depths in gravelly zones (> 1m). Enhanced site details concerning the wetland and uplands at PBP can be found elsewhere (e.g., Young *et al.* 2018; Young, 2019).

Study sites in Iceland which pertain to this investigation include the hillslope area Fimmvörðuháls (516 m a.s.l.) just east of Eyjafjallajökull (63°36'N 19°25'W), a lava rise pit (depression) (63.9°N, 17.7°W) and sandur-wetland area in SE Island (63°55'N, 17°41'W), near the glacial margin of Vatnajökull about 17 km from Grimsövn (Figure 2) (Scheffel, 2018). A small, drained patchy wetland site (Figure 2f) near Kirkjubæjarklaustur (63° 50'N, 18°02' W) was also chosen due its receipt of frequent ash inputs from Grimsövn (see Perera & Young, 2019). Iceland is near the boundary between the mid-latitude westerlies and the polar easterlies; cyclones pass frequently, and shifts between frost and thaw are common. The mean annual range of precipitation is 400-2000 mm. The mean annual range of temperature is 2-6°C, with the mean July range being 6-10°C (Ágústsdóttir, 2015). The southern coast routinely receives heavy rainfall, reaching 1500 mm/year, while the interior upland is much drier (Ágústsdóttir, 2015). The study sites likely do not contain permafrost, though patches of sporadic permafrost can occur in the uplands and interior.

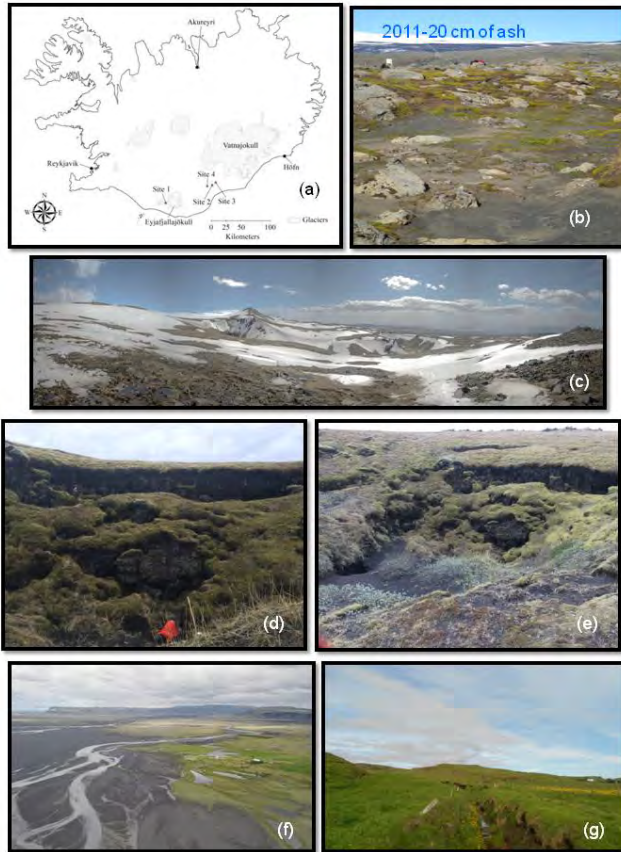


Figure 2. (a) General map of Iceland showing the study locations: 1=upland hillslope; 2=lava rise pit, 3=sandur-wetland, and 4=drained, patchy wetland; (b-c) are photographs of the upland site including ash thickness in 2011; (d-e) are photographs of the lava rise pit taken May, 2015. The depth of the pit is about 6.5 m. The distribution of ash and plant cover in the pit are also shown; (f) aerial view of the sandur-wetland area, June 2016; and (g) is a drained, small, patchy wetland near Prestbakki, Iceland, June, 2018.

3. METHODOLOGY

3.1 Canadian High Arctic – Polar Bear Pass

Young *et al.* (2018) showed how the distribution of snowcover differed from the northern part of the pass (southern aspect) to the southern part (northern aspect), and the effect that this had on both snowmelt and the streamflow regime (Young, 2019). Seasonal winds blow predominantly from the northern sector here (Young & Labine, 2010), and in low snow years (2009) sediments can be eroded from the upper polar desert plateau onto the late-lying snowbed and adjoining wetland enhancing melt, but not in years when the plateau has a deeper snowpack (2010) (Young *et al.* 2013). Here, we investigate the seasonality of dust emissions by identifying the timing and frequency of surficial erosion on the plateau at PBP. Earlier studies in the High Arctic have demonstrated that aeolian processes happen year round (Fosheim Peninsula-Woo *et al.* 1991), while others show that it typically occurs during the spring-summer season (Melville Island-Lewkowitz & Young, 1991). Bullard & Mockford (2018) indicate that dust inputs to soils and water bodies can have substantial ecological impacts. An automatic weather station (AWS) was established at PBP on the plateau near the

main cabin in the early 1980's and the climate data (e.g. radiation, temperature, wind) were used for ecological studies. Instruments were updated in 2006 and 2011-2012, and a tipping-bucket rain gauge and an external Campbell Scientific camera were added in 2011. Complete details on the instrumentation can be found in Young *et al.* 2018. These continuous climate data have been quality checked since 2006. Recent dust studies in high latitudes show that the threshold speed for saltation ranges from about 5 to 6 m/s at 10 m (Crusius *et al.* 2011; Heldmann *et al.* 2012; Bullard & Mockford, 2018). There is of course always a need to consider other controls on dust emission beside the wind regime, which can include surface soil moisture, snow cover, and sediment supply. The threshold for aeolian sediment transport can also be moderated by temperatures and humidity (Bullard & Mockford, 2018). For instance, Bullard & Mockford (2018) found that if soils are moist, speeds required for saltation can approach 10.3 m/s.

In this study, we specifically use the daily windspeed/direction data (height=4 m) and consider snow sensor depth information from 2007-2013 – years when we were in the field. To be compatible with other studies, the wind speeds were adjusted to a height of 10 m assuming a z_0 of 0.001 m (Oke, 1987). Analyzing the climate data, we determined the number of days when the windspeed was > 6 m/s and was blowing from NW to NE. We also considered days when the snowcover was less than 5 mm on the plateau. The time periods examined were from January to May (winter to early spring); June to August (late spring to summer) and September to December (early fall to early winter).

3.2 Iceland-Southern Coast

In 2015, as part of a hillslope catchment study, small infiltration studies employing double-ring infiltrometers were conducted on hillslope materials near the site of the Eyjafjallajökull eruption in 2009. In June 2018, infiltration studies were also performed in a series of small, drained, patchy wetlands (< 1 hectares) showing varying thicknesses of tephra layers, indicative of volcanic activity. These small wetlands were drained after World War II to increase food supply in Iceland, but now many are abandoned and little is known of their hydrology. Although guidelines exist to protect large wetlands (> 3 hectares) from development, 55% of undisturbed wetlands (~30% of which are < 1 hectare) are still unprotected, despite the view that all wetlands in Iceland, including the small, drained wetlands, are critical habitats for native and migratory birds (Arnalds *et al.* 2016b; Perera & Young, 2019).

Groundwater is an essential source of household and industrial water in Nordic countries. In Iceland, 95% of household water is sourced from groundwater (Kløve *et al.* 2017). On the SE coast, we were interested to know how volcanic ash impacted the Eldhraun (Laki) lava field (562 km²) (Ágústsdóttir, 2015), which is an important recharge/discharge area for groundwater. In August 2014 we selected a lava rise pit (see Guilbaud *et al.* 2005) to explore the effect of ash on groundwater. This incised depression, like others in the area, acts as a sediment trap during wind storms. Others have documented glacio-aeolian sediment in lava depressions such as lava tubes (see Kiernan *et al.* 2003). We measured water level at the bottom of the site with a Hobo pressure transducer (± 3 mm). A Hobo temperature ($\pm 0.5^\circ\text{C}$) and light sensor and a series of copper-constantan thermocouples ($\pm 0.5^\circ\text{C}$) monitored the air and near-surface thermal regime. The light sensor measured light intensity in Lux and was converted into W/m^2 using the conversion $0.0079 \text{ W}/\text{m}^2$ per Lux for visible sunlight. Daily precipitation (mm) was monitored with a Hobo tipping-bucket raingauge (± 0.1 mm). A vegetation survey and limited volumetric soil moisture measurements (0-15 cm) with a Theta soil moisture probe were also made.

In 2015-2016 we examined water level dynamics across a sandur-wetland boundary at the Hvoll farm (located about 17 km to the east of Kirkjubæjarklaustur). Here, we consider only the role of a dust storm in triggering water level rise. Transects of groundwater wells were installed across the sandur and wetland. Continuous water level measurements were made with Hobo pressure transducers and verified with regular spot water level measurements. The Iceland Meteorological Office (IMO) provided both climate and hydrometric data, including water levels and conductivity of nearby glacial streams. Further details can be found in Scheffel (2018).

4. RESULTS AND DISCUSSION

4.1 Frequency of Aeolian Erosion-Polar Bear Pass

There have been numerous studies that document the role of dust and volcanic ash on the albedo and its impact on snowmelt (e.g., Woo & Dubreuil, 1985; Heldmann *et al.* 2012 and Skiles *et al.* 2018). Our recent studies at Polar Bear Pass (Young *et al.* 2018; Young, 2019) reveal the interactive role of aspect, wind (direction+speed), and dust on the snowmelt and streamflow pattern out of the wetland. The prevailing winds at PBP erode sediments from the plateau during snowmelt (often June

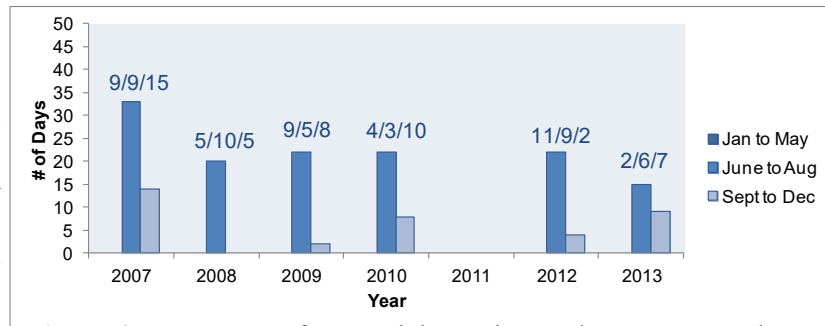


Figure 3. Frequency of ‘potential’ erosion, Polar Bear Pass plateau (2007 to 2013). Note data is missing for 2011 due to datalogger errors. Numbers on top of June to Aug bars refer to the number of occurrences in months June, July and August. For instance in 2007, there were 9 days in June, 9 days in July and 15 days in August when conditions were favourable for erosion (i.e., winds blew from the northern sector (NW to NE), wind speed at 10 m was > 6 m/s, and snowcover < 5 mm).

and July) and transport sediment onto the late-lying snowbed and adjoining wetland. These areas (south-facing) melt-out first (Young *et al.* 2018) and in most years the first pulse of streamflow is due to these meltwaters. The cleaner snow on the southern edge of the Pass melts out later, contributing to the second pulse of streamflow peaks (Young, 2019). Figure 3 validates this pattern as the highest episodes of erosion occur during the spring-summer period. The timing of dust is important (Painter *et al.* 2012; Bullard & Mockford, 2018), as dust deposition during spring and summer can accelerate snowmelt, while winter dust will usually become covered by more snow. However, Walker & Everett (1987) found that a winter dust fall can have major ecological effects along Alaskan roads, especially during the early phase of melt-off.

4.2 Impact of Volcanic Ash on Infiltration

4.2.1 Hillslope catchment

In this catchment we evaluated the infiltration response of low arctic soils impacted by volcanic ash using a double-ring infiltrometer. Vegetation cover in the basin is predominantly short grass with some mossy-grassy hummocks. Bare ash patches often crawl over vegetation via aeolian processes and when dirty snow melts out. Our field observations indicate that during high wind storms hummocky patches often intercept windblown ash, while stretches of ground vegetation can be stripped away, leading to water ponding during precipitation events. Non-ash,

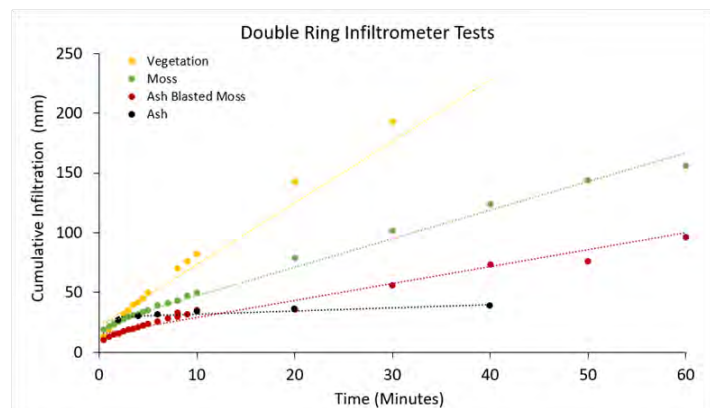


Figure 4. Double-ring infiltrometer tests over surficial material types, which were representative of the upland hillslope catchment near Eyjafjallajökull, June 2016.

vegetated surfaces show the greatest infiltration rates in contrast to ash surfaces (Figure 4.0). The fine texture of ash seals the ground surface, inhibiting drainage, often creating water ponding (e.g., Mallik, 1984; Scheffel, 2018).

4.2.2 Small, drained patchy wetland

At Prestbakki, infiltration rates in the patchy wetland adjacent to a drainage ditch ranged from 80 mm/hr to 340 mm/hr as ponded water in the centre of the wetland patch precluded measurements. April and May are generally dry months in Iceland but in 2018 rainfall across Iceland was exceptionally high (~129 mm – Reykjavik). However, these infiltration rates and cumulative totals

fell within the range found for volcanic soils near Selfoss (Orradottir *et al.* 2008), at the wetland-sandur complex at Hvoll (Scheffel, 2018), and for peaty soils at the Agricultural University of Iceland, NW Iceland (see Figure 5a). Tephra occurred in the top 0.15 m soil horizons along with organic material and dominated at a depth of 0.16-0.2 m to 0.4-0.55 m (presence at lower depth seen in Figure 5b). Tephra volumetric soil moisture content ranged from 63%-100%, which was generally lower than most surface soil measurements (0-15 cm) taken inwards along transects 15 m from the ditch. Soil pits with a tephra presence showed more variation in soil moisture than the NW site, which had peat soils and did not have any tephra horizons (Figure 5c).

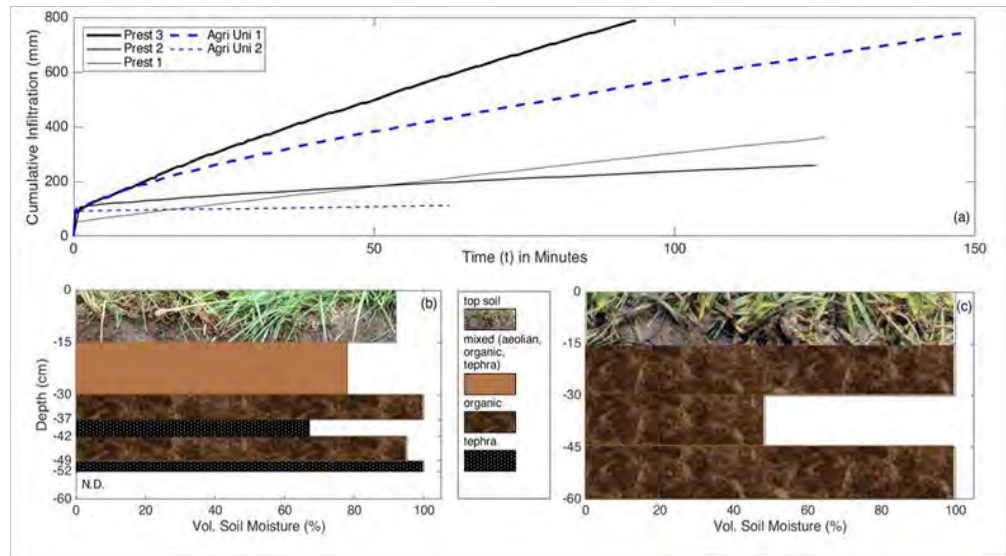


Figure 5. (a) Cumulative infiltration shown at Prestbakki near Grimsvötn – 3 trials: Prest 1-3 (solid lines) and at the Agricultural University of Iceland, NW Iceland-2 trials: Agri Uni 1-2 (dashed lines). Soil pit horizons and volumetric soil moisture at Prestbakki (b) and Agricultural University of Iceland, NW Iceland (c). N.D. indicates no data for that layer.

4.3 Impact of a Dust Storm on the Water Levels (Sandur, Wetland)

(1) Throughout the summer of 2016, we observed several dust events at the sandur-wetland field site. One severe wind event occurred on June 19 – 20 after a drought of 14 days. Spot wind gusts ($n = 4$) reached over 22 m/s and dust devils were observed picking up glacial flour and fine sediments from the sandur. Visibility was poor and a thick yellow tainted cloud of fine particles rising ca. 250 m above the ground blew north towards the Sidhujökull and Vatnajökull glaciers. Water tables rose on June 20, 2016 (1900h) as a result of ‘rapid’ glacial melt. The skies were partially cloudy and air temperatures were warm ($>24^{\circ}\text{C}$) (Figure 6). Glacial meltwater discharge likely increased as a result of the dust lowering the Sidhujökull glacier’s albedo, enhancing Q^* receipt, while the warm air temperatures and windy conditions would have enhanced sensible heat exchange. Elevated discharge along the Brunná River lowered the water conductivity on June 20 (40 to 25 $\mu\text{S}/\text{cm}$), but then it rose back up to 50 $\mu\text{S}/\text{cm}$ once the flood had passed. Another severe

wind event occurred on August 7, 2016 with wind gusts reaching 25 m/s at Hvoll and 19 m/s at Höfn (data not shown). However, previously wet conditions over the sandur prevented fine materials from becoming suspended. Others have remarked on the effect of dust storms on the surrounding landscape in Iceland (Arnalds *et al.* 2016a). Dust storms are generally quite frequent in Iceland, which experiences between 34 to 135 days with dust storms annually (Arnalds *et al.* 2016a). These frequencies are similar to values found in Mongolia, Iran, and major deserts around the world (Dagsson-Waldhauserova *et al.* 2014).

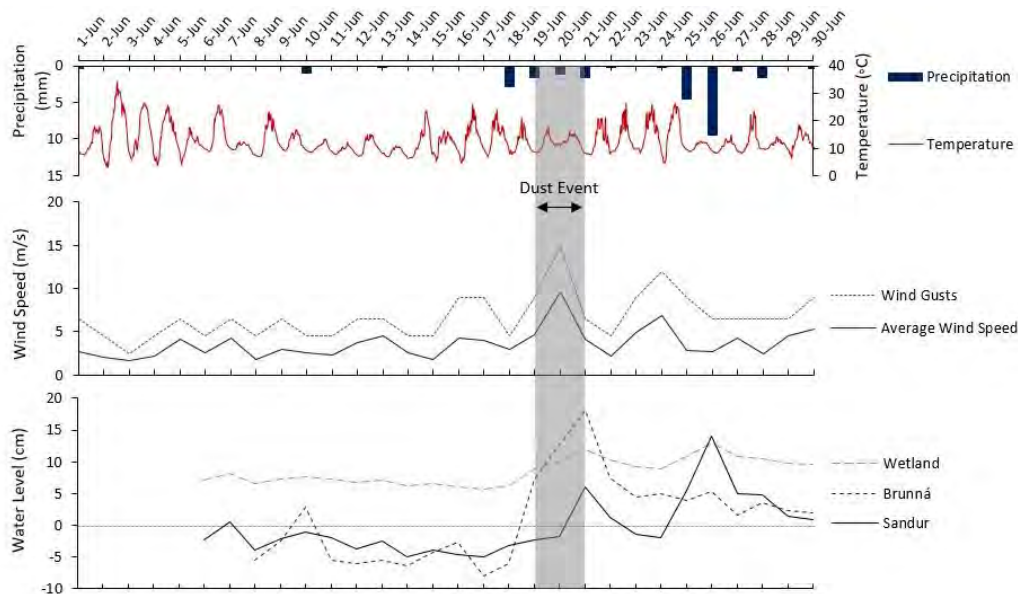


Figure 6. Rise of water levels in the Brunná River, sandur and adjoining wetland at Hvoll in June, 2016 in response to a dust event, which triggered a small jökulhlaup (glacial outwash flood).

4.4 Volcanic Ash on Surfaces - Lava Rise Pit ('depression')

Water levels at the bottom of the lava rise pit fluctuated from 0 to 11 mm but they were not in sync with rainfall inputs, which might indicate rapid drainage in this karst-like landscape even during heavy or prolonged rainstorms (see Hartmann *et al.* 2017) (Figure 7). The slight increase in water level over the summer season suggests that elevated air temperatures probably melted some of the ashy snow buried in deep cracks and crevices. Dripping icicles and ice melt from sheltered walls in May 2015 confirmed other sources of water seeping into these porous features.

While it was difficult to directly tie the impact of ash and dust on groundwater dynamics in the lava pit, the occurrence of bare ash or ash mixed with some vegetation in the pit was critical in raising surface temperatures (Figures 8, 9). Others have also documented the impact of ash on vegetation (Walker & Everett, 1987; Ágústsdóttir, 2015). Large tephra events can leave behind barren and sterile surfaces that might require decades or even centuries of natural primary succession to restore. They can damage vegetation by direct burial, heat, or breakage; inhibit photosynthesis; and modify water budgets, by altering drought, surface flow, or water logging episodes. Wind erosion with tephra-laden air causes abrasion and desiccation and uncovers plant roots, as well as reducing the soil depth (Ágústsdóttir, 2015). Cryptograms (moss) are heavily impacted by dust/ash blankets. Most are affected by desiccation and in some cases the smothering can eliminate them (Walker & Everett, 1987).

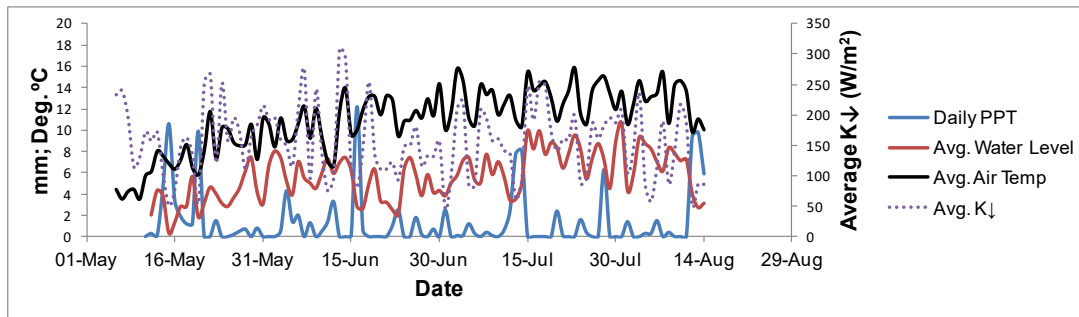


Figure 7. Groundwater level (mm) in the lava rise pit (depression) in response to daily rainfall (mm), average air temperature (°C) and incoming solar radiation (W/m²). Total rainfall over the season was 134 mm.

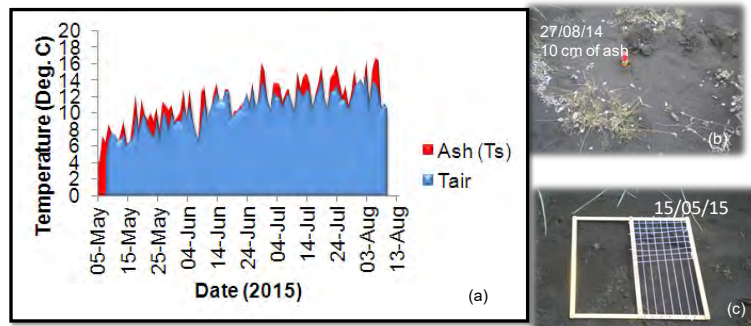


Figure 8. (a) Surface temperature of bare ash in the lava rise pit (depression). Photos (b) and (c) provide indications of ash thickness and use of the plant quadrat in the site.

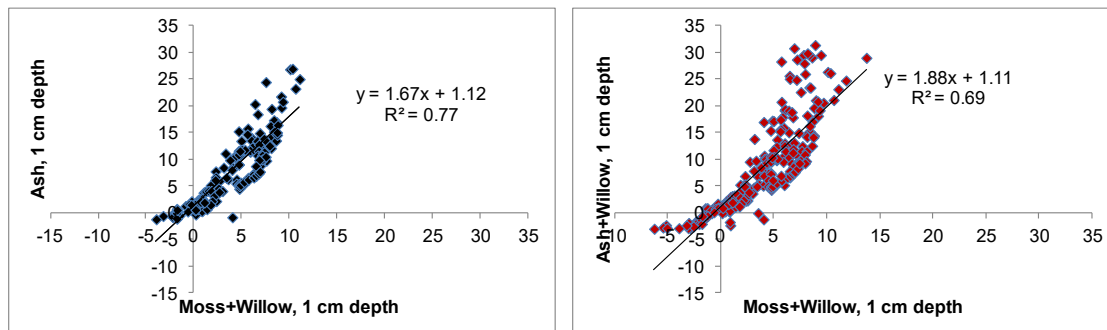


Figure 9. Diagram showing the role of ash in raising surface temperatures in vegetated areas: (a) ash versus (no ash)-moss+willow location; and (b) ash+willow versus (no ash)-moss+willow.

4.5 Climate Change – Hydrology Expectations for Arctic Landscapes

Arctic ecosystems have undergone major changes over the past century (Hinzman *et al.* 2013) and much of the change is driven by higher temperatures. This warming is enhanced relative to lower latitudes (Anderson *et al.* 2017) but other stressors exist including dust. As the climate warms and glaciers retreat, outwash plains will increase in size as will the availability of windblown sediments (fine sands) (Heldmann *et al.* 2012). Increasing amounts of impurities in Arctic snow have been suggested to originate from local sources. Earlier melt of the seasonal snow cover may thus affect dust mobilization and subsequently snow and ice albedo, which is important for snow ablation. For

instance, small decreases in fresh snow albedo of 1% can lead to surface mass losses of 27 GT/yr from the Greenland ice sheet (Groot Zwaaftink *et al.* 2016).

Changes in volcanic activity are expected in Iceland (Ágústsdóttir, 2015). Volcanism in Iceland has a marked periodicity and this factor together with climatic change and reduced surface pressure from melting glaciers (isostatic rebound-Compton *et al.* 2015) implies renewed activity. Specifically, there is an increased probability of activity in the East Iceland volcanic zone, where 80% of all historical eruptions have occurred and where four of the most active volcanoes are located. An eruption can be expected every 2-7 years at Grimsvötn, with parallel activity in nearby Barðabunga (Ágústsdóttir, 2015).

5. CONCLUSIONS

- (1) Local dust in arctic catchments can enhance snow ablation. At Polar Bear Pass, Bathurst Island, a transfer of dust and sediments from the plateau onto the wetland occurs predominantly in the spring-summer period;
- (2) Volcanic ash and ensuing dust storms play a role in the local hydrology of small, low arctic catchments. It can impact infiltration of water in ashy-covered hillslope landscapes potentially causing ponding and overland flow. Multiple tephra layers in patchy, drained wetlands can modify soil moisture levels but our limited experiments suggest that infiltration rates remain little changed from organic soils, especially during rainy seasons. Dust can lead to modest glacial jökulhlaups inundating both downstream sandar and raising water levels in adjoining wetlands;
- (3) Future climate warming in arctic landscapes will lead to longer thaw seasons, and sediments available for erosion, especially from glacial catchments. Volcanic eruptions may become more frequent in Iceland due to glacial retreat (isostatic rebound), ultimately leading to enhanced frequency of dust storms and disruption to landscape hydrological processes.

ACKNOWLEDGEMENTS

Over the years our research in the Canadian High Arctic has been supported by the Polar Continental Shelf Program (PCSP), Natural Science & Engineering Research Council (NSERC), ArcticNet and Government of Canada Northern Student Training Program (NSTP). In Iceland, our research over the years has been supported by York University, NSTP, MITAC (travel grant to H-A. Scheffel), American-Scandinavian Foundation (ASF) and Society of Wetland Scientists (SWS) (travel grants to E.A. Perera). We are indebted to Drs. Ólafur Arnalds, Hlynur Óskarsson and Sigmundur Brink, Agricultural University of Iceland for their assistance in 2018 (site selection) and for allowing us to store soil samples at their university facility prior to shipment to Canada. We would especially like to thank Kristinn Guðjónsson, Borgarholtskóla who over the years remains a treasured friend, along with his wife Helga always providing good advice, logistical support, and valuable help in the field.

REFERENCES

- Ágústsdóttir, A.M. 2015 Ecosystem approach for natural hazard mitigation of volcanic tephra in Iceland: building resilience and sustainability. *Nat. Hazards* 78, 1669-1691.
- Anderson, N.J., Saros, J.E., Bullard, J.E., Cahoon, S. M.P., McGowan, S., Bagshaw, E.A. *et al.*

- 2017 The Arctic in the 21st century: Changing biogeochemical linkages across a paraglacial landscape of Greenland. *BioScience*, 67(2), 118-133.
- Arnalds, Ó. 2010 Dust sources and deposition of aeolian materials in Iceland. *Icel. Agric. Sci.* 23, 3-21.
- Arnalds, Ó. 2013 The influence of volcanic tephra (Ash) on ecosystems. *Adv. in Agron.*, 21, 331-380.
- Arnalds, Ó., Dagsson-Waldhauserova, P. & Olafsson, H. 2016a The Icelandic volcanic Aeolian environment: Processes and impacts – A review. *Aeolian Res.* 20, 176-195.
- Arnalds, Ó., Guðmundsson, J., Oskarsson, H., Brink, S. & Gisladóttir, F. 2016b Icelandic inland wetlands: characteristics and extent of draining. *Wetlands*, 36(4), 759-769.
- Bullard, J.E. & Mockford, T. 2018 Seasonal and decadal variability of dust contributions in the Kangerlussuaq area, West Greenland. *Arctic, Antarct. & Alpine Res.* 50 (1), S10011, doi: 10.1080/15230430.2017.145854.
- Church, M. 1972 Baffin Island sandar: a study of arctic fluvial processes. *Geol. Survey of Can. Bull.* 216, 1-208.
- Compton, K., Bennett, R.A. & Hreinsdóttir, S. 2015 Climate-driven vertical acceleration of Icelandic crust measured by continuous GPS geodesy. *Geophys. Res. Lett.* 42, 743-750.
- Crusius, J., Schroth, A.W., Gasso, S., Moy, C.M., Levy, R.C. & Gatica, M. 2011 Glacial flour dust storms in the Gulf of Alaska: Hydrologic and meteorological controls and their importance as a source of bioavailable iron. *Geophys. Res. Lett.* 38, L06602, doi:10.1029/2010GL046573.
- Dagsson-Waldhauserova, P., Arnalds, O. & Ólafsson, H. 2013 Long-term frequency and characteristics of dust storm events in Northeast Iceland (1949–2011). *Atmos. Environ.* 77, 117-127.
- Dagsson-Waldhauserova, P. Arnalds, O. & Ólafsson, H. 2014 Long-term variability of dust events in Iceland (1949–2011). *Atmos. Chem. and Phys.* 14(24), 13411-13422.
- Gilbert, R. 1983 Sedimentary processes of Canadian arctic fjords. *Sediment. Geol.* 36, 147-175.
- Groot Zwaafink, C.D., Grythe, H., Skov H., & Stohl, A. 2016 Substantial contribution of northern high-latitude sources to mineral dust in the Arctic. *J. Geophys. Res. Atmos.* 121(13), 678-697.
- Guilbaud, M.-N., Self, S., Thordarson, T. & Blake, S. 2005 Morphology, surface structures, and emplacement of lavas produced by Laki, AD 1783–1784. *Geol. Soc. of Amer. Spec. Papers*, 396, 81-102.
- Hartmann, A., Gleeson, T., Wada, Y. & Wagener, T. 2017 Enhanced groundwater recharge rates and altered recharge sensitivity to climate variability through subsurface heterogeneity. *PNAS*, 114(11), 2842-2847.
- Heldmann, J., Marinova, M., Williams, K., Lacelle, D., Mckay, C., Davila, A. *et al.* 2012 Formation and evolution of buried snowpack deposits in Pearse Valley, Antarctica, and implications for Mars. *Antarct. Sci.* 24(3), 299-316.
- Hinzman, L.D., Deal C.J., McGuire, A.D., Mernild, S.H., Polyakov, I.V. & Walsh, J.E. 2013 Trajectory of the Arctic as an integrated system. *Ecol. Appl.* 23, 1837–1868.
- Kiernan, K., Wood, C. & Middleton, G. 2003 Aquifer structure and contamination risk in lava flows: insights from Iceland and Australia. *Environ. Geol.* 43, 852-865.
- Kløve, B., Kvitsand, H.M.L., Pitkanen, T., Gunnarsdottir, M.J., Gaut, S., Gardarsson, S.M., Rossi, P.M. & Miettinen, I. 2017 Overview of groundwater sources and water-supply systems, and associated microbial pollution, in Finland, Norway and Iceland. *Hydrogeo. J.* 25, 1033-1044.
- Lewkowicz, A.G. 1998 Eolian sediment transport during winter, Black Top Creek, Fosheim Peninsula, Ellesmere Island, Canadian Arctic. *Perm. and Perigl. Process.* 9, 35–46.
- Lewkowicz, A. & Young, K.L. 1991 Observations of Aeolian transport and niveo-aeolian deposition at three lowland sites, Canadian Arctic Archipelago. *Perm. and Perigl. Process.* 2, 197-210.
- Lewkowicz, A.G. and Guðjonsson, K.A. 1992. Slope hummocks on Fosheim Peninsula,

- Northwest Territories. *Current Res., Part B, Geol. Surv. of Canada Paper* 92-1B, 97-102.
- Marren, P. M. 2002 Fluvial–lacustrine interaction on Skeiðarársandur, Iceland: Implications for sandur evolution. *Sedimen. Geol.* 149, 43–58.
- McKenna Neuman, C. 1990a Observations of winter aeolian transport and niveo-aeolian deposition at Crater lake, Pangnirtung Pass, N.W.T., Canada. *Perm. and Perigl. Process.* 1, 235-247.
- McKenna Neuman, C. 1990b Role of sublimation in particle supply for aeolian transport in cold environments. *Geog. Ann.* 72A, 329-335.
- McKenna Neuman, C. 1993 A review of aeolian transport in cold environments. *Prog. in Phys. Geog.* 17, 137-155.
- McKenna-Newman, C. & Gilbert, R. 1986 Aeolian processes and landforms in glaciofluvial environments of southeastern Baffin Island, N.W.T., Canada. In: Nickling, W.G. (ed.), *Aeolian Geomorphology*. The Binghampton Symposia in Geomorphology: International Series, no. 17, Allen and Unwin, Boston, pp 213-235.
- Oke, T.R. 1987 *Boundary Layer Climates* (2nd Edition). Routledge, Great Britain
- Orradottir, B., Archer, S.R., Arnolds, O., Wilding, L.P. & Thurow, T.L. 2008 Infiltration in Icelandic andisols: The role of vegetation and soil frost. *Arctic and Antarctic. and Alpine Res.* 40, 4012-4021.
- Painter, T.H., Bryant, A. & Skiles, S.M. 2012 Radiative forcing by light absorbing impurities in snow from MODIS surface reflectance data. *Geophys. Res. Lett.* 39 L17502, doi:10.1029/2012GL052457, 2012.
- Perera, E.A. & Young, K.L. 2019 Initial surface hydrology characteristics of Icelandic, drained, patchy wetlands. *Wetland Sci. & Practice*, April 2019, 83-90.
- Scheffel, H-A. 2018 *Hydrology of a Sandur-Wetland in a Volcanic Environment, Southeast Iceland*. Master's Thesis, Department of Geography, York University, Toronto, Ontario, Canada, unpublished.
- Skiles, S.M., Flanner, M., Cook, J.M., Dumont, M. & Painter, T.H. 2018. Radiative forcing by light-absorbing particles in snow. *Nat. Clim. Change* 8, 964-971.
- Vincent, 2018. The effect of arctic dust on the retrieval of satellite derived sea and ice surface temperatures. *Sci. Reports*, 2018, 8:9727. doi: 10.1038/451598-018-280-24.
- Walker, D.A. and Everett, K.R. 1987 Road dust and its environmental impact on Alaskan taiga and tundra. *Arctic & Alpine Res.* 19(4), 479-489.
- Whittmann, M., Groot-Zwaafink, C.D., Schmidt, L.S., Guðmundsson, S. Pálsson, F. & et al. 2017 Impact of dust deposition on the albedo of Vatnajökull ice cap, Iceland. *Cryosphere*, 11, 741-754.
- Woo, M.K. & Dubreuil, M-A. 1985 Empirical relationship between dust content and arctic snow albedo. *Cold Regions Sci. and Tech.* 10, 125-132.
- Woo, M.K., Edlund, S.A. & Young, K.L. 1991 Occurrence of early snow-free zones on Fosheim Peninsula, Ellesmere Island, N.W.T. *Current Res., Part B, Geol. Surv. of Canada Paper* 91-1B, 85-93.
- Young, K.L. 2019 Swings in runoff at Polar Bear Pass: an extensive low-gradient wetland, Bathurst Island, Canada. *Hydrol. Res.* 50(2), 778-792.
- Young, K.L. & Labine, C. 2010 Summer hydroclimatology of an extensive low-gradient wetland: Polar Bear Pass, Bathurst Island, Nunavut, Canada. *Hydrol. Res.* 41.6, 492-502.
- Young, K.L., Assini, J., Abnizova, A. & Miller, E. 2013 Snowcover and melt characteristics of upland/lowland terrain: Polar Bear Pass, Bathurst Island, Nunavut, Canada. *Hydrol. Res.* 44(1), 2-20.
- Young, K.L., Brown, L. & Labine, C. 2018 Snow cover variability at Polar Bear Pass, Nunavut. *Arctic Sci.* 4, 669-690.

Mercury inputs to the Mackenzie River and Beaufort Sea: Future impacts of permafrost thaw

Christian Zdanowicz¹, Staffan Åkerblom², Anne Soerensen³, Karin Eklöf⁴, Holger Hintelmann⁵

¹*Department of Earth Sciences, Uppsala University, Uppsala, Sweden.*

²*Unit for Environment and Environmental Economics
Statistics Sweden, Stockholm, Sweden.*

³*Department of Analytical Chemistry and Environmental Science, Stockholm University,
Stockholm, Sweden.*

⁴*Department of Aquatic Sciences and Assessment, Swedish University of Agricultural Sciences,
Uppsala, Sweden.*

⁵*School of the Environment, Trent University, Peterborough, Canada*

**Corresponding author's email address: christian.zdanowicz@geo.uu.se*

ABSTRACT

Recent studies highlighted the existence of a large reservoir of mercury (Hg) stored in frozen soils and peat of the circumarctic, and evidence is accumulating that this Hg is being released by permafrost thaw to streams and lakes in the northern Yukon and Northwest Territories. This raises the question whether such releases will increase the net export of Hg by large Arctic rivers to marginal seas of the Arctic Ocean, and thus potentially negating some of the long-term environmental benefits of Hg emissions reductions under the United Nations Minamata Convention.

In 2018 we initiated a Swedish-Canadian research project to investigate the sources of Hg entering the Mackenzie River, using an approach that combines measurements of multiple water quality parameters, including isotopes of Hg and carbon (dissolved and particulate). We carried out a sampling survey across the Mackenzie River Basin (MRB) in the summer of 2018, and will extend this with additional sampling in 2019.

We will present our initial findings from this study, with a focus on the implications for climate change on the cycling of terrestrial Hg between the MRB and Beaufort Sea.

KEYWORDS

Arctic environments; mercury; rivers; Arctic; subarctic; climate; permafrost.

